Dissertation
submitted to the
Combined Faculties for the Natural Sciences and for Mathematics
of the Ruperto-Carola University of Heidelberg, Germany
for the degree of Doctor of Natural Sciences

presented by
Paola Sofía Kuri Rodríguez, MSc
born in: Monterrey, Mexico
Oral examination: 09.09.2016

Teleost fish models for the *in vivo* study of inflammasome signaling

Referees: Prof. Dr. Detlev Arendt

Prof. Dr. Joachim Wittbrodt

Table of contents

Table of figures

Summary

Inflammation is an organism's concerted response to damage and infection. For an inflammatory signal to spread it relies on specific signaling pathways to activate proinflammatory genes. One is set off by receptors that, after detecting an appropriate stimulus, nucleate the assembly of a large multimolecular signaling platform called the inflammasome.

Currently, thanks to the advances in live microscopy, questions in immunology that can only be solved by live imaging are beginning to be addressed. In this work, we have established zebrafish and medaka as vertebrate model systems for the visualization of inflammasome signaling by three approaches. Since inflammasome assembly is driven by the aggregation of the adaptor molecule ASC, one approach was to study the dynamics of this molecule's switch from a cellular cytoplasmic localization to a single aggregate, called a speck, using zebrafish. We saw that speck formation leads to pyroptosis, a proinflammatory type of cell death, *in vivo*. This is the first time this process is visualized in a live organism. Furthermore, we generated a zebrafish transgenic line with endogenously tagged ASC that can be used to study the role of inflammasome activation live in zebrafish infection models.

Second, we used medaka to study the proinflammatory cytokine interleukin-1 (*il1*), whose activation is downstream of inflammasome assembly. We generated a transgenic line to track the transcriptional activation of the gene and the protein's cleavage. Based on our results, we propose that *il1* genes in teleost fish correspond genetically and functionally to both *il1* paralogues in mammals, instead of only for *il1β*.

Lastly, we generated a zebrafish reporter line to visualize and quantify NF-κB activity, a master regulator of proinflammatory genes. We show that the line has potential to be used in high-throughput screens.

Overall, this work reveals unknown features of the functional role of the inflammasome signaling cascade in fish and its evolution.

Zusammenfassung

Durch Entzündungsreaktionen kann ein Organismus koordiniert auf Infektionen und Verletzungen reagieren. Membranständige Rezeptoren erkennen entsprechende Stimuli und lösen den Aufbau eines Mulitprotein-Komplexes, des Inflammasoms, aus. Spezifische Signalwege sorgen daraufhin für die Ausbreitung der Entzündung durch Aktivierung proinflammatorischer Gene.

Idealerweise werden solche Prozesse direkt durch Live-Mikroskopie auf molekularer Ebene verfolgt. In dieser Arbeit wurden zwei Fischarten, Zebrafisch und Medaka, als Wirbeltier-Modelle für die Visualisierung von Inflammasom-Signalwegen in drei unterschiedlichen Ansätzen etabliert. Da der Aufbau des Inflammasoms durch die Ansammlung des Adaptormoleküls ASC vorangetrieben wird, entschieden wir uns im ersten Ansatz dazu, die Lokaliesierung von ASC im Zytoplasma und die Bildung von Aggregaten, auch Specks genannt, im Zebrafisch zu untersuchen. Wir zeigten, dass die Ausbildung dieser Specks zu Pyroptose, einer Form des programmierten Zelltods, führt. Dies ist der erste Nachweis dieses Processes im lebenden Organismus. Ausserdem verknüpften wir endogenes ASC mit einem fluoreszenten Reportermolekül in einer neuen transgenen Zebrafisch-Linie, welche zur Untersuchung der Inflammasom-Aktivierung in Infektionsmodellen verwendet werden kann.

Im zweiten Ansatz erforschten wir das proinflammatorische Zytokin Interleukin-1 (*il1*), welches vom Inflammasom aktiviert wird. Wir entwickelten eine transgene Linie in Medaka, die es erlaubt, sowohl die Epxression als auch die Spaltung von *il1* zu verfolgen. Unsere Resultate legen nahe, dass *il1* in Fischen genetisch und funktionell beiden *il1* Paralogen in Säugetieren entspricht, statt wie bisher geglaubt nur *il1β*.

Schließlich erzeugten wir eine Reporterlinie im Zebrafisch, welche die Visualisierung und Quantifizierung von NF-κB, eines Regulators von proinflammatorischen Zytokinen, ermöglicht.

Insgesamt zeigte diese Arbeit bisher unbekannte, funktionelle Merkmale der vom Inflammasom ausgehenden Signalwege auf und gestattet Rückschlüsse auf deren Evolution von Fisch zum Menschen.

Acknowledgements

It is very hard to describe the learning process one goes through while working towards a PhD. In my experience, a significant part of the journey was spent learning how to do science rather than just doing the work. In this sense, it is also an extreme individual experience of self-improvement and discipline. However, although we do the steep climbing by ourselves we are frequently pointed in the right direction by mentors, provided with better gear by colleagues, and given a shoulder to rest our heads on by friends and family.

First and foremost, I need to thank Maria, who offered me the incredible chance of doing a PhD in the rich scientific environment that is EMBL. Thank you, Maria, for sharing your enthusiasm for science, for trusting me with this project and for giving me the room to grow with it. Special thanks also to Eilish who always managed to fit me in Maria's schedule!

My sincerest thanks to Darren, Jochen and Detlev: first, for agreeing to being my TAC members and second, for their remarkable interest in the project and in my scientific development. Their suggestions and criticism lead to significant progress throughout my PhD. Many thanks also to Dr. Steeve Boulant, who kindly agreed to join the thesis defense committee.

Sometimes we are fortunate enough to find true friends in our colleagues. Renjith, Sanjita and Sara are no longer in the lab, but were there at the start. They taught me how to play the game and gave me a sincere friendship that kept me going during tough times. Sara, you are my second sister.

Many thanks to the current members of the lab for help, advice and support: Martina, Parisa, Julio, Benedikt and Matteo. Special thanks go to Baubi, with whom I collaborated in several projects, for our scientific discussions and for introducing me to medaka. Heartfelt thanks go to Sinja,

who made my wishes come true all the time (and spoiled me with chocolate!), Sourhab, whose is always up for coffee and an eccentric conversation; and Daniel, my Mexican teammate, for all the advice and jokes… so many good ones would be wasted without you!

Because I was the only person in my lab working with zebrafish, I heavily relied on the support that Francesca Peri and Darren Gilmour together with the members of both labs provided throughout the years. Francesca opened the doors of EMBL to me when I joined her lab as a Master student and she has continued being generous and supportive all my time here. I also need to thank the members of her lab, all of whom I constantly shared expertise and worked alongside with (especially in the fish room!): thank you Fargol, Fede, Timm, Ale, Shynia, Marvin, Joergen and Ambra. An honorable mention goes to Kerstin, a friend to who I am greatly indebted for help with countless protocols and reagents, but also for the all the laughs we shared. None of this work would have been possible without the dedication and invaluable assistance of Natalia and Conny, who diligently take care of our fish. I also want to thank the Gilmour lab for their willingness to share reagents, expertise and ideas, especially Andreas, Lionel, Sevi and Erika.

I must also thank the all staff here at EMBL who have given me outstanding technical support throughout the years, including Paul Collier and Vladimir Benes at GeneCore, Julia Rossmanith and Hüseyin Besir at PepCore, and Mandy Jeske and Joanna Kirkpatrick at the Proteomics facility. Because microscopy was such as important part of my PhD, I want to especially thank the ALMF staff for their technical assistance: Stefan Terjung, Yury Belyaev and Christian Tischer. Thanks also to my colleagues in DB who never say no when you need help.

I also want to thank the people who made my time in Heidelberg more enjoyable. To the members of LaBrat, friends with whom I shared countless rehearsals and unforgettable gigs: Dan, Gustavo, Wieschy, Nik, Marzia, Sean, Nils and Christoph. Thank you for the music! To all the good friends I made here, especially Alejandro, Christophe, Paul, Natalia, Aastha, Paola, Simone,

Leo and Andrea. I especially want to thank Joana, Giorgia, Chiara and Doris who always had words of understanding and encouragement and became friends truly close to my heart. Last but not least, my family in Germany, AKB. Irena, Siv, Marta, Mateusz and Víctor: we "came here to work", but got so much more in between.

Ever present in spite of being physically absent, I want to thank my whole family for their unwavering support and their unconditional love. To my parents, who have been my compass all my life, and who made sure all doors were open to me. My sister, who is always there for me, lights up my life with hers. Saying that I am eternally grateful does not begin to cover it.

¡Gracias!

I. Introduction

1 Inflammatory signaling in the innate immune system

Vertebrates rely on their innate and adaptive immune systems to recognize and deal with threats. The innate immune system, however, always responds first, providing the first line of defense by being the main driver of the inflammatory response. The classical definition of inflammation summarizes the response in five characteristic macroscopic symptoms: redness, swelling, heat, pain and loss of function. At the cellular level, these acute inflammatory symptoms are the result of a complex and carefully orchestrated response triggered upon the detection of pathogens, noxious stimuli andor physical injury, its basic purpose being to combat the source and consequences of the insult (Newton and Dixit, 2012). The activation of inflammatory signaling cascades is not limited to innate immune cells such as macrophages, dendritic cells, and circulating leukocytes; epithelial cells, endothelial cells, and fibroblasts also contribute to a global inflammatory response (Peeters et al., 2015; Yazdi et al., 2010).

The inflammatory response is also crucial for tissue and wound repair but should subside once the initial insult has been dealt with, i.e. the pathogen has been cleared or the tissue damage has been repaired. Failure to resolve the inflammatory response can occur when the offending agent is not removed or as a result of dysregulation of inflammatory signaling cascades, leading to a chronic inflammatory state or autoimmune disorders (Broderick et al., 2015; Newton and Dixit, 2012).

1.1 PRRs: germline-encoded sensors for pathogen and danger signals

The ability of the innate immune system to recognize and limit threats relies on elements that, for the most part, are constitutively present and ready to be mobilized immediately upon infection. Initial recognition is based on Pattern Recognition Receptors (PRRs), a fixed set of germ-line encoded receptors that

survey the extra and intracellular environment and are responsible for immune activation (Mogensen, 2009). PRRs are responsible for the recognition of conserved structures among microbial species that indicate the presence of a foreign organism. These include components of the microbial cell wall, secretion systems and microbial nucleic acids. However, some endogenous molecules released from damaged cells are also recognized by PRRs. These molecules are released by damaged host cells and alert the body to tissue damage. Molecules that belong to these two categories are known as PAMPs and DAMPs, for Pathogen Associated Molecular Patterns and Danger Associated Molecular Patterns respectively (Newton and Dixit, 2012; Takeuchi and Akira, 2010). Although, the recognition of DAMPs implies self-reactivity by PRRs, it can be beneficial in the context of infection since pathogens that escape recognition by conserved PAMPs may nonetheless lead to cellular damage (Fig. I.1.1). Therefore, mounting an inflammatory response to molecules indicative of compromised cellular integrity is an indirect way to sense invading microbes (Kono et al., 2014). This is probably why inflammatory responses during infection can be very similar to those induced by sterile stimuli (Chen and Nuñez, 2010).

PRRs can be broadly subdivided in transmembrane receptors found in the plasma membrane and in endosomes, where they can survey the extracellular milieu. This category includes Toll-like receptors (TLRs) and C-type lectin receptors (CLRs). The class of PRRs that reside in the intracellular environment is comprises the RIG-I-like receptors (RLRs), the AIM2-like receptors (ALRs) and NOD-like receptors (NLRs). Sensing of PAMPs or DAMPs by PRRs results in the release of cytokines and chemokines as well as the upregulation of a broad range of molecules, including cell adhesion molecules, immunoreceptors and further synthesis of chemokines and cytokines themselves. One of the main activators driving this transcriptional response is nuclear factor-κB (NF-κB) (Lamkanfi and Dixit, 2014; Mogensen, 2009; Takeuchi and Akira, 2010).

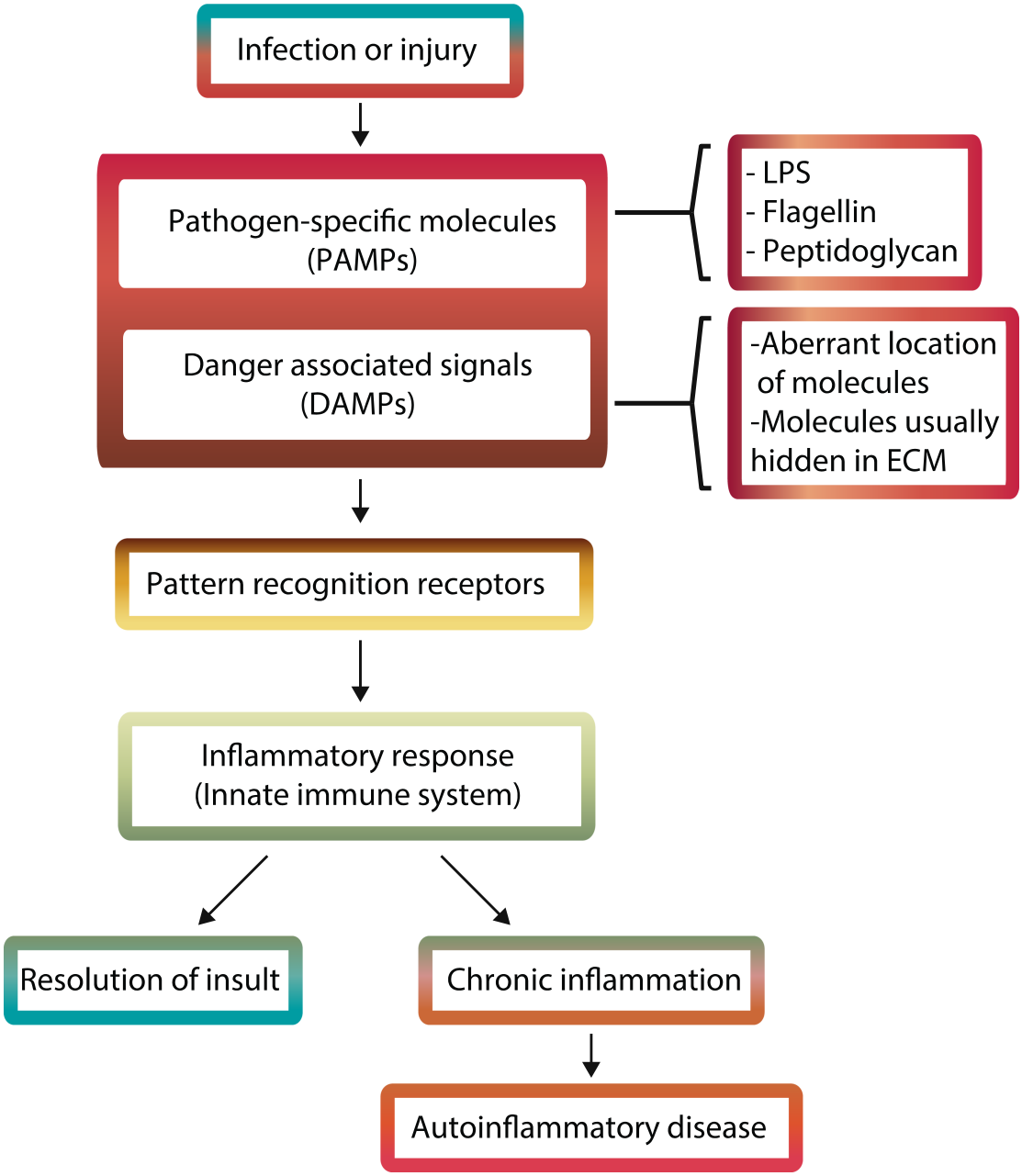

Figure I.1.1. Innate immune recognition by PRRs sets off the inflammatory response. During infection or injury, endogenous intracellular danger-associated molecules (DAMPs) are released by dying cells and alert to damage. Conserved molecular structures from pathogens (PAMPs) imply a foreign threat. Both DAMPs and PAMPs are recognized by pattern recognition receptors (PRRs). Activation of PRRs triggers a signaling cascade that sets off an inflammatory response and activates the innate immune system to elicit a response. Inflammation should subside after the insult has been dealt with. Failure to do so can lead to chronic inflammation and autoinflammatory disease. Figure modified from Mogensen (2009).

1.2 The modular structure of NOD-like receptors

Members of the NLR family are cytosolic immune regulatory proteins that share structural homology to the apoptosis-activating factor Apaf-1, the sensor protein of the apoptosome. Most NLRs have a tripartite modular structure consisting of a variable N-terminal domain; a central nucleotide-binding and oligomerization domain (NOD, also called NACHT domain, for NAIP, CIITA, HET-E and TP1, based on proteins sharing these domains) and C-terminal leucine-rich repeats (LRRs) that vary both in composition and number. This domain architecture is thought to be the key property that confers NLRs the ability to translate sensing into downstream signaling through intramolecular conformational changes. The central NOD domain contains a nucleotide binding domain (NBD), a helical domain (HD1) and a winged helix domain (WHD). NLRs function as binary molecular switches, with a monomeric "off" state in which ADP is bound to the NDB and allows the interaction between the WHD and LRR to act as a lock (Lechtenberg et al., 2014). Ligand binding leads to a remodeling of the protein that allows the replacement of ADP by ATP. The ATP-bound form of the NBD represents the "on" state and results in the oligomerization of multiple NBD domains (Fig. I.1.2) (Chai and Shi, 2014). The LRRs have been traditionally considered the ligand-binding as well as autorepression domain. However, the precise structural mechanism of ligand sensing has remained elusive and other domains have been shown to carry out this function (Tenthorey et al., 2014). The variable N-terminal domain contains one of several death-fold domains and is involved in the recruitment of downstream effector molecules. Subfamilies within the mammalian NLRs are classified based on their N-terminal effector domains: NLRA or Class II transactivator contain an acidic transactivation domain, NLRB or neuronal apoptosis inhibitor proteins (NAIPs) have a baculovirus inhibitor of apoptosis protein (IAP) repeat (BIR), NLRCs possess a caspase activation and recruitment domain (CARD), and NLRPs a pyrin domain (PYD) (Barbé et al., 2014; Ting et al., 2008). These death-fold domains recruit effector molecules via homotypic domain interactions (e.g., a CARD-CARD and PYD-PYD) to mediate downstream signaling (Chai and Shi, 2014).

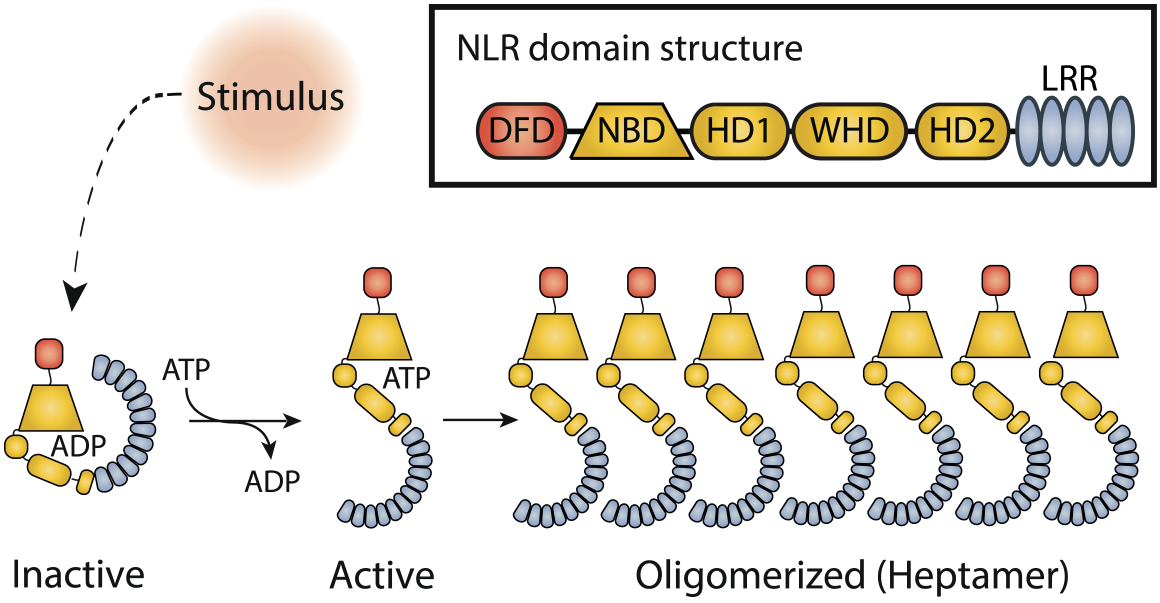

Figure I.1.2. Principles of NLR activation.
NOD-like receptors (NLRs) are capable of sensing a wide variety of DAMPs and PAMPs. In a resting state, monomeric cytoplasmic NLRs are kept in an autoinhibited inactive conformation by the interaction between the WHD and the LRR. Upon sensing a stimulus, the NBD exchanges ADP for ATP and the receptor switches to an active conformation, which can oligomerize with other active NLRs into heptamers. The N-terminal DFD recruits downstream signaling molecules that trigger the signaling cascade. Figure modified from Broderick et al. (2015).

1.3 Activated NLRs can form inflammasomes

Almost 15 years ago, an overexpression system was used to show for the first time that, in its oligomerized state, the NLR protein NLRP1 can form part of a high-molecular weight cytosolic complex that also contained ASC (apoptosis-associated speck-like protein containing a CARD) and caspase-1 (Martinon et al., 2002). This molecular complex, named the "inflammasome", was found to be responsible for the processing of the proinflammatory cytokine interleukin-1β (IL-1β). Macrophages lacking inflammasome components are deficient in their ability to activate caspase-1 or secrete activated IL-1β in response to infection (Mariathasan et al., 2004). A second NLR, NLRP3, was later shown to be responsible for the activation of caspase-1 following exposure to lipopolysaccharide (LPS) and ATP (Mariathasan et al., 2006). Other members of the NLR family as well as AIM2, an ALR PRR family member, have been found to form inflammasomes in response to a wide variety of stimuli. In addition to NLRP1 and NLRP3, these include NLRP6, NLRP7, NLRP12, NLRC4 and the NLRB proteins (Fig. I.1.3) (Barbé et al., 2014; Broderick et al., 2015). Although

until recently each NLR was thought to form distinct inflammasome scaffolds, it has been shown that more than one NLR can be recruited to the same inflammasome complex (Man et al., 2014; Qu et al., 2016). Additionally, a non-canonical caspase-11-dependent inflammasome that does not require a PRR and whose activation indirectly leads to IL-1β secretion has also been described (Kayagaki et al., 2011).

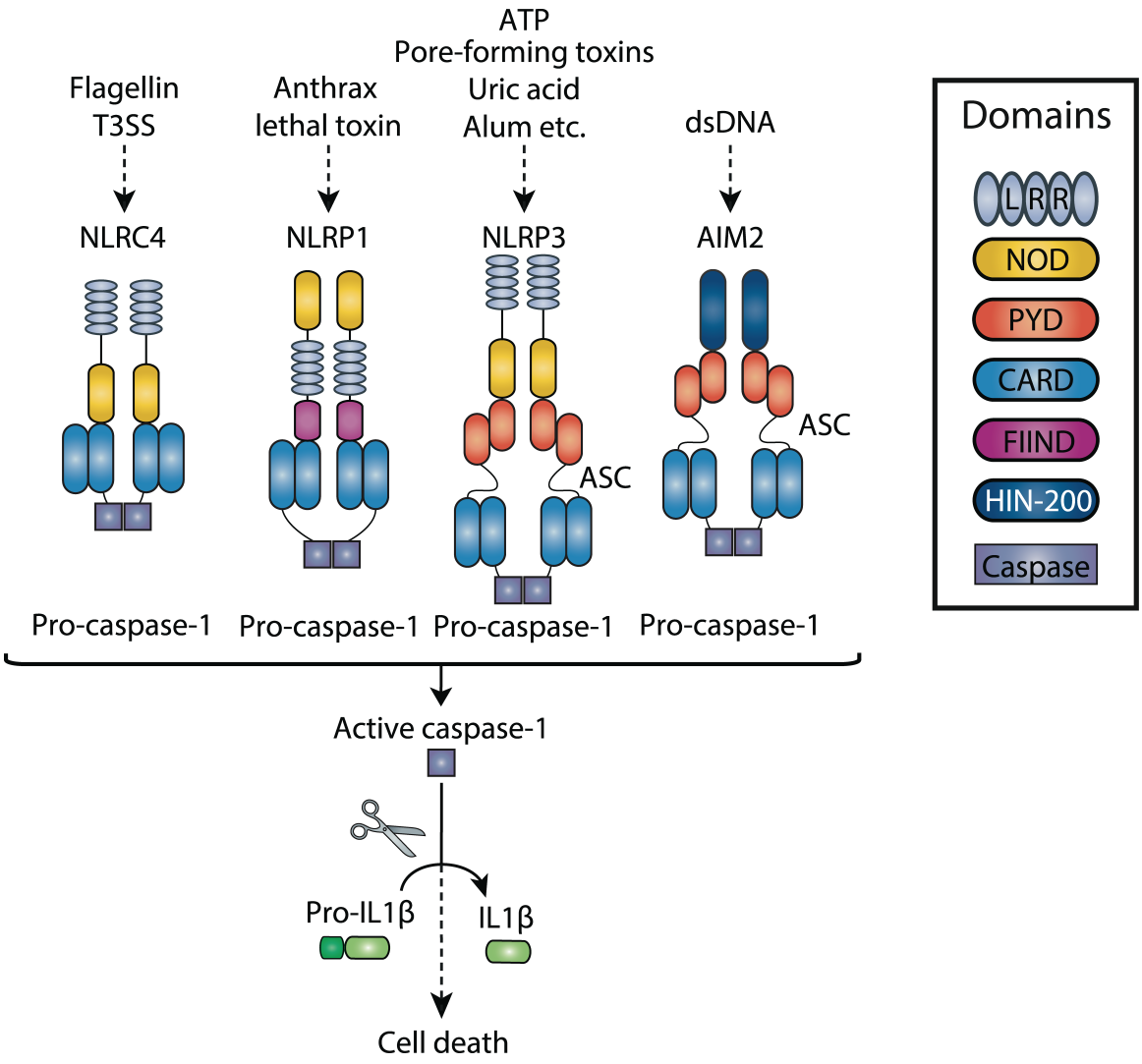

Figure I.1.3. The assembly of inflammasomes relies on homotypic domain interactions. Different NLRs are activated by specific stimuli. The downstream molecules are recruited through DFD homotypic interactions with the N-terminal domain of the NLRs. NLRs with a PYD domain recruit the adaptor molecule ASC, which is composed of a PYD and a CARD domain. The immature form of the inflammatory caspase-1, pro-caspase-1, is then recruited via its CARD domain. NLRs that have an N-terminal CARD domain can recruit pro-caspase-1 directly. Caspase-1 is activated via proximity-induced autoproteolytic cleavage and is the main effector molecule of the inflammasome. Activated caspase-1 cleaves its downstream targets, including the proinflammatory cytokine, IL-1β, and can also cause cell death. Figure modified from Vanaja et al. (2015).

In a manner thought to be analogous to the formation of the apoptosome, oligomerization of NLRs represents the first nucleation step in inflammasome formation. Like Apaf-1 for the apoptosome, which oligomerizes into heptamers upon activation, the NLR protein would form the scaffold of the complex (Chai and Shi, 2014). Afterwards, through its PYD domain, the NLR recruits ASC to act as an adaptor. ASC contains both a PYD and a CARD domain, which allow it to interact with both the PYD-containing NLR and CARD-containing pro-caspase-1. In cases where the NLR has a C-terminal CARD domain instead of a PYD, pro-caspase-1 can be recruited through direct interaction with the CARD domain. Once recruited to the inflammasome, pro-caspase-1 is activated and can then proteolytically activates a number of proteins to further spread the inflammatory signal in the tissue (Latz et al., 2013).

Inflammasomes play a key role in the innate immune system. Mutations in sensors are behind several autoinflammatory diseases, such as familial Mediterranean fever (FMF) and Cryopyrin-associated periodic syndrome (CAPS). Inflammasomes are implicated in chronic inflammation accompanying diseases such as gout, atherosclerosis, Alzheimer's disease and Type 2 Diabetes (Broderick et al., 2015; Guo et al., 2015); and also have a role in cancer progression and therapy (Kolb et al., 2014; Zitvogel et al., 2012). The wide range of inflammasome involvement in disease underscores the potential for therapeutic benefit of studying these complexes.

1.4 Death-fold domains in detail

As already stated, interactions between PYD and CARDs determine the logic of inflammasome assembly. Both domains are members of the death domain fold (DDF) superfamily and possess the characteristic six anti-parallel α-helices with a hydrophobic core and an outer surface composed of charged residues. Variations on length and orientation of these α-helices result in different charged and hydrophobic surface pockets that largely determine the specificity of protein-protein interactions (Dorfleutner et al., 2015). PYD domains are usually about 90 amino acids long and are always located at the N-terminus of proteins. The structures of PYD domains (evident from the available PYD structures of

NLRP1, NLRP3, NLRP7, NLRP12 and AIM2, among others) show that two acidic patches formed by residues in the α2 and α3 helices and basic patches formed by residues in the α1 and α4 helices are conserved among PYD domains. A likely source of variation among PYD domains is the sequence and length of the α2- α3 loop region (Chu et al., 2015). Because PYD domains have a high propensity for aggregation, NMR and X-ray crystallography structures were obtained by preparing the proteins at low pH, which modifies the surface charge potential and thus prevents complementarity-induced aggregation (Hauenstein et al., 2015).

CARD domains were first described as an interaction motif between apoptotic caspases and their adaptor molecules (as is the case for the apoptosome). However, the role of CARDs in signaling has been expanded to include assembly of signaling complexes in inflammation and NF-κB. Many caspase zymogens contain a CARD in their N-terminal domains, including human inflammatory caspases -1, -4, and -5, and mouse inflammatory caspases -1 and -11 (Kao et al., 2014).

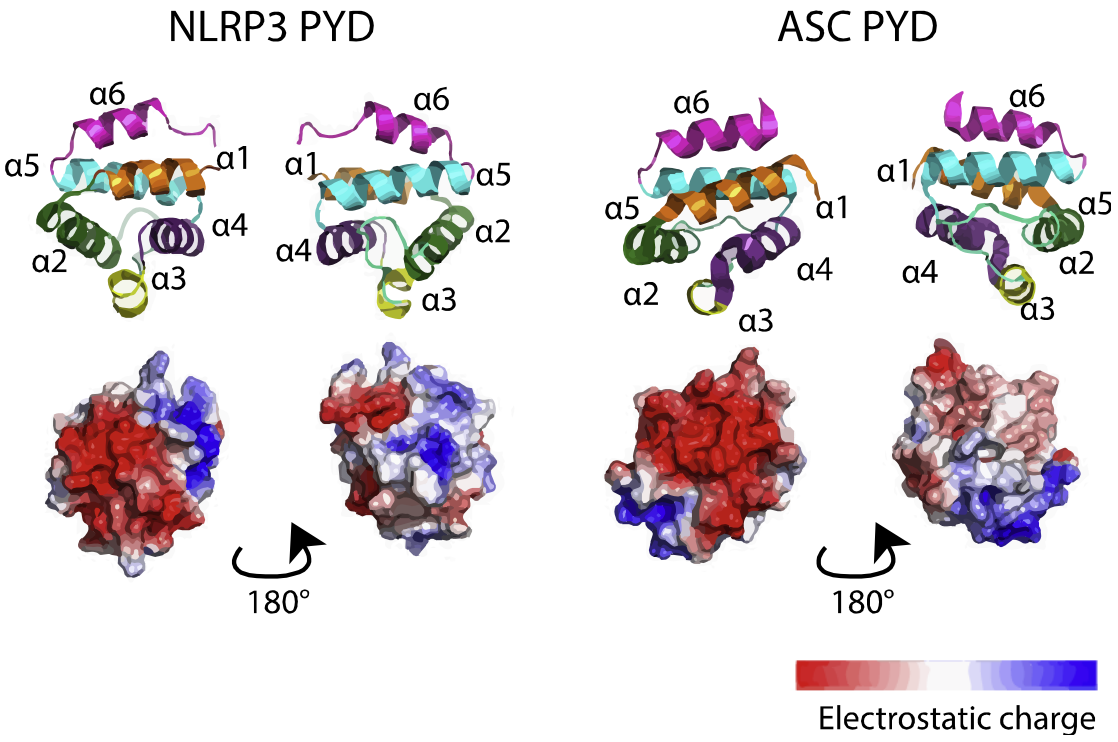

Figure I.1.4. The structure of PYD domains determine the specificity of protein interactions.
ASC and NLRP3 PYD domains, here shown in ribbon diagram, are composed of 6 antiparallel α-helices that make up a hydrophobic core with the charged residues on the outer

surface. Electrostatic surface representations show negative (red) and positively (blue) charged residues. The specificity of PYD-PYD domain interactions is determined by these differently charged and hydrophobic surface pockets. Figure modified from Chu et al. (2015).

1.5 Inflammasome activation requires two signals

Mainly from the methodology that has been used to trigger inflammasome formation in cell-culture studies, activation of inflammasomes is thought to be a two-step process that requires two signals. Signal 1 functions as the priming signal. It can be provided by the activation of NF-κB or by other innate immune receptors and was thought to be necessary for the NF-κB-mediated upregulation of *NLRP3* and *il1β*. *NLRP3* upregulation would influence the susceptibility to inflammasome activation triggers and more IL-1β would strengthen the inflammatory signaling (Latz et al., 2013). However, current views suggest priming can also happen independently of the upregulation of inflammasome components, for example, though post-translational modifications. So far only ubiquitination and phosphorylation have been investigated (Barbé et al., 2014; Elliott and Sutterwala, 2015). Signal 2 is considered the direct trigger of inflammasome assembly through the recognition of PAMPs and DAMPs themselves by NLRs, although other signals such as potassium efflux, generation of mitochondrial reactive oxygen species (ROS), cathepsin release as a result of lysosomal membrane disruption and calcium signaling have also been reported to activate the inflammasome assembly (Elliott and Sutterwala, 2015; Vanaja et al., 2015). Signal 1 and 2 are always delivered one after the other to cells in culture, so their significance in a live situation in which cells sense and integrate multiple signals simultaneously, is unclear.

2 ASC: an inflammasome adaptor molecule

In its role as an adaptor molecule, ASC is frequently considered a central link in inflammasome assembly. ASC was discovered using monocolonal antibodies developed against the TritonX-100 insoluble components of the promyeloleukemic cell line HL-60 after induction of apoptosis. The protein, described as a 22-kD novel member of the CARD-containing adaptor family, was

located in the cytoplasm and nucleus of unstimulated HL-60 cells. However, upon treatment with retinoic acid or antitumor drugs, the protein relocalized to a single aggregate, called a speck, in the cell. At the time, specks were thought to be related to apoptotic cell death (hence the name) (Masumoto et al., 1999). Subsequent work has revealed the central role that ASC plays in inflammasome signaling as a crucial mediator of the assembly of this complex (Lu and Wu, 2014).

2.1 ASC forms speck-like aggregates upon stimulation

Fernandes-Alnemri et al. (2007) coined the term "pyroptosome" to describe the spherical ASC specks of around 2μm in diameter formed *in vitro* by THP-1 macrophages. Cells stably expressing ASC fused to a fluorescent protein would form specks large enough to be visualized by light microscopy. The assembly of the ASC pyroptosome, from visualization of the first aggregate until all cytoplasmic protein was recruited to the speck took less than 3 min (Fernandes-Alnemri et al., 2007). This study also noted that in hypotonic THP-1 lysates, incubation at 37°C results in the spontaneous formation of specks. Therefore, aggregation of ASC inside a cell seems to mimic a snowball effect in which the entire soluble pool of ASC protein in the cytoplasm is recruited to single subcellular location. Indeed, when using a fluorescently tagged version of ASC, the switch from a weak, diffuse signal present throughout the cell, including the nucleus, to one single bright point in a stimulated cell is currently considered a read-out for inflammasome activation (Stutz et al., 2013). The combined use of antibodies and flow cytometry has also allowed the quantification of endogenous inflammasome activation in mixed cell populations and its activation *in vivo* (Sester et al., 2015).

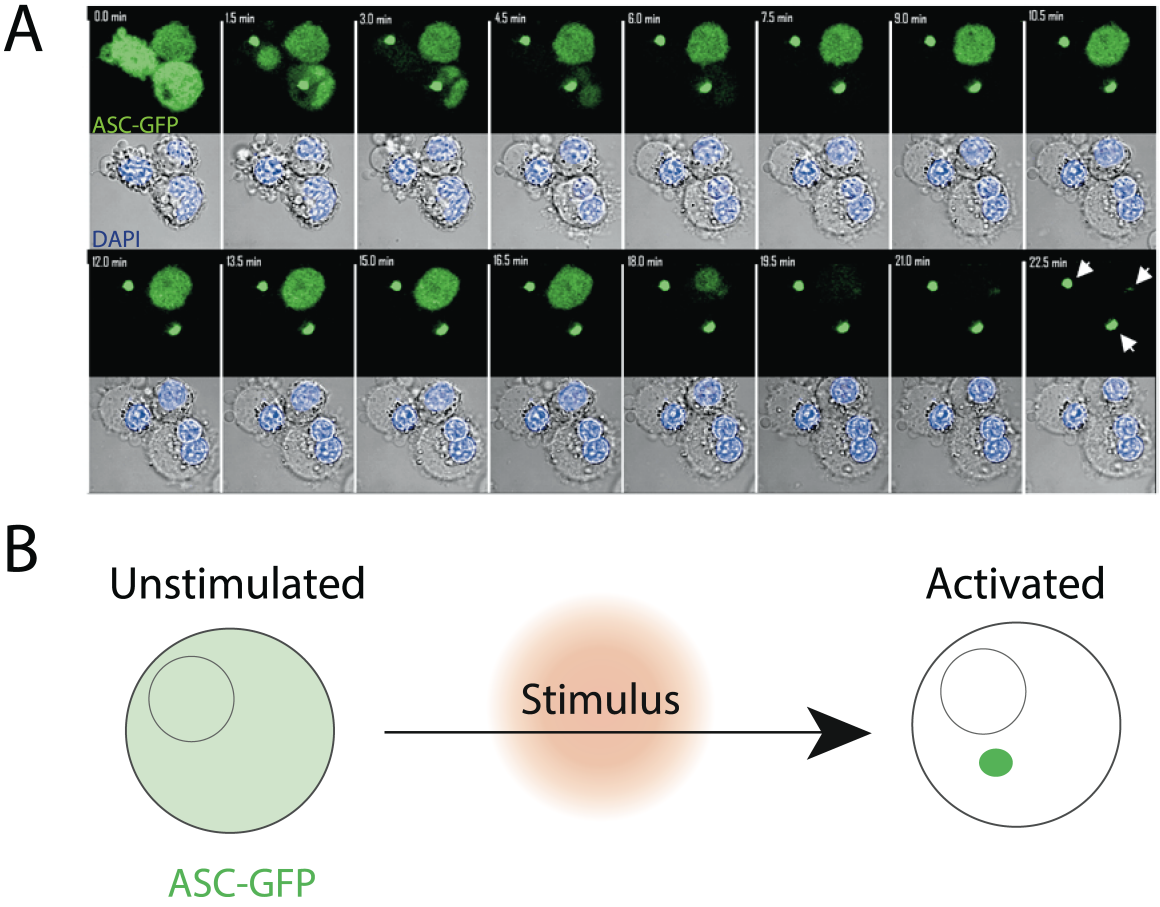

Figure I.2.1. The inflammasome adaptor ASC aggregates into specks.
THP-1 macrophages stably expressing ASC-GFP show a switch from a cytoplasmic distribution of ASC to a single point in the cell after stimulation with LPS (white arrowheads). The concomitant morphological changes visible in the bright field show that THP-1 cells undergo cell death after assembly of ASC speck (A). After exposure to an inflammatory stimulus, all the protein in the cell is recruited to the speck. Speck formation is a proxy for inflammasome activation. Panel A modified from Fernandes-Alnemri et al. (2007) and panel B modified from Sester et al. (2015).

ASC redistribution happens in a variety of cell types in response to stimuli that activate inflammasomes, including LPS, infection, and viral proteins (Bryan et al., 2009; Fernandes-Alnemri et al., 2007; McAuley et al., 2013). Overexpression of NLRP3, which colocalizes with ASC specks, also leads to speck formation (Hornung et al., 2009). Furthermore, since transfection of ASC leads to speck formation in cell types such as HeLa, HEK-293, and COS cells (Cheng et al., 2010; Fernandes-Alnemri et al., 2007; Masumoto et al., 1999); the ability to form specks seems to be an innate property of ASC.

2.2 Structural aspects of ASC speck formation

The bipartite nature of ASC is crucial for its function in inflammasome assembly. An NMR high-resolution structure of ASC obtained under acidic conditions showed that the PYD and CARD of ASC (from here onwards referred to as PYD_{ASC} and $CARD_{ASC}$, respectively) are structurally independent and connected by a 23bp flexible linker (Fig. I.2.2) (de Alba, 2009). Subsequent studies have built upon this structure by using site-directed mutagenesis to unravel the role of specific residues in the interaction surface of individual ASC proteins (Lu and Wu, 2014; Sahillioglu et al., 2014).

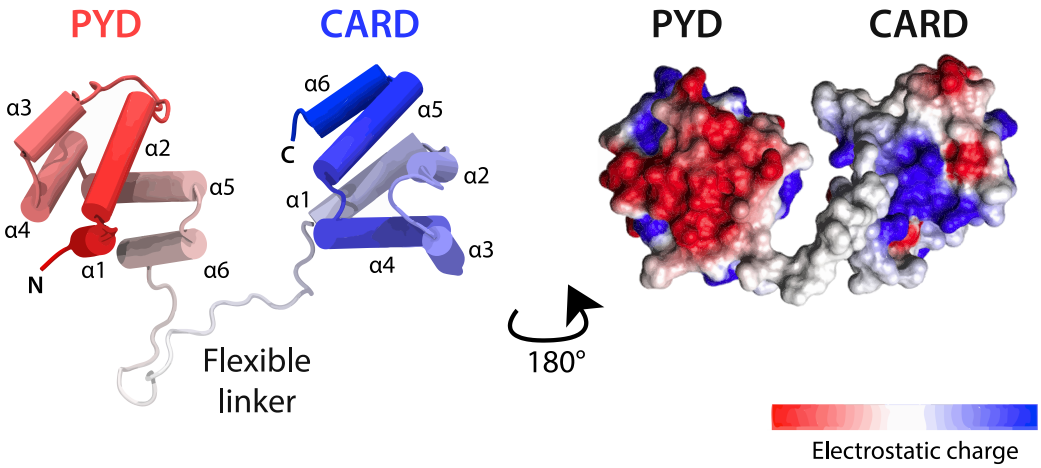

Figure I.2.2. Structure of full-length human ASC.
An N-terminal PYD and a C-terminal CARD joined by a flexible linker make up ASC (right panel). Both death-fold domains have the typical 6 α-helices structure and a variably charged surface as shown by an electrostatic surface representation (left panel). NMR structure was originally solved by de Alba, (2009) (PDB ID 2KN6). Right panel modified from Sahillioglu et al. (2014) and left panel from de Alba (2009).

Homotypic interactions between PYD or CARD domains are weak and no K_D for these interactions has been reported (Lechtenberg et al., 2014). This is likely the reason why in the absence of a stimulus, ASC molecules have low affinity for one another and the likelihood of nucleation is very low. Changes in the protein concentration, however, will alter the aggregation kinetics (Cheng et al., 2010). Only two years after its discovery, it was shown that overexpressing ASC results in filament-like aggregates. Both PYD_{ASC} and $CARD_{ASC}$ also independently form filament-like aggregates when overexpressed separately, suggesting that oligomerization of the domains could play a role in speck formation (Masumoto et al., 2001). Two recent in-depth studies addressing

assembly mechanics of ASC polymers confirmed this (Cai et al., 2014; Lu et al., 2014). Both studies showed that, after priming (as an initial required nucleation step), PYD_{ASC} has a very strong tendency to self-associate into long hollow filaments. Using cryo-EM, Lu et al. (2014) solved the structure of PYD_{ASC} filaments. They found that filaments have a helical symmetry with the subunits densely packed in a spiral, ultimately giving rise to a cylinder-like structure with a three-fold symmetry. Using a yeast prion assay to test the aggregation properties of ASC, Cai et al. (2014) found that ASC is able to induce prion conversion. PYD_{ASC} forms fibers that can convert inactive ASC into an active prion form that is both necessary and sufficient for downstream signaling. Mutations that abolished the prion-like activity prevented the activation of reconstituted inflammasomes in HEK-293 cells, but replacing the PYD_{ASC} with a yeast prion protein did not affect the ability of ASC to activate pro-caspase-1 (Cai et al., 2014). This prion-forming ability seems to be unique to the PYD_{ASC}, since the PYD of NLRP3 and that of other proteins are unable to induce yeast prion conversion. A model in which the structure of full-length ASC is superimposed into the filaments formed by the PYD_{ASC} domains, shows that the PYD_{ASC} localizes at the core of the filaments and the flexibly linked $CARD_{ASC}$ is directed outwards, forming a second layer that goes around the entire filament (Fig. I.2.3) (Lu et al., 2014).

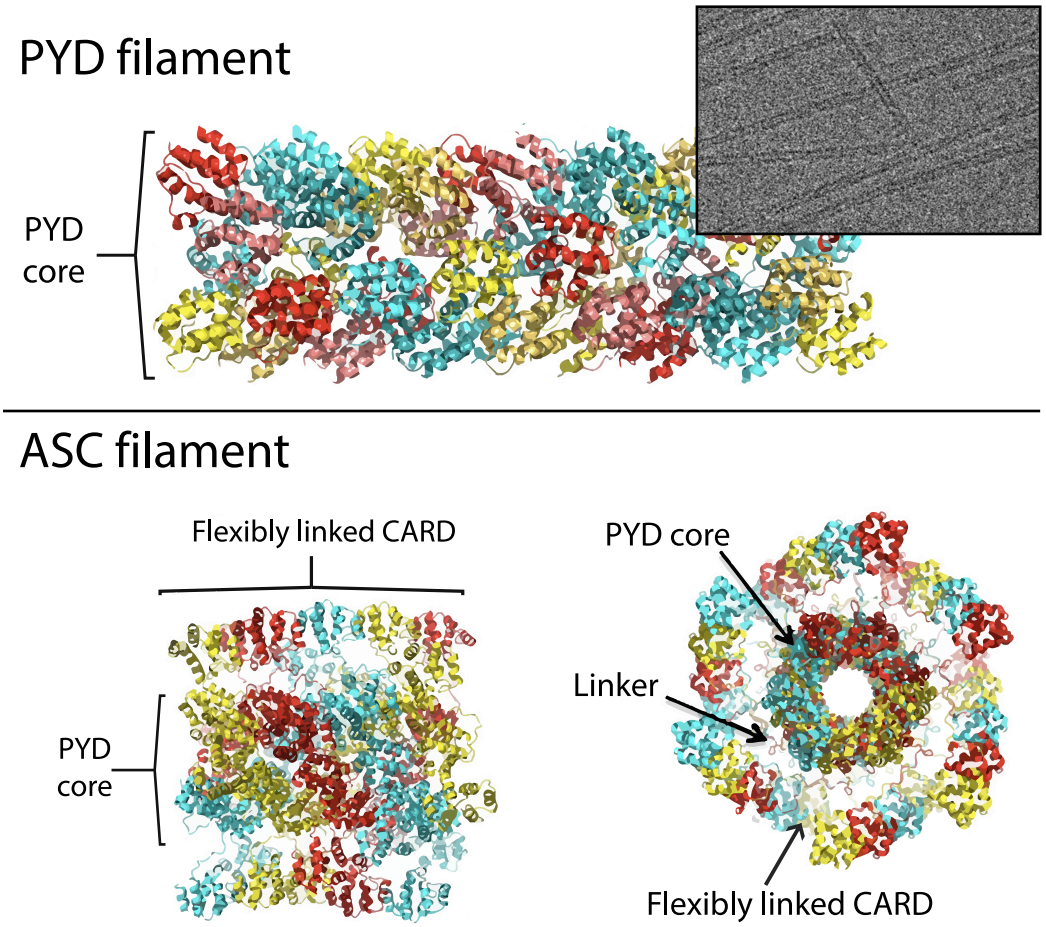

Figure I.2.3. PYD_{ASC} assembles in filament structures.
Upper panel: PYD_{ASC} filaments form a three start helical assembly. Each strand is represented by red, cyan and yellow as shown in a ribbon representation. Structure of PYD_{ASC} filaments was solved by cryo-EM (inlay corresponds to cryo-EM image) from PYD_{ASC} filaments that assembled spontaneously *in vitro*. Lower panel: A superimposition of the full-length ASC (PDB ID 2KN6) on the PYD_{ASC} filament model depicts the peripheral location of the flexibly linked $CARD_{ASC}$ domain from the side (left) or in a cross-section (right). Figures modified from Lu et al. (2014).

2.3 ASC properties: implications for inflammasome assembly

Inflammasome formation was initially thought to occur in a manner analogous to apoptosome assembly. Recently, the fact that activation of signaling induces a prion-like polymerization of ASC into filaments has shifted the common view regarding inflammasome formation from an apoptosome-based model to one centering on PYD and CARD filaments, where inflammasome assembly is ASC-dependent (Lu and Wu, 2014; Ruland, 2014).

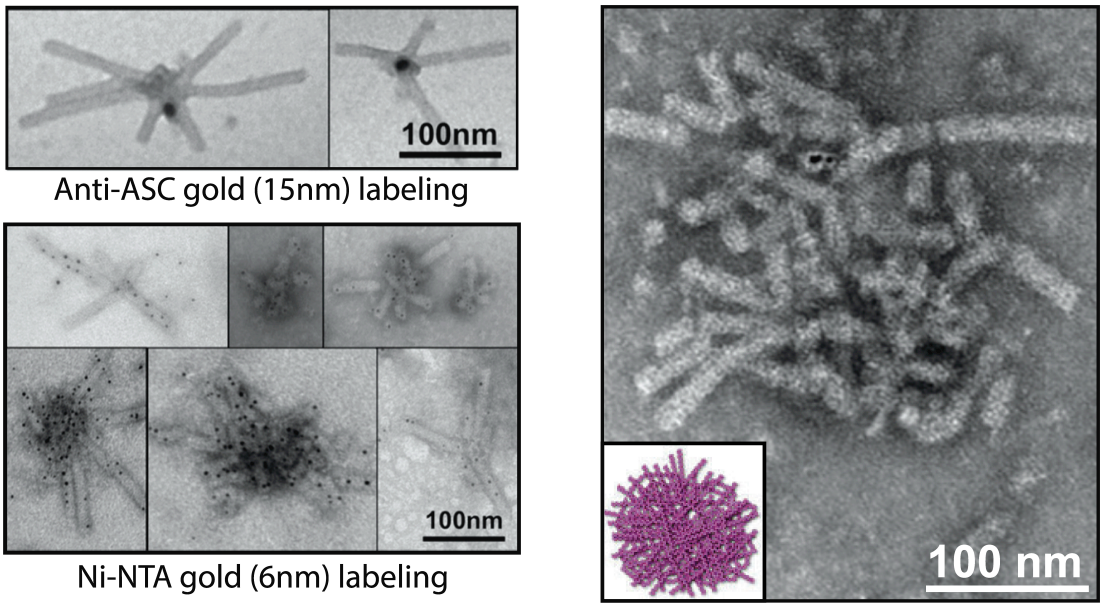

Figure I.2.4. *In vitro* reconstitutions of the inflammasome.
Left panels: Electron micrographs of star-shaped ternary inflammasome complex assembled *in vitro* from purified AIM2 PYD domain, full-length ASC and the His-GFP labeled CARD domain of caspase-1. Labeling of the ternary complex with anti-ASC gold (upper panel) or Ni-NTA gold (lower panel) showed ASC is located at the center of the structure whereas caspase-1 locates along the protruding star filaments. Right panel: *In vitro* reconstituted inflammasomes incubated overnight. Inlay image shows model of the filamentous sphere formed through the aggregation of multiple filaments. Figures modified from Lu et al. (2014) and Lu and Wu (2014).

Inflammasome assembly deviates from a 1:1 molecular stoichiometry (Elliott and Sutterwala, 2015). *In vitro* reconstitution reactions showed that PYD domains of ASC can be nucleated into forming filaments with sub-stoichiometric amounts of the PYD domains of the receptor proteins AIM2 or NLRP3. Furthermore, in a reconstituted AIM2/ASC/caspase-1 complex visualized by EM, full-length ASC induced the formation of caspase-1 filaments, which were themselves overstoichiometric to ASC. Using gold labeling, it was shown that the receptors were located at the tips of these filament bodies, with numerous filaments growing out from the site of receptor nucleation in a star shaped pattern (Lu et al., 2014). Over time, these *in vitro* structures further aggregate into filamentous spheres, which could represent the ASC speck formed by cells *in vivo* (Fig. I.2.4) (Lu and Wu, 2014). Furthermore, the PYD domains of AIM2 and NLRP3 are able to convert ASC into a self-perpetuating prion through PYD-PYD interactions (Cai et al., 2014). Therefore, in what has been called a branching tree

model (Elliott and Sutterwala, 2015), receptors detect a damage, assemble into heptamers and induce the formation of ASC filaments in which the PYD_{ASC} acts as building block that forms an inner core. The outer ring of flexibly linked CARDs on the filament's surface can then further nucleate filament formation of pro-caspase-1 (Hauenstein et al., 2015; Ruland, 2014).

2.4 Supramolecular organizing centers

Structural studies give insight into the molecular basis of assembly of high-order signaling complexes in cells (Lu and Wu, 2014). It has become clear in recent years that these signaling complexes, called supramolecular organizing centers (SMOCs), provide a phenomenological explanation for the punctate morphology that is often observed for protein regulators in innate immunity. supramolecular organizing centers do not constitute random aggregates but instead, as has been seen in the case of ASC filaments, have a defined molecular basis of assembly (Fig. I.2.5) (Kagan et al., 2014; Wu, 2013). What are the properties of these signaling systems? First: effector enzymes drive the allosteric changes required for their activation. Second: immense signal amplification that enables a response threshold to be reached. In the case of the inflammasome, this ensures that once the cascade is activated, almost all pro-caspase-1 molecules in the cell are processed, which represents the maximum level of activation. Third: the modularity of the system, where numerous upstream stimuli converge in common downstream module. Fourth: supramolecular organizing centers may provide spatial regulation through transient compartmentalization of the complexes which, due to their size, do not easily diffuse (Kagan et al., 2014; Wu, 2013).

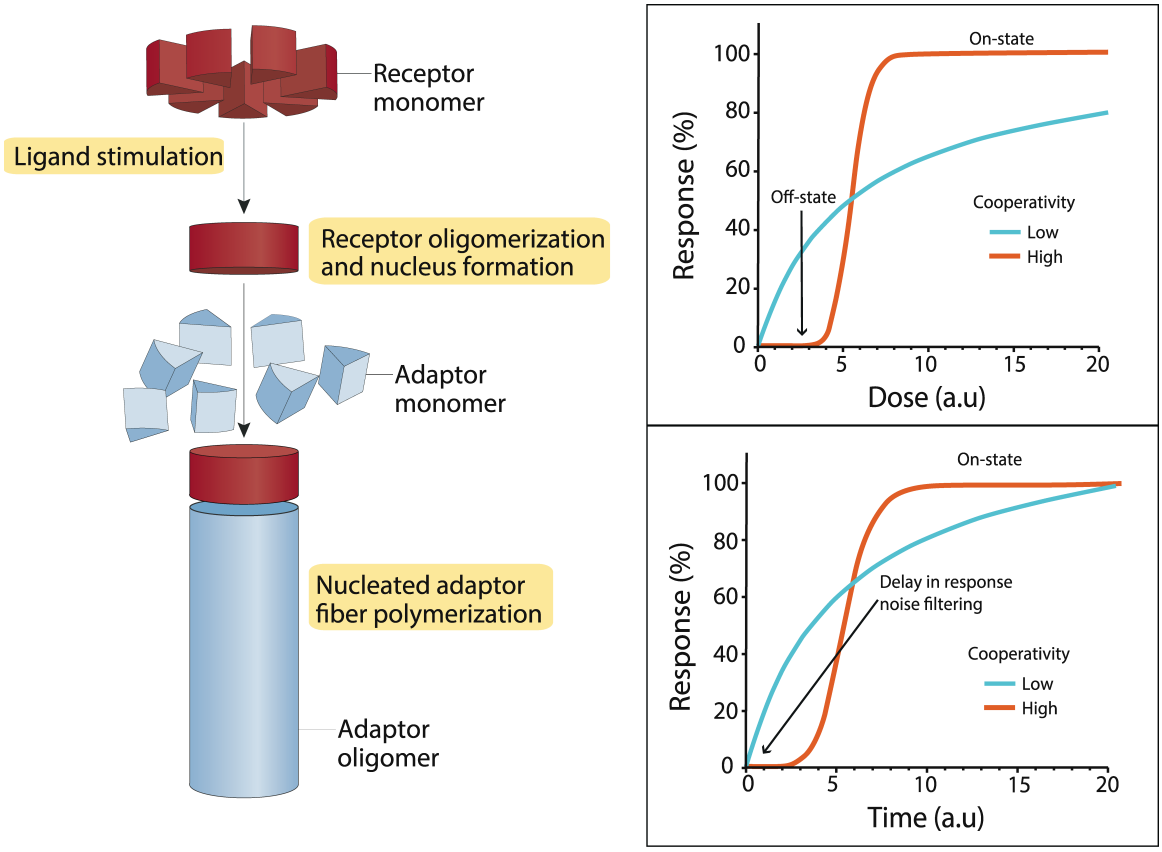

Figure I.2.5. Nucleated polymerization driven assembly of supramolecular organizing centers. Left panel: Supramolecular organizing centers can be assembled via a nucleated polymerization mechanism in which the oligomer of a receptor (NLR), formed upon stimulation, constitutes the nucleus to which the adaptor (ASC) can bind and use as a seed for a filamentous polymerization. Right panel: Simulated response curves as a function of dosage (up) or time (down) for processes highly or lowly cooperative. In highly cooperative processes the transition between an "off" and an "on" state shifts abruptly upon overcoming a certain concentration threshold. Time-wise, assembly of cooperative processes would proceed with slow kinetics at first, as seeds assemble. A time delay could help overcome transient and stochastic variations in the stimuli, thus functioning as a noise filter. Right panel modified from Kagan et al. (2014) and left panel from Wu (2013).

An obvious issue that arises from the formation of stable and large aggregates such as the inflammasome is how the cell manages to disassemble them. However, whether a mechanism for this purpose exists is unknown. From a biophysics standpoint, supramolecular organizing centers should exhibit slow dissociation kinetics, making a spontaneous disassembly highly unlikely. Furthermore, specks may be too large to be efficiently degraded by standard cellular protein degradation machinery (Kagan et al., 2014; Wu, 2013), although they could be delivered to autophagosomes and destroyed there after ubiquitination (Shi et al., 2012). However, inflammasomes can also persist as stable aggregates for a long time (discussed below).

2.5 Regulation of inflammasome assembly via ASC post-translational modifications

How is the assembly of inflammasomes regulated? Given that ASC plays a central role in inflammasome assembly, post-translational modifications that regulate its aggregation can promote or inhibit inflammasome activation (Man and Kanneganti, 2015a). Thus far, only ubiquitination and phosphorylation have been investigated (Elliott and Sutterwala, 2015). As mentioned previously, polyubiquitination of ASC can target the inflammasome to autophagosomes (Shi et al., 2012). On the other hand, linear ubiquitination of ASC by the linear ubiquitination assembly complex (LUBAC) is a requirement for NLRP3 inflammasome assembly (Rodgers et al., 2014). Phosphorylation of ASC as an indirect consequence of Syk and Jnk kinase activation is a checkpoint for inflammasome activation, since treatment with inhibitors of either kinase abolished speck formation. Phosphorylation of specific sites likely functions as a licensing step, with Y144 a critical phosphorylation site for speck formation. However, the kinase that is directly responsible has not been identified (Hara et al., 2013). The fact that ASC is modified by several post-translational modifications suggests that different cellular processes target this protein as prerequisite for assembly (Man and Kanneganti, 2015a).

3 Pyroptosis

Cells die. This can happen accidentally, for example, after a mechanical, physical or chemical insult causes cell destruction. However, cell death can also be "regulated" when it is engaged by a predestined molecular mechanism. Types of regulated cell death can be separated according to the immune response they elicit, if the cell's membrane integrity is maintained, as in apoptosis, the cell death is "immunologically silent". On the other hand, if membrane integrity is compromised, the cell death acts as an inflammatory activator (Stephenson et al., 2015). Another distinction is that different regulated cell death programs require the activation of different signaling pathways and specific subsets of caspases, cysteine proteases that cleave after aspartic acid residues. Caspases are expressed

as zymogens in many tissues and organs both by immune and non-immune cells. They can be classified as apoptotic and inflammatory caspases. The first include initiator caspases -2, -8, -9 and -10, which receive the apoptotic signal and activate the downstream effector caspases -3, -6 and -7, which then cleave target proteins. Inflammatory caspases are involved in the activation of inflammasomes and in the induction of a lytic cell death called pyroptosis. These include caspase-1, -4 and -5 (humans), and -11 (mice) (Man and Kanneganti, 2015b). In spite of the distinction between apoptotic and inflammatory caspases, there is increasing evidence of cross-talk between pathways leading to the activation of caspases in either group (Aachoui et al., 2013).

3.1 Caspase-1 is activated by the inflammasome

Caspase-1 was originally termed interleukin-converting enzyme (ICE) based on its ability to cleave pro-IL-1β into its mature secreted form. The zymogen of caspase-1, pro-caspase-1, contains an N-terminal CARD domain that gets cleaved off during activation. The C-terminal domain also undergoes cleavage to yield two subunits, p20 and p10, which heterodimerize to form active caspase-1 (Thornberry et al., 1992). As has been reported for apoptotic caspases, cleavage may lead to the stabilization of the active site, which is essential for the processing of pro-IL-1β (Boucher et al., 2014). As mentioned previously, activation of caspase-1 occurs after its recruitment to the inflammasome. In macrophages, discrete foci of caspase-1 colocalize with ASC and NLRP3 specks (Bryan et al., 2009) and IL-1β can be recruited to the ASC speck in a caspase-1-dependent manner that is unaffected by addition of a caspase-1 inhibitor (Broz et al., 2010b). This would suggest that IL-1β is processed by caspase-1 within the ASC focus (Miao et al., 2011). Similar to PYD_{ASC}, Caspase-1 CARD forms filaments *in vitro*. A recent study solved the structure of these Caspase-1 CARD filaments by cryo-EM and showed that the $CARD_{ASC}$ nucleates the assembly of these filaments (Lu et al., 2016). As pro-caspase-1 clusters in this cylindrical arrangement, they are thought to activate and heterodimerize. Whether these structures are also formed *in vivo* is unclear (Hauenstein et al., 2015).

3.2 Inflammasome activation leads to pyroptosis though caspase-1

One of the most prominent physiological functions of caspase-1 that is unrelated to the cleavage of pro-IL-1β is pyroptosis. The name comes from the Greek word *pyro*, fire, to denote a "screaming, alarm-ringing proinflammatory" type of regulated cell death (Cookson and Brennan, 2001). Pyroptosis depends on the activation of inflammasomes (either the canonical caspase-1-dependant or the non-canonical caspase-11-dependent inflammasome) and is independent of apoptotic caspases. Although targets downstream of caspase-1 and -11 driving pyroptosis had remained elusive, two recent studies independently found that Gasdermin D is a pro-pyroptotic substrate of caspase-1 or -11 whose cleavage is sufficient to drive pyroptosis as a response to inflammasome activation (Kayagaki et al., 2015; Shi et al., 2015). The morphological features of pyroptosis include loss of plasma membrane integrity, due to which the cell permeable to small molecules, water and ions. This influx of molecules causes the cell to swell, rupturing the membrane and leading to cell lysis (Jorgensen and Miao, 2015). Mitochondria of pyroptotic cells also lose membrane integrity and release their contents (Man and Kanneganti, 2015b).

Speck assembly induces pyroptosis in macrophages in a caspase-1-dependent manner within seconds after speck formation (Fernandes-Alnemri et al., 2007). Caspase-1 can also trigger pyroptosis independently of both ASC and autoproteolytic cleavage of the p20 and p10 subunits of the enzyme. The catalytic activity of the enzyme, though, was shown to be indispensable for pyroptosis and cells expressing a catalytically inactive caspase-1 were resistant to this type of cell death. This suggests that two distinct activation states of caspase-1 are behind IL-1β processing and pyroptotic cell death (Broz et al., 2010a). In the absence of caspase-1, inflammasome stimuli do not lead to pyroptosis and cells instead undergo apoptosis much more slowly (Pierini et al., 2012; Sagulenko et al., 2013). In this case, apoptotic death occurs in an ASC-dependent manner via an unusual heterotypic PYD-DED domain interaction in which caspase-8 DED filaments assemble as an extension to the PYD_{ASC} filaments in the direction of filament growth (Vajjhala et al., 2015). It is possible that the recruitment of

caspase-8 to the ASC speck represents a back up mechanism in case the pathogen manages to somehow obstruct pyroptosis (Boucher et al., 2014).

3.3 Pyroptosis as a defense mechanism

The existence of pyroptosis was first suggested by experiments in which macrophages infected with *Shigella flexneri* underwent a form of death similar to apoptosis (Zychlinsky et al., 1992), which was later also observed upon infection with *Salmonella enterica* serovar Typhimurium (*S*. Typhimurium) (Boucher et al., 2014). Subsequent studies showing mice deficient in the inflammatory caspases that trigger pyroptosis are susceptible to intracellular bacterial pathogens that induce inflammasome formation, indicated that pyroptosis is an effective mechanism to deal with intracellular pathogens (Jorgensen and Miao, 2015), even in the absence of IL-1β (Miao et al., 2010). How does a pyroptotic cell contribute to the host response against pathogens? First, because the intracellular contents are released, intracellular pathogens are deprived of an environment in which they can survive and reproduce, exposing them to extracellular defenses and making them susceptible to engulfment by a secondary phagocyte, like a neutrophil (Fig. I.3.1). The observation that neutrophils activate caspase-1 and release IL-1β, but do not undergo concomitant pyroptosis upon various inflammatory stimuli supports this notion (Chen et al., 2014). Second, the released intracellular contents contain DAMPs such as ATP and IL-1α that activate an inflammatory response in the surrounding tissue. Lastly, other intracellular components released during pyroptotic cell death have direct anti-microbial activity (Stephenson et al., 2015). *In vivo*, it is likely that inflammasome-dependent cell death and cytokine production work together to promote microbial clearance, although the individual contributions of each probably differ depending on the pathogen (Aachoui et al., 2013).

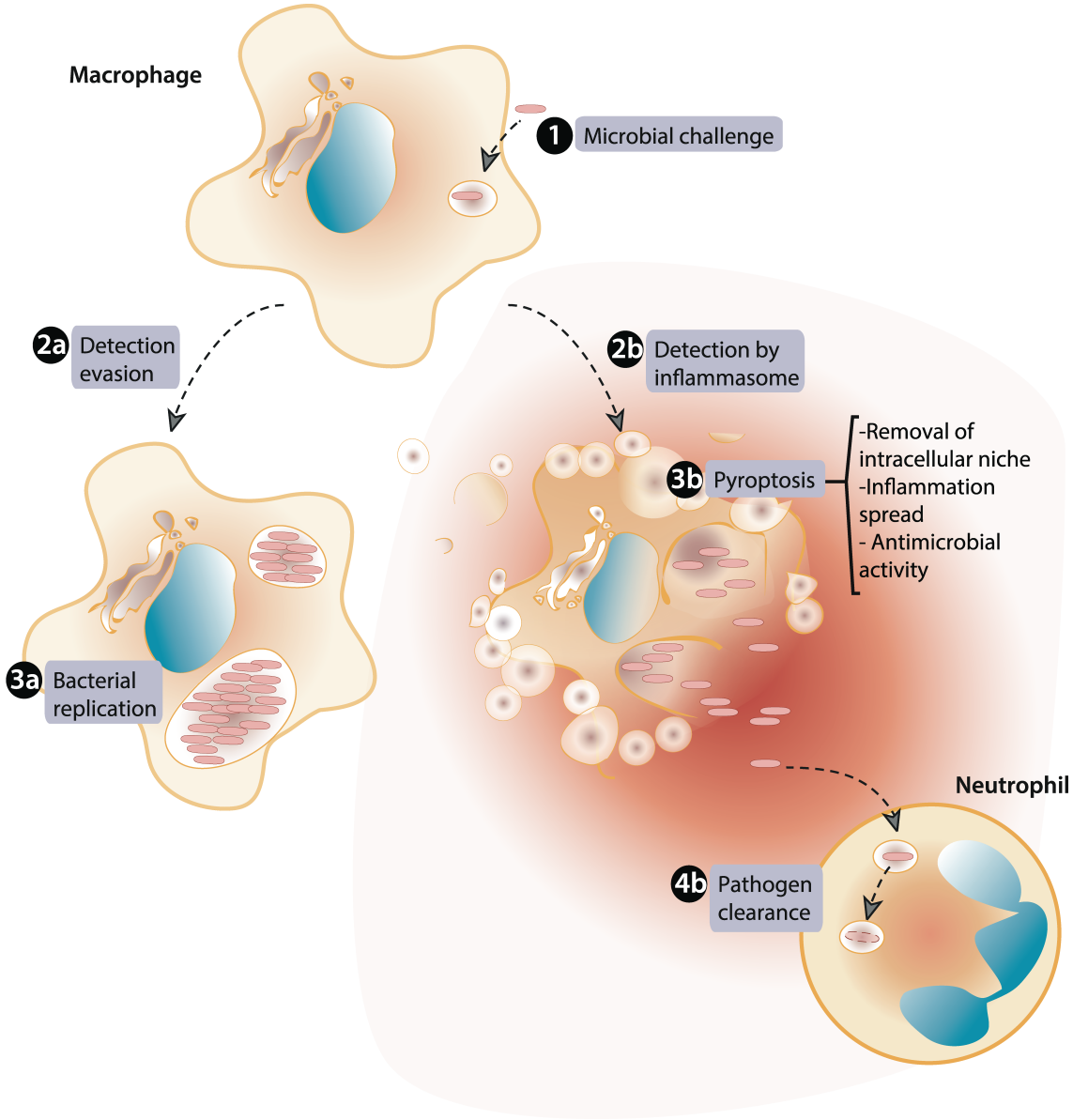

Figure I.3.1. Pyroptosis can aid in the clearance of intracellular pathogens.
After a pathogenic microbe is engulfed by a macrophage (1), if it evades detection (2a) it can replicate inside the host cell (3a), eventually leading to its release in greater numbers. Instead, pathogen recognition by the inflammasome (2b) will trigger a pyroptotic response and the pathogen will be released to the extracellular space (3b). Released bacteria lose their replicative niche and are exposed to the additional clearance mechanisms including clearance by neutrophils, which do not undergo pyroptotic cell death (4b). Figure modified from Miao et al. (2011) and Broderick et al. (2015).

3.4 Extracellular specks spread inflammation

It was recently reported that ASC specks persist can *in vivo* during *Pseudomonas aeruginosa* infection, in chronic lung inflammation and in serum of patients with active CAPS (Baroja-Mazo et al., 2014; Franklin et al., 2014). Furthermore, antibodies against ASC were found in patients with autoimmune

diseases (Franklin et al., 2014). Rather than this being a consequence of an active secretion mechanism, inflammasomes (or specks) are released passively together with the rest of the intracellular contents during pyroptosis (Broderick and Hoffman, 2014)

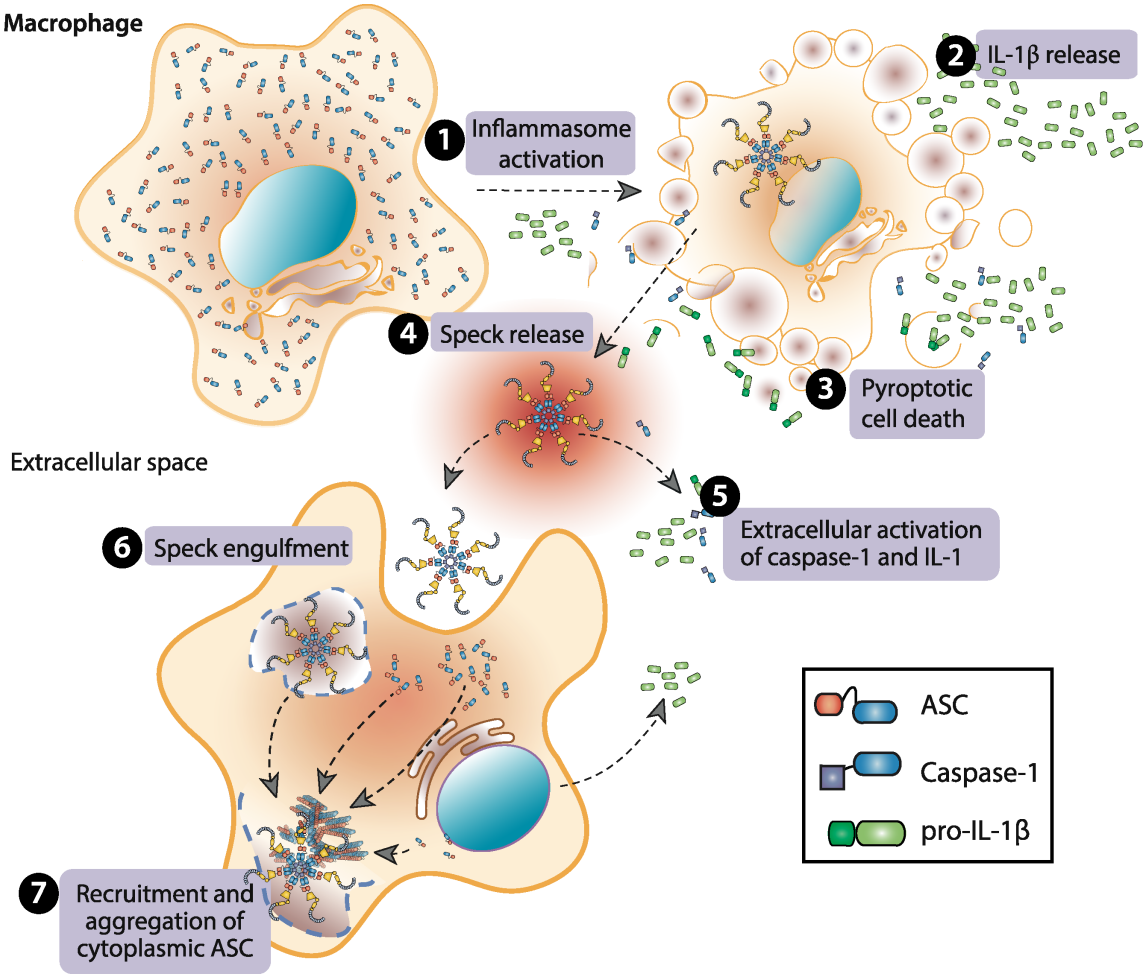

Figure I.3.2. Specks released after pyroptosis can spread inflammation.
Upon activation of the inflammasome (1), specks recruit all cytoplasmic ASC to a single speck, which leads to IL-1β release (2) and can also cause pyroptotic cell death (3). After pyroptosis, the cell's intracellular contents, including unprocessed caspase-1 and IL-1β, are released together with the ASC speck (4), which continues to activate the former two (5). Extracellular specks can be ingested by phagocytes (6) and, in the long term, cause phagolysosomal damage that leads to their release into the cytoplasm and the recruitment of the host cell's soluble ASC (7). Figure modified from Broderick et al. (2015)

Specks in the extracellular environment continue to activate pro-caspase-1 and pro-IL-1β. The engulfment of these extracellular specks by macrophages

results in inflammasome activation in the recipient cell (Franklin et al., 2014). This suggests that the effects of initial inflammasome activation might have long-lasting effects due to resistance to extracellular protease-mediated degradation (Broderick and Hoffman, 2014), moreover, it indicates that inflammasomes can function as endogenous danger signal that could be accumulated in sites of tissue damage, leading to persistent inflammation (Broderick et al., 2015).

3.5 Inflammasome activation in non-myeloid cells

Most progress in understanding inflammasome function has been made in cells of the innate immune system. However, cell types other than immune cells can also activate the inflammasome, release IL-1β and undergo pyroptotic cell death. The need for an innate immune surveillance in these cells becomes evident when considering that certain cell types, like epithelial cells, are located at interfaces between the body and the environment and are therefore directly exposed to threats (Yazdi et al., 2010). Keratinocytes activate the inflammasome as a response to UVB irradiation (Feldmeyer et al., 2007), contact hypersensitivity (eczema) (Watanabe et al., 2007), and *Human papillomavirus* (HPV) infection (Reinholz et al., 2013). Infected intestinal epithelial cells are extruded from the gut epithelium likely as a mechanism to prevent enteric pathogens from crossing the epithelial barrier. Although caspase-1 activation is involved in this process, the fact that intestinal epithelial cells dislodge from the epithelium without losing plasma membrane integrity means the process might not be entirely analogous to pyroptosis in macrophages (Sellin et al., 2015). Other epithelial tissues that have been reported to secrete IL-1β in response to inflammatory stimuli include airway epithelial cells lining the respiratory tract, glomerular and tubular epithelial cells in the kidney and genital epithelia such as cervical and prostate epithelial cells (Peeters et al., 2015). Hematopoietic progenitor cells also activate the inflammasome and pyroptosis in response to stress induced by chemotherapy or viral infection, a response that led to cytopenia and immunosuppression (Masters et al., 2012).

4 Zebrafish as a model to study the inflammasome

Most knowledge of the inflammasome comes from studies in human cell lines and mice, and knowledge of the role the inflammasome in innate immunity of other vertebrate species is limited. However, the increasing number of available genome sequences has greatly increased the information on the repertoire of innate immune genes in many organisms (Bryant and Monie, 2012). Fish are a link to early vertebrate evolution and important models in comparative immunology, whose study improve our understanding of fish immunology as well as the evolution of the immune system (Zhu et al., 2013). In particular, zebrafish (*Danio rerio*) has emerged as a genetically and optically accessible *in vivo* model organism for diseases and drug screening (Renshaw and Trede, 2012; Torraca et al., 2014; van der Vaart et al., 2012), where evolutionary and functional aspects of the inflammasome can be studied (Angosto and Mulero, 2014).

4.1 The NLRs family is expanded in teleost fish

The number of NLRs encoded in the genomes of animal species varies considerably. There are around 22 NLRs in humans and 34 in mouse (Bryant and Monie, 2012; Ting et al., 2008), whereas the genome of some early diverging metazoans like the sea urchin, contain a repertoire of over 200 NLRs (Rast et al., 2006). In teleost fish, NLRs seems to have undergone an expansion into several hundreds of predicted genes. They posses possible orthologues for both the NLRC and NLRP subfamilies, but also have an additional unique group of NLRs (Bryant and Monie, 2012). The N-terminus of the NLR teleost proteins contains a range of effector domains (including PYD domains, but also novel NLR effector domains like B30.2 and fish-specific domains), suggesting that the downstream signaling network is diverse (Bryant and Monie, 2012). Moreover, NLR sequences identified in fish species group mostly on species-specific branches indicating further species-specific expansions of NLR subfamilies (Stein et al., 2007). The zebrafish genome contains over 350 NLRs, however, it lacks clear

orthologues of some of the best characterized inflammasome-forming NLRs in mammals, like NLRP1, NLRP3 and NLRC4 (Hansen et al., 2011; Howe et al., 2016; Stein et al., 2007). Overall, the variation observed in range and numbers of NLRs across species underscores that these sensor genes of the innate immune system are under strong evolutionary pressure. The divergence may be reflective of the types of threats commonly faced by each species (Bryant and Monie, 2012).

4.2 ASC might have a functional orthologue in zebrafish

Teleost fish contain *asc* genes that in some cases seem to correspond to functional orthologues (Hansen et al., 2011). The *asc* gene has been cloned and characterized to some extent in the Japanese flounder (*Paralichthys olivaceus*) (Li et al., 2016), the mandarin fish (*Siniperca chuatsi*) (Sun et al., 2008), and in zebrafish (Masumoto et al., 2003). In the last two, ASC fused to a fluorescent protein transiently expressed in mammalian cells in culture appeared to form specks (Masumoto et al., 2003; Sun et al., 2008). Masumoto et al. (2003) also identified a zebrafish homologue of *caspase-1* (*caspy*, currently named *caspa*). Although Caspa has an N-terminal PYD domain instead of a CARD, when co-transfected with zebrafish ASC in mammalian cells the two proteins colocalize in a single speck. Furthermore, the expression of Caspa induces cell death in mammalian cells, which is enhanced by enforced zebrafish ASC oligomerization (Fig. I.4.1).

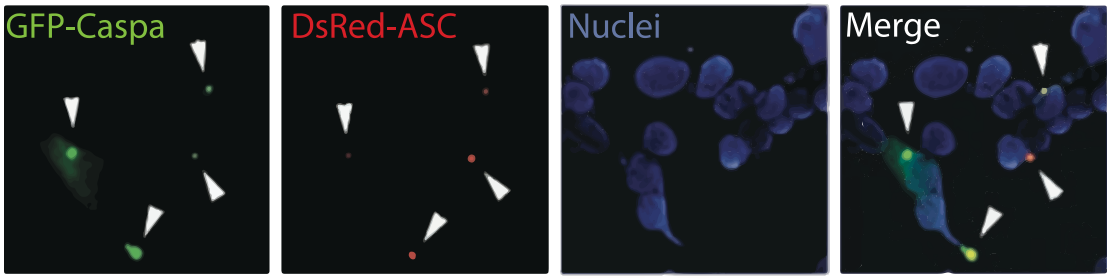

Figure I.4.1. The zebrafish ASC orthologue forms specks in mammalian cells.
Constructs for expression of zebrafish ASC fused to DsRed and Caspa fused to GFP were transfected in COS-7 cells that were then fixed after 24h and stained with DAPI. DsRed-ASC and GFP-Caspa colocalize in a single speck. Figure from Masumoto et al. (2003).

In zebrafish larvae, *asc* and *caspa* are expressed in pharyngeal arches. Knockdown of *caspa* is associated with a defective formation of the cartilaginous

pharyngeal skeleton (Masumoto et al., 2003). Overall, the study suggested that the interaction between these two inflammasome components is conserved in zebrafish. The role of caspase-1 homologues in fish in IL-1 maturation is discussed below. A summary of the number of inflammasome components identified in humans, mouse and zebrafish can be found in Table I.4.1.

Table I.4.1. Number and domain structure of inflammasome components in human, mouse and zebrafish.
Summary of *nlr*, *asc* and *caspase-1* homologous genes in human, mouse and zebrafish including number of genes and domain composition. NLR subfamily nomenclature is based on Ting et al. (2008) although some domain compositions were simplified. The single member of the NLRX1 family was excluded. Its N-terminal domain shows no strong homology to that of any other NLR subfamily. In the case of zebrafish only genes annotated in ENSEMBL are included except for the estimation of total *nlr* gene number, which is based on Howe et al. (2016). Abbreviations: AD, acid domain; BIR, baculovirus inhibitor of apoptosis protein repeat; NOD, nucleotide oligomerization domain.

Organism\ Gene	***nlr***	***asc***	***caspase-1***
Human (*Homo sapiens*)	22 NLRA: AD-NOD-LRR (1) NLRB: BIR-NOD-LRR (1) NLRC: CARD-NOD-LRR (5) NLRP: PYD-NOD-LRR (14)	1 PYD-CARD	1 CARD-Casp
Mouse (*Mus musculus*)	34	1 PYD-CARD	1 CARD-Casp
Zebrafish (*Danio rerio*)	>350	1 PYD-CARD	2 Caspa:PYD-Casp Caspb:PYD-Casp

4.3 Inflammasome signaling in fish

There is some evidence that inflammasome activators lead to an increase in caspase-1-like activity in fish. Caspase-1 is activated in sea bream macrophage cultures in response to bacterial infection and a triggered cell death that was abolished by treatment with a pan-caspase inhibitor (Angosto et al., 2012). In zebrafish leukocytes, caspase-1-like activity was detected after *F. noatunensis* infection and treatment with caspase-1 inhibitor prevented the cleavage and release of IL-1 (Vojtech et al., 2012), whereas treatment with a caspase inhibitor

diminished IL-1 activation in response to UVB irradiation and sterile injury (Banerjee and Leptin, 2014; Ogryzko et al., 2014b). Macrophages were also seen to activate *caspa* expression in response to viral infection (Varela et al., 2014) and *caspa* knockdown partly rescued the mortality of a *L. monocytogenes* infection in zebrafish larvae (Vincent et al., 2015). Overall, although specific sensor molecules have not been identified, the activation of caspase-1 as an inflammatory response seems to be conserved in fish.

5 Interleukin-1 signaling

The IL-1 family of cytokines in human includes 11 genes, all of which are major mediators of innate immune reactions and probably arose from the duplication of a common ancestral gene (Sims and Smith, 2010). Two of its members, Interleukin-1α and β (IL-1α and IL-1β) were the first interleukins identified. Because they are sensed by virtually all cell types, these cytokines are central mediators of innate immunity and inflammation and are involved autoinflammatory, infectious and degenerative diseases (Garlanda et al., 2013b; Van de Veerdonk and Netea, 2013).

5.1 IL-1α: a second proinflammatory member of the IL-1 family

Il1α and *Il1β* are encoded by two genes located adjacent to one another in the human genome. Although they share only 26% amino acid sequence, IL-1α and IL-1β have similar biological properties, mainly because they signal through the same IL-1 receptor (IL-1R) cell surface receptor complex, and elicit the same downstream signaling events. However, despite engaging the same receptor and signaling pathways, these cytokines are not redundant, their differences mostly due to varying localization, expression and release mechanisms in different cell types (Afonina et al., 2015). Both IL-1α and IL-1β are synthesized as 31kDa precursor pro-proteins, with cleavable N-terminal pro-domains of approximately 100 amino acid residues, and lack a classical signal peptide (Sims and Smith, 2010). IL-1α expression is widespread, being constitutively present in all epithelial cells, including the entire gastrointestinal tract, thymic epithelium,

lung, liver, kidney, keratinocytes, endothelial cells and astrocytes. In contrast, IL-1β is produced in hematopoietic cells like blood monocytes, tissue macrophages, skin dendritic cells and microglia. It is strongly inducible and expressed mostly in response to inflammatory stimuli such as TLR activation, activated complement components and other cytokines (including IL-1 itself) (Garlanda et al., 2013a; Joosten et al., 2013).

5.2 The different processing of IL-1α and IL-1β

Since IL-1β cannot bind to its receptor in its immature form, the cleavage of pro-IL-1β downstream of inflammasome assembly determines the activity of the molecule. On the other hand, IL-1α is active in its unprocessed form, but cleavage strongly enhances its binding receptor affinity (Afonina et al., 2015). After caspase-1 cleavage into a 17kDa processed form, IL-1β is selectively released from cells via an active secretion mechanism for which more than one pathway is available, including exocytosis by secretory lysozymes, microvesicle shedding from the plasma membrane or release of multivesicular bodies containing exosomes (Joosten et al., 2013). The mechanism varies depending on cell type, culture conditions and stimulus applied (Carta et al., 2013). In the case of IL-1α, because pro-IL-1α is constitutively present in cells, it can act as an alarm signal as it is passively released during a lytic cell death (Carta et al., 2013; Kim et al., 2013). Pyroptosis leads to a strong inflammatory response and the infiltration of immune cells because of the release of both, IL-1β and pro-IL-1α (Aachoui et al., 2013; Stephenson et al., 2015). Pro-IL-1α is directly cleaved into its 18kDa mature form in an inflammasome dependent or independent manner by calpains, a family of Ca^{2+}-dependent proteases activated downstream of the inflammasome (Rider et al., 2013). Strong inducers of Ca^{2+} influx, like the Ca^{2+} ionophore ionomycin, lead to inflammasome-independent cleavage and release of IL-1α, whereas NLRP3 inflammasome activators induced cleavage and release of both IL-1α and IL-1β in an inflammasome-dependent manner in bone marrow-derived cells (Fig. I.5.1). Both interleukins were actively released with similar kinetics prior to cell death (Groß et al., 2012).

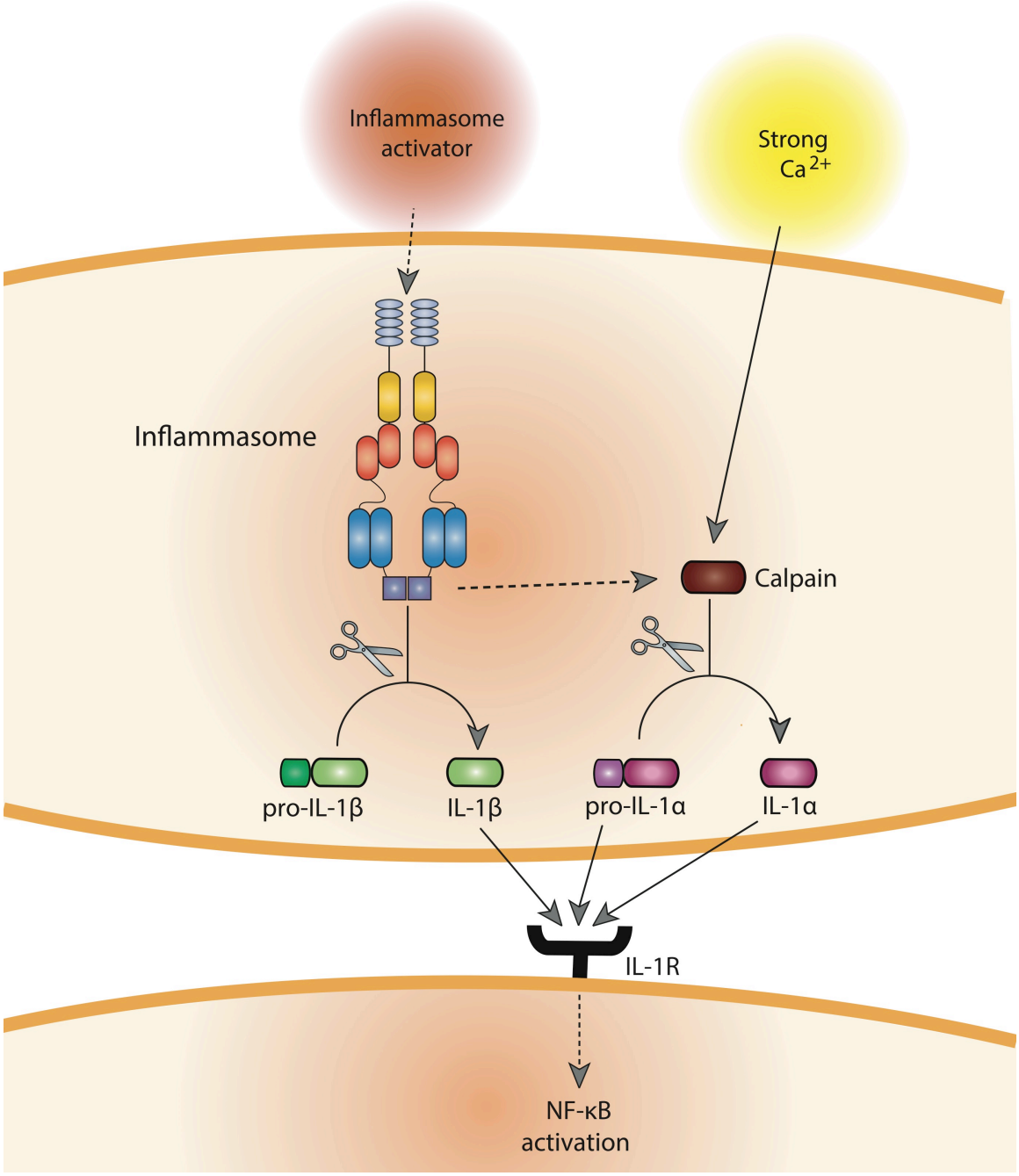

Figure I.5.1. IL-1α can be secreted by inflammasome-dependent or independent mechanisms. IL-1β cleavage takes place downstream of inflammasome activation and is actively released in its mature form. Inflammasome-dependent IL-1α cleavage takes place when calpain proteases responsible for it become activated as a consequence of inflammasome signaling. Ca^{2+} influx activates calpains and leads to inflammasome-independent maturation and secretion of IL-1α. Also depicted is the binding to IL-1 receptor (IL-1R). IL-1α, in its processed and unprocessed form can act as ligand, whereas only the mature IL-1β can bind the receptor. Binding to the IL-1R leads to the activation of NF-κB signaling. Figure modified from Groß et al. (2012).

Binding of both IL-1α and IL-1β to the ubiquitously expressed receptor, type I IL-1 receptor (IL-1R), results in activation of the NF-κB pathway, which drives expression of proinflammatory cytokine genes, including the *il1* genes

themselves. Therefore, IL-1 signaling serves as a positive feedback loop that amplifies the inflammatory response (Joosten et al., 2013). The different properties of IL-1α and IL-1β are listed in Table I.5.1.

Table I.5.1. Functional characteristics of mammalian IL-1α and IL-1β.

Property	**IL-1β**	**IL-1α**
Sources	Blood monocytes, tissue macrophages, skin DCs and microglia	Epithelial cells, primary cells, endothelial cells and astrocytes
Expression	Inducible	Constitutive
Precursor	Inactive	Active
Mature form	Active	Active
Cleaved by	Caspase-1	Calpain-like proteases
Signal peptide	Absent	Absent
Receptor	IL-1R	IL-1R

5.3 IL-1 conservation in teleost fish

Throughout vertebrate evolution, there have been several expansions of the IL-1 family members. One of them is thought to have resulted in the divergence of *Il1α* and *Il1β* (Ogryzko et al., 2014b). Although an *il1* gene has been cloned from many species of teleost fish, including salmonids (salmon and trout), cyprinids (carp and zebrafish), perciforms (sea bream, sea bass, nile tilapia) and tetraodontiform (pufferfish) (Secombes et al., 2011), there is no evidence that there are any orthologues in fish corresponding to this expansion of the *il1* locus, which took place roughly at the same time as mammals emerged (Ogryzko et al., 2014b). Some species of teleost fish contain more than one *il1* gene, in some cases due to genome duplication events in particular lineages and in others due to local gene duplications (Husain et al., 2012). Although *il1* genes identified in fish have been designated specifically as *il1β* orthologues, the difference between IL-1 protein sequences in fish and tetrapods is quite high, with a maximum of 30%

shared identity and different exon organization. Therefore, it is difficult to determine which mammalian *il1* gene teleost IL-1 are closest to (Ogryzko et al., 2014b). Furthermore, the caspase-1 cleavage site located after an aspartic acid residue in exon 5 in mammalian pro-IL-1β is absent in fish IL-1 (Bird et al., 2002).

In spite of the differences, IL-1 seems to have a similar role in teleost innate immunity as its mammalian homologues. In zebrafish larvae *il1* expression is induced after UVB irradiation (Banerjee and Leptin, 2014) and in leukocytes following sterile injury (Ogryzko et al., 2014a). Furthermore, a zebrafish transgenic *il1:GFP* reporter showed both constitutive expression in epithelial cells and a strong induction of *il1* following bacterial infection. This increase in IL-1 signaling was required for recruitment of neutrophils (Nguyen-Chi et al., 2014). The *il1* gene is also strongly inducible in trout spleen of infected adult trout (Secombes et al., 2011), and in head kidney macrophages of after phytohaemagglutinin (PHA) treatment (Husain et al., 2012), indicating the cytokine's role as a prominent proinflammatory molecule is conserved.

5.4 Cleavage of fish IL-1

The literature regarding cleavage of IL-1β in fish is inconsistent, with studies in different species coming to different conclusions. Sea bream macrophages infected *ex vivo* with *S*. Typhimurium, released an 18 kDa mature form of this species' pro-IL-1β, which was unaffected by treatment with Caspase-1 inhibitors. However, the inhibitors did prevent sea bream macrophage cell death after *S*. Typhimurium infection. Therefore, although caspase-1 is involved in the inflammatory response to infection in this model, it is not required for the activation of pro-IL-1β (Angosto et al., 2012). In zebrafish, primary leukocytes were also shown to secrete a processed form of IL-1β in a partly caspase inhibitor-sensitive manner after infection with *Francisella noatunensis*. Coexpression of Caspa and a second zebrafish homologue of caspase-1, Caspb, with zebrafish IL-1β in HEK293 cells resulted in cleavage of the latter in two aspartic acid sites, which were validated by mutation analysis (Vojtech et al., 2012). Direct cleavage of IL-1 by caspase-1 was also shown *in vitro* for sea bass, where caspase-1 was able to cleave IL-1β after it underwent autoproteolytic

cleavage during incubation of the two recombinant proteins (Reis et al., 2012), although the result could be an artifact of the *in vitro* system used for the experiments (Ogryzko et al., 2014b). Some evidence for cleavage had also been obtained for carp (Mathew et al., 2002) and trout (Hong et al., 2004) by using antibodies, although in both cases the protease behind the cleavage was not investigated. A summary of these studies can be found in Table I.5.2.

A general conclusion regarding the conservation of IL-1 cleavage by caspase-1 in fish cannot be reached due the lack of rigorous *in vivo* analyses. However, a consistent observation across fish species is that the cytokine is inducible and proinflammatory, which suggests that IL-1's role in inflammation is conserved. Therefore, it is possible that the association between caspase-1 activation and IL-1 developed later in evolution, as a function coopted to act downstream of inflammasomes (Denes et al., 2012; Ogryzko et al., 2014b)

Table I.5.2. Summary of evidence for IL-1 cleavage in teleost fish.

Organism	**Finding**	**Reference**
Carp (*Cyprinus carpio*, Cypriniformes)	Processed IL-1 is detected in supernatants of carp leukocytes after stimulation with PHA.	(Mathew et al., 2002)
Rainbow trout (*Oncorhynchus mykiss*, Salmoniformes)	Processed IL-1 is detected in supernatants of a trout macrophage cell line, independently of LPS stimulation.	(Hong et al., 2004)
Sea bream (*Sparus aurata*, Perciformes)	Isolated sea bream leukocytes release mature IL-1 in response to *S.* Typhimurium but not in response to inflammasome activators.	(Angosto et al., 2012)
	Pharmacological inhibition of sea bream caspase-1 did not prevent IL-1 processing, but prevented cell death.	
	Ectopically expressed caspase-1 did not cleave IL-1.	
Sea bass (*Dicentrarchus labrax*, Perciformes)	Sea bass IL-1 is cleaved by caspase-1 *in vitro* after 4h of incubation of the two recombinant proteins. Sea bass caspase-1 also cleaves recombinant human pro-IL-1 in the same experimental setup.	(Reis et al., 2012)
Zebrafish (*Danio rerio*, Cypriniformes)	Processed IL-1 is detected in supernatants of isolated zebrafish leukocytes in a caspase-dependent manner following *Francisella noatunensis* injection. IL-1 aspartic acid cleavage sites following coexpression with Caspa and Caspb in HEK293 cells were identified and confirmed via mutational analysis.	(Vojtech et al., 2012)

6 Nuclear factor-κB (NF-κB) signaling

The NF-κB transcription factor signaling cascade has long been considered a prototypical proinflammatory pathway because it is activated by proinflammatory cytokines (IL-1 included) and downstream of PRRs (Lawrence, 2009). However, NF-κB is also involved in the regulation of many other cellular and developmental functions including growth, differentiation and apoptosis through the activation of hundreds of genes (Gilmore and Wolenski, 2012). NF-κB activity must therefore be tightly regulated, and its inappropriate activation is linked to autoimmunity, chronic inflammation and cancer (Hoesel and Schmid, 2013; Rinkenbaugh and Baldwin, 2016).

6.1 The core NF-κB pathway

The NF-κB transcription factor is a dimer composed of two members of the ubiquitously expressed NF-κB/Rel protein family, all of which share a highly conserved Rel homology region (RHR), a DNA-binding domain that enables these proteins to homo and heterodimerize. In unstimulated cells, NF-κB, in one of its dimeric forms, is sequestered in the cytoplasm through an interaction with the IκB inhibitory protein, whose binding of NF-κB masks the latter's nuclear localization signal (NLS). As long as NF-κB remains in the cytoplasm it cannot activate its targets. Upon activation by a physiological signal, the IκB kinase (IKK) phosphorylates IκB, which targets IκB for proteasomal degradation. The released NF-κB translocates to the nucleus, and activates its targets by direct DNA binding to its specific sites. As is the case for dimeric NF-κB transcription factor, multiple genes can take the role of IκB and IKK (Napetschnig and Wu, 2013).

6.2 Conservation of NF-κB pathway

The core NF-κB pathway is conserved in all vertebrates. In mammals there are five NF-κB transcription factors, seven IκB-like inhibitors, and four IKKs whereas zebrafish contains five NF-κB family members, five IκB-like inhibitors, and four IKKs (Gilmore and Wolenski, 2012), some of which have been cloned and functionally characterized (Correa et al., 2005; 2004). Aside from its conserved role in innate immune signaling (van der Vaart et al., 2012) roles for NF-κB in zebrafish have been identified in notochord development (Correa et al., 2004), cell cycle coordination during gastrulation (Liu et al., 2009), epidermal differentiation (Fukazawa et al., 2010), gonad formation and sex determination (Pradhan et al., 2012).

6.3 NF-κB binding sites determine downstream targets

One major source of complexity in the NF-κB pathway are κB sites, 9 to 11 bp long DNA binding sites to which the NF-κB dimers bind. Although a κB consensus sequence has been found, it is highly degenerate and several κB sites that strongly deviate from this consensus are still able to attract certain NF-κB dimer combinations with high affinity. However, there are no clear correlations between specific dimer combinations and κB sequences in target genes and while some genes require specific combinations of NF-κB proteins for activation, others are able to recruit all NF-κB proteins without apparent specificity. An additional source of complexity arises from the fact that dimers can be exchanged at a given promoter or enhancer site over time (Natoli, 2006). Recently, Siggers et al. (2012) carried out a comprehensive analysis of DNA binding by NF-κB dimers from mouse and human to discover these dimer-specific differences and identified lower affinity, new non-traditional sites as well as high affinity ones. Furthermore, the authors provided a database and search tool to analyze potential κB sites and to predict the affinity of specific dimer combinations (Siggers et al., 2012).

6.4 Visualizing and quantifying NF-κB activity via reporters

Given the importance of the NF-κB pathway, there has been great interest

in establishing reporters that allow the tracking of activation via imaging of *in vitro* and *in vivo* systems. This has been done by placing a minimal promoter downstream of one or several copies of κB sequences and cloning a reporter gene for visualization (fluorescent protein) of activity or for quantification (luciferase gene) (Badr et al., 2009; Matsuda et al., 2007).

Kanther et al. (2011) generated a transgenic *nfkb:EGFP* zebrafish reporter line containing a single NF-κB binding site. The reporter enabled the authors to visualize endogenous patterns of NF-κB activity by tracking GFP expression during zebrafish larval development. The authors also analyzed the activation of NF-κB in the digestive tract as a response to colonization by commensal microbiota (Kanther et al., 2011). That same reporter line was later used to visualize the NF-κB activity as an indicator of inflammatory response to wounding (Ogryzko et al., 2014a) and high-cholesterol diet in zebrafish larvae (Progatzky et al., 2014). A second transgenic zebrafish reporter line was developed by Banerjee et al. (2014) using three copies of a consensus NF-κB binding sequence located upstream of the Kal4:UAS system driving *EGFP* expression. The line was used to track the inflammatory response of zebrafish larvae to UVB irradiation live (Banerjee and Leptin, 2014). These studies underscore the potential of the zebrafish as a model in which inflammatory responses, both constitutive and inducible, can be visualized live.

II. Motivation and aims

In spite of the significant contribution cell culture studies have made to the understanding of the molecular processes underlying inflammation, results are highly dependent on culturing conditions as well as cell type. Furthermore, because most studies focus on cells of the immune system, very little is known of the capabilities of other cells to respond to inflammatory stimuli. Therefore, studies using whole organisms are necessary to address the dynamics of signaling and activation *in vivo*, which have yet to be studied.

Teleost fish are becoming a widely used model for studying the innate immune system, especially because of the ease with which live imaging can be done. This enables us to visualize the response to inflammatory stimuli in multiple cell types simultaneously and to integrate the role of cells not traditionally considered part of the immune system within a global response towards an insult. Furthermore, through the use of teleost fish we learn about the degree of conservation of inflammatory molecules and signaling mechanisms across different vertebrate lineages, allowing us to uncover how immune response have been shaped throughout vertebrate evolution.

In the present study we chose to take advantage of two teleost model systems to address aspects of innate immune signaling, mostly surrounding inflammasome signaling. The specific aims were the following:

I) Adapt the zebrafish (*Danio rerio*) model for the study of dynamics of the inflammasome by focusing on the visualization of adaptor molecule ASC and the downstream effects of its activation.

II) Use the medaka model (*Oryzias latipes*) to study the *in vivo* activation of the inflammatory cytokine Interleukin-1.

III) Generate a qualitative and quantitative zebrafish *in vivo* reporter *nfκB*, suitable for high throughput studies of inflammatory activation.

III. Results

7 ASC

7.1 Analysis of *asc* expression

We first carried out a genetic characterization of *asc* by studying the expression of the gene and protein in several stages during embryo development.

7.1.1 *asc* is expressed from early stages of development in epithelial tissues

To find out when *asc* expression begins during zebrafish development, we performed Reverse Transcription PCR (RT-PCR) on cDNA obtained from mRNA extracted at several stages: morula, blastula, and 1, 2, 3 and 8dpf, as well as the two adult hematopoietic tissues, head kidney and spleen (Fig. III.1.1A). Our results showed that the expression of *asc* starts early during embryo development and is still present at 8dpf and that adult hematopoietic tissues also express *asc*. To determine which embryonic tissues expressed the *asc* we carried out *in situ* hybridization (*is*h). It had been reported that in 2dpf larvae, *asc* is expressed most strongly in the pharyngeal arches, but also slightly in the epidermis and mouth (Masumoto et al., 2003). We assessed the expression pattern in the whole larva at a slightly older stage, 3dpf (Fig. III.1.1B). We found that, although expression is strongest in the area around the pharyngeal arches and gills, *asc* is also expressed in the entire epidermis. We used a sense probe as a negative control and observed no background staining (Fig. III.1.1C). To determine whether the observed expression is limited to the epidermis or extends into the underlying tissues we performed sections on the plastic-embedded *is*h samples at different angles (marked by colored lines in Fig. III.1.1D). Different sections allowed us to determine that the expression is limited to the external epidermal layers surrounding the entire body (Fig. III.1.1E, F and G) including that of the lateral fins (Fig.

III.1.1G') and specific organs exposed to the surface like gills (Fig. III.1.1I). We also observed that expression is absent from the muscles (Fig. III.1.1E and 1.1E'). The expression of *asc* is also present in the epithelium lining the mouth opening (Fig. III.1.1H), and very likely throughout the whole intestine, since the expression in intestine was found at all sections that included these organs (Fig. III.1.1F, G and G''). We also found that certain cells in the brain expressed *asc* strongly (Fig. III.1.1G and G'''). Overall, at 3dpf zebrafish larvae express *asc* in epithelial tissues at levels strong enough to be detected by *in situ* hybridization.

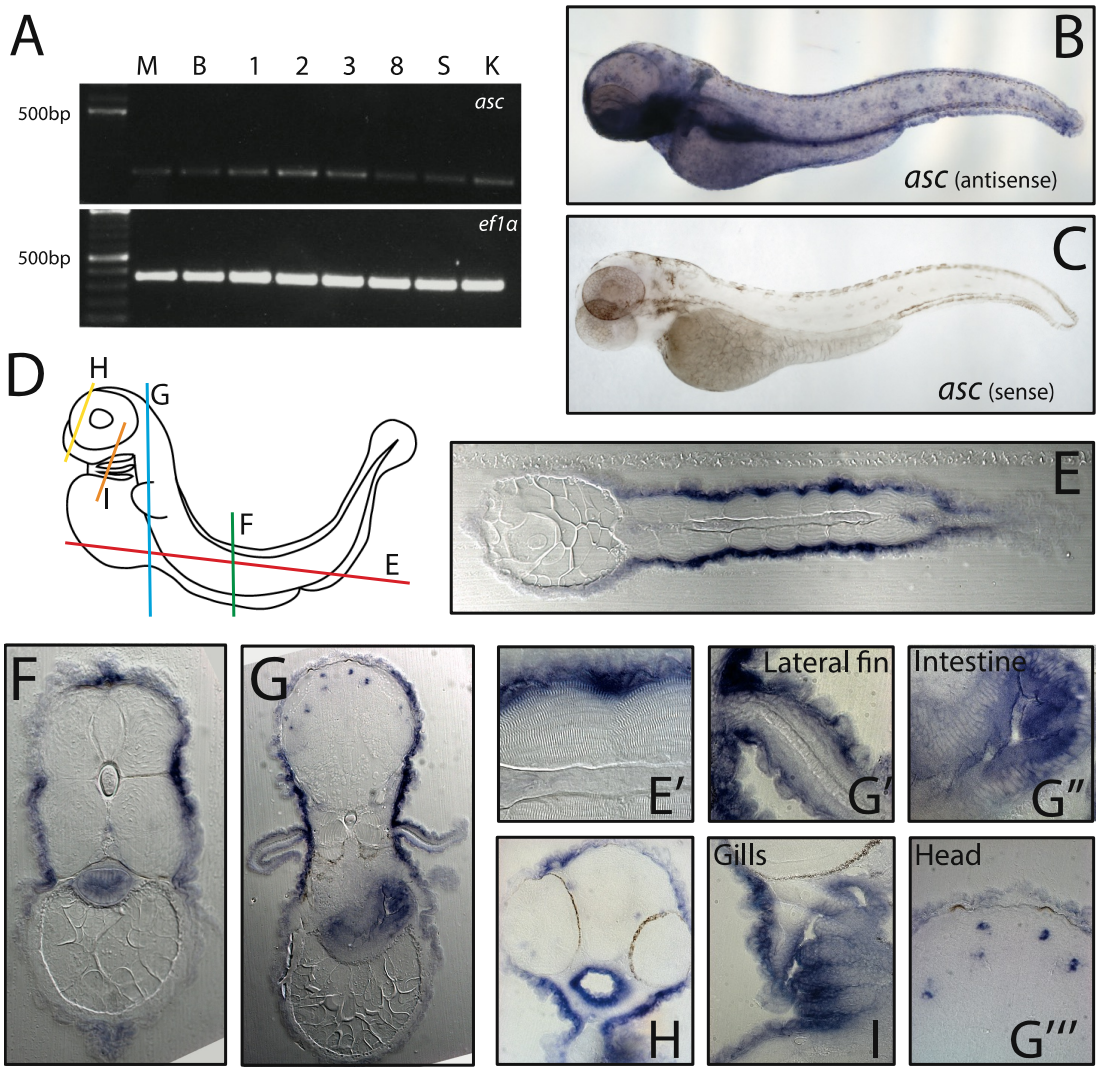

Figure III.1.1. *asc* is expressed in epithelial tissues during early development in zebrafish. RT-PCR of *asc* during early development in Morula (M), Blastula (B), 1 (1dpf), 2 (2dpf), 3 (3dpf), 8 (8dpf) and adult spleen (S) and head kidney (K). *ef1a* is used as housekeeping gene control [A]. *asc in situ* hybridization (*is*h) in 3dpf zebrafish larvae [B] *asc* sense probe is used

as a negative control [C]. Diagram depicting sectioning on plastic-embedded *is*h sample [D]. Lack of expression in muscle cells is shown in longitudinal section and magnification [E, E'] as well as in mid-body cross section [F]. Expression in fins and intestine, as well as expression in brain cells is shown in a more anterior cross section with respective magnifications [G, G',G'',G''']. The two anterior most cross sections show expression in mouth and pharyngeal arches [H, I].

7.1.2 ASC protein is present in epithelial tissues

To determine the localization of ASC during larval stages, we carried out whole-mount immunostainings. Due to lack of a commercial antibody for the protein, we generated an antiASC polyclonal antibody in-house by purifying the full-length recombinant protein and injecting it in rabbits (a more detailed description on antibody production is available in Materials and Methods).

We first tested the antiASC antibody's specificity by performing an immunostaining both with the purified antibody and preimmunization serum collected prior to antigen immunization. The preimmunization serum was used at a 10 fold higher dilution. The immunostaining showed a defined staining with the purified antibody (Fig. III.1.2A), but not with the preimmunization serum (Fig. III.1.2B). Immunostainings on whole larvae showed that the protein is present in the tissues where expression had been detected using *is*h, most prominently, in the epidermis (Fig. III.1.2A') and the gut epithelia (Fig. III.1.2A''). Additional stainings at earlier and later stages showed that expression in the epidermis is present from 1dpf and retained at least until 5dpf (Fig. III.1.2C left and right panels, respectively).

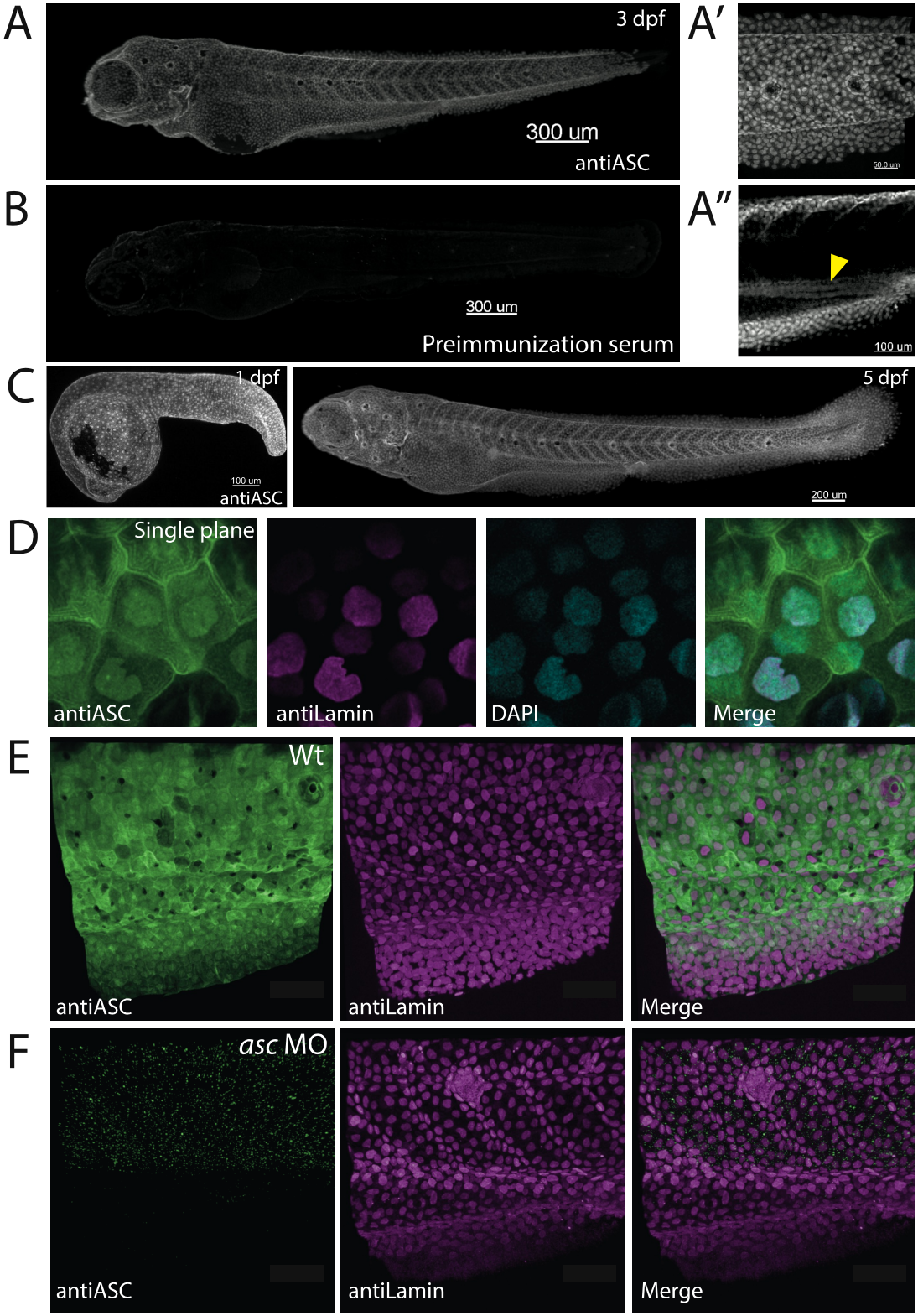

Figure III.1.2. ASC is expressed in larvae and localizes to cytoplasm and nucleus. Immunostaining of 3dpf larva with antiASC [A]. Magnifications highlight staining in epithelial cells [A'] and intestine [yellow arrowhead, A''']. Preimmunization serum is used as primary antibody in negative control [B]. Immunostaining of 1 and 5dpf larvae [C]. Single plane of immunostaining with antiLamin and DAPI as nuclear markers [D]. Immunostainings on wild type (Wt) [E] and *asc* morphant 3dpf larvae [F]. AntiLamin was used as the immunostaining positive control.

From the immunostainings it seemed that ASC was localized not only in the cytoplasm but also in the nuclei of epithelial cells. Costaining with DAPI and a nuclear envelope marker (Lamin) (Fig. III.1.2D) showed that ASC is found in the nuclei of cells. To further test the specificity of the antibody we used an ATG-morpholino to knock down the expression of *asc*. We observed that *asc* morphant larvae did not display any obvious morphological phenotype. We therefore repeated the immunostaining of ASC and the nuclear envelope, as a positive control for the staining, in *asc* morphant and wild type fish (Fig. III.1.2E). The ASC staining was completely absent in the morphants, whereas the nuclear envelope staining was unaffected. This not only confirmed the specificity of the morpholino, but also that of the antibody.

To confirm the identity of the epidermal cells expressing ASC, we performed immunostainings on the transgenic lines *krt4:GFP* and *krt19:tomato-CAAX*. At this stage, zebrafish has only two layers of keratinocytes in the epidermis and only the outermost monolayer, called enveloping layer (EVL), is labeled in the *krt4:GFP* line, whereas the *krt19:tomato-CAAX* labels both the EVL and the monolayer beneath it, composed of basal keratinocytes (Fischer et al., 2014). Immunostainings on 3dpf larvae from the *krt4:GFP* line showed that all cells that expressed GFP were also labeled by antiASC (Fig. III.1.3A, left panels). Furthermore, a cross-section of the lateral fin showed that in addition to the EVL, the second epidermal layer beneath it also expresses ASC (Fig. III.1.3A, right panels). This was confirmed by staining the *krt19:tomato-CAAX* line in which most cells were double positive (Fig. III.1.3B). However, epidermal cells seem to express the protein at variable levels.

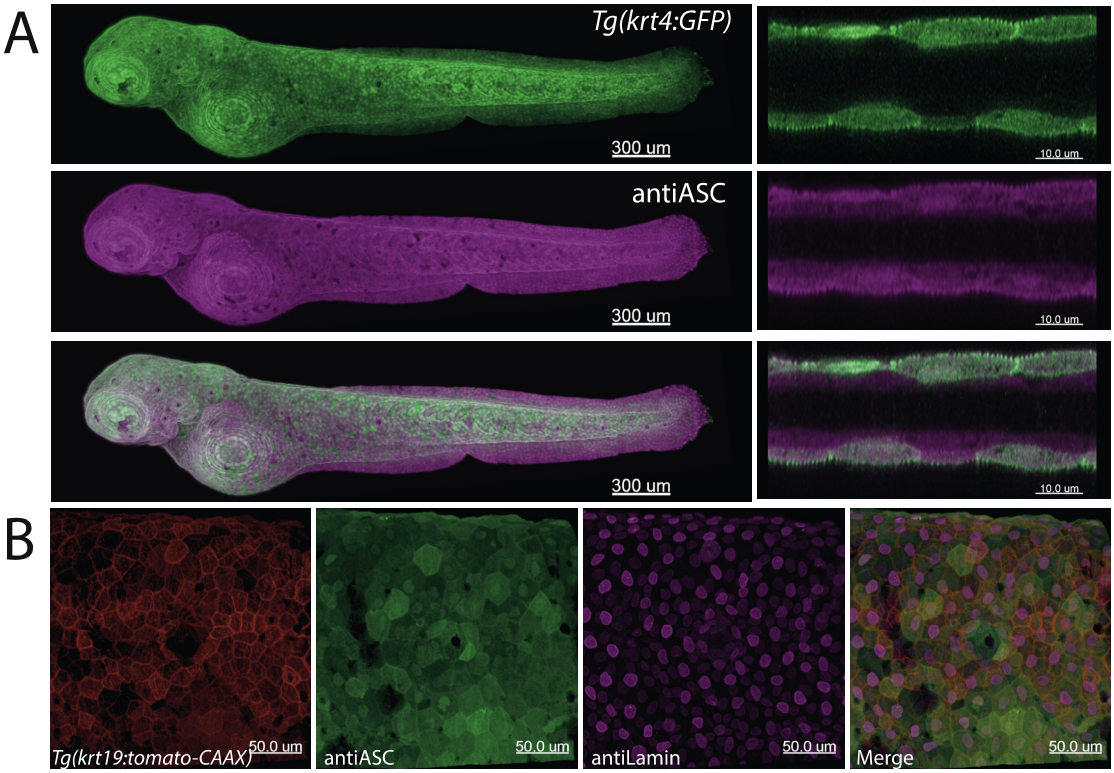

Figure III.1.3. ASC is expressed in epidermal layers.
Immunostaining of *krt4:GFP* transgenic 3dpf larva [A]. Cross sections of lateral fin show GFP expression only in enveloping layer (EVL), and antiASC staining on EVL and basal epidermal layers [A, right panels]. Immunostaining of *krt19:tomato-CAAX* transgenic 3dpf larva shows coexpression in basal and EVL epidermal cells [B].

Although ASC is present in the epidermis of mammals (Feldmeyer et al., 2010), inflammasome signaling is mainly studied in cells belonging to the innate immune system, predominantly macrophages. To find out whether ASC is also present in cells of the innate immune system we performed immunostainings on transgenic lines that label all myeloid-derived cells (*pU1:tagRFP*), macrophages (*mpeg1:EGFP*) and neutrophils (*lysC:DsRed2*) (Fig. III.1.4A and B, C, and D, respectively). In the *pU1:tagRFP* line we observed that only a subset of cells was labeled (Fig. III.1.4A). However, in stainings of the *mpeg1:EGFP* line (Fig. III.1.4C) all cells were double positive, indicating that all macrophages express ASC. Furthermore, all red cells in the head area of *pU1:tagRFP* larvae (Fig. III.1.4B) were also ASC positive. The only cells in the zebrafish brain that are labeled by *pU1:tagRFP* are microglia, the tissue-resident macrophages of the brain (Peri and Nüsslein-Volhard, 2008). The labeled microglia likely correspond to the positive cells localized to the brain in the *in situ* hybridization (Fig. III.1.1G''). That all microglia also express ASC

further supports the statement that all macrophages contain ASC. In the case of neutrophils, we observed a higher degree of variation in the levels of ASC expression, with some cells expressing at high levels and others at barely detectable ones (Fig. III.1.4D). Therefore, some of the *pU1:tagRFP* cells that do not express ASC could be neutrophils.

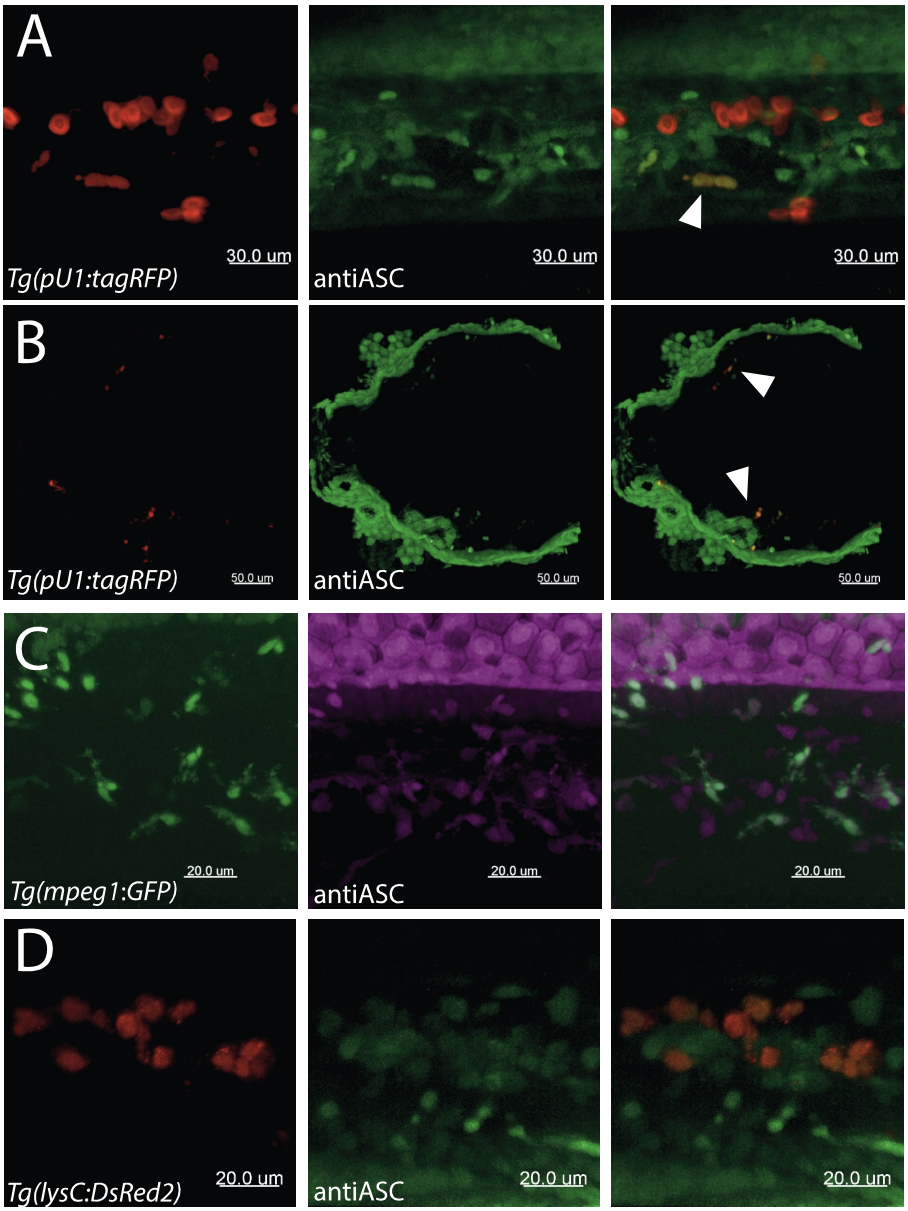

Figure I.1.4. Myeloid cells expressed ASC.
Caudal hematopoietic tissue (CHT) region of antiASC immunostaining of 3dpf *pU1:tagRFP* larva with myeloid cells labeled with tagRFP. Only one expresses ASC [A, white arrowhead]. In head region of immunostaining all tagRFP cells (microglia) express ASC [B, white arrowheads]. Immunostaining of *mpeg:EGFP* in a 3dpf larva shows macrophages (green) express ASC [C]. 3dpf *lysC:DsRed2* larva immunostaining shows neutrophils (red) express ASC.

In summary, ASC is expressed in zebrafish from early stages in the epidermis, localizing to both the nuclear and cytoplasmic compartments, and is also expressed in innate immune cells such as macrophages.

7.2 Misexpression studies of ASC

ASC speck formation is a defining features of classical inflammasome activation (Man and Kanneganti, 2015a), but how the protein behaves in zebrafish has not been studied. Therefore, in order to study the behavior of the protein live we used several strategies to misexpress the protein and then used live imaging to visualize its localization *in vivo*.

7.2.1 Heat shock-driven expression of ASC-mKate2 leads to speck formation in zebrafish larvae

In order to visualize ASC live while controlling its expression, we generated a construct containing ASC tagged with a fluorescent protein (mKate2) under the control of a heat shock promoter (Bajoghli et al., 2004). We injected the construct in wild type embryos at the one-cell stage and gave a heat shock at 2.5dpf to induce expression. We first tested whether ASC-mKate2 could be stably transiently overexpressed. We carried out immunoblotting using antiASC against whole-larva lysates and detected both tagged and untagged versions of ASC. As a negative control we used the preimmunization serum (Fig. III.1.5A). The antiASC antibody recognized a 23kDa band corresponding to the endogenous protein. In the samples from larvae that had been induced to transiently expressed ASC-mKate2, an additional higher band of approximately 50kDa corresponding to the fusion protein was detected. Both bands were absent when using preimmunization serum as primary antibody. This confirmed that the fluorescently tagged protein could be stably expressed in zebrafish larvae.

To visualize the protein live, we imaged larvae a certain period after heat shock. We observed that the transient expression of ASC-mKate2 led to the formation of specks over the entire larva. On the other hand, expression of

mKate2 alone had a cytoplasmic distribution (Fig. III.1.5B). Specks were also formed in cells that do not endogenously express *asc*, such as muscle cells. This finding suggests that speck formation is an intrinsic behavior of the protein, independent of the presence of endogenous, untagged ASC.

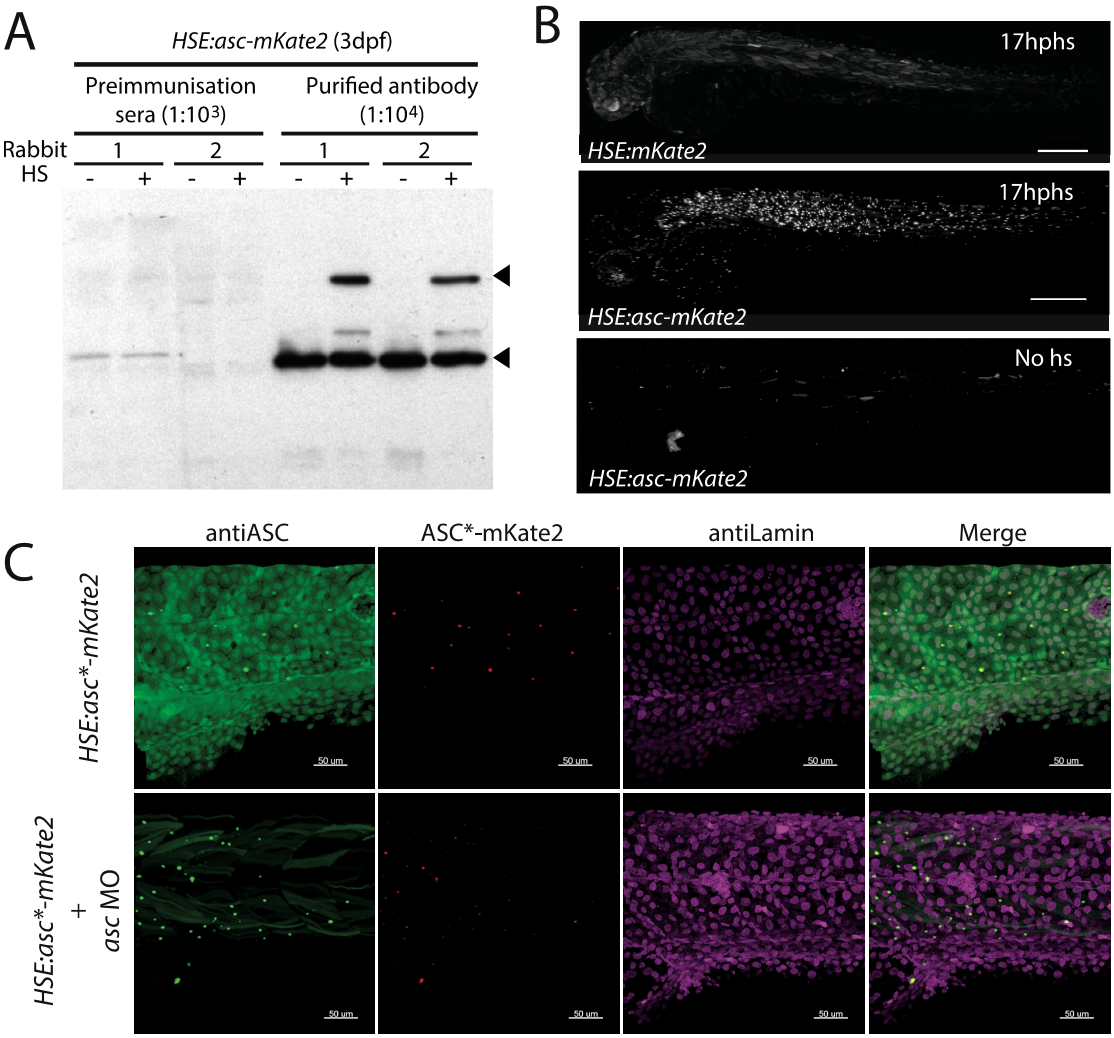

Figure III.1.5. ASC-mKate2 can be stably misexpressed by heat shock and results in specks formation.
Immunoblot of 3dpf whole-larvae lysates with or without heat shock-induced transient expression of ASC-mKate2 collected 24 after induction [A]. Using antiASC 1 and 2, a band of approx. 23kDa corresponding to endogenous ASC is detected in all samples (lower black arrowhead). After heat shock an additional band of approx. 50kDa corresponding to ASC-mKate2 appears (upper black arrowhead). Preimmunization serum is used as primary antibody in negative control. 3dpf larvae were imaged 17 h after heat shock-induced transient expression of *HSE:mKate2* (upper panel) or *HSE:asc-mKate2* (middle panel). Specks only form in larvae injected with *HSE:asc-mKate2* [B]. Immunostaining of 3dpf larvae after heat-shock induced expression of a morpholino-resistant *asc-mKate2* containing 6 silent mutations (*asc*-mKate2*). Endogenous *asc* expression was knocked down using *asc* ATG morpholino. Speck formation of ASC-mKate2 is unaffected in *asc* morphants [C].

To test this hypothesis, we carried out immunostainings of misexpressed ASC-mKate2 in the *asc* morphant background. This would also allow us to reject that lack of staining in the muscle cells was due to a penetration issue. We therefore generated a version of the heat shock construct (ASC*-mKate2) resistant to the *asc* ATG-morpholino, by introducing 6 silent mutations in the *asc* region targeted by the morpholino. These point mutations would prevent the morpholino from binding to the mRNA coming from the transiently expressed construct, while not affecting its ability to silence endogenous *asc* expression. As observed when expressing ASC-mKate2, transient expression of ASC*-mKate2 in a wild type background resulted in speck formation (Fig. III.1.5C upper row). After silencing the endogenous *asc* with the ATG-morpholino, we observed that ASC*-mKate2 is still expressed and also able to form specks (Fig. III.1.5C lower row). That antiASC recognized specks formed inside muscle cells, indicates that the antibody is able to penetrate in muscle cells and confirms that muscle cells do not endogenously express the protein. Second, it shows that the antibody is able to recognize ASC after speck formation. Furthermore, in both cases we also observed muscle cells expressing ASC*-mKate2 either contained a speck or had a uniform cytoplasmic distribution of the protein, suggesting that upon speck formation all protein is recruited to a single site in the cell.

7.2.2 Alternative tags and overexpression methods also result in speck formation of ASC

To discard the possibility that speck formation was a result of an artifact of our heat shock-induced misexpression system we tested two alternative misexpression strategies (mRNA and a drug inducible system) as well as different fluorescent protein tags. First, we produced mRNA of *asc-mKate2* and of an additional construct where ASC was fused to turboGFP (tGFP, Evrogen). We imaged larvae at 1dpf and 2dpf and observed that specks were uniformly distributed already at 1dpf and were still present at 2dpf. This was the case irrespective of the fluorescent protein used (Fig. III.1.6A). The second misexpression strategy used the LexPR drug inducible

system (Emelyanov and Parinov, 2008), in which the LexPR transactivator induces expression of the genes downstream of the Lex operator (LexOP) upon addition of Mifepristone to the water. Therefore, the LexPR/OP system allows for timed control of gene expression. We used a ubiquitous promoter (*ubi*) to drive expression of LexPR. Just as we observed with heat shock, drug-induced misexpression of ASC led to speck formation over the entire larva (Fig. III.1.6B).

These two experiments showed that overexpressed ASC forms specks regardless of the expression method. One possible explanation for speck formation is that the process is being driven by ASC's fluorescent protein tag. To confirm that speck formation did not only occur when ASC is fused to a fluorescent protein, we returned to the heat shock overexpression system. We overexpressed ASC* (the morpholino resistant version) fused to an HA (Human influenza hemagglutinin) tag and an untagged version. To visualize the overexpressed protein we performed immunostainings on these larvae (Fig. III.1.6C). Indeed, we observed that both proteins retained their ability to form specks. In the case of ASC*-HA, the specks were labeled by staining with antiHA. A single plane of the ASC* speck reveals that, as seen before, only one speck is formed per cell, with cells expressing the transgene having an otherwise uniform cytoplasmic distribution of the protein. These results indicate that speck formation is a property intrinsic of ASC, with the protein being able to aggregate in these structures when overexpressed irrespective of the method or the tag used to visualize it.

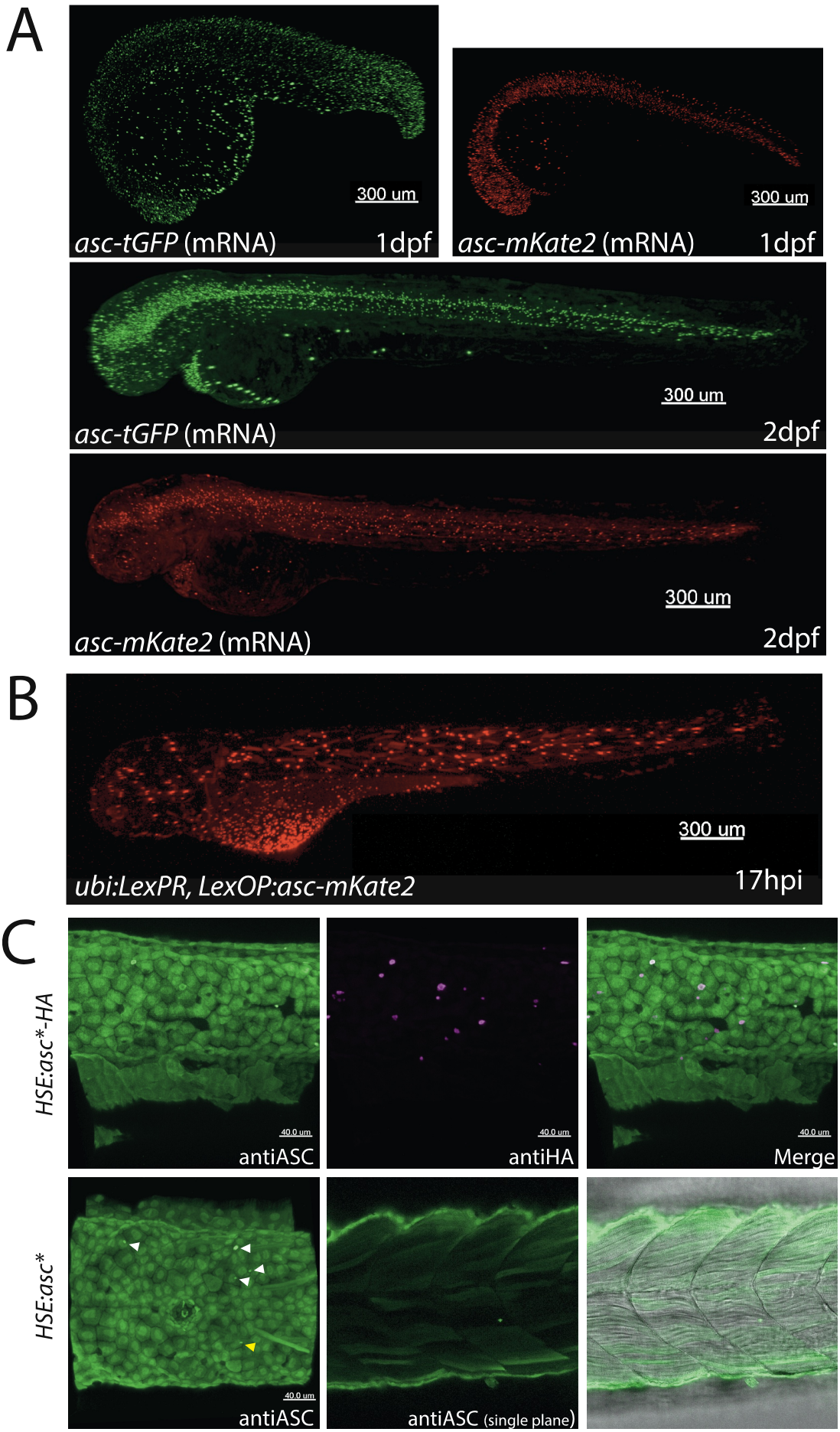
A
300 um
asc-tGFP (mRNA)
1dpf
300 um
asc-mKate2 (mRNA)
1dpf
300 um
asc-tGFP (mRNA)
2dpf
300 um
asc-mKate2 (mRNA)
2dpf
B
300 um
ubi:LexPR, LexOP:asc-mKate2
17hpi
C
HSE:asc*-HA
40.0 um
antiASC
40.0 um
antiHA
40.0 um
Merge
HSE:asc*
40.0 um
antiASC
antiASC (single plane)

Figure III.1.6. ASC misexpression *in vivo* leads to speck formation.
asc-mKate2 or *asc-tGFP* mRNA injected embryos at 1 and 2 dpf [A]. Drug-induced expression of *asc-mKate2* by transiently expressing the driver LexPR (under the *ubiquitin* promoter), and placing *asc-mKate2* downstream of the LexPR operator, LexOP. Specks are observed 17h after addition of Mifepristone to the media allows LexPR to bind to the LexOP sequence and drive expression of *asc-mKate2* [B]. AntiASC immunostaining of 3dpf larvae after heat-shock induced expression of *asc*-HA* (upper row) or *asc** (lower row) [C]. Specks of ASC-HA are labeled by antiHA. White arrowheads highlight ASC specks. The speck in the middle panel is indicated by a yellow arrowhead in the left panel.

7.2.3 Mutation of potential phosphorylation sites impair speck formation

Several recent studies have studied the aggregation properties of ASC by mutating key residues required for speck formation (Hara et al., 2013; Lu et al., 2014; Sahillioglu et al., 2014). One performed an *in silico* analysis of mouse ASC to predict Syk and JNK phosphorylation sites, and showed that mutating these potential post-translational regulation sites affected the protein's ability to form specks (Hara et al., 2013). We therefore carried out a phosphorylation site prediction analysis of ASC using the same software and parameters as reported (Fig. III.1.7A). By aligning the protein sequences, we saw that 3 of the 4 predicted phosphorylation sites identified in the CARD domain (Y152, T160 and T170) were highly conserved with those identified in mouse ASC (Fig. III.1.7B). We therefore targeted these three sites as well as one additional site in the PYD_{ASC} domain (T38) by site-directed mutagenesis (Fig. III.1.7B, residues boxed in red). All threonines (T) were mutated into alanines (A) and the tyrosine (Y) into phenylalanine (F). Thus, the final protein contained the following mutations: T38A, Y152A, T160A and T170A. We transiently expressed a construct containing all mutations (*HSE:asc(4xmut)-mKate2*). In order to avoid interference from the wild type ASC, we analyzed the mutant phenotypes only in muscle cells, which do not express *asc* (Fig. III.1.7C). The mutated ASC (T38A, Y152A, T160A, T170A) displayed a striated pattern or formed large clumps when expressed in muscle cells, in contrast to the wild type ASC, in which the protein is concentrated in a single site in the cell. We then expressed constructs with single mutations and observed that the Y152F mutation alone disrupted speck formation, similar to that of all 4 mutations together (Fig. III.1.7D). Mutations

in the corresponding site in mouse ASC was sufficient to abrogate speck formation *in vitro* (Hara et al., 2013). These results indicate that speck formation in zebrafish may be under the control of the same regulatory mechanisms as in mice.

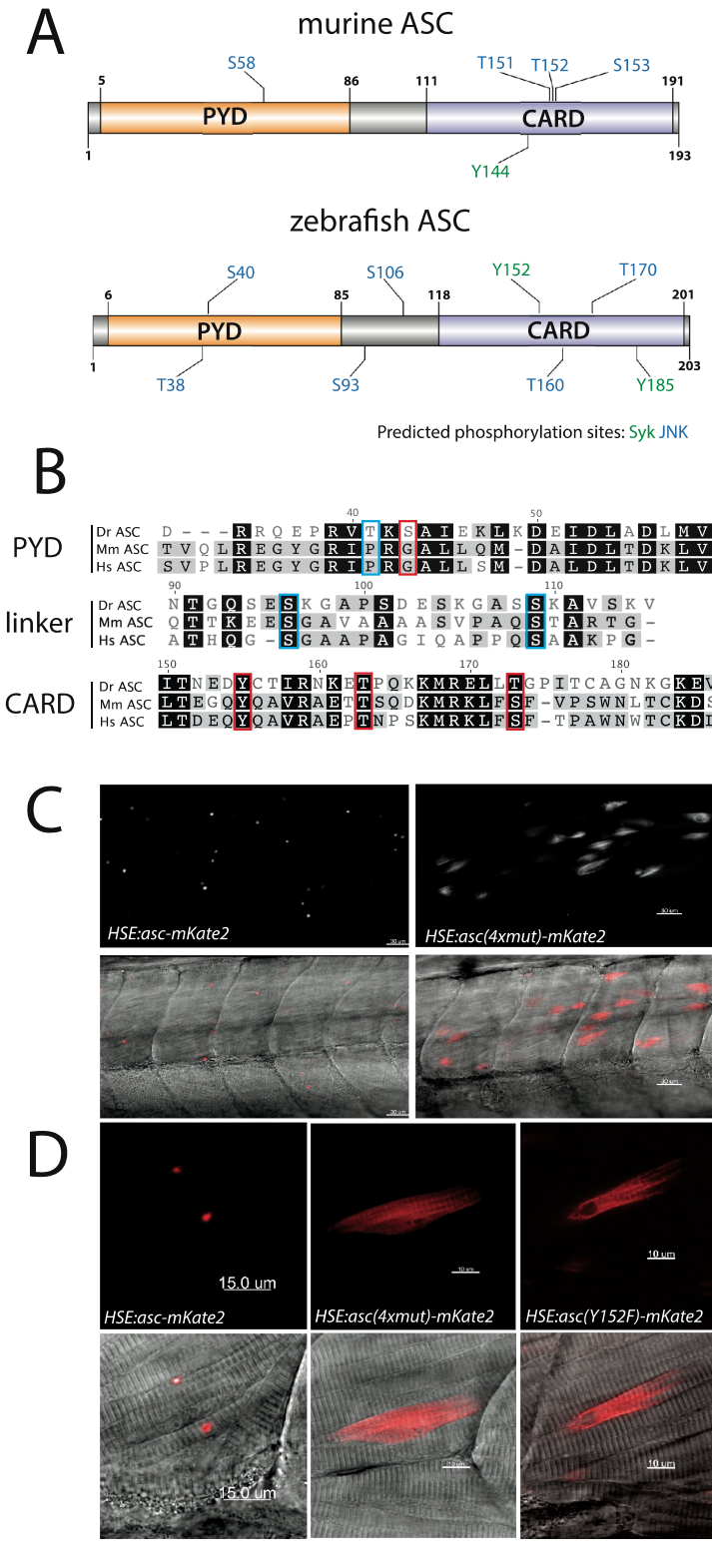

Figure III.1.7. Mutations targeting potential phosphorylation sites abolish speck formation.
Results from phosphorylation sites analysis using the online GPS 2.1.1 (Xue et al., 2011) depicting Syk and JNK-specific predicted phosphorylation sites in zebrafish ASC and those previously published using the same analysis for mouse ASC (Hara et al., 2013) [A]. Sections of full protein alignment of zebrafish (Dr), mouse (Mm) and human (Hs) ASC orthologues separated by domain. Amino acids boxed represent sites that were identified in the analysis. In red, are those chosen for single site mutagenesis [B]. Larvae transiently expressing either *asc-mKate2* or *asc(4xmut)-mKate2*, which contains base pair changes that lead to 4 missense mutations (T38A, Y152F, T160A and T170A) [C]. Single muscle cell in larvae transiently expressing *asc-mKate2*, *asc(4xmut)-mKate2* or *asc(Y152F)-mKate2*. The last construct only contains the Y152F missense mutation [D].

7.2.4 Generation of a stable *HSE:asc-mKate2* transgenic line

Inducing transient expression of ASC-mKate2 via heat shock allowed us to visualize the effects of speck formation, but because integration of the transgene is random, it does not occur in all cells and can happen multiple times and in different sites in the genome. Labeling is therefore not uniform throughout the organism, and quantifications of a large number of larvae are unreliable. To circumvent this issue, we generated the stable line *HSE:asc-mKate2*. We used time-lapse imaging of the whole larva after heat shock to visualize speck formation after induction of ASC-mKate2. We then quantified the number of specks in the entire embryo throughout the time-lapse (Fig. III.1.8A). Only 2.5 hours post heat shock (hphs), speck numbers began to rise steadily until a plateau was reached at ca. 20hphs (Fig. III.1.8B).

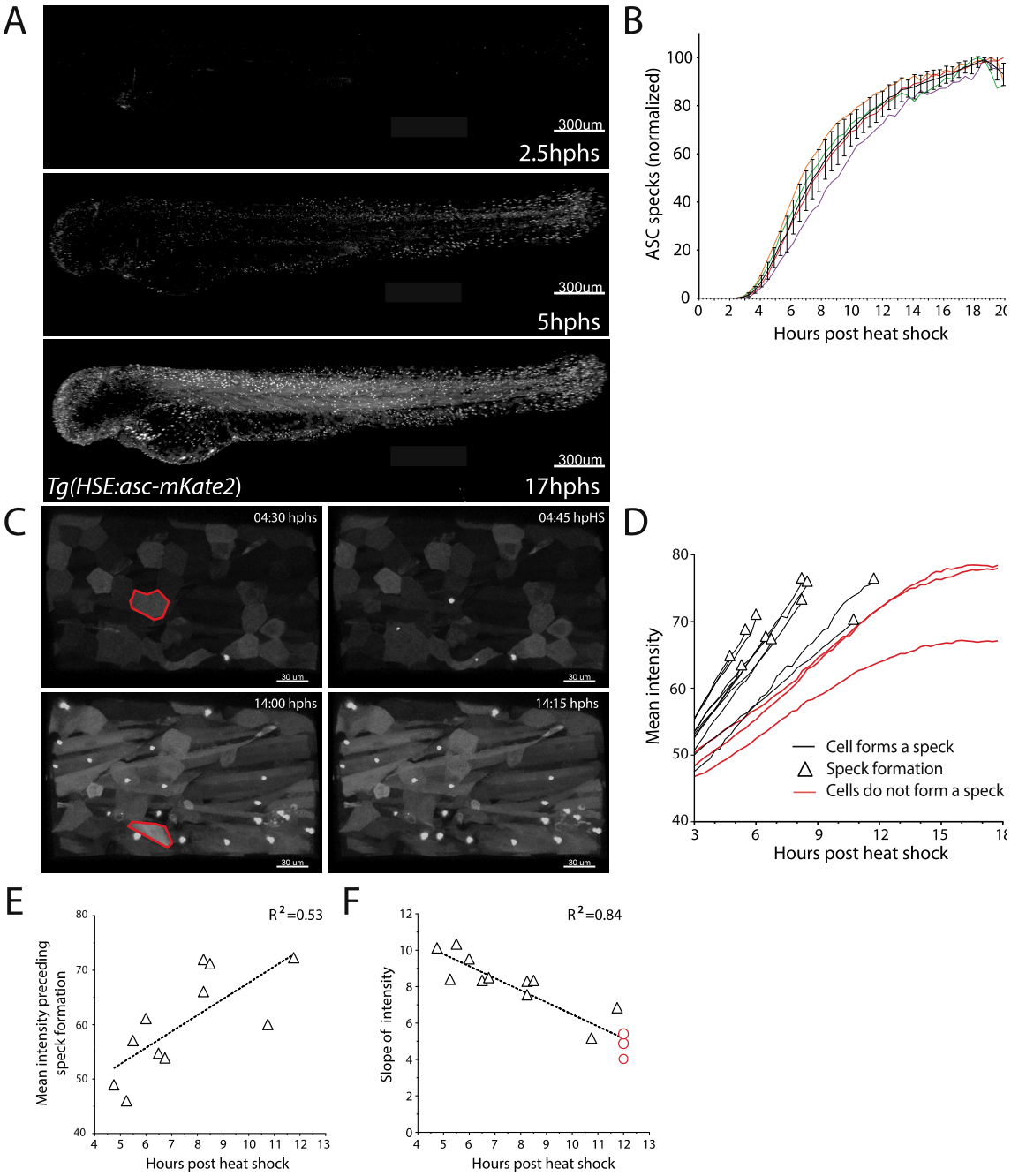

Figure III.1.8. Ubiquitous speck formation in the *HSE:asc-mKate2* transgenic line.
Larvae of the *HSE:asc-mKate2* transgenic line were heat shocked at 2.5dpf and imaged overnight [A]. Speck formation in several larvae over the time-lapse was quantified using 3D image analysis software [B]. Time-lapse of a higher magnification allowed for the manual segmentation of individual epidermal cells (demarcated in red) in order to quantify and follow the change in fluorescence intensity from 3h after heat shock until speck formation [C]. Plot depicting the change in mean intensity of individual cells (n=14) over time until speck formation. Dashed lines represent cells that do not form a speck before end of time-lapse [D]. Plot of individual slope values of linear phase of fluorescence intensity increase (from 3 to 12hphs) in all cells vs. time-point of speck formation. Inverted triangles represent cells that do not form a speck by 12hphs [E]. Plot of mean intensity values in time-point before speck formation in all cells that form a speck vs. time of speck formation [F]. In both plots, the dashed line represents linear regression whose R^2 value is depicted at the top right corner.

The rising speck numbers led us to ask whether speck formation in a certain cell type is concentration-dependent and whether all cells form a speck once a specific concentration threshold is passed. To answer this, we carried out time-lapse imaging at a magnification that enabled us to visualize speck formation in single epidermal cells (Fig. III.1.8C). We then quantified the average pixel intensity of each cell at every time-point prior to speck formation (Fig. III.1.8C left column). These values we took as a proxy for the concentration of ASC-mKate2. By plotting the increase in concentration over time for each cell (Fig. III.1.8D), we observed that cells did not form a speck at the same concentration of ASC-mKate2. Furthermore, some cells that did not form a speck eventually reached the highest concentration levels detected (Fig. III.1.8D, red lines). We plotted the average intensity values at the time-point immediately preceding speck formation and saw that ASC-mKate2 concentration did not strongly correlate with time-point of speck formation (R^2=0.53, Fig. III.1.8E). We then calculated the slope of the linear increase in ASC-mKate2 for every cell until the time-point of speck formation or until 12hphs for cells that did not form a speck. We plotted these values with time of speck formation, and saw that the rate of protein accumulation highly correlated with time-point before speck formation (R^2=0.84, Fig. III.1.8F). The data imply that the faster cells accumulate ASC-mKate2, the faster and likelier it is that they will form a speck. Cells whose rate of increase is too low will not not form a speck even at relatively high concentrations of ASC-mKate2. These results suggest that the rate of ASC-mKate2 increase is a better predictor for speck formation time-point than concentration of the protein.

7.3 Studying cell type-specific consequences of speck formation

Pyroptosis, an inflammatory form of cell death, is thought to occur as a consequence to speck formation (Boucher et al., 2014). During pyroptosis, the cell membrane collapses, spilling cytoplasmic contents into the extracellular space thus spreading the inflammatory response to all nearby tissues. Pyroptosis as a consequence of speck formation has never been observed in zebrafish. The transgenic line, *HSE:asc-mKate2*, allowed us to induce speck

formation throughout the larva simultaneously, and it provided us with the possibility to look at downstream effects of speck formation in different cell types live.

7.3.1 Speck formation has cell-type specific consequences

We first tested whether speck formation caused by overexpression of ASC was enough to drive cell death in zebrafish larvae. We stained *HSE:asc-mKate2* transgenic larvae and the negative siblings as controls with the fluorescent dye acridine orange, which labels dying cells and can be used in zebrafish larvae *in vivo* (Peri and Nüsslein-Volhard, 2008). Given that we already know the time course of speck formation in the larvae after heat shock (Fig. III.1.8B, left panel), we stained transgenic larvae and negative siblings (with non-heat shocked larvae as control for both) at an early time-point where very few if any specks have formed and at a later one where specks are distributed throughout the larvae, namely 2.5 and 15hphs (Fig. III.1.9A). We then used 3D image analysis software to segment the trunk region including the fins to exclude autoflorescence from pigment cells in the head and from the yolk (Fig. III.1.9B, white outline). In the segmented region we quantified the acridine orange spots (Fig. III.1.9B, white spots). Spots that were also red were assumed to be bleed-through from specks and were excluded from the final numbers (Fig. III.1.9B, magenta spots). We observed there was no significant difference in the amount of cell death from all groups at an early time-point (2.5hphs). However, by 15hphs, the number of acridine orange spots was significantly higher ($p<0.001$) in transgenic larvae that had been heat shocked as compared to all other groups (Fig. III.1.9B, right panel dark orange bar). This indicates expression of ASC-mKate2 induces cell death, but only at a time-point where specks are abundant.

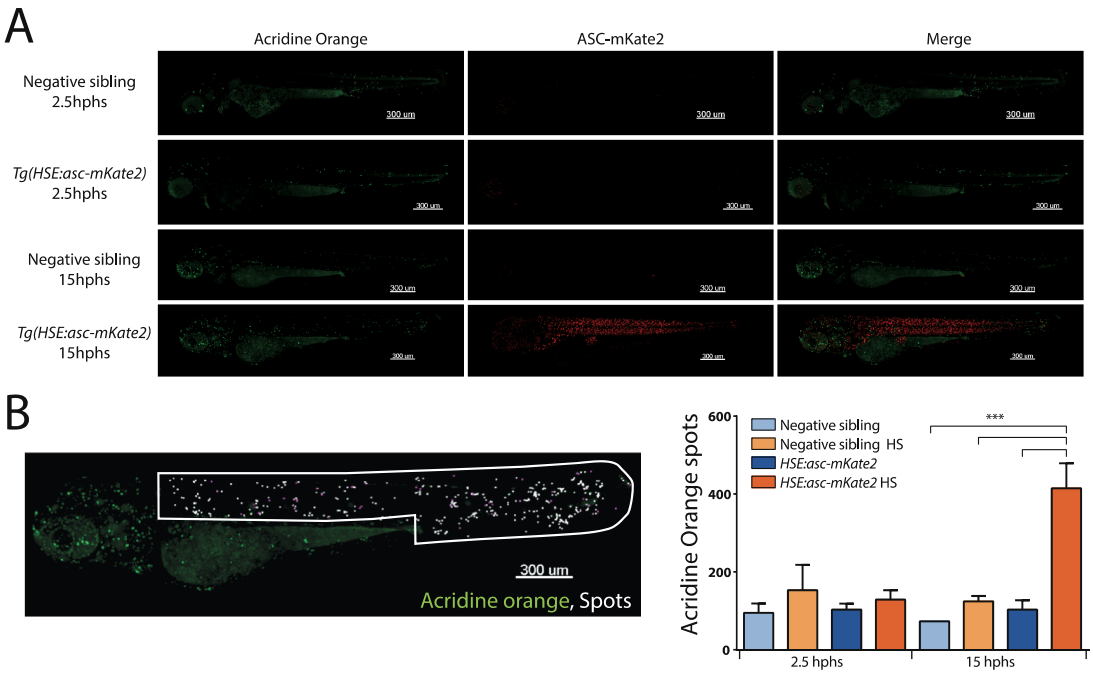

Figure III.1.9. ASC overexpression causes increase in cell death.
HSE:asc-mKate2 transgenic larvae and their negative siblings were heat shocked and stained for cell death using the live stain acridine orange. Whole larvae were imaged 2.5 and 15hphs [A]. 3D rendering of individual larvae were manually segmented to exclude the head, heart and yolk regions. Acridine orange spots in the segmented region were quantified using 3D image analysis software [white spots, left panel, B]. Spots also positive in the red channel (indicative of pigment cells or cross excitation from specks) were excluded from the analysis [magenta spots, left panel, B]. Plot depicting number of acridine orange spots in each group of larvae. The only group with a significant increase in cell death detected was the *HSE:asc-mKate2* transgenic larvae 15hphs ($p<0.0001$) [right panel, B].

An optical cross section of the larva (Fig. III.1.10A) showed that the acridine orange signal was most prominent at the epidermal layer of the trunk, suggesting that these cells may be particularly susceptible to cell death. To test this, we performed time-lapse imaging of *HSE:asc-mKate2* transgenic larvae after heat shock and staining with acridine orange (Fig. III.1.10B). We observed that within 2 hours after speck formation, epidermal cells accumulated acridine orange positive cellular debris in the vicinity of the speck. Muscle cells in the same time period did not.

Bright-field field images of these cells show that, in addition to the acridine orange-labeled debris, epidermal cells respond to speck formation by the dramatic morphological changes typical of pyroptotic cell death (Fig. III.1.10C, upper row). Within 15 minutes after speck formation, the cells round up and dislodge themselves from the surrounding epidermal layer.

The plasma membrane of the rounded up cell eventually collapses and the speck remains in the extracellular environment. A muscle cell imaged in the same time-lapse (Fig. III.1.10C, lower row) does not display any changes in cell morphology even 4 hours after speck formation. Overall, these results indicate that after speck formation, epidermal cells, but not muscle cells, undergo morphological changes that resemble pyroptosis and eventually lead to cell death, as shown by the acridine orange staining.

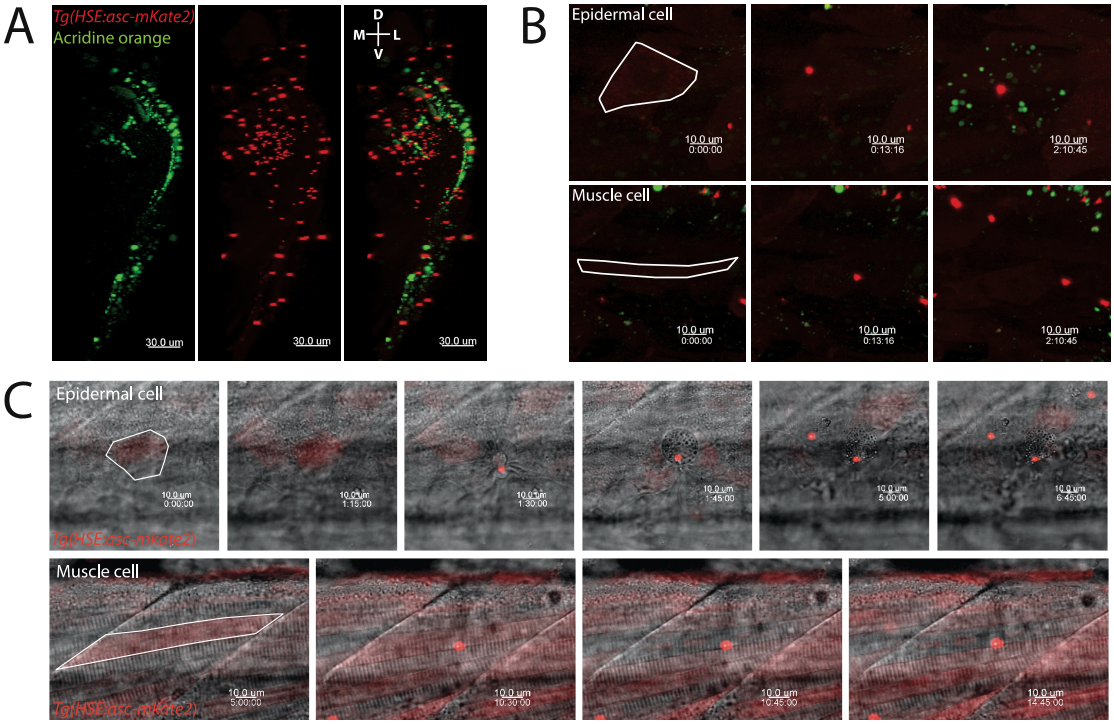

Figure III.1.10. Speck formation has cell type-specific consequences.
A cross section of a *HSE:asc-mKate2* transgenic larvae 15hphs stained with acridine orange showing cell death is mostly located in the lateral side [A]. *HSE:asc-mKate2* transgenic larvae were stained with acridine orange 3hphs and individual epidermal cells (top row) and muscle cells (bottom row) were imaged in a time-lapse to visualize debris accumulation in the vicinity of the cells. This only occurred after speck formation in epidermal cells [B]. Time-lapse of individual epidermal cells (top row) and muscle cells (bottom row) *HSE:asc-mKate2* transgenic larvae to visualize changes in cell morphology brought about by speck formation by imaging the bright-field [C]. Drastic morphological changes were only observed in the case of epidermal cells.

7.3.2 Epidermal cells undergo a pyroptotic-like cell death after speck formation

To determine the identity of the cells that undergo cell death after speck formation, we turned again to the keratinocyte labeling lines *krt4:GFP*

and *krt19:tomato-CAAX*. In the *krt4:GFP* and *HSE:asc-mKate2* double transgenic line transgenic line after heat shock, cells labeled by GFP underwent the same form of cell death as we had observed previously after speck formation. The loss of cytoplasmic GFP signal indicates that the plasma membrane integrity is compromised and the cytoplasmic contents are leaked to the extracellular environment, a feature of pyroptosis (Fig. III.1.11A, white arrowhead). Furthermore, in the bright-field, we again saw that the cell detaches from the surrounding epidermal tissue and rounds up (Fig. III.1.11A'). To visualize speck formation in the *krt19:tomato-CAAX* line, we transiently expressed the *HSE:asc-tGFP* construct. Because in this transgenic line the membranes of epidermal cells are labeled, we were able to observe the changes that the plasma membrane undergoes after speck formation (Fig. III.1.11B). Once speck formation takes place, the plasma membrane fragments into vesicles that likely correspond to the debris labeled by acridine orange. In this case, even after the cell has died, the speck can remain in the extracellular environment as stable aggregate.

These experiments confirmed that epidermal cells are indeed susceptible to cell death after speck formation, whereas in other cell types, such as muscle cells, misexpressed ASC can form specks without causing cell death.

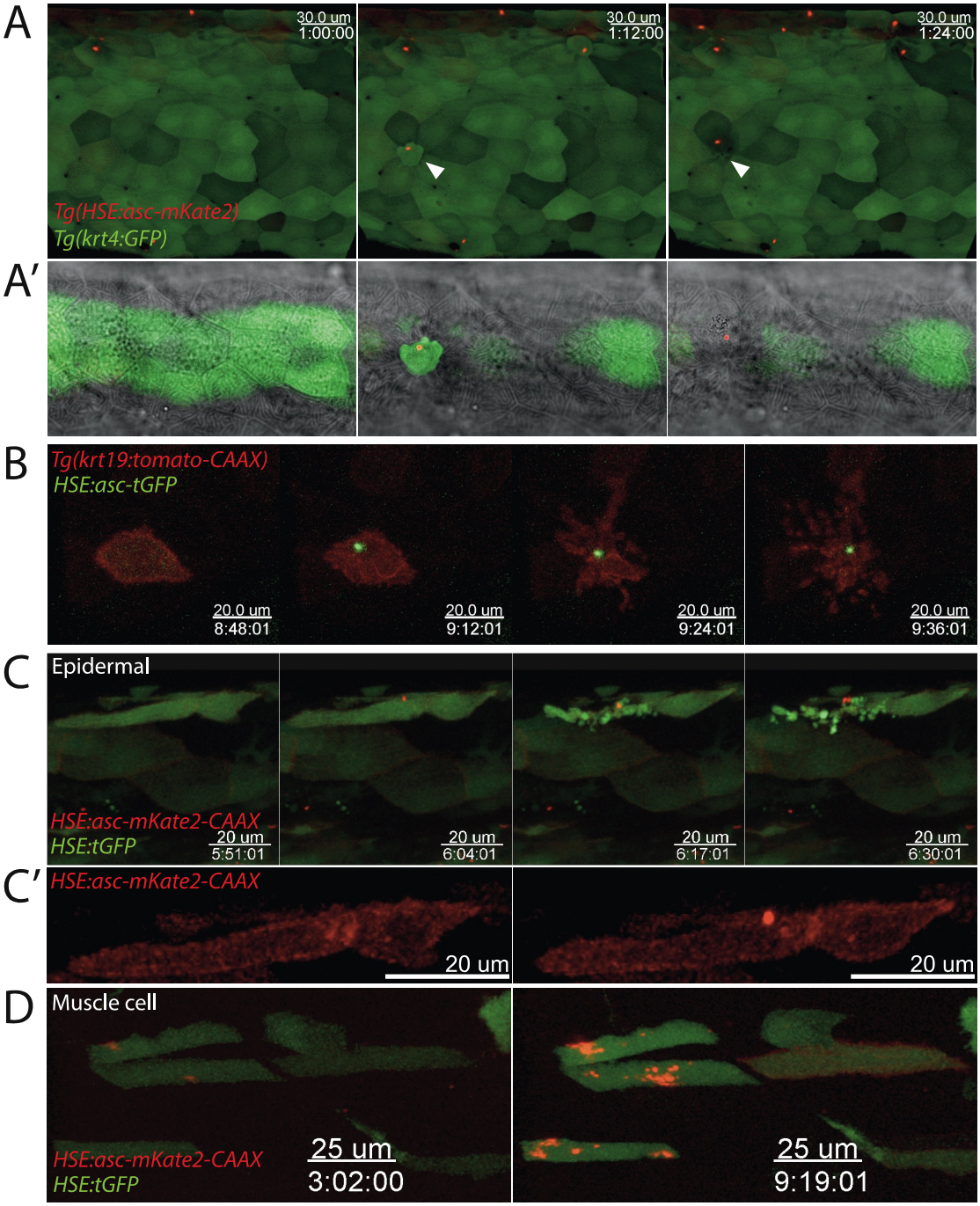

Figure III.1.11. Speck formation leads to cell death of epidermal cells.
Time-lapse imaging of the double transgenic line *HSE:asc-mKate2, krt4:GFP* after heat shock showing an epidermal cell disappearing after speck formation [white arrowhead, A]. Magnification of a single plane merged with the bright-field of the epidermal cell showing changes in cell morphology after speck formation [A']. Time-lapse imaging *krt19:tomato-CAAX* transiently ASC-tGFP, shows that speck formation leads to collapse of the plasma membrane and the formation of debris [B]. Time-lapse imaging of transient coexpression of a membrane anchored version of ASC (ASC-mKate2-CAAX) and GFP. Speck formation caused cell death in epidermal cells [C]. Magnification of the red channel in the time-points before and after speck formation, showing local recruitment of membrane anchored ASC to form a speck [C']. Time-lapse imaging of in muscle cells expressing the same construct [D].

7.3.3 Anchoring ASC-mKate2 to the membrane does not prevent cell death after speck formation

Thus far we have seen epithelial cells die after ASC forms a cytoplasmic speck. We therefore wondered if, by targeting ASC to specific subcellular localization we could inhibit its cytoplasmic aggregation and subsequently, cell death. To test this we used the construct *HSE:asc-mKate2-CAAX*, which contains the CAAX farnesylation sequence at the C-terminus of the mKate2, which targets the fusion protein to the plasma membrane (Fig. III.1.11C and D). Surprisingly, we found that, although the construct localized to the plasma membrane of epidermal cells it could nonetheless form local ASC aggregates. In these cells, cell death ensued without all of the available ASC-mKate2-CAAX to relocalizing to the speck (Fig. III.1.11C'). In muscle cells (Fig. III.1.11D), the protein often aggregated before reaching the plasma membrane (without causing cell death), but sometimes also localized to the plasma membrane entirely.

7.3.4 Intranuclear speck formation also results in cell death

Specks have been seen in intranuclear, perinuclear or cytoplasmic locations. In a cell line in which speck formation does not lead to pyroptosis, specks that formed in either the nucleus or the cytoplasm first depleted the pool of ASC only in the respective compartment prior to speck formation (Cheng et al., 2010). We therefore looked at the localization of specks relative to the nucleus in epidermal cells. To visualize the nucleus we used a *βactin:NLS-tagBFP* transgenic line, in which nuclei are labeled throughout the whole larva. To visualize the cytoplasm, GFP was coexpressed with ASC-mKate2 under the heat shock promoter, which is bidirectional (Bajoghli et al., 2004). We induced expression and observed that specks can form both in the cytoplasmic and the nuclear compartments of the cell (Fig. III.1.12A, yellow arrowheads). If the speck forms in the cytoplasm, the cytoplasmic pool of ASC-mKate2 is depleted immediately with the nuclear pool still being visible after speck formation (Fig. III.1.12B). Conversely, if the speck forms inside the

nucleus (Fig. III.1.12C), it is this compartment's pool of ASC-mKate2 that is depleted to form the speck with the cytoplasm seemingly retaining its pool of ASC-mKate2 until cell death. We confirmed this by quantifying plot profile (white line) intensity levels in all three channels before and after speck formation in the case depicted in Fig. III.1.12C (Fig. III.1.12D). After speck formation, both green and cyan channels are unaffected, however, in the red channel, the nuclear pool is relocalized to a single saturated spot. The red channel's cytoplasmic signal remains unchanged. Regardless of speck localization, however, disintegration of the nuclear compartment and cell death consistently take place after speck formation. These downstream events appear to occur more rapidly if the speck is formed in the cytoplasm than in the nucleus (roughly three times faster, 15 min vs. 45 min). Therefore, in epidermal cells, specks can form in or outside of the nucleus using that compartment's pool of ASC with speck formation leading to cell death in each case.

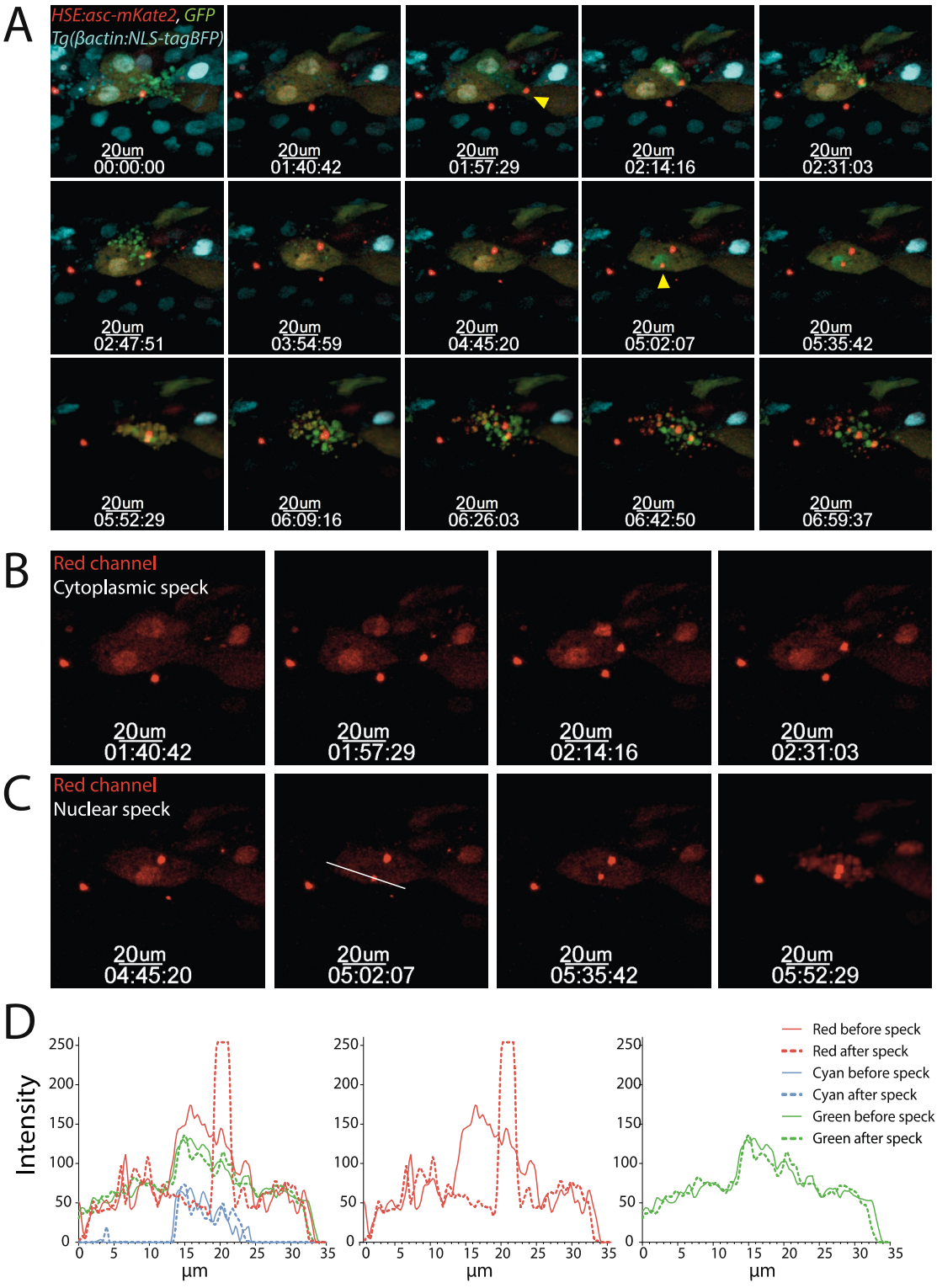

Figure III.1.12. Speck formation can occur in the nucleus or cytoplasm of epidermal cells. Time-lapse imaging of transient heat-shocked induced coexpression of ASC-mKate2 and GFP in the transgenic line *βactin:NLS-tagBFP* [A]. Yellow arrowheads highlight localization of two specks assembled during time-lapse. Red channel from time-lapse showing depletion of ASC-mKate2 pool in cytoplasmic [B] and nuclear compartments [C]. Intensity plot profile of line marked in second panel of [B] for all three channels [C]. The plot profiles shown correspond to the time-points before and after speck formation, the latter in dashed lines. The middle and right panels contain plot profiles of green and red channels separately.

7.3.5 Macrophages can engulf cellular debris generated from speck formation-induced cell death

We had previously observed that a large amount of cellular debris was generated after a pyroptotic-like cell death both by staining with acridine orange (Fig. III.1.9A) and visualizing the membrane of epidermal cells (Fig. III.1.11C). Furthermore, we had seen that specks seem to persist after cell death and remain in the extracellular environment. Therefore, we wondered whether phagocytes cleared the cellular debris after speck formation.

We used the transgenic line *mpeg1:EGFP*, which labels macrophages, crossed with the *HSE:asc-mKate2* and imaged the larvae after heat shock (Fig. III.1.13A). We observed that macrophages were capable of engulfing cellular debris containing ASC specks, and that they can contain multiple phagosomes with specks. In the example presented in Fig. III.1.12A, we see that more than an hour after speck formation, although there are two macrophages in the vicinity of the debris that is later engulfed (signaled by the white arrow) only the macrophage on the right (which already contains several specks inside phagosomes from previously ingested material) branches out and engulfs the speck in a phagocytic cup, which can be seen in the bright-field of a single merged z plane of time-point 6 (Fig. III.1.13A'). In this case, the macrophage accumulates debris-containing specks, but it is unclear whether the material was being digested or not. Further imaging of such events, this time using the *pU1:tagRFP* to label macrophages and transient expression of *HSE:asc-sfGFP* showed that indeed they can. As depicted in Fig. III.1.13B, a macrophage (as judged by cell morphology) engulfs cellular debris containing a speck and afterwards seemingly digests the engulfed material, as shown by the vanishing speck fluorescent signal 2 hours after engulfment. These experiments indicate that the cellular debris resulting from speck formation-induced cell death can be cleared up by professional phagocytes and that the latter are able to process the engulfed material.

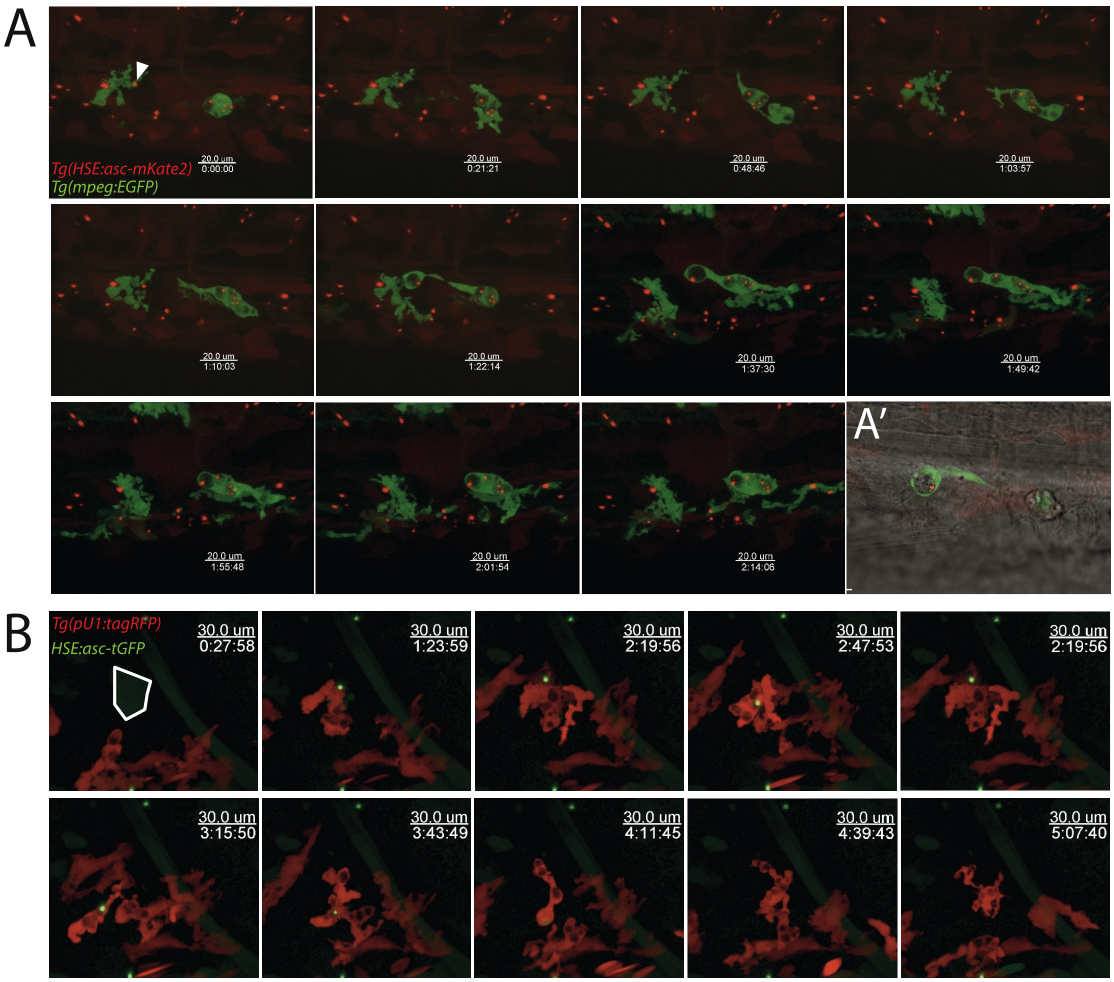

Figure III.1.13. Macrophages phagocytize specks.
Time-lapse imaging of the double transgenic line *HSE:asc-mKate2, mpeg:EGFP* after heat shock shows macrophage engulfing a speck (white arrowhead) [A]. Single plane merge with bright-field of time-point when phagocytic cup surrounds the speck [A']. Time-lapse imaging of heat-shock induced transient expression of *HSE:asc-tGFP* in the *pU1:tagRFP* transgenic line. Movie starts before cell (white border) forms speck A myeloid phagocytic cell in the vicinity engulfs the speck. Movie ends when speck inside the phagosome is no longer visible [B].

7.4 A caspase-1 homologue as a downstream effector molecule

In mammals, the ASC speck recruits the immature form of the downstream effector molecule caspase-1 (pro-caspase-1). Caspase-1 undergoes autoproteolytic activation and the mature form of caspase-1 is released into the cytoplasm, becoming the major effector driving pyroptotic cell death (LaRock and Cookson, 2013). Given the similarity between the response we observed after specking in epidermal cells and pyroptosis, we speculated that caspases could be involved in this response. We focused on Caspa, a zebrafish caspase whose catalytic domains have the highest

homology to those of human caspase-1 (Masumoto et al., 2003).

7.4.1 Caspase inhibition reduces cell death in the *HSE:asc-mKate2* line

To determine whether caspases were involved in the cell death resulting form speck formation we treated larvae from *HSE:asc-mKate2* the with the pan-caspase inhibitor Q-VD-OPh hydrate (Sigma) after heat shock. We imaged the larvae 15hphs and compared the amount of cell death between DMSO-treated transgenic larvae and negative siblings treated with the inhibitor by staining with acridine orange (Fig. III.1.14). Treatment with the inhibitor significantly diminished cell death in *HSE:asc-mKate2* larvae compared to DMSO-treated controls. This result indicated that caspases were involved in the cell death caused by speck formation.

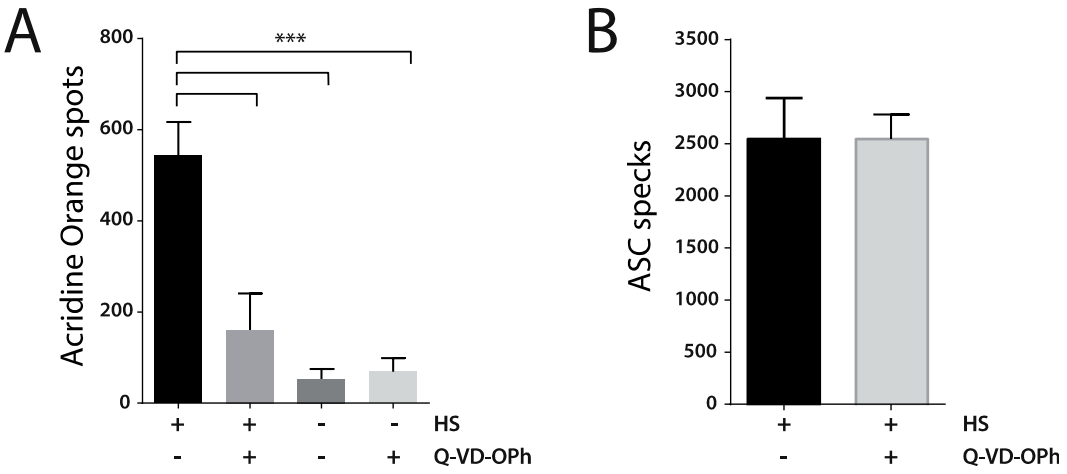

Figure III.1.14. Caspase inhibitors reduce cell death caused by speck formation.
Plot depicting number of acridine orange spots in stained *HSE:asc-mKate2* transgenic larvae with and without heat shock and with or without treatment with the pan-caspase inhibitor Q-VD-OPh (100 μM) imaged 17h after heat shock [A]. Spots in the manually segmented regions of 3D rendering of individual larvae were quantified using 3D image analysis software. Spots also positive in the red channel (indicative of pigment cells or cross excitation from specks) were excluded from the analysis. A significant reduction in cell death was observed in heat-shocked larvae treated with Q-VD-OPh ($p<0.0001$). Quantification of specks in the segmented region of each larva belonging to a group where ASC-mKate2 expression was induced showing treatment with inhibitor does not affect speck formation [B].

7.4.2 Caspa overexpression is highly toxic

Since we knew caspases were involved in the cell death induced by speck formation, we visualized the downstream cellular consequences brought about by the activation of the two mammalian *caspase-1* homologues in zebrafish, *caspa* and *caspb*. Both Caspa and Caspb have N-terminal PYD domains. To compare levels of cell death, we used an apoptotic caspase that lacks a PYD domain, Casp3a, the orthologue of mammalian caspase-3. We generated heat shock overexpressing constructs for all three (*HSE:caspa-EGFP*, *HSE:caspb-EGFP* and *HSE:cas3a-EGFP*). To concomitantly observe the response of myeloid cells, we transiently expressed these constructs in *pU1:tagRFP* transgenic larvae (Fig. III.1.15).

In larvae transiently overexpressing Caspa (Fig. III.1.15A), we observed a high amount of cellular debris in the epidermis, indicative of cell death. The debris is visible from 3hphs, a time after which the cell has barely accumulated enough fluorescent protein for it to be detectable. Myeloid cells were frequently seen ingesting green-labeled material. Therefore, epidermal cells appeared to be especially susceptible to cell death after induction of Caspa expression. Muscle cells were also affected by Caspa expression, but at later time-points after induction, with a detached plasma membrane and a darkening cytoplasm visible from 17hphs (Fig. III.1.15B). This suggests that expression of Caspa itself is sufficient to trigger cell death in both of these cell types. We only observed this drastic response when we expressed Caspa. Transient expression of either Caspb (Fig. III.1.15C) or Casp3a (Fig. III.1.15D) did not result in any obvious defects in either epidermal cells (top rows) or muscle cells (bottom rows) in the same time period. These results indicate that Caspa activation is capable of causing cell death swiftly both in epidermal cells and muscle.

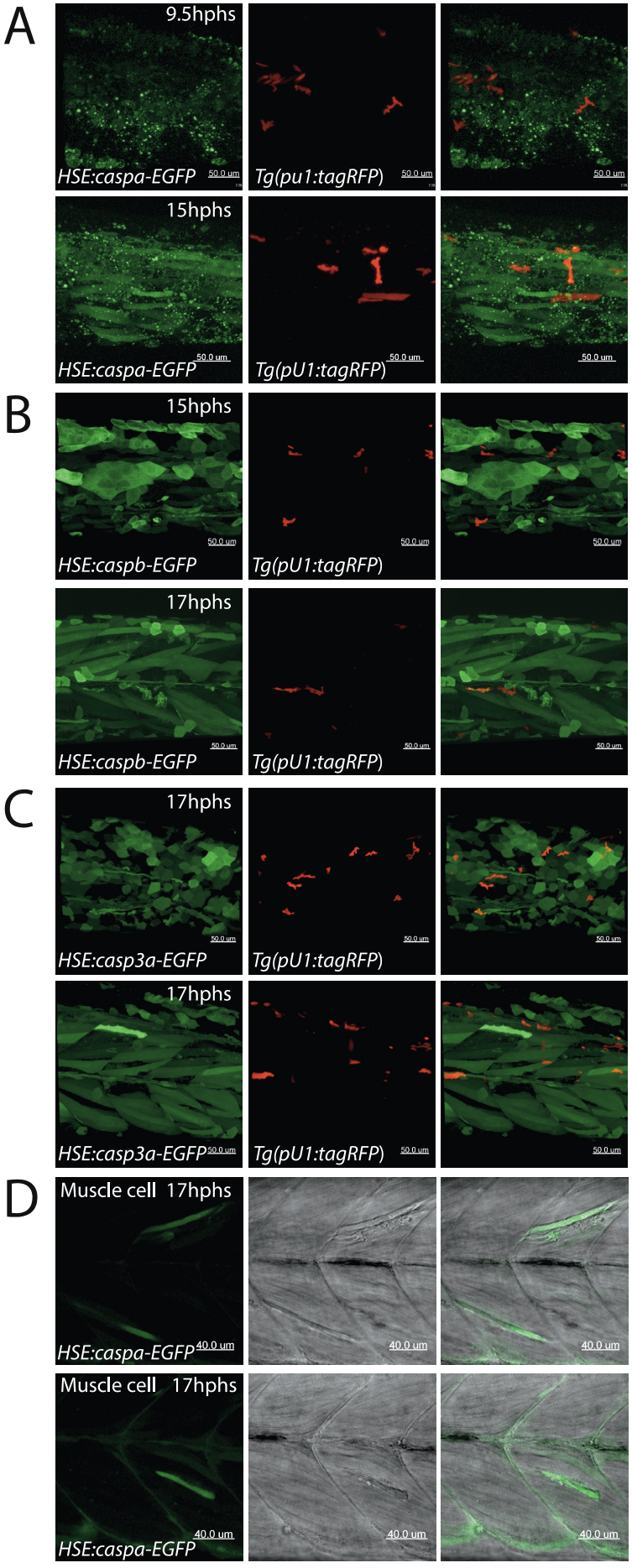
A
9.5hphs
HSE:caspa-EGFP
Tg(pu1:tagRFP)
15hphs
HSE:caspa-EGFP
Tg(pU1:tagRFP)
B
15hphs
HSE:caspb-EGFP
Tg(pU1:tagRFP)
17hphs
HSE:caspb-EGFP
Tg(pU1:tagRFP)
C
17hphs
HSE:casp3a-EGFP
Tg(pU1:tagRFP)
17hphs
HSE:casp3a-EGFP
Tg(pU1:tagRFP)
D
Muscle cell 17hphs
HSE:caspa-EGFP
Muscle cell 17hphs
HSE:caspa-EGFP

Figure III.1.15. Caspa overexpression causes cell death.
Imaging of heat-shock induced transient expression of *HSE:caspa-EGFP* [A], *HSE:caspb-EGFP* [B] or *HSE:casp3a-EGFP* [C] in the *pU1:tagRFP* transgenic line, between 9 and 17hphs. Massive amounts of cellular debris in the epidermis are only evident in the case of Caspa-GFP overexpression. Single plane of *HSE:caspa-EGFP* transient expression merged with bright-field showing muscle cells' morphological change in response to Caspa-GFP overexpression 17hphs [B].

7.4.3 Caspa is recruited to ASC speck

Caspase-1 in mammals is recruited to the speck, where it undergoes autoproteolytic activation. Therefore, recruitment to the speck is the key downstream effector event that unleashes pyroptosis. To find out whether Caspa can be recruited to the ASC speck. We transiently coexpressed *HSE:asc-mKate2* and *HSE:caspa-EGFP* and used the *HSE:caspb-EGFP* and *HSE:casp3a-EGFP* as control. Because muscle cells show no response to speck formation, we used these cells as an *in vivo* test for recruitment of the different caspases to the speck. Imaging the larvae coexpressing different combinations of *asc* and caspase constructs revealed that speck formation is unaffected by caspase expression (Fig. III.1.16A). Moreover, if the two proteins were coexpressed in the same cell, we observed recruitment only in the case of Caspa-GFP (Fig. III.1.16B). These experiments confirmed that Caspa is recruited to the speck but another PYD-domain containing caspase is not.

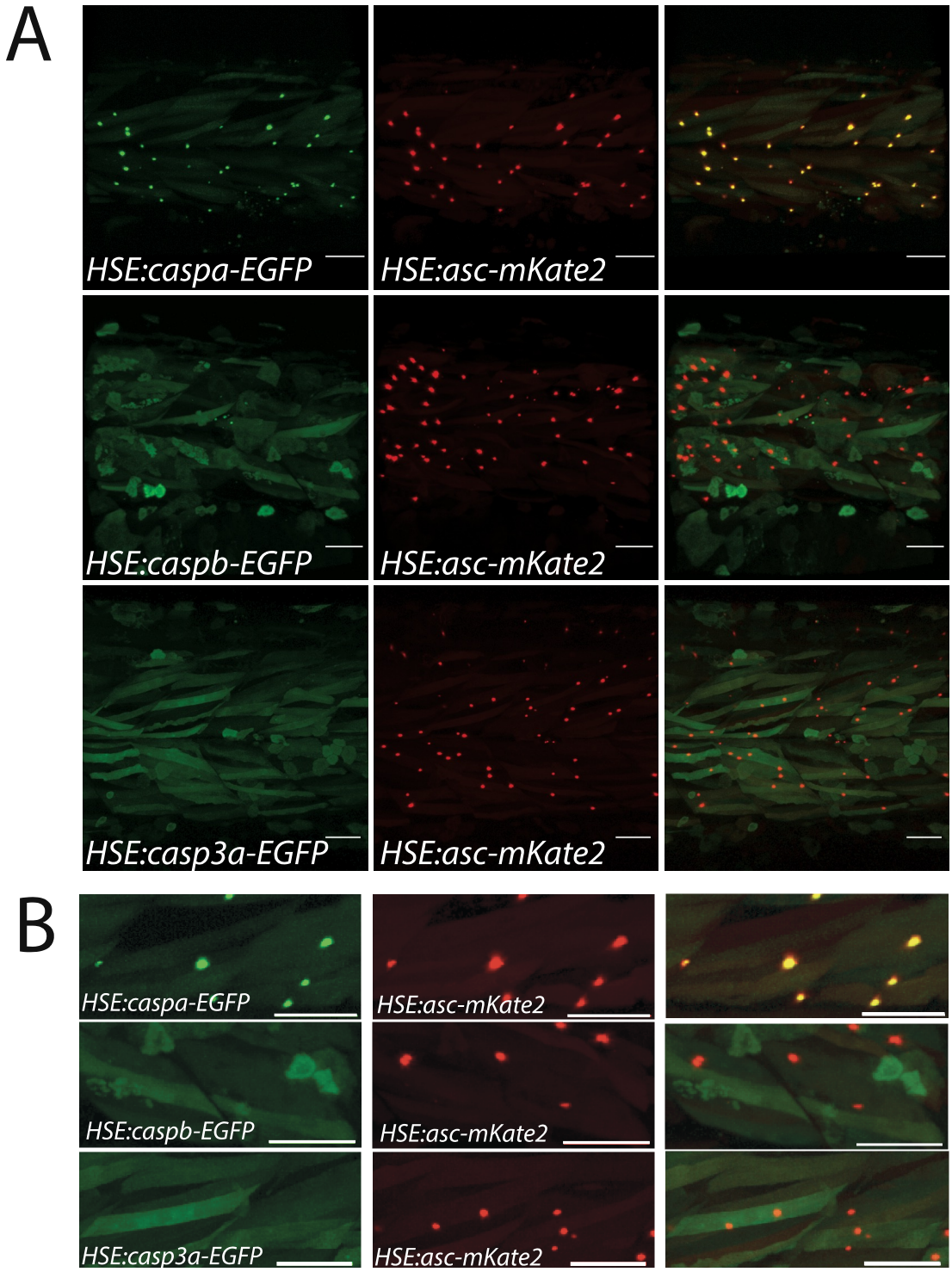

Figure III.1.16. Caspa is recruited to the ASC speck.
Imaging of heat-shock induced transient expression of *HSE:caspa-EGFP*, *HSE:caspb-EGFP* or *HSE:casp3a-EGFP* with transient expression of *HSE:asc-mKate2* [A]. Single cells show that recruitment of a caspase to the ASC specks only happens in the case of Caspa-EFGP coexpression with ASC-mKate2 [B].

7.4.4 Caspa and ASC interact via their PYD domains

It had been previously shown that ASC and Caspa colocalized in a PYD-dependent manner when coexpressed in mammalian cells (Masumoto et al., 2003). To test whether Caspa is recruited to the ASC speck via its PYD domain (PYD_{Caspa}) *in vivo* we generated heat shock constructs containing each domain for both Caspa and ASC separately, namely *HSE:*PYD_{Caspa}*-EGFP* and *HSE:*$Casp_{Caspa}$*-EGFP*, in the case of Caspa, and *HSE:*PYD_{ASC}*-mKate2* *HSE:*$CARD_{ASC}$*-mKate2* for ASC (Fig. III.1.17-1.19). We coexpressed combinations of these constructs transiently in larvae and focused on muscle cells to visualize the interaction without the background of endogenous ASC. Expressing either PYD or CARD domains of ASC (PYD_{ASC} or $CARD_{ASC}$, respectively) resulted in abnormal speck formation, with fibril-like aggregates forming instead of a single speck. We first coexpressed the separate domains of Caspa fused to GFP (PYD_{Caspa}-GFP and $Casp_{Caspa}$-GFP), or GFP alone as a negative control, with PYD_{ASC}-mKate2. The coexpressed protein tagged with GFP colocalized with the PYD_{ASC}-mKate2 aggregates exclusively when the GFP fusion contained the PYD_{Caspa} (Fig. III.1.17). Namely, we only observed an interaction between PYD_{ASC}-mKate2 and the full-length protein, and between PYD_{ASC}-mKate2 and PYD_{Caspa}-GFP. When we performed the converse experiment expressing $CARD_{ASC}$-mKate2, none of the GFP-tagged proteins colocalized with the aggregates of $CARD_{ASC}$-mKate2 (Fig. III.1.18). We then coexpressed the ASC-mKate2 with the separate domains of Caspa. In this case, PYD_{Caspa}-GFP but not $Casp_{Caspa}$-GFP was recruited to a properly assembled speck (Fig. III.1.19A). When expressed alone, PYD_{Caspa}-GFP and $Casp_{Caspa}$-GFP had a cytoplasmic distribution alone in muscle cells (Fig. III.1.19B), as observed for the full-length protein (Fig. III.1.15). These results indicate that the recruitment of Caspa to the ASC speck *in vivo* is dependent on their PYD domains.

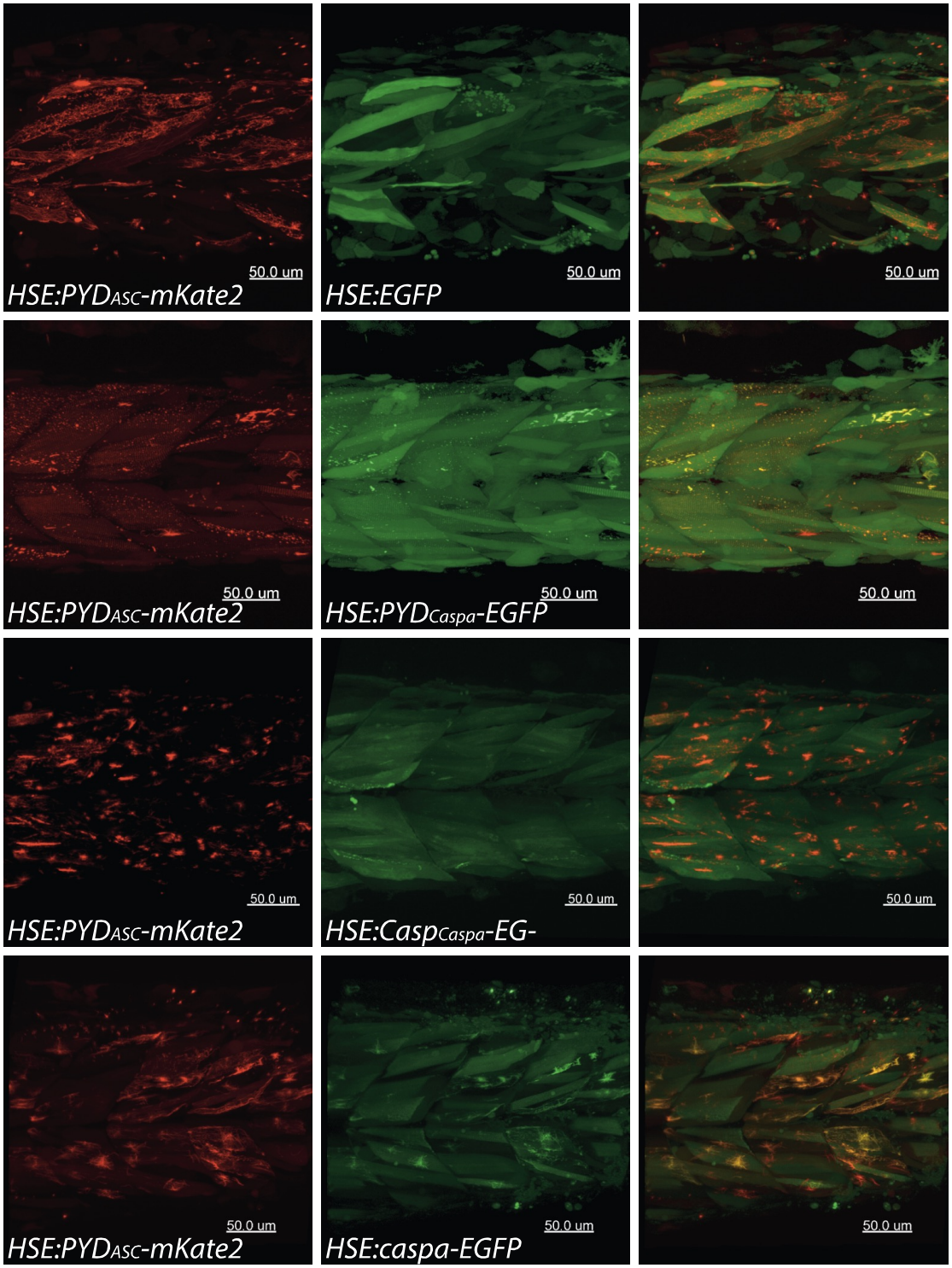

Figure III.1.17. ASC PYD (PYD_{ASC}) recruits Caspa via its own PYD.
Imaging of heat-shock induced transient expression of *HSE:PYD_{ASC}-mKate2* with *HSE:EGFP*, *HSE:PYD_{Caspa}-EGFP*, *HSE:$Casp_{Caspa}$-EGFP* and *HSE:caspa-EGFP*. Colocalization of GFP fusion proteins with PYD_{ASC} is only seen in cases where PYD_{Caspa} domain is included.

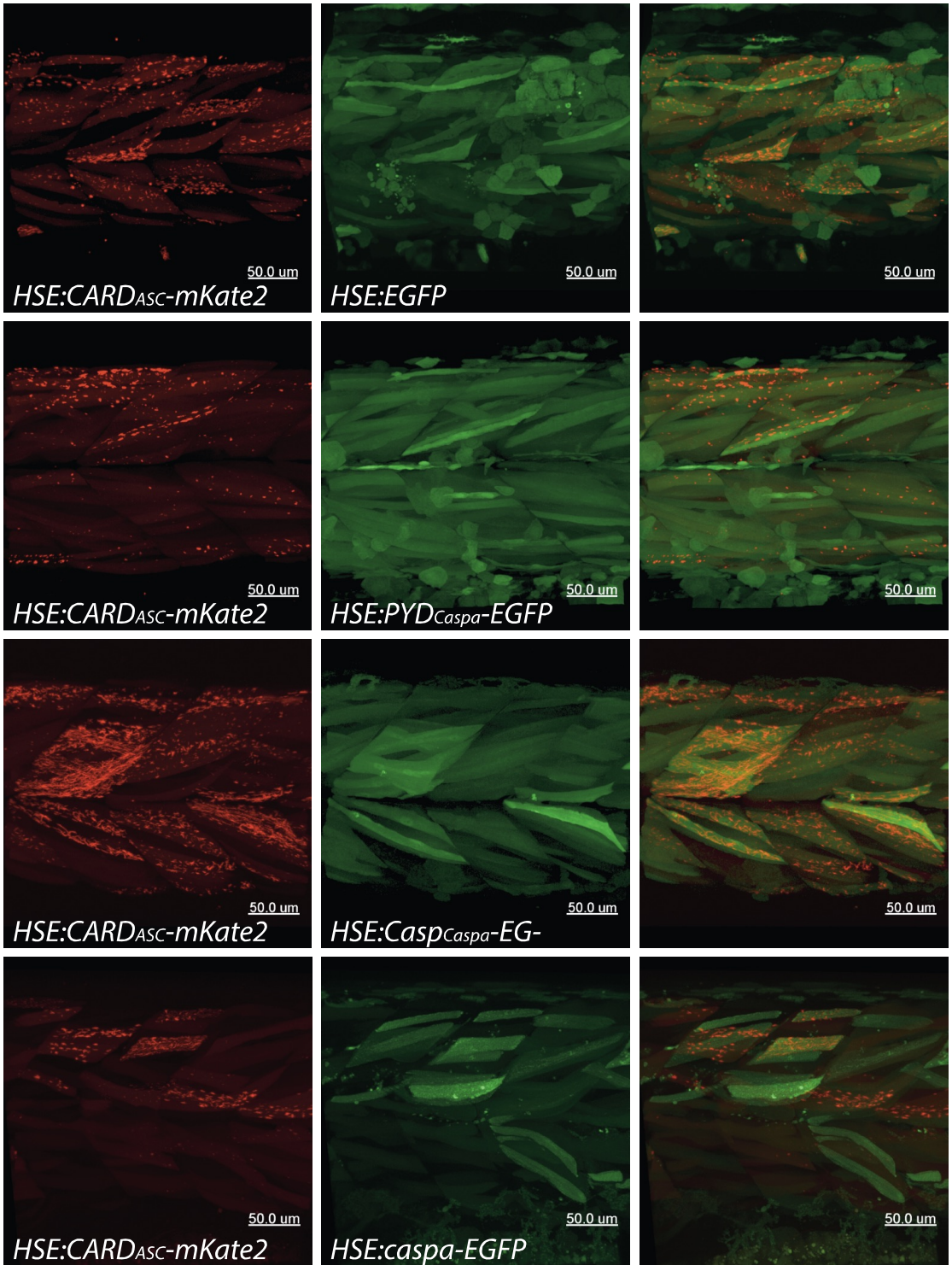

Figure III.1.18. ASC CARD ($CARD_{ASC}$) is not involved in recruitment of Caspa to the speck.

Imaging of heat-shock induced transient expression of *HSE:$CARD_{ASC}$-mKate2* with *HSE:EGFP*, *HSE:PYD_{Caspa}-EGFP*, *HSE:$Casp_{Caspa}$-EGFP* and *HSE:caspa-EGFP*. No colocalization is observed.

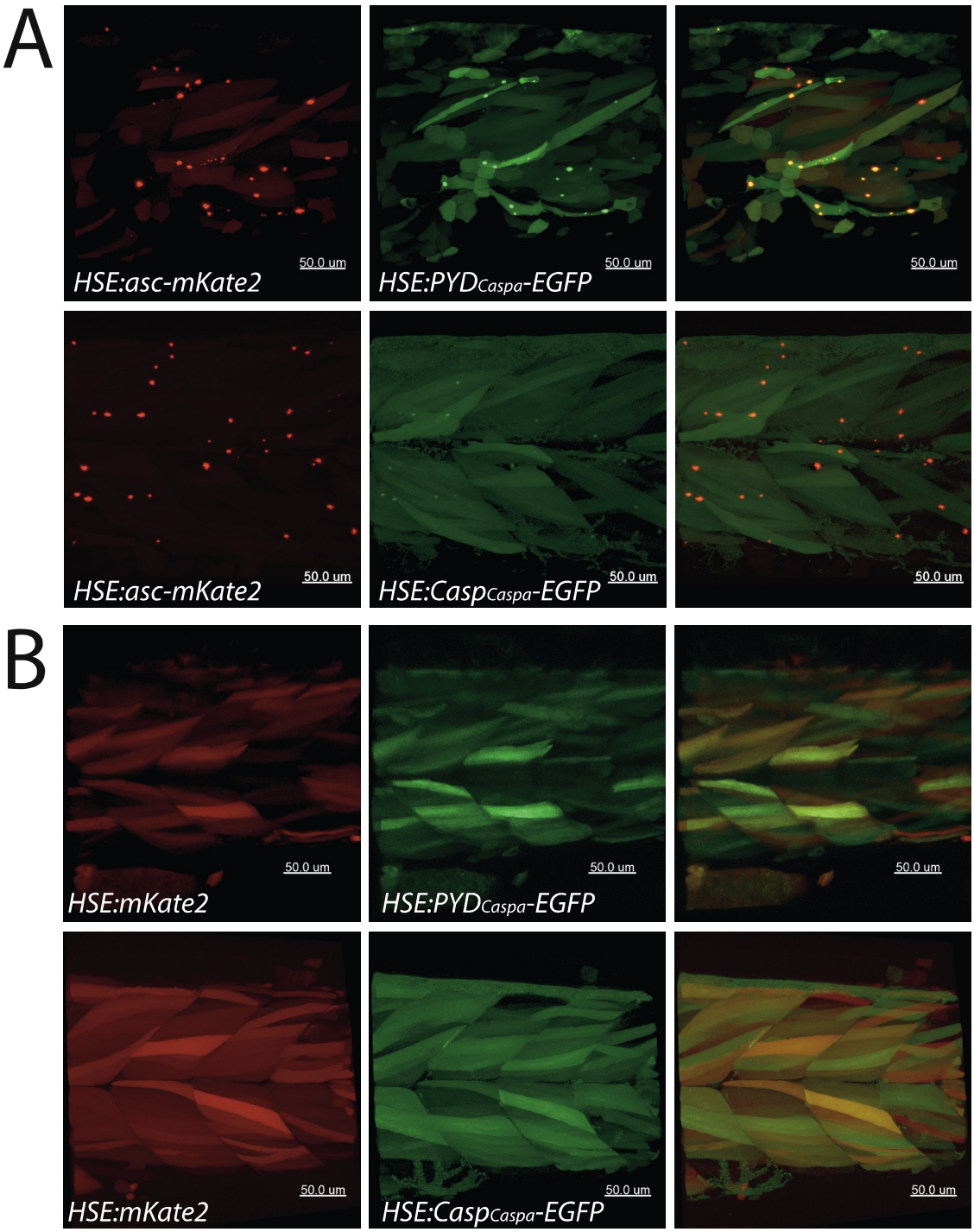

Figure III.1.19. Caspa is recruited to ASC speck through a PYD-PYD interaction.
Imaging of heat-shock induced transient expression of *HSE:asc-mKate2* with *HSE:PYD$_{Caspa}$-EGFP* and *HSE:Casp$_{Caspa}$-EGFP*. The only domain in Caspa required for recruitment to the speck is PYD$_C$ [A]. Imaging of heat-shock induced transient expression of *HSE:mKate2* with *HSE:PYD$_{Caspa}$-EGFP* and *HSE:Casp$_{Caspa}$-EGFP*, showing that both constructs have a cytoplasmic cellular localization [B].

7.4.5 Caspa is expressed in the epidermis

For Caspa to be the downstream effector driving pyroptotic cell death in the epidermis it would need to be expressed by these cells. To determine the endogenous expression pattern of *caspa*, we performed an *in situ* hybridization on 3dpf zebrafish larvae (Fig. III.1.20A). Similar to the expression pattern we had observed for *asc* (Fig. III.1.1B), *caspa* is strongly expressed in the area of the gills and mouth and in the intestinal area. We also saw expression, albeit at low levels, in epidermal cells covering the main body of the fish and in fins, but no expression in muscle cells (Fig. III.1.20B). This suggests that Caspa in epidermal cells could be a downstream effector of pyroptosis after speck formation, where as muscle cells, lacking Caspa, do not undergo cell death upon speck formation.

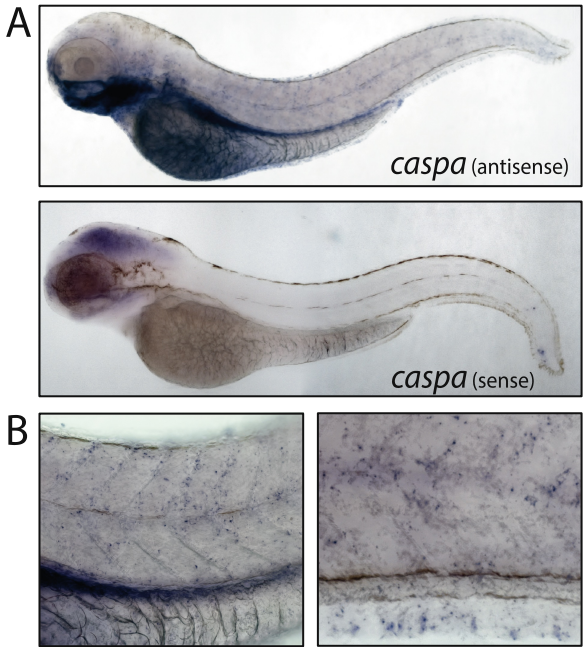

Figure III.1.20. *caspa* is expressed in the epidermis.
caspa in situ hybridization (*is*h) in 3dpf zebrafish larvae. Sense probe is used as a negative control [A]. Magnification of *caspa wish* showing expression in epidermis and ventral fin [B].

7.4.6 Generation of a *caspa* CRISPR mutant

To test whether *caspa* is necessary to drive cell death after speck formation in epidermal cells we generated a zebrafish knockout using CRISPR/Cas9. We generated two different small guide RNAs (sgRNAs) targeting the first exon of the *caspa* gene, *caspa* Guide 1 and 2 (Fig. III.1.21A).

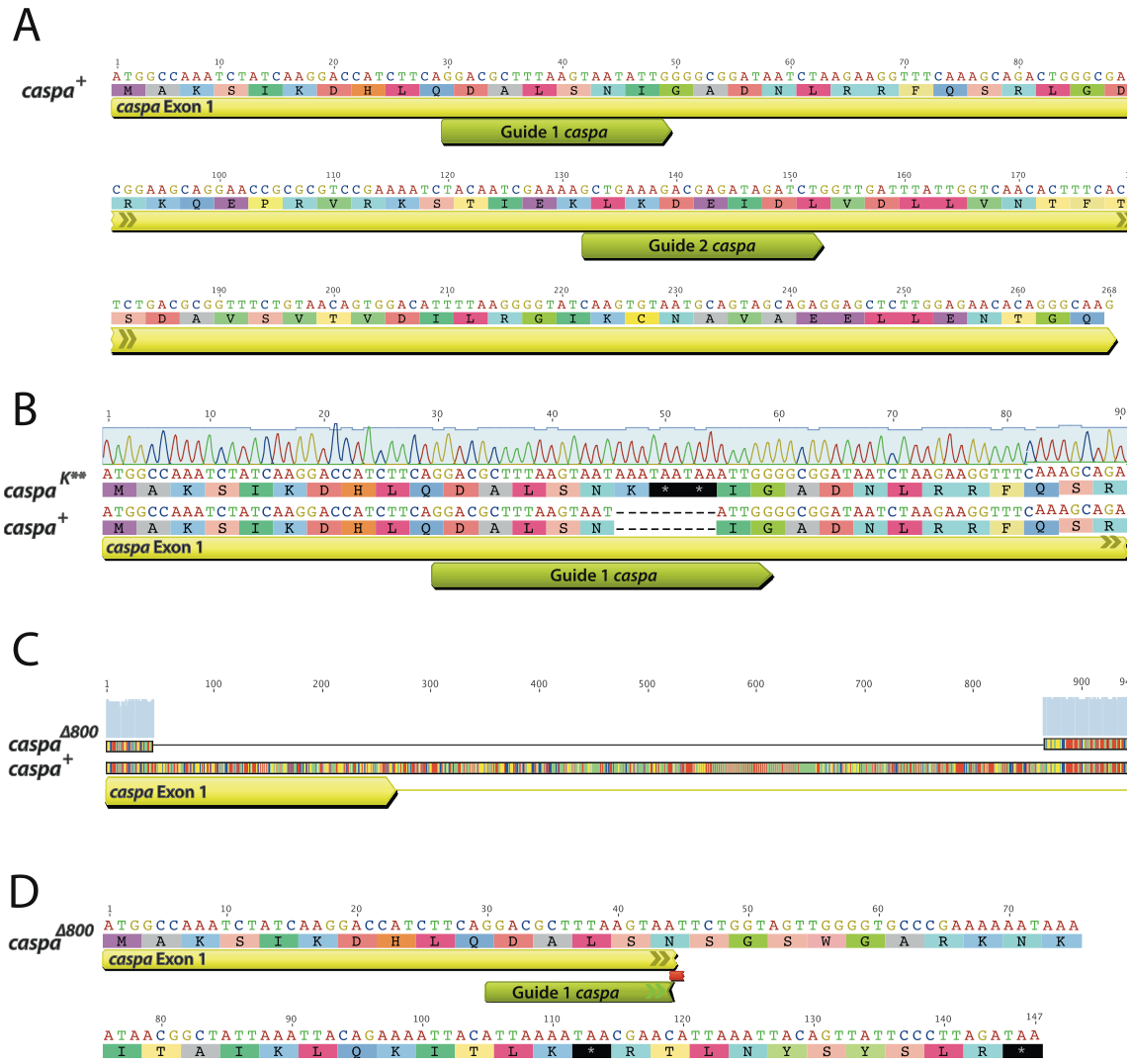

Figure III.1.21. Generation of two *caspa* mutant alleles by use of CRISPR-Cas9.
Sequence of first exon of *caspa* gene (yellow) showing target sites of two sgRNAs, Guide1 and Guide 2 *caspa* (lime green), designed using the online tool at http://crispr.mit.edu [A]. Sequence of first *caspa*$^{-}$ allele after genotyping F1 of incross between *caspa* Guide1-injected F0, *caspa*^{K**}. NHEJ led to insertion of 9 base pairs resulting in the addition of one lysine (K) and two STOP codons in the *caspa* reading frame [B]. Sequence of second mutant allele, *caspa*$^{\Delta 800}$, which lacks an 800bp fragment that includes 224bp of Exon 1 and the first 596bp from Intron 1 [C]. The translation of *caspa*$^{\Delta 800}$ results causes a frame shift and the insertion of a STOP codon after 37aa[D].

To test whether the sgRNAs were effectively targeting *caspa*, we performed injection trials with either sgRNA. The injection of both sgRNAs led to mutations in the *caspa* gene. *Caspa* Guide 1 was much more efficient and caused mutations in 75% of injected embryos vs. 25% of injected embryos in the case of *caspa* Guide 2. We therefore raised embryos injected with *caspa* Guide 1 (F0). Adults from the F0 were genotyped by tail fin clipping and those with detected mutations were incrossed to give rise to F1, which were

also raised to adulthood. Adults from F1 were genotyped to find mutant alleles. We found several F1 adults that carried two different *caspa* alleles that resulted in a knockout of the protein, which we named *caspa*^{K**} and the *caspa*$^{\Delta 800}$ alleles. In the case of the *caspa*^{K**}allele, a 9 bp insertion resulted in the introduction of two STOP codons in the reading frame (Fig. III.1.21B), which would result in either early degradation of the mRNA or the production of a truncated protein of 16 amino acids (aa). The *caspa*$^{\Delta 800}$ allele (Fig. III.1.21C) corresponds to a large deletion spanning the last 224bp of Exon 1 and the first 596bp from Intron 1. This deletion results in the translation of product that is truncated after 37 aa. The first 15 aa correspond to *caspa*, but the last 22 are entirely different (Fig. III.1.21C). Therefore, the adult F1 fish carrying these two alleles were already *caspa* loss of function mutants (*caspa*^{K**}/*caspa*$^{\Delta 800}$). We detected no obvious phenotypes resulting from the knock down. To obtain F2 mutants homozygous for the *caspa*^{K**}and the *caspa*$^{\Delta 800}$ alleles (*caspa*^{K**}/*caspa*^{K**} and *caspa*$^{\Delta 800}$/*caspa*$^{\Delta 800}$), the *caspa*^{K**}/*caspa*$^{\Delta 800}$ F1 fish were incrossed and the F2 generation was raised to adulthood.

7.5 Endogenous speck formation

Thus far, all the experiments in which ASC was misexpressed in the zebrafish larvae led to speck formation in both epidermal and muscle cells. Although we found no defined threshold of ASC-mKate2 concentration that needs to be surpassed for a cell to form a speck (Fig. III.1.8B), it is probable that the process is concentration-dependent since all the methods used to visualize speck formation up to this point rely on the addition of more copies of the gene or increasing amounts of mRNA. This was true for all cell types observed, including the ones that do not endogenously express *asc*. That the additional layer of expressed protein is driving the speck formation process could also explain why we do not observe specks with immunostainings, although a technical issue cannot be discarded. In order to find out whether the endogenous ASC can form specks we followed two approaches: immunostainings of larvae after an inflammatory stimulus and the generation of a transgenic CRISPR knock-in line.

7.5.1 Immunostainings of larvae after inflammatory stimuli do not show specks

To test whether endogenous ASC forms specks as a response to inflammatory stimuli we first performed immunostainings of larvae that had been subjected to UVB exposure (Banerjee and Leptin, 2014) or tail fin wounding (de Oliveira et al., 2013; Ogryzko et al., 2014a). Both have been reported to activate interleukin-1 signaling in fish, which is connected to inflammasome signaling. Furthermore, both assays target epidermal cells directly, one through direct injury and another one by causing DNA damage.

UVB treatments were performed on the *krt4:GFP* line, in order to be able to visualize the damage to the external layer of epidermal cells (EVL) directly. Embryos were fixed for immunostaining at several time-points after irradiation. We saw the strongest tissue damage at 24hpt (Fig. III.1.22A), with cells losing their normal shape, stretching along the AP axis and appearing to adopt the shape of the muscle tissue underneath instead of forming a smooth layer. A further indication of epidermal cell damage is the cellular debris at the surface and the fact that some patches of epidermis lacked GFP expression, but had normal ASC expression (Fig. III.1.22A, white arrowheads). In spite of the evident damage, however, we could not detect any clear cases of speck formation. Although we observed certain cases where a spot was seemingly labeled by antiASC; in the midst of a high amount of cellular debris, it is impossible to confirm whether the spot actually corresponds to a speck.

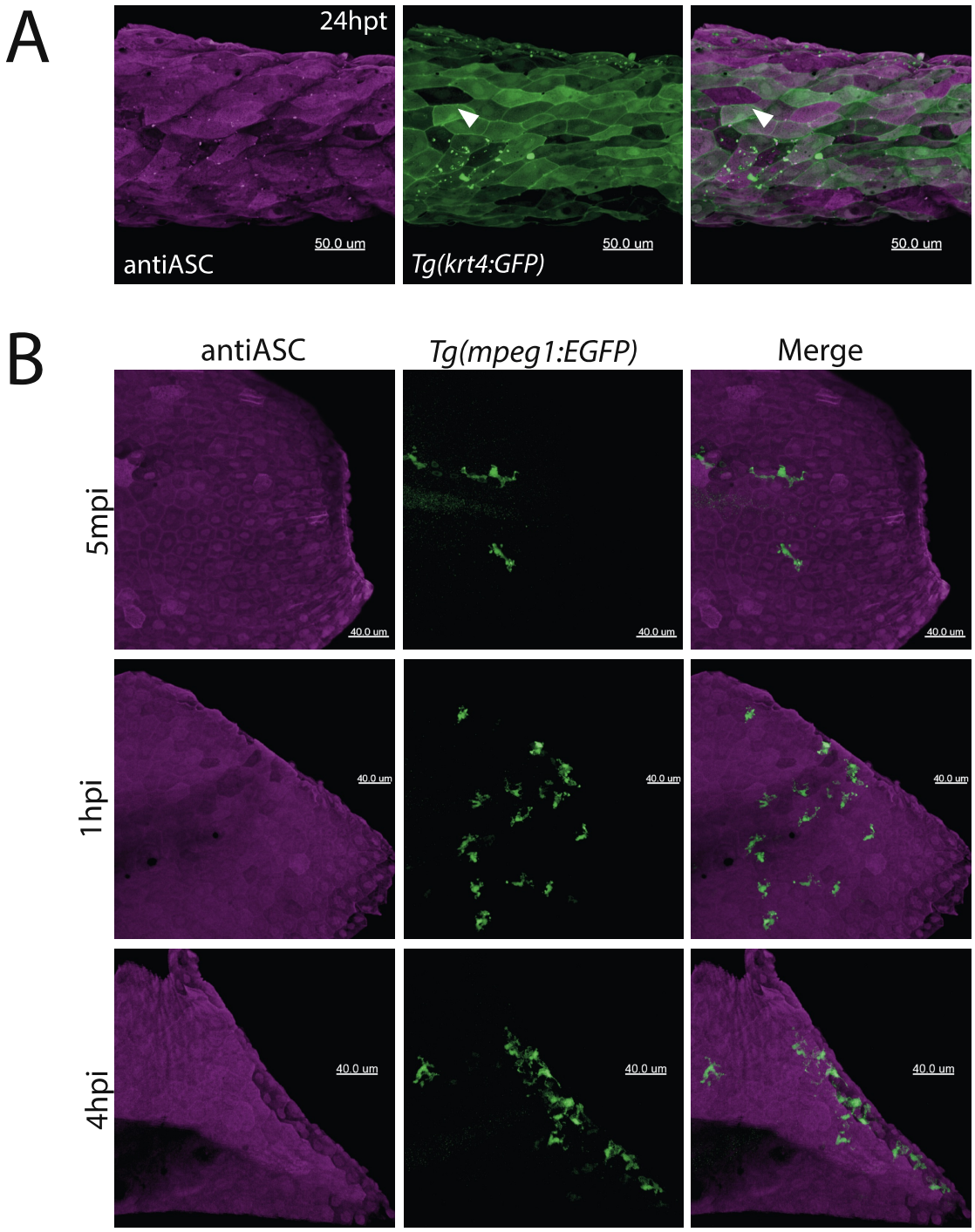

Figure III.1.22. Endogenous specks are not detected in immunostainings of larvae after inflammatory stimuli.
AntiASC immunostaining of *krt4:GFP* transgenic larva at 4dpf, 24h after UVB irradiation. Although the overall morphology of the epidermis is abnormal and debris is visible, no specks were observed [A]. AntiASC immunostaining of *mpeg:EGFP* transgenic larva at several time-points (5 min, 1h and 4h) after tail fin wounding [B]. Recruitment of macrophages to the site of injury increases with passing time, but no specks are observed [B].

We then turned to a second assay, fin tail wounding. Because it was previously reported (Ogryzko et al., 2014a) that this type of assay results in

recruitment of both macrophages and neutrophils to the site of injury in an interleukin-1 signaling-dependent manner, we used the *mpeg1:EGFP* line to visualize macrophage recruitment to the injury site. Larvae were fixed for immunostaining at several time-points after injury (Fig. III.1.22B). We observed increased recruitment of macrophages after the injury. However, we did not detect any signs of speck formation either in epithelial cells or in macrophages.

7.5.2 Generation of an *asc:asc-EGFP* CRISPR knock-in line via homologous recombination

To visualize endogenous speck formation live, we inserted a *linker-EGFP* sequence into the endogenous *asc* locus by CRISPR/Cas9 genome editing (Auer and Del Bene, 2014). The exogenous DNA was inserted while leaving all intronic sequences as well as the 3'UTR of the *asc* gene intact. We used a previously published method for both sgRNA and donor vector design (Stemmer et al., 2015). The CCTop CRISPR/Cas9 target online predictor was used to design sgRNAs targeting the 3' end of the protein. Two sgRNAs whose predicted cleavage site was located upstream of the STOP codon were found suitable, Guide 1 and Guide 2 *asc* (Fig. III.1.23A).

We tested whether the sgRNAs could successfully target the genomic locus. Trial injections with only sgRNAs and Cas9 showed that Guide 2 *asc* successfully targeted the region in close to 100% of injected embryos, whereas Guide 1 *asc* had an efficiency of close to 70%. We therefore used only Guide 2 *asc* for further injections.

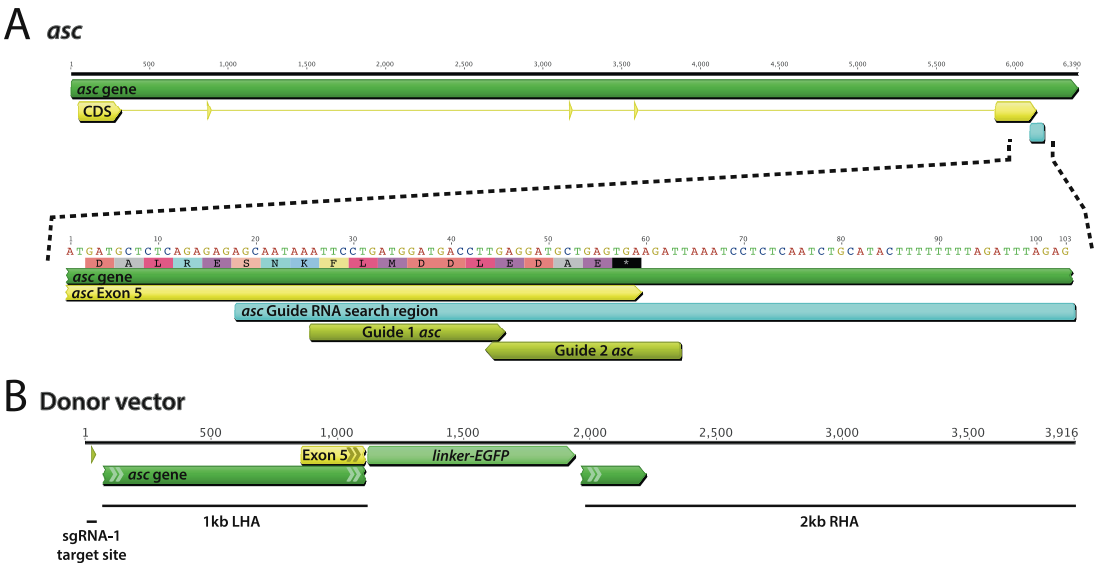

Figure III.1.23. Design of sgRNAs and donor vector for endogenous tagging of *asc*.
Diagram of full *asc* gene (green) with exons (yellow) showing region chosen to search for candidate sgRNAs (teal) using the online design tool at http://crispr.cos.uni-heidelberg.de. Chosen sgRNAs, Guide1 and Guide 2 *asc* (lime green) are located at the end of the gene's last exon [A]. Donor vector was designed included 1 and 2kb left and right homology arms (LHA and RHA) flanking a linker-*EGFP* CDS. The homology arms ended (LHA) or started (RHA) at the predicted cutting site for Guide 2 *asc* sgRNA [B].

The DNA insertion was carried out by homology directed repair. This method relies on coinjecting a donor vector in which two homology arms (for the 5′ and 3′ ends) flank a linker sequence upstream of a fluorescent protein. Following an approach for donor vector design published previously (Hisano et al., 2015), we designed homology flanks specific to Guide 2 *asc*, meaning that homology flanks extended up to the cutting site of Cas9 specific for the sgRNA used. The total length of the two the 5′ and 3′ homology flanks was 1kb and 2kb in length, respectively (Fig. III.1.23B). The 5′ homology flank covered a genomic region that included the last exon, whereas the 3′ region covered that of the 3′ UTR of *asc* and part of the 3′ UTR of a second gene on the opposite strand, *scn1b* (ENSDARG00000070170). Because it has been seen that recombination is more efficient when the donor vector is linearized *in vivo* by Cas9 after injection (Irion et al., 2014), we included the sgRNA-1 target site (Stemmer et al., 2015) for linearization upstream of the 5′ homology flank (Fig. III.1.23B, green arrowhead). All elements were assembled in the final donor vector using the Golden GATEway cloning system (Kirchmaier et al., 2013) (a more detailed description on the donor vector cloning strategy is

available in Materials and Methods). The final donor vector was injected in combination with Cas9 and the sgRNAs (Guide 2 *asc* to target the genomic locus and sgRNA-1 to linearize the donor vector). At 2dpf embryos were screened for those with GFP expression pattern reflected that of the *asc* mRNA and protein (Fig. III.1.1 and 1.2). We observed some embryos with patchy expression of GFP in the epidermis in an extremely low ratio. In total, we obtained approximately one positive embryo for every 150 injected, although the success rate varied, occasionally being as high as 1 in 50 or with no positive embryos found at all. Due to the low number of embryos with GFP expression we abstained from genotyping at this stage and instead raised all positive F0 fish to adulthood.

7.5.3 The GFP expression in the *asc:asc-EGFP* CRISPR knock-in line reflects RNA and protein expression pattern

The F1 was screened for positive integration in the germline by outcrossing the F0 adults with wild type fish. We obtained one founder whose progeny with GFP expression was approximately 30%. We tested for successful integration by amplifying the region containing the Guide 2 *asc* sgRNA target site. Amplification of the wild type allele would yield a PCR product of 260bp, whereas amplification of an allele where recombination had been successful would give a longer 1.1kb product containing the 850bp corresponding to the GFP and the linker sequences. Indeed, we observed that GFP positive embryos contained both alleles, whereas GFP negative embryos were homozygous for the wild type allele (Fig. III.1.24A). Sequencing of the 1.1kb PCR product (Fig. III.1.24B) confirmed that the fragment corresponded to the *linker-EGFP* tag from the donor vector inserted via homologous recombination in the genome (Fig. III.1.23B).

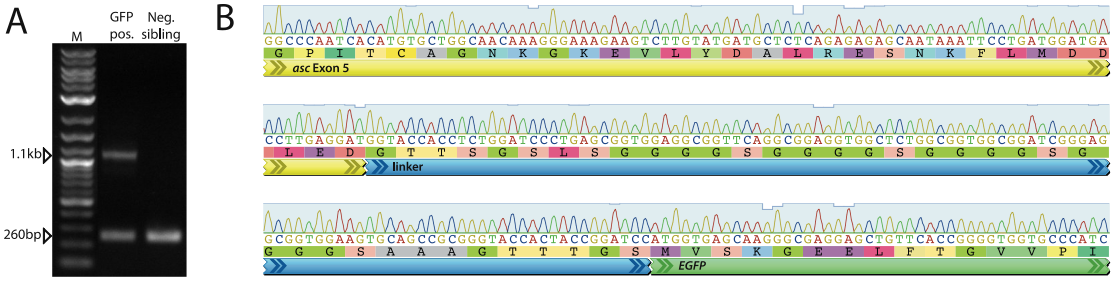

Figure III.1.24. Genotyping of F1 progeny of *asc:asc-EGFP*.
F0 was outcrossed and F1 progeny, screened based on GFP expression, was genotyped via PCR by using primers flanking the Guide 2 *asc* sgRNA target site. Amplification of the wild type allele yields 260bp product, whereas amplification of *asc:asc-EGFP* allele results in a 1.1kb product containing the 850bp linker-*GFP* sequence [A]. Sequence of the 1.1kb *asc:asc-EGFP* allele PCR product [B].

After genotyping, we imaged the larvae at different stages to visualize the endogenous expression pattern of *asc* (Fig. III.1.25 and 1.26). We observe expression of *asc-EGFP* throughout the entire epidermis from 1dpf (Fig. III.1.25A). Expression is seen also at 2dpf (Fig. III.1.25B and C), 3dpf (Fig.1.26A and A') and 5dpf (Fig. III.1.26B). At all stages examined, muscle cells never express *asc*, as can be seen in a sagittal sections of the 3dpf larva (Fig. III.1.25C and 1.26C). The protein has both a cytoplasmic and nuclear localization (Fig. III.1.25B') and is expressed in epithelial tissues that were also seen to express *asc* mRNA as judged by *is*h, such as gills (Fig. III.1.25C') and intestine (Fig. III.1.26C'). Furthermore, we also observe cells in the brain that were also strongly expressing GFP (Fig. III.1.26C''), again reflecting the mRNA expression pattern.

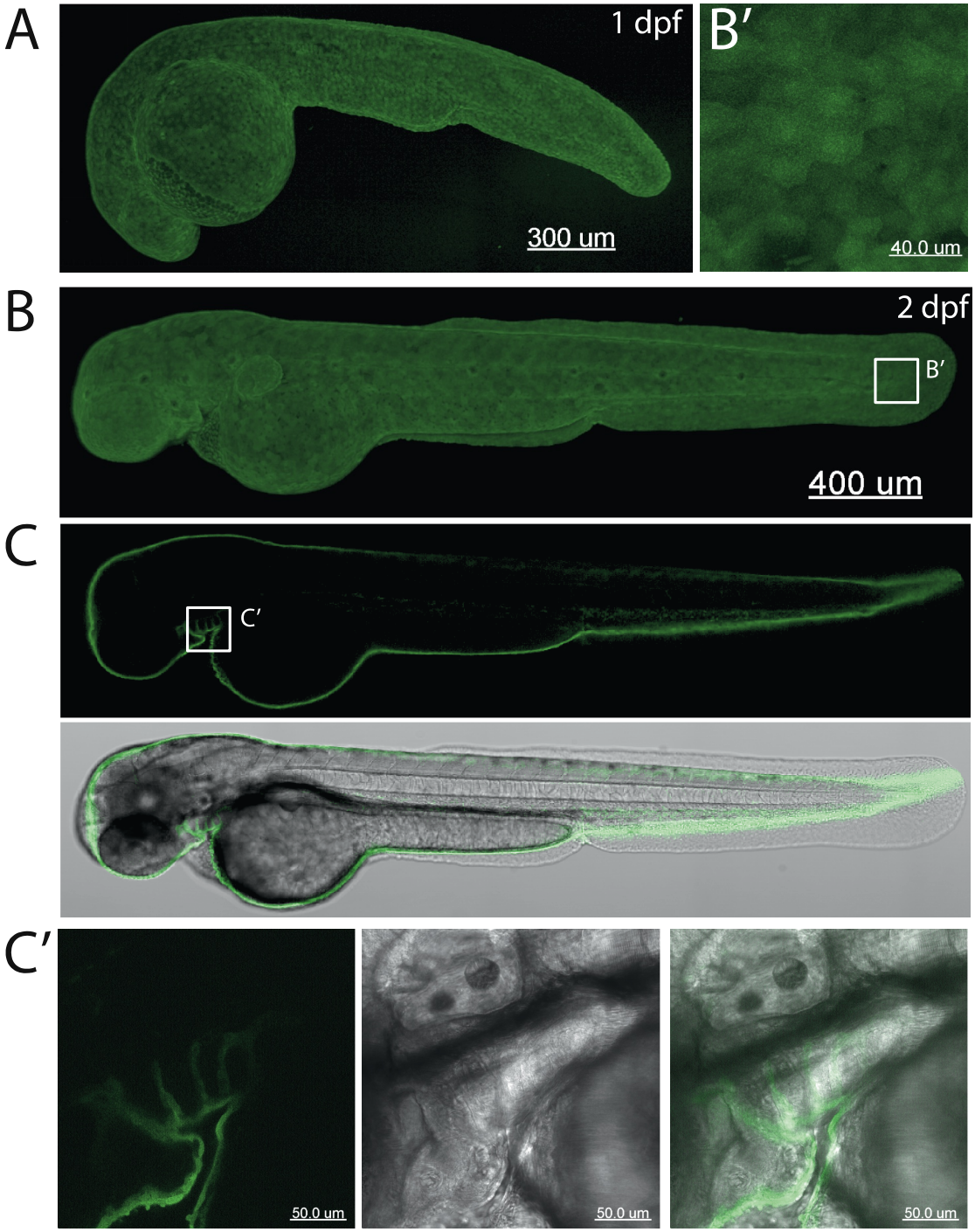

Figure III.1.25. ***asc:asc-EGFP*** **shows expression in epidermis at 1 and 2dpf.**
Live imaging of *asc:asc-EGFP* F1 during early development showing expression patterns at 1dpf [A] and 2dpf [B]. Imaging epidermal cells shows ASC-GFP localizing also to the nucleus of epidermal cells [B′]. Optical sagittal section of 2dpf larva showing no expression in muscle cells [C] and expression in the pharyngeal branches [C′].

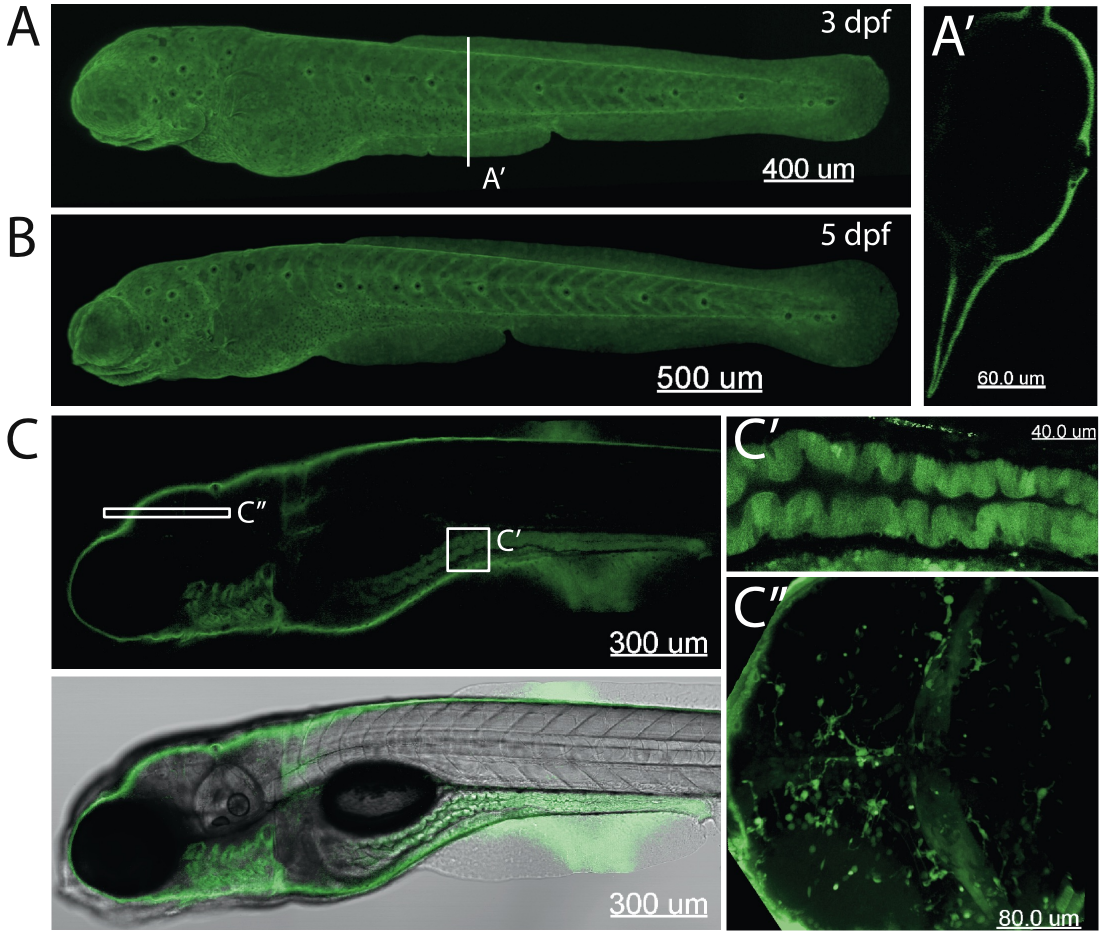

Figure III.1.26. Epithelial tissues show expression of *asc:asc-EGFP*.
Live imaging of *asc:asc-EGFP* F1 shows expression patterns of larvae at 3dpf [A] and 5dpf [B]. Optical cross section of 3dpf larvae showing expression in epidermis also in dorsal and ventral fins [A′]. Optical sagittal section of 5dpf larva [C] showing expression in intestine [C′]. Transversal optical sectioning of the brain showing expression pattern in the head [C′′].

To determine whether myeloid cells were GFP positive in the *asc:asc-EGFP* line, we crossed the founder with the *pU1:tagRFP* line and imaged the offspring at 3dpf. We observed that myeloid cells labeled by the *pU1:tagRFP* line coexpressed GFP. These included microglia (Fig. III.1.27A), macrophages (judging by morphology) in the muscle tissue (Fig. III.1.27B) and myeloid cells in the caudal hematopoietic tissue (CHT, Fig. III.1.27C). In the CHT, we observed other cells that expressed *asc*, but were not labeled by *pU1* (Fig. III.1.27C, white arrowhead).

Overall, the observed GFP expression pattern confirms the antiASC immunostaining showing that myeloid cells in the *pU1:tagRFP* contain ASC protein (Fig. III.1.4A and B).

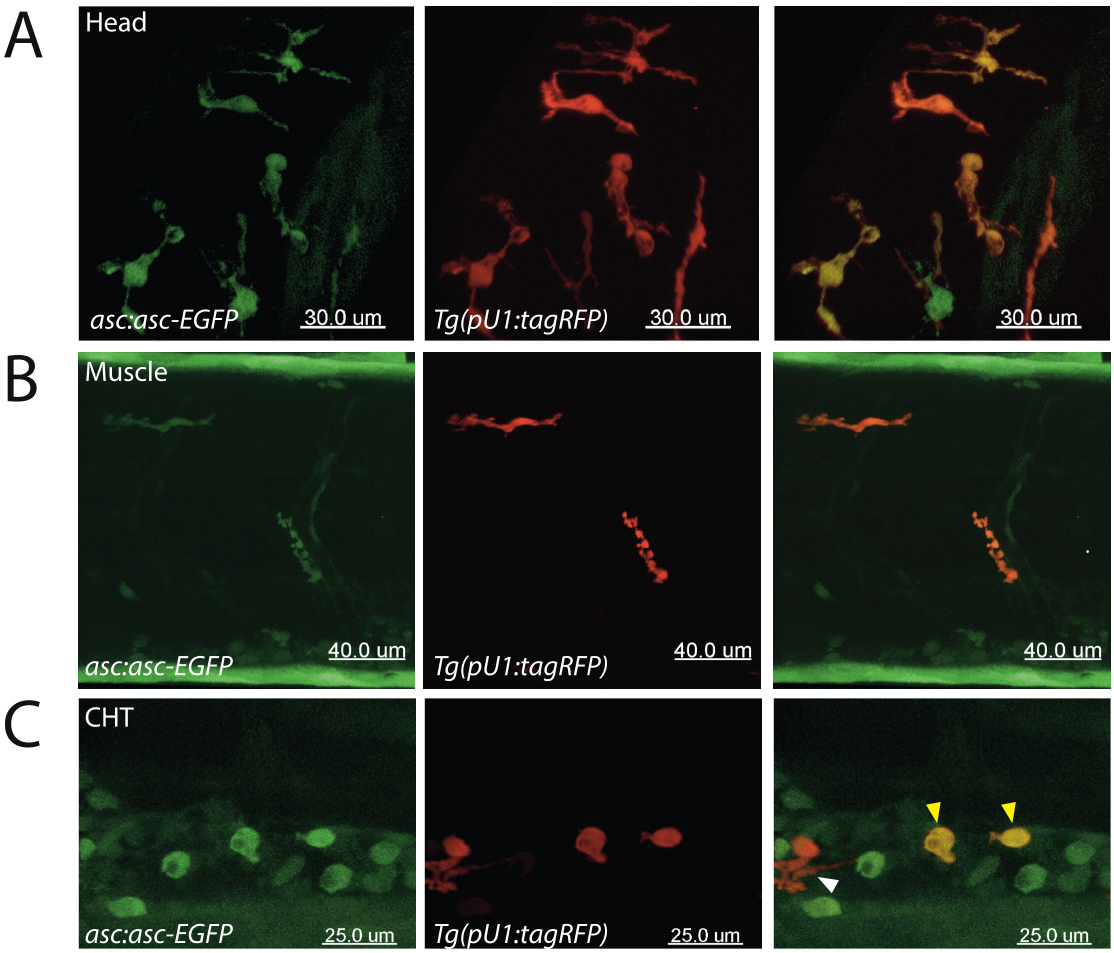

Figure III.1.27. Myeloid cells express *asc-EGFP*.
Live imaging of a 3dpf *asc:asc-EGFP, pU1:tagRFP* transgenic larva in the head region shows coexpression in microglial cells [A] and macrophages in muscle tissue [B]. Imaging the CHT region revealed some myeloid cells expressing high levels of *asc* (yellow arrowheads) whereas in others *asc* expression was barely detectable (white arrowhead). Other cells in the CHT that were not tagRFP positive were also seen to express *asc* [C].

7.5.4 Specks in the *asc:asc-EGFP* CRISPR knock-in line happen concomitantly with cell death

While imaging the *asc:asc-EGFP* line, we noticed the occasional appearance of GFP specks without any experimental stimuli. Upon closer examination, we observed that, without exception, specks were contained in what appear to be dead or dying cells in the epidermis as shown in the bright-field (Fig. III.1.28A). A time-lapse of the events following one case of speck formation (Fig. III.1.28B) showed that the speck is contained within the seemingly dying cell. Afterwards, the appearance of a second cell

surrounding it is visible in the bright-field (Fig. III.1.28B, yellow arrowhead). The cells remain in contact until the dying cell collapses (Fig. III.1.28B, orange arrowhead). Afterwards, the speck seems to shrink and disappear. We observed specks appearing also in epidermal cells in fins. The example in Fig. III.1.28C (first time-point), shows a speck inside a dying cell in the dorsal fin. We again followed the events by time-lapse imaging and saw that after a period of time in which the speck remains in the vicinity of the dead cell, the speck seems to fade and disappear (Fig. III.1.28D, yellow arrowhead). The reason for speck formation in these examples is unclear. These events confirm that speck formation happens in zebrafish with endogenous levels of ASC and that it leads to cell death. The causes leading to speck formation can now be further studied using our newly developed *in vivo* model.

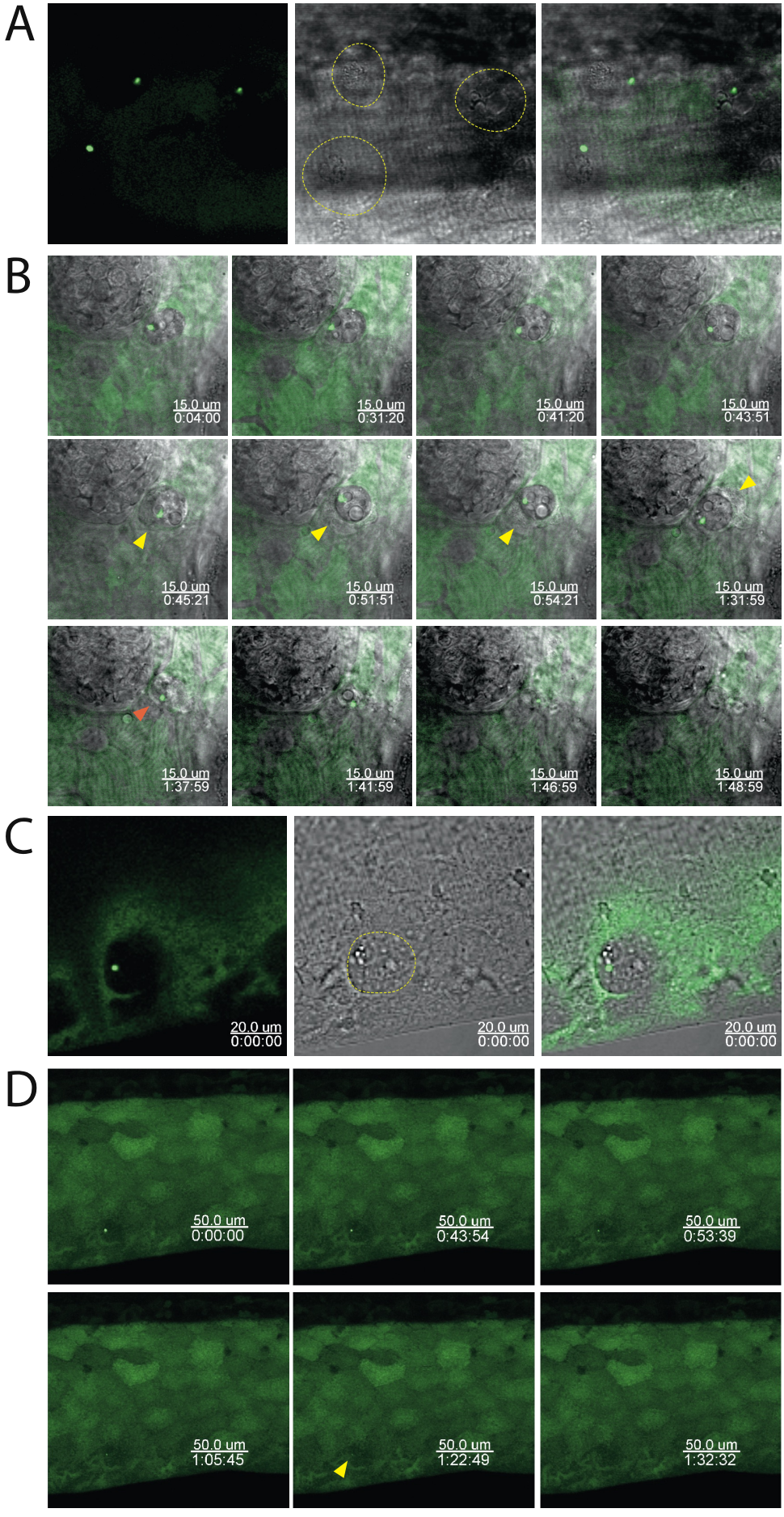
A
B
15.0 um
0:04:00
15.0 um
0:31:20
15.0 um
0:41:20
15.0 um
0:43:51
15.0 um
0:45:21
15.0 um
0:51:51
15.0 um
0:54:21
15.0 um
1:31:59
15.0 um
1:37:59
15.0 um
1:41:59
15.0 um
1:46:59
15.0 um
1:48:59
C
20.0 um
0:00:00
20.0 um
0:00:00
20.0 um
0:00:00
D
50.0 um
0:00:00
50.0 um
0:43:54
50.0 um
0:53:39
50.0 um
1:05:45
50.0 um
1:22:49
50.0 um
1:32:32

Figure III.1.28. Speck formation occurs *in vivo*.
Live imaging of the dorsal region of 3dpf *asc:asc-EGFP* larva where three specks have formed. Merge with bright-field plane shows all specks are within a cell displaying altered morphology (circled by a yellow dashed line) [A]. Time-lapse imaging of an epidermal cell after speck formation. A single plane merged with the bright-field to display cell features is shown. Yellow arrowheads highlight a cell that approaches the one containing a speck and appears to engulf it over the course on almost an hour. Orange arrowhead shows degradation of the cell body, which marks the subsequent disappearance of the speck [B]. Example of speck formation in dorsal fin, shown in a single plane merged with the bright-field. The speck-containing cell displays altered morphology (circled by a yellow dashed line). Time-lapse of cell in [C] in 3D rendering, showing speck slowly fading 90 min after movie start [yellow arrowhead, D].

8 Interleukin-1

The hallmark of inflammasome activation in mammals is the release of the mature form of IL-1β after it is cleaved by caspase-1. We therefore set out to characterize Interleukin-1 in fish to understand its role as an inflammatory cytokine in the context of what is known about the two *Il1* paralogues in mammals, *Il1α* and *β*. This project was carried out using medaka (*Oryzias latipes*).

8.1 Teleost fish Interleukin-1 orthologues lack conserved caspase-1 cleavage site

Humans and mice, where interleukins are well characterized, have two paralogues of the *Il1* gene, *Il1α* and *Il1β*. The divergence of these genes form a single locus roughly coincides with the emergence of mammals. IL-1 family members have been described in fish, however, there is no evidence that the expansion of the IL-1 locus (that includes *Il1α* and *Il1β*, among other genes) also took place in fish (Ogryzko et al., 2014b). Regardless, because *il1* genes in fish possess an IL-1 family signature and have an overall higher homology to IL-1β than IL-1α, they have generally been considered orthologues of the latter (Bird et al., 2002; Ogryzko et al., 2014b).

It has been previously reported that the caspase-1 cleavage site, which in mammalian pro-IL-1β is located after an aspartic acid residue in exon 5, is not revealed by sequence alignments analysis of the corresponding regions in mammalian and fish IL-1 (Huising et al., 2004; Secombes et al., 2011). To test

whether the reported cleavage site for IL-1α was conserved in fish IL-1, we performed alignments using the protein sequences of both IL-1 mammalian paralogues (in their immature forms) and available IL-1 sequences from a number of teleost fish species (Fig. III.2.1). As previously reported (Bird et al., 2002), the alignment showed that the cleavage site of pro-IL-1β (Fig. III.2.1, aspartic acid in red) is not conserved in any of the IL-1 sequences of fish species included in the analysis. However, the reported calpain cleavage site for pro-IL-1α (Fig. III.2.1, serine in blue) is conserved in most analyzed sequences, including both medaka and zebrafish. This led us to hypothesize that *il1* in fish, instead of being the functional orthologue of either mammalian *Il1α* or *Il1β*, retained genetic and functional characteristics of the ancestral il1 that gave rise to both paralogues during the mammalian IL-1 family expansion.

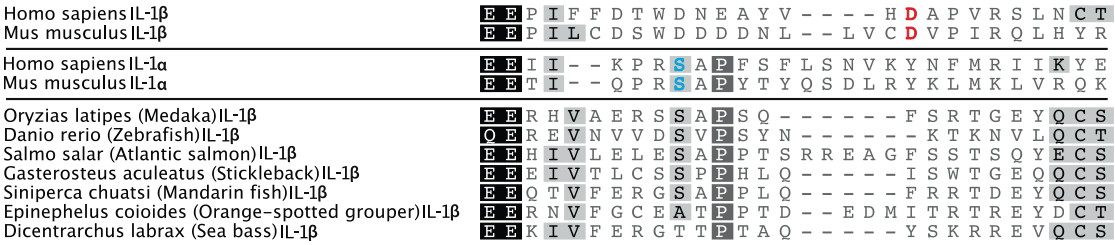

Figure III.2.1. Conservation of mammalian Interleukin-1 cleavage sites in fish.
Fragment of alignment of protein sequences from human and mouse IL-1α and IL-1β with IL-1 sequences from various species of teleost fish. Cleavage site of IL-1β is printed in red (D, aspartic acid) and that of IL-1α in blue (S, serine). Alignment by Baubak Bajoghli.

8.2 The expression of *interleukin 1* in medaka larvae is both constitutive and inducible

In mammals, *Il1α* is expressed constitutively in epithelial layers whereas *Il1β* expression is induced in myeloid cells such as monocytes, macrophages and dendritic cells as a response to inflammatory stimuli (Garlanda et al., 2013a). To test whether *il1* in medaka was constitutively expressed and/or inducible, we used two approaches. We first examined the expression pattern of the gene in medaka. *In situ* hybridization on naïve medaka embryos, showed that expression of *il1* is not detectable at this stage. However, infection of the embryo with bacteria (*Escherichia coli*) leads to an

upregulation that is detectable using the same assay (Fig. III.2.2).

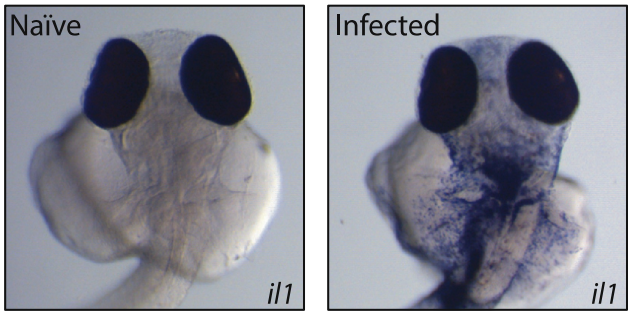

Figure III.2.2. Induced, but not basal, expression of *il1* is detectable by *in situ* hybridization in medaka larvae. *In situ* hybridization of 6dpf medaka larvae in a naïve situation and after bacterial injection. Expression of *il1* is only detected in the latter. Experiment performed by Baubak Bajoghli.

Second, to track the spatiotemporal induction of *il1* after an inflammatory stimulus live, we generated a transgenic reporter line for the gene. The *il1:EGFP-t2a-il1-HA* vector used to generate this line is depicted Fig. III.2.3A. We used the 7kb region upstream of the *il1* CDS as promoter and inserted an *EGFP* directly downstream. The expression of GFP is a proxy for the transcriptional activation of *il1*. To determine whether the protein is being cleaved *in vivo*, we included the *il1* CDS tagged with a C-terminal HA downstream of the *EGFP*. The two sequences were separated by a T2A sequence to produce two separate proteins (Provost et al., 2007).

The *il1:EGFP-t2a-il1-HA* transgenic line expressed GFP from very early in development, namely the blastula stage (Fig. III.2.3C). To corroborate the early expression of the gene we performed a RT-PCR on cDNA produced from morula, blastula, 1dpf and 2dpf medaka wild type embryos (Fig. III.2.3B). The gene is indeed endogenously expressed from the blastula stage, and present at 1 and 2dpf, indicating that the temporal expression of the *il1:EGFP-t2a-il1-HA* transgenic line reflects that of the endogenous gene. Transgenic larvae showed a basal level of expression in the epidermis as well as in specific organs such as the gills, intestine and thymus (Fig. III.2.3D).

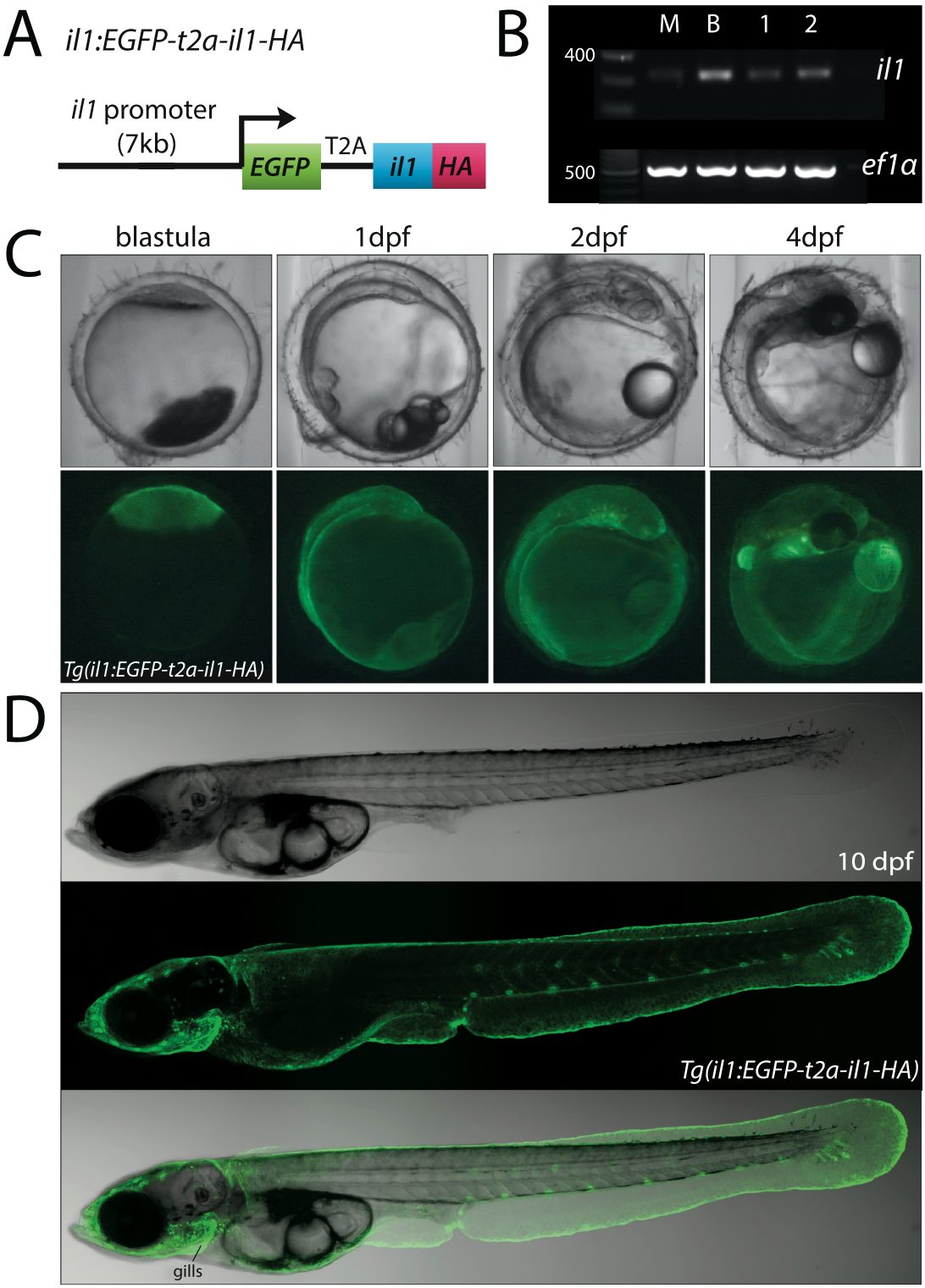

Figure III.2.3. The *il1:EGFP-t2a-il1-HA* transgenic reporter line shows endogenous expression pattern of *il1* in medaka larvae.
The 7kb region upstream of the *il1* transcriptional start site drives expression of *EGFP* and the *il1* CDS tagged C-terminally with HA with a T2A sequence in between [A]. RT-PCR of *il1* during early developmental stages: morula (M), blastula (B), 1 dpf (1) and 2dpf (2). *ef1a* is used as housekeeping gene control [B]. Live imaging of the *il1:EGFP-t2a-il1-HA* line showing endogenous expression patterns at early developmental stages [C]. At 10dpf *il1:EGFP-t2a-il1-HA* transgenic larvae shows expression in the epidermis and gills [D].

We tested whether the *il1:EGFP-t2a-il1-HA* reporter would respond to inflammatory stimuli. We used the tail fin wounding assay (de Oliveira et al., 2013; Ogryzko et al., 2014a) in medaka larvae (Fig. III.2.4A). Time-lapse imaging after the insult revealed a strong activation in the area surrounding the cut 6 hours after injury. The induction continues to increase with more elapsed time, indicating the inducibility of the reporter and therefore of *il1*. We next tested another localized injury by injecting bacterial lipopolysaccharides (LPS) directly into the muscle tissue (Fig. III.2.4B) and performing time-lapse imaging. Because LPS induces *il1* in zebrafish larvae (Novoa et al., 2009; Watzke et al., 2007), we tested whether it would result in an increased *in vivo* response of the reporter. As a control we injected PBS (Fig. III.2.4C). After PBS injection activation began at 7.5 hours after injection and after LPS at 6 hours after injection. This indicates that the injury sustained during injection itself is sufficient to activate *il1*. However, LPS does cause a heightened response, with larger numbers of cells in the surroundings showing *il1* activation. The muscle cells immediately adjacent to the site of injury do not activate *il1* (Fig. III.2.4D). Because myeloid cells can be a major source of *il1* activation in zebrafish (Banerjee and Leptin, 2014), it is possible that the induction we see corresponds to myeloid cells drawn to the site of injury and activating *il1* expression.

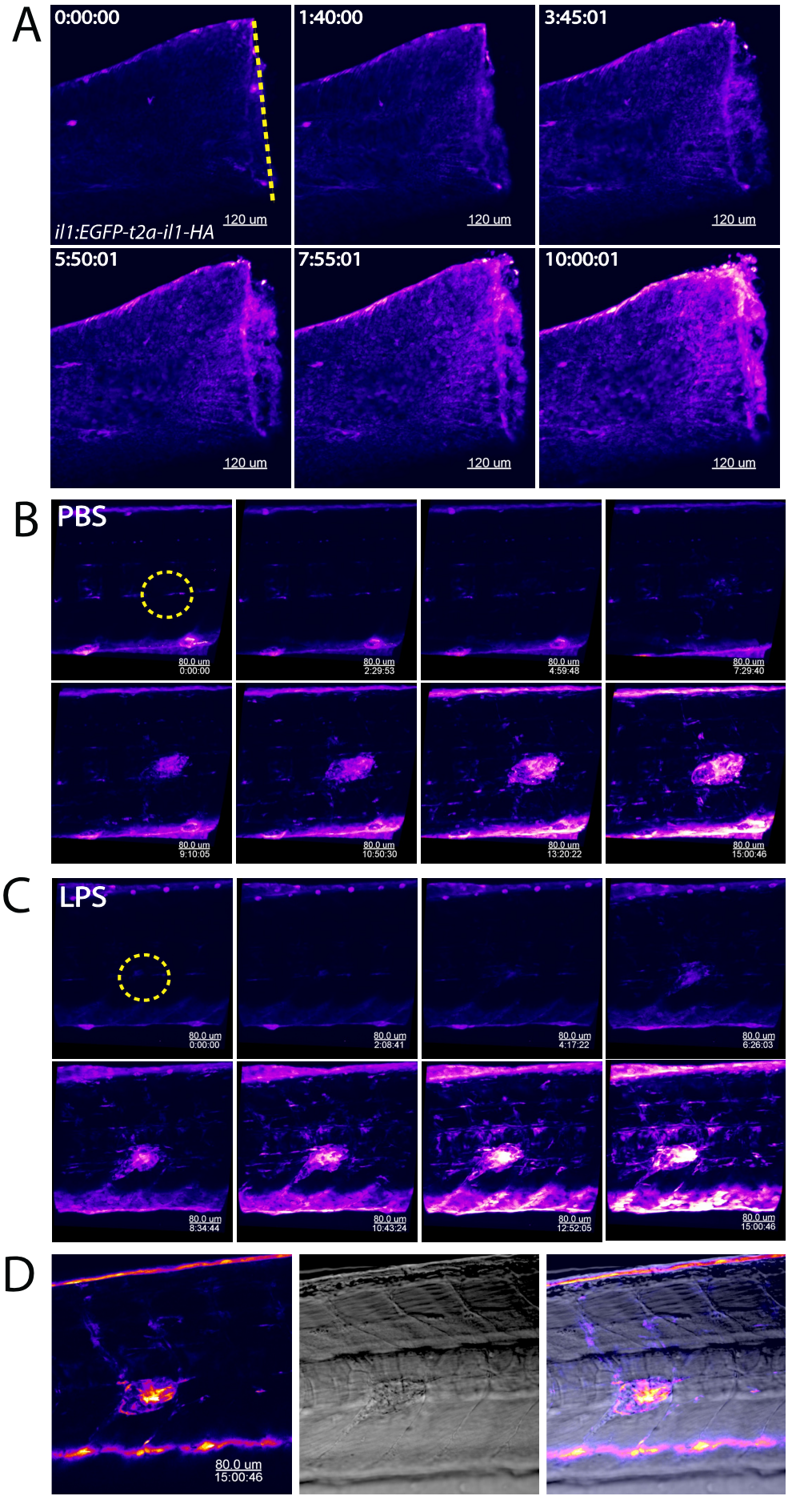
A
0:00:00
1:40:00
3:45:01
il1:EGFP-t2a-il1-HA
120 um
5:50:01
7:55:01
10:00:01
B
PBS
C
LPS
D
80.0 um
15:00:46

Figure III.2.4. Expression of *il1* is induced in reporter line as a response to injury.
Time-lapse imaging of an *il1:EGFP-t2a-il1-HA* transgenic larvae after tail fin wounding, cut is depicted by a dashed yellow line. [A]. Time-lapse imaging of an *il1:EGFP-t2a-il1-HA* transgenic larvae after injection of PBS [B] or LPS [C]. Single plane of last time-point from LPS injection time-lapse is merged with the bright-field [D]. In all images, green channel is displayed using a color lookup table.

Thus far, our experiments show that *il1* is inducible after an insult and that the *il1:EGFP-t2a-il1-HA* reporter line recapitulates this inducibility. Furthermore, the reporter line also revealed *il1*'s endogenous expression pattern, showing that there is constitutive expression of the gene in the epidermis that is below the *is*h detection limit.

8.3 Adult myeloid cells express *interleukin 1*

To test whether *il1* expression was constitutive and/or inducible in myeloid cells, we used flow cytometry of samples from medaka adults. As an inflammatory stimulus, adults were first injected intraperitoneally with fluorophore-conjugated *E. coli*. Blood, spleen and head kidneys were collected 16 hours post infection (hpi). We saw that close to 6% of all cells in blood samples constitutively expressed GFP. No GFP^+ cells were found on wild type controls (Fig. III.2.5A, left and middle panels). In blood samples from injected fish, one fifth of this population became double positive (RFP^+/GFP^+) indicating that fluorescent bacterial were phagocytized *in vivo*. The GFP^- fraction remained unchanged (Fig. III.2.5A, right panel). That no RFP^+/GFP^- cells were found suggests that all phagocytic cells in the blood constitutively express *il1*. When blood samples were gated for myelomonocytic cells (Fig. III.2.5B, left panel), the percentage of GFP^+ cells increased to more than 70% of the total population, indicating that myelomonocytic cells represent a major fraction of the cells constitutively expressing *il1* in the blood (Fig. III.2.5B, middle panel). Furthermore, in blood samples from injected fish, we observed that the GFP^+ myelomonocytic population slightly increased suggesting these cells can upregulate *il1* upon inflammatory insult (Fig. III.2.5B, middle panel).

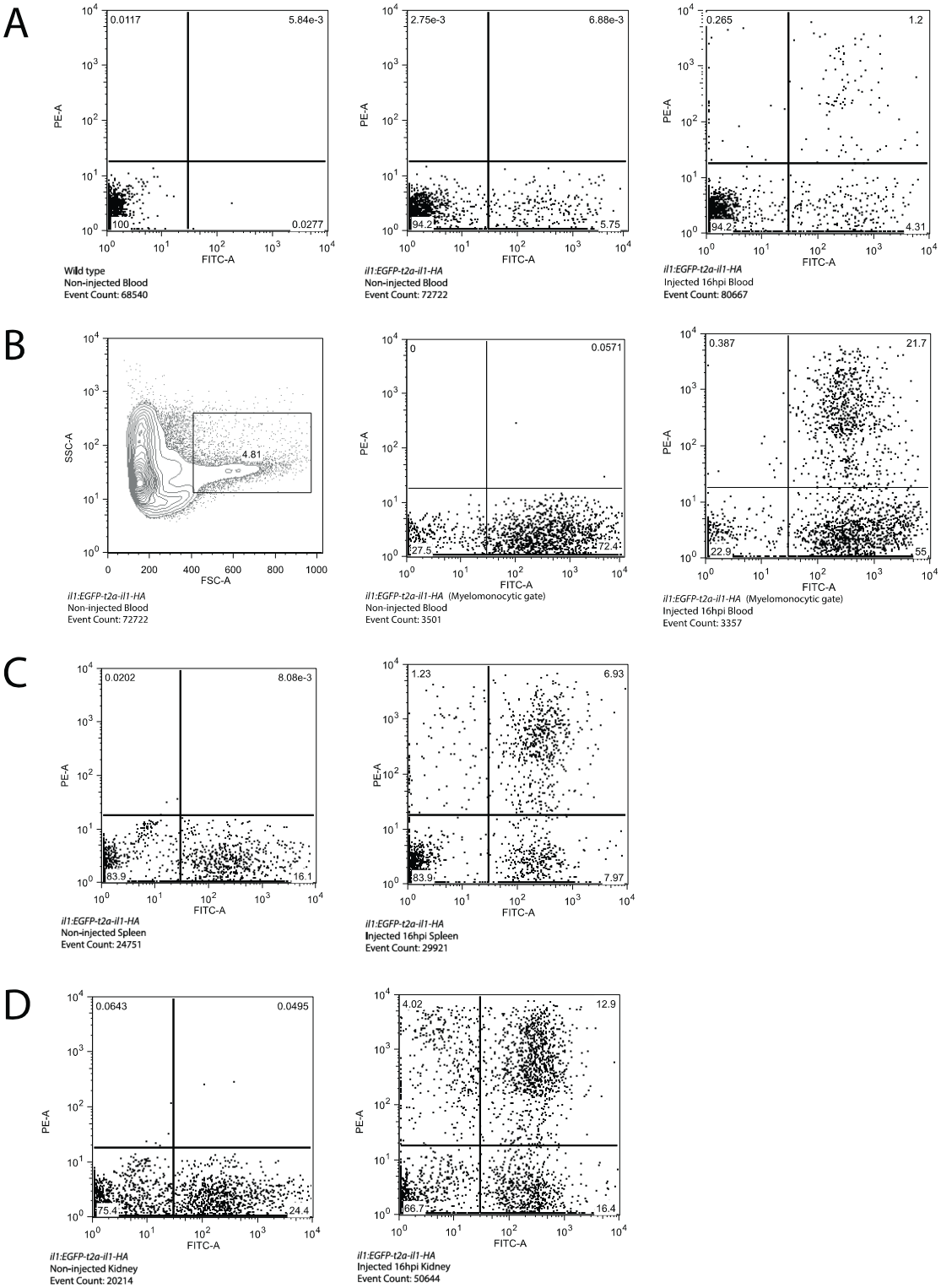

Figure III.2.5. Myeloid cells in adult induce *il1* expression after inflammatory stimuli.
Single cell suspensions of blood [A], spleen [C] and head kidney [D] collected from medaka *il1:EGFP-t2a-il1-HA* adults 16h after intraperitoneal injection with red fluorescent *E. coli* were analyzed by flow cytometry with non injected and wild type controls. Cells are plotted according to GFP (FITC axis) and red (PE-A) fluorescence intensity. Cells in right quadrants express *il1*. Cells in the top quadrants engulfed red-labeled bacteria. The myelomonocytic cell population was gated according to forward (FSC-A) and side (SSC-A) scatter [B].

We found that the spleen and kidney had a higher ratio of GFP^+ cells than the blood (Fig. III.2.5C and 2.5D, respectively), with one out of every 4 cells being GFP^+ in the kidney. Injecting the fish with bacteria resulted in a 20% increase in the GFP^+ population in the kidney, indicating that the gene is constitutively expressed but also inducible in this organ. In contrast to blood samples, both spleen and kidney GFP^+ and GFP^- fractions were able to engulf bacteria, suggesting that a phagocytic cell type that does not express *il1* is absent in the blood but is present in both these organs.

Overall, the experiments confirm that *il1* is constitutively expressed in some adult cell types and that the expression increases upon inflammatory stimuli.

8.4 Medaka IL-1 is cleaved *in vivo*

Treatment of mammalian cells *in vitro* with the K^+ ionophore nigericin results in cleavage of both IL-1α and IL-1β cleavage whereas treatment with the Ca^{2+} ionophore, ionomycin, results only in cleavage of IL-1α (Groß et al., 2012). To test if we could detect cleavage of the IL-1HA, we treated *il1:EGFP-t2a-il1-HA* and wild type larvae as controls with either nigericin or ionomycin. The drug was added directly to the water and protein lysate samples were collected after 30 min of exposure. To visualize cleavage we performed an immunoblot using antiHA (Fig. III.2.6A). We detected a band of 31kDa corresponding to the full-length IL-1-HA as well as a band of around 60kDa corresponding to the GFP-T2A-IL-1-HA protein. Given that it has been reported that the cleavage of the T2A peptide is not 100% efficient in zebrafish (Kim et al., 2011), this was expected. Both bands were absent in the wild type controls. Upon addition of ionomycin and to a slightly lesser extent, nigericin at a concentration of 10µm, two bands of lower molecular weight appeared in the antiHA blot, of around 20 and 18kDa. These bands were absent in the wild type sample, suggesting that they correspond IL-1-HA whose N-terminal domain is cleaved off in two different sites. Because the ratio of the cleaved to immature IL-1-HA was extremely low, we included a pretreatment with LPS to induce activation of *il1* and increase the ratio of cleaved protein,

as is frequently done in *in vitro* experiments (Groß et al., 2012) (Fig. III.2.6B). Samples pretreated with LPS showed greater induction of the reporter, as shown by the increase in antiGFP signal. However, this increase did not directly translate into a higher ratio of the cleaved fragments to immature IL-1-HA.

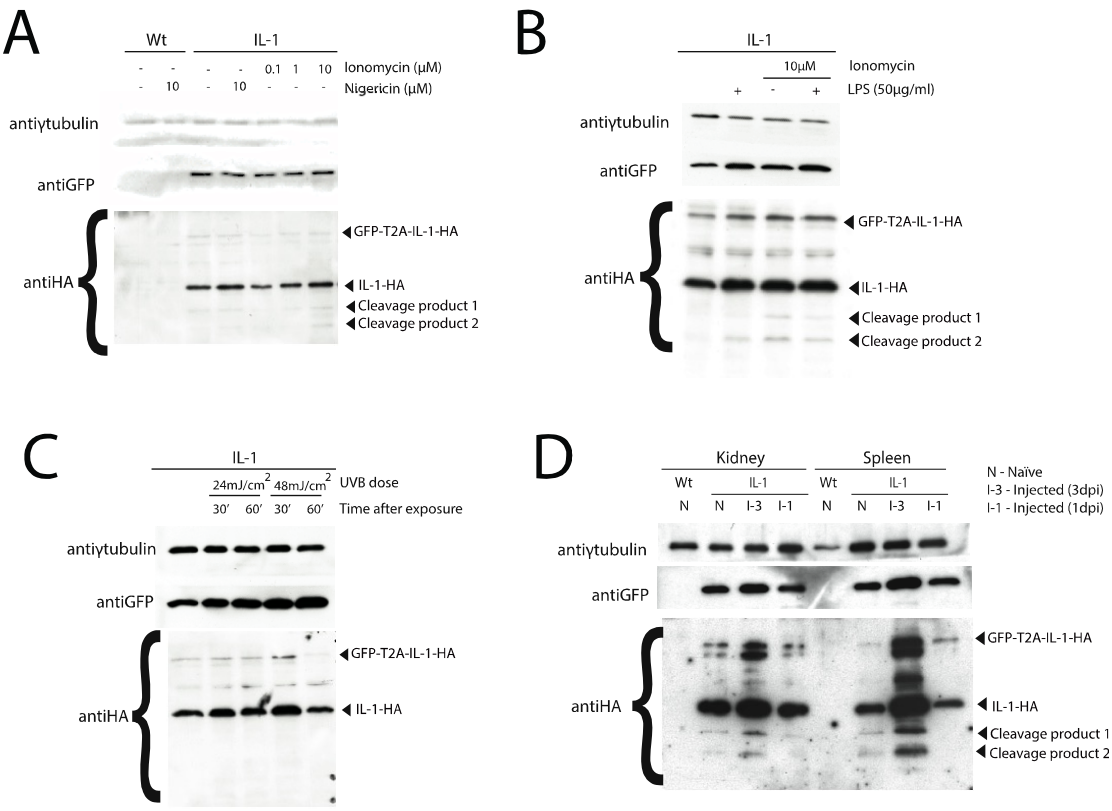

Figure III.2.6. IL-1-HA is cleaved *in vivo* after exposure to inflammatory stimuli.
Immunoblots of protein lysates of 10-14dpf *il1:EGFP-t2a-il1-HA* medaka larvae after a 30 min treatment with nigericin or ionomycin in the concentrations shown. Wild type larvae were used as negative controls. γtubulin is used as loading control. Possible cleavage products of IL-1 appear in antiHA blot as bands of lower molecular than the full-length IL-1-HA, these and the band corresponding to protein GFP-T2A-IL-1-HA are highlighted by black arrowheads [A]. Immunoblots of protein lysates of 10-14dpf *il1:EGFP-t2a-il1-HA* medaka larvae exposed to 3 hours of LPS pretreatment followed by 30 min of 10 μM ionomycin treatment [B]. Immunoblots of protein lysates of 10-14dpf *il1:EGFP-t2a-il1-HA* medaka larvae exposed to 3 hours of LPS pretreatment followed by 30 min of 10 μM ionomycin [B]. Immunoblots of protein lysates of 10-14dpf *il1:EGFP-t2a-il1-HA* medaka larvae exposed to either 24 or 48 mJ/cm² of UVB irradiation, 30 or 60 min after exposure. No cleavage of IL-1-HA was observed at the selected time-point after insult [C]. Immunoblots of head kidney and spleen protein lysates of *il1:EGFP-t2a-il1-HA* medaka adults collected 1 (I-1) or 3 (I-3) days after intraperitoneal injection with *E. coli*. Wild type samples were used as negative control [D].

Because we had seen that the epidermis expresses *il1* constitutively, we hypothesized that an inflammatory treatment that affects these cells directly might lead to IL-1-HA cleavage in a higher ratio than what we had observed with ionophore treatment. Since UVB irradiation leads to increase in *il1* expression in zebrafish larvae (Banerjee and Leptin, 2014) we chose this inflammatory stimulus. We used two doses of irradiation and collected the samples 30 and 60 min after treatment (Fig. III.2.6C). The UVB treatment did lead to an induction of il1 expression, but we could not detect the cleaved fragments in these samples.

We therefore suspected that the cleavage was not taking place in epidermal cells, but in other cell types constitutively expressing *il1*. Since we had seen that these cell types could be found in adult blood, spleen and head kidneys (Fig. III.2.5), we tested if we could detect cleaved fragments in these organs. We again used intraperitoneal bacterial injection to induce an inflammatory response and, because we had seen the largest GFP^+ populations in spleen and kidney (Fig. III.2.5C and 2.5D) we collected these organs 1 and 3 days post injection (dpi) (Fig. III.2.6D). Expression of *il1* was induced in both organs strongly at 3dpi, especially in the spleen. This increased expression also translated into a higher concentration of both cleaved fragments, which had the same molecular size as those appearing in whole larva lysates. Taken together, these experiments suggested that IL-1-HA was being cleaved *in vivo* as a response to inflammatory stimuli both in medaka larvae and adults.

8.5 IL-1-HA cleaved fragments can be immunoprecipitated and their identity confirmed by MS

To confirm the identity of the cleaved fragments we decided to use Mass Spectrometry (MS). Given that the entire proteome is too complex a sample to analyze by MS, we first enriched for the proteins of interest via immunoprecipitation (IP) using beads covalently bound to antiHA antibody. This allowed us to recover both the full-length IL-1-HA and the cleaved fragments. Because we had seen the highest ratio of cleaved fragments to full-

length IL-1-HA in adult spleens collected from fish injected with bacteria (Fig. III.2.6D), we used this sample for an IP. As a negative control we used lysate from a spleen collected from a wild type fish (Fig. III.2.7A). To avoid antibody contamination from the beads, the sample was eluted with HA peptide. We assessed the efficiency of elution by boiling the beads ("beads sample") to visualize the protein that remained bound after HA peptide elution. Both cleaved fragments and the full-length IL-1-HA were present in the eluate, thus showing that the fragments were specifically bound by HA antibodies. We could no longer detect GFP or γtubulin in the eluted fraction showing that unspecific binding was minimized. We detected some full-length IL-1-HA in the beads sample, indicating that the elution method was not 100% efficient. However, because using HA peptide meant avoiding contamination from the antibody in the beads (Fig. III.2.7A, red dash), we did not switch to a more aggressive elution method. We proceeded with MS using the eluate sample. To confirm the identity of the full-length IL-1-HA and the cleaved fragments separately, eluates were separated by SDS-PAGE and stained with Coomassie (Fig. III.2.7B). Coomassie is an insensitive staining method, but we could nonetheless detect both the full-length and the cleaved fragments. The gel was cut to separate the section containing the full-length IL-1-HA and the cleavage products (Fig. III.2.7B, black lines) and samples were subsequently processed separately for MS. The MS results from these "Upper" and "Lower sections" are depicted in Fig. III.2.7C. Also depicted are results from MS using the full eluate without SDS page separation. Each colored block represents a peptide detected. We identified peptides belonging to IL-1HA in all samples, but only the full eluate contained a peptide belonging to GFP. This confirmed the identity of the cleaved fragments, since full-length IL-1HA would not be present in the lower section of the gel. We also noticed that the peptide containing the predicted cleavage site of IL-1-α was present in both the full eluate and the upper section, but absent from the lower section. This could suggest that the cleavage site is within the region containing amino acids 81-113, but further experiments would be required to confirm this.

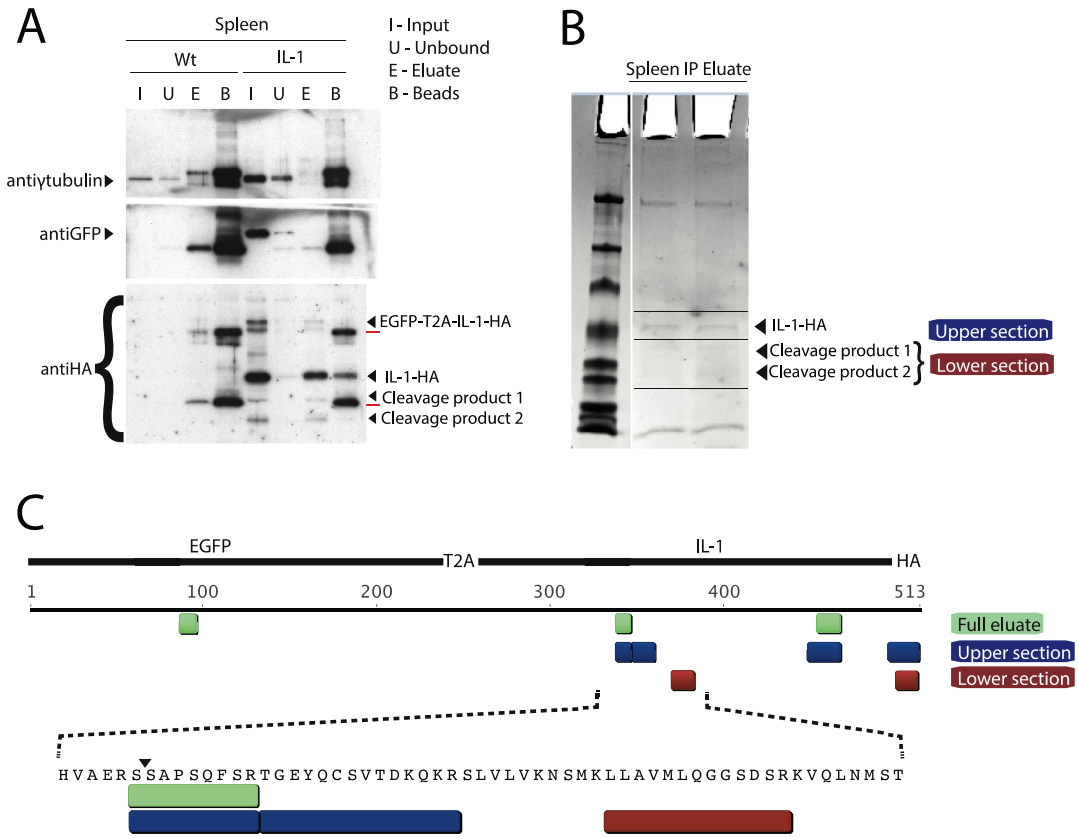

Figure III.2.7. Immunoprecipitation of cleavage products and identification by MS. Immunoblot of immunoprecipitation using antiHA-conjugated sepharose beads of protein lysates of spleen samples of *il1:EGFP-t2a-il1-HA* medaka adults collected 3 days after intraperitoneal injection with *E. coli*. Bound fraction (E) was eluted using HA peptide, bead sample (B) was obtained by boiling beads after elution. Red lines show unbound antiHA antibody (light and heavy chain) originating from beads [A]. Coomassie stain of SDS-PAGE containing elution sample from spleen antiHA immunoprecipitation. Black lines mark gel sections that were analyzed separately with mass spectrometry. "Upper section" contains full-length IL-1-HA and "Lower section" the cleaved fragments. A "Full elute" sample corresponding to the eluate not separated by SDS-PAGE was also included. [B]. MS results showing identified peptides marked by colored blocks for each sample: full eluate (green), upper section (blue) and lower section (red). Peptides corresponding to IL-1 were found in all samples, but in the "lower section" peptides identified correspond to sections of the protein downstream of the conserved IL-1α (SSAPS) cleavage site [C].

Overall, the combination between IP and MS strengthen the claim that the fragments detected correspond to cleaved products of IL-1HA, produced in response to inflammatory stimuli *in vivo*.

9 NF-κB

After the mature forms of IL-1α or IL-1β are secreted from the cell, they can bind to IL-1 receptors in neighboring cells. This activates a signaling cascade that eventually leads to the translocation of NF-κB to the nucleus, thus activating the expression of proinflammatory genes, including that of *il1* itself. Therefore, as an additional and more general tool to visualize and quantify the immune response live we generated a reporter line for the activation of NF-κB. This project was carried out in zebrafish.

9.1 The NF-κB zebrafish reporter shows endogenous activation

A previous study addressing the DNA-binding properties of different NF-κB dimers found a high-affinity palindromic binding sequence for a diverse combination of dimers using a an NF-κB-specific protein-binding microarray (Siggers et al., 2012). To generate a new more sensitive NF-κB reporter, we used an 8x multimer of this sequence (5'-GGGAATTCCC-3') as a promoter upstream of an *EGFP* in one strand and a *Renilla* luciferase gene (*luc*) on the other (Fig. III.3.1). The simultaneous induction of a fluorescent protein and the luciferase gene would allow the activation of NF-κB to be visualized by live imaging and also to be quantified (*nfκb:EGFP,luc*).

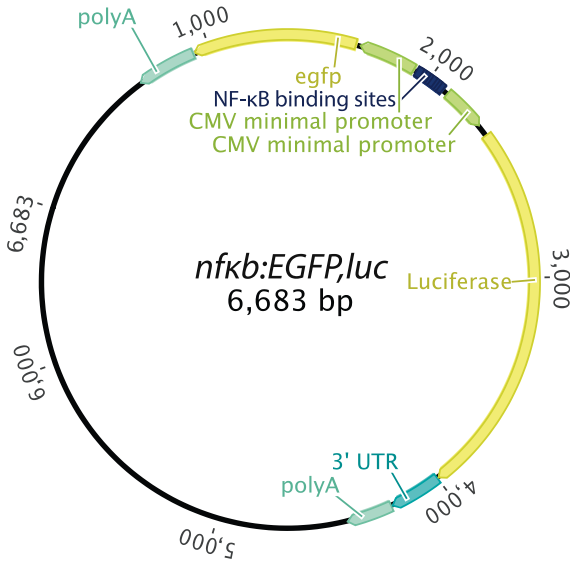

Figure III.3.1. Map of *nfκb:EGFP,luc* NF-κB binding sites (8 multimers of 5'-GGGAATTCCC-3') are located between the *Renilla* luciferase and *EGFP* CDS, located on opposing strands. Each reporter gene also has a CMV minimal promoter immediately upstream.

We generated a transgenic zebrafish line using this construct. We identified a founder, outcrossed it and then incrossed the F1. We raised these fish and imaged their progeny and that of the next generation (F2 and F3) (Fig. III.3.2A-E). The *nfκb:EGFP,luc* line allowed us to visualize the endogenous pattern of NF-κB activation during early development. The strongest early expression appeared at 1dpf (Fig. III.3.2A, white arrowhead), in two symmetric groups of neurons in the head, which likely correspond to the olfactory placodes (Whitlock and Westerfield, 2000). The activation of the reporter at 2dpf was reduced in the olfactory placodes and the lateral line, the proctodeum and epithelial cells around the edges of the fins became positive (Fig. III.3.2B). This expression pattern remained at 3dpf (Fig. III.3.2C), with the activity in cells lining the proctodeum (which will become the anal passage) increasing (Fig. III.3.2C'). By 5dpf (Fig. III.3.2D), we observed that in addition to the signal remaining in the lateral line, fins and proctodeum; cells in the intestinal lining became positive (Fig. III.3.2D). This activation coincides with the stage in which the larva begins to feed.

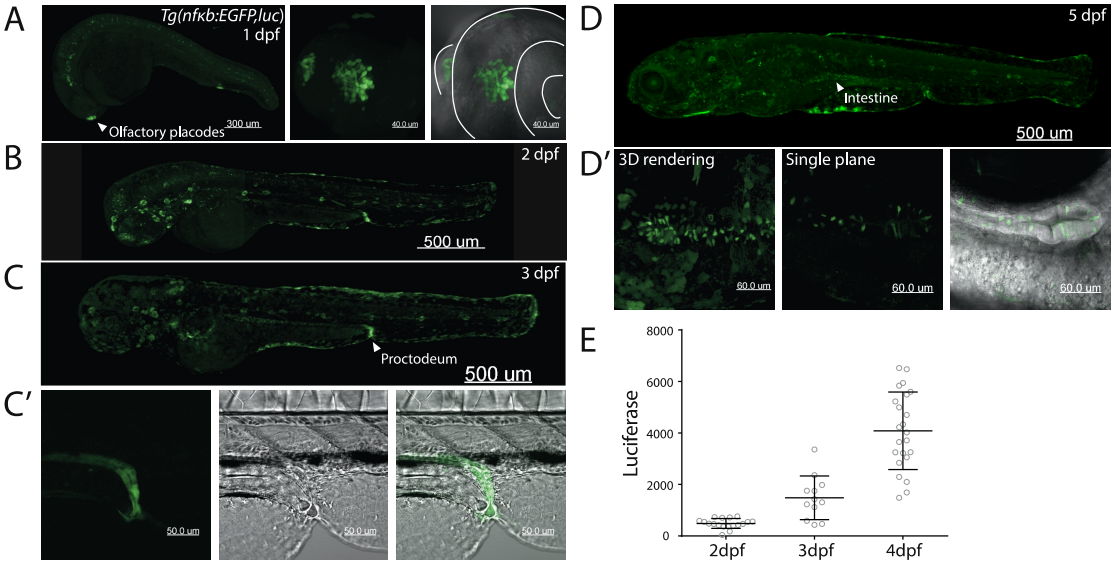

Figure III.3.2. The *nfκb:EGFP,luc* transgenic reporter line reveals endogenous NF-κB activation pattern during early zebrafish development.
Live imaging of the *nfκb:EGFP,luc* transgenic reporter line during early development showing endogenous NF-κb activation pattern at 1dpf [A] with expression in the olfactory placodes [A']; 2dpf [B]; 3dpf [C] a single plane merge with the bright-field showing activation in the proctodeum [C']; and 5dpf [D], highlighting activation in the intestine [D'] in a 3D rendering of the organ and a single plane merge with the bright-field. Quantification of luciferase reporter levels in 2, 3 and 4dpf embryos, shows increase in NF-κb activation with age [E].

We tested whether the early activation of NF-κB in the reporter line could be quantified using a previously published method for *in vivo* bioluminescence measurement in zebrafish larvae (Lahiri et al., 2014). Because measurements are carried out in 96-well plates and the luminescence reagent is added directly to the water, the method is non-invasive and easily scalable. We observed that in the first 4 dpf, concomitant with the broadening of the GFP expression pattern, luciferase expression increases approximately 10 fold. This confirmed that the palindromic sequence was successfully driving expression of both *EGFP* and *luc* genes. Therefore, the line is suitable for both live visualization and quantification of NF-κB activity, the latter in high throughput.

9.2 NF-κB is active from blastula stages

NF-κB begins to activate its transcriptional targets from early embryogenesis. In zebrafish, it has been shown to play a role in mesoderm formation (Correa et al., 2004) and in coordinating the cell cycle with cell movements during gastrulation (Liu et al., 2009). Since we had seen that the *nfκb:EGFP,luc* reporter line is sensitive enough to detect the endogenous pattern of NF-κB activity, we tested whether we could visualize the early activation using live microscopy. We imaged the whole embryo at the gastrula stage, from around 6hpf through the beginning of the segmentation stage. In order to image the entire embryo at this stage with minimum photodamage we used light-sheet microscopy (Reynaud et al., 2008). We were able to detected uniform GFP signal already at shield stage, with the animal pole entirely labeled (Fig. III.3.3A). Cells retained approximately the same level of expression throughout the rest of the gastrula stage and into the segmentation stage. Right before the onset of somitogenesis, individual cells distributed throughout the embryo had higher levels of reporter activity (Fig. III.3.3A, white arrowhead). Furthermore, light-sheet imaging also allowed us to delineate the time frame at which expression in the proctodeum increases (Fig. III.3.3B, white arrowhead). Shifting to a frontal view allowed us to visualize that the strongly labeled cells line the notochord (Fig. III.3.3B', white

arrowhead).

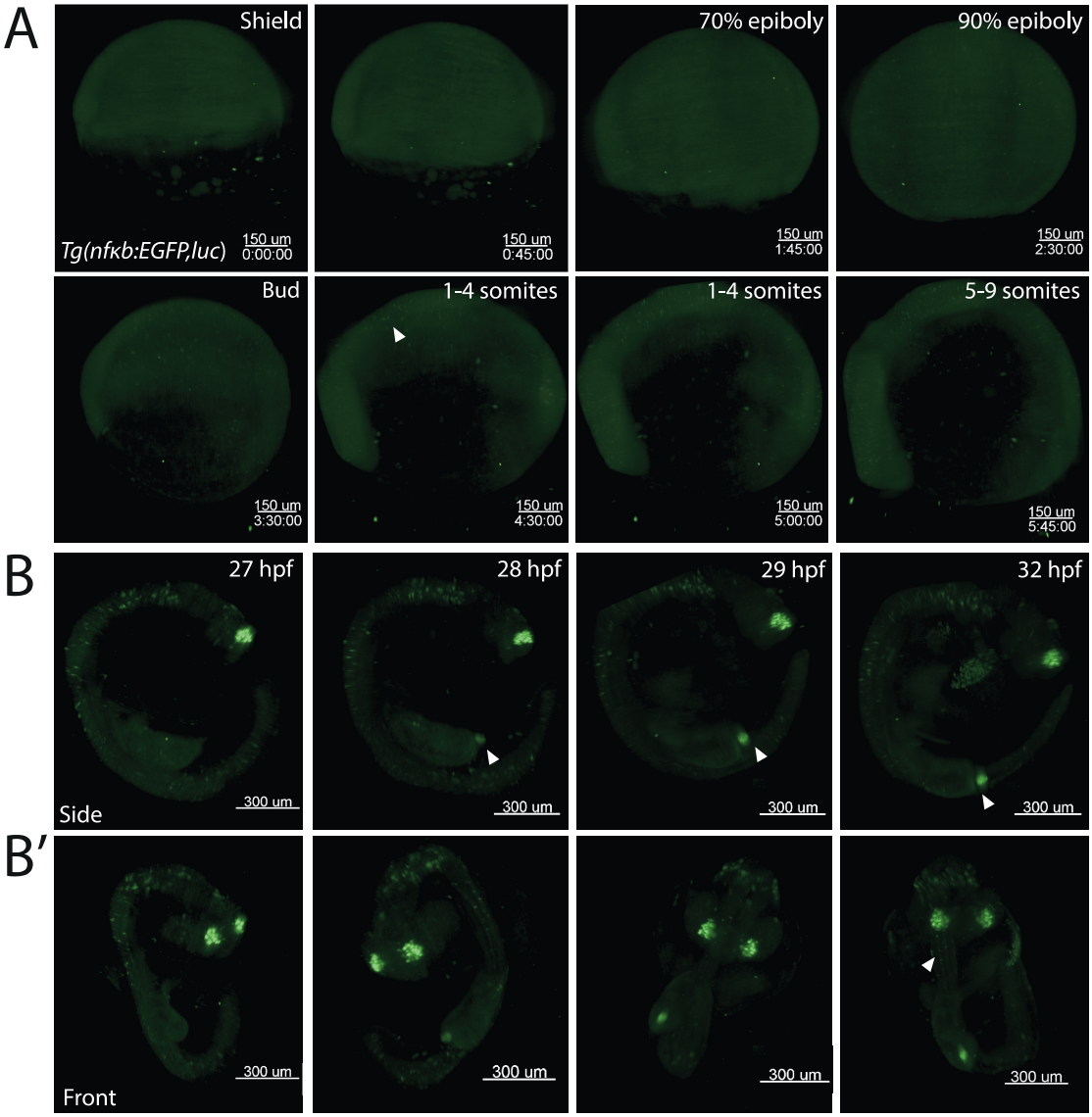

Figure III.3.3. NF-κB is activated transcription from gastrula stage.
Time-lapse imaging of *nfκb:EGFP,luc* transgenic reporter line using light-sheet microscopy from the gastrula stage until segmentation stages [A]. Time-lapse imaging of the entire *nfκb:EGFP,luc* embryo within the chorion using light-sheet microscopy at 1dpf to visualize activation of expression in proctodeum [B].

9.3 Knocking down *nfκbiαa* results in increased reporter activation

In the cytoplasm, NF-κB is bound by an inhibitory protein, NF-κBiαa, that prevents its translocation to the nucleus (Correa et al., 2004). As a confirmation that we observed NF-κB activation with our reporter, we genetically reduced *nfκbiαa* expression by using a previously published

morpholino (He et al., 2015). To test whether NF-κB activation was increased in the absence of the inhibitor we measured luciferase levels in embryos injected with a low and high morpholino dose. Morpholino injection resulted in a dose-dependent increment in NF-κB activation in 2 and 3dpf embryos (Fig. III.3.4A and E). This increase in NF-κB activation led to severe embryo malformation, especially in embryos injected with the high dose (Fig. III.3.4D and H). These experiments confirmed that reporter activity in the *nfκb:EGFP,luc* line is linked to NF-κB activation, and further underscore that precise regulation of NF-κB is crucial during early developmental processes.

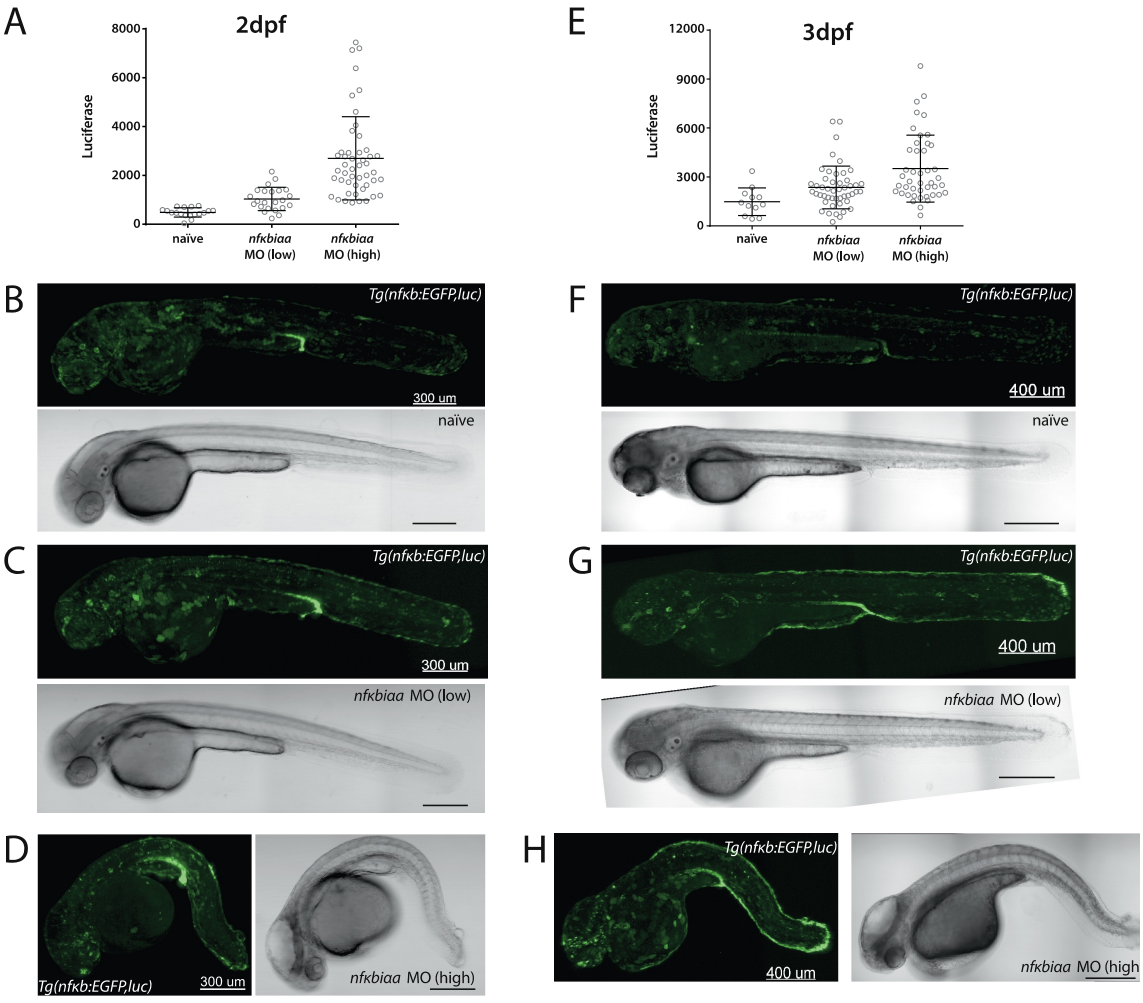

Figure III.3.4. *nfκbiaa* MO of the *nfκb:EGFP,luc* reporter line show increase NF-κB activation and developmental defects.
nfκbiaa expression was knocked down using a morpholino injected at a low (0.3mM) or high (1mM) concentrations. The luciferase activity of larvae belonging to all groups was quantified 2 [A] and 3dfp [E] and individual larvae were imaged to visualize GFP activation also at 2 [B-D] and 3dpf [F-H].

9.4 Injury leads to increase in NF-κB activation

To test whether the *nfκb:EGFP,luc* reporter responds to an inflammatory stimulus we used the tail fin wounding assay (de Oliveira et al., 2013; Ogryzko et al., 2014a). To distinguish activation in epidermal cells for these experiments we crossed the *nfκb:EGFP,luc* reporter line with the *krt19:tomato-CAAX* transgenic line (Fig. III.3.5). In an uninjured tail fin of a 4dpf larva (Fig. III.3.5A), we observe the previously described basal activation in cells at the tail fin edge (Fig. III.3.2C). At 16hpi we see that the reporter is active in epithelial cells surrounding the wound edge of injured larvae (Fig. III.3.5B'). These results indicate that the activation of NF-κB in response to an inflammatory stimulus can be visualized in the *nfκb:EGFP,luc* reporter line.

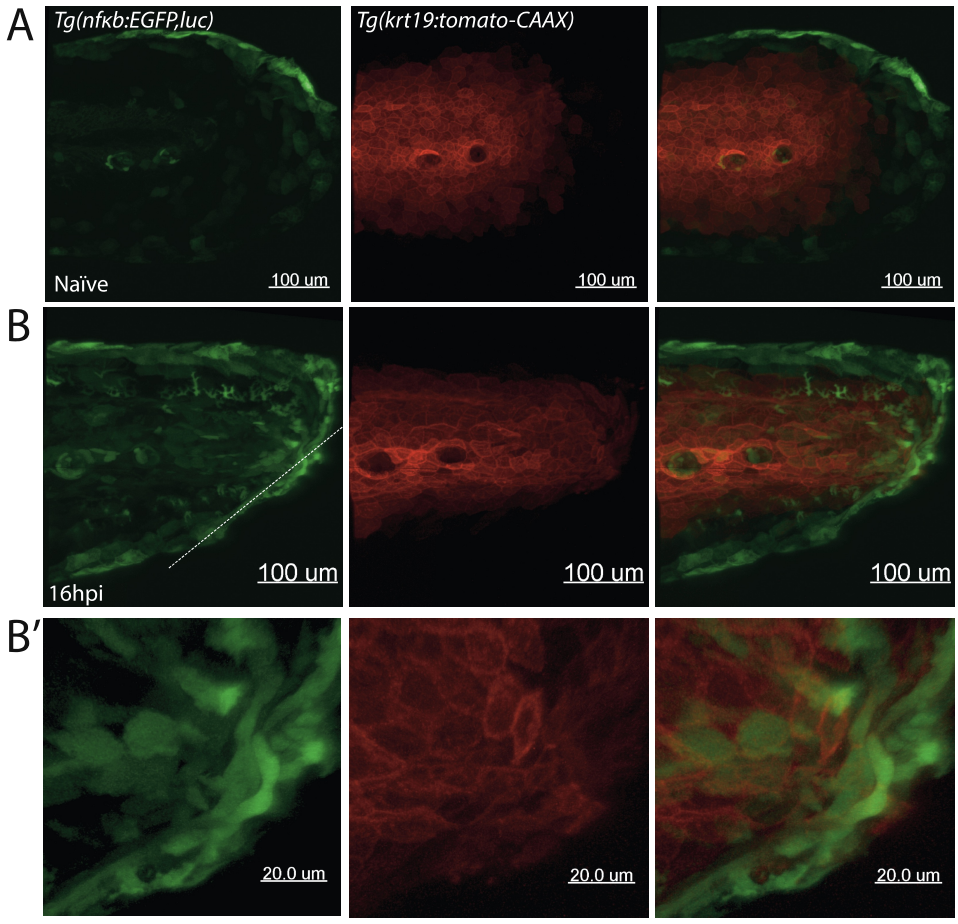

Figure III.3.5. *nfκb:EGFP,luc* reporter line shows activation after injury.
Imaging of naïve *nfκb:EGFP,luc/krt19:tomato-CAAX* double transgenic larvae [A] and 16h after tail fin wounding, cut is depicted by a dashed white line [B]. Magnification of epithelial cells shows activation of the reporter after wounding [B′].

IV. Discussion

1 Using teleost fish models to visualize inflammation

In this study we characterized diverse aspects of inflammasome activation in teleost fish by use of two species. We used zebrafish to visualize speck formation and its downstream consequences in a whole organism for the first time by developing a misexpression and a knock-in transgenic line. Also in zebrafish we developed a tool to visualize and quantify NF-kB activation, a master transcriptional regulation of proinflammatory genes. To address the issue of IL-1 cleavage in fish we developed a transgenic reporter line in medaka to visualize both the induction and the cleavage of IL-1 in larvae and adults *in vivo*.

1.1 Inflammasome conservation in zebrafish

Previous work in the lab characterized the repertoire of innate immunity genes in the zebrafish genome and found that the NLR genes in zebrafish have undergone a massive expansion, resulting in more than 350 genes with varying domain structures (Howe et al., 2016). This gene amplification and diversification could imply that NLR receptors in fish have wider direct detection abilities than in mammals or that the variety is analogous to the multiple isoforms of mammalian gene families (Ogryzko et al., 2014b).

The zebrafish genome has only a single orthologue of *asc* that retains the domain composition of one PYD and CARD domain of its mammalian counterpart and (Masumoto et al., 2003). This appears to be the case for at least two other teleost fish in which *asc* has been cloned (Li et al., 2016; Sun et al., 2008). The ASC speck is the central platform upon which inflammasomes are built (Vanaja et al., 2015) and its formation and assembly are considered a proxy for inflammasome activation (Sester et al., 2015; Stutz et al., 2013). Although it is unclear whether fish can assemble NLR inflammasomes, we

focused on the adaptor, which might have a more general function than any of the NLRs in the zebrafish genome. As has been reported for mammals, overexpression of ASC led to speck formation, and, by generating a knock-in line, we also observed speck formation of tagged ASC expressed at endogenous levels under its own promoter. While certain aspects of inflammasome activation had been studied in fish using isolated cells (Angosto et al., 2012; Reis et al., 2012) or larvae (Vincent et al., 2015; Vojtech et al., 2012), to our knowledge no previous study had visualized speck formation and its consequences by *in vivo* imaging in the otherwise intact organism.

Another aspect in inflammation that this study addressed was the role of IL-1 *in vivo* using medaka fish. The activation observed with a *il-1* transgenic reporter indicated that gene expression is strongly induced and also undergoes proteolytic cleavage after an inflammatory stimulus. Both of these aspects are reported downstream of inflammasome activation in mammals (Garlanda et al., 2013b).

2 ASC speck is formed *in vivo*

2.1 ASC overexpression drives speck formation

The fact that ASC was discovered because it formed aggregates (Masumoto et al., 1999) is a clear indicator of how intrinsic a behavior speck formation is to this protein. Since then, the fact that ASC is prone to aggregation has been well documented. To generate a clonal inflammasome reporter macrophage line in which ASC is tagged to a fluorescent protein, Stutz et al. (2013) indicates that following transgene insertion, there will be cells that form specks autonomously. The paper also notes that selecting cells with a precise level of fluorescence is crucial given that highly fluorescent cells are prone to speck formation without addition of inflammatory stimuli (Stutz et al., 2013). Similarly, Sester et al. (2015) observed a dose-dependent increase in spontaneous speck formation when transfecting ASC-GFP in HEK293 cells (Sester et al., 2015).

Masumoto et al. (2003) had previously shown that expressing zebrafish ASC fused to a fluorescent protein in mammalian cells resulted in speck formation without any external stimuli. Indeed, one previous study using *asc-GFP* mRNA injection to assess speck formation in a zebrafish *Listeria monocytogenes* infection model as a proxy for inflammasome activation, found that PBS injected controls contained the same number of specks as larvae infected with wild type bacteria. Only infection with an *L. monocytogenes* strain engineered to express flagellin exogenously resulted in higher numbers of specks than negative controls (Vincent et al., 2015). However, which cell types formed the specks and whether those would actually express *asc* endogenously was not investigated. These results, together with our own experiments using heat-shock, drug induction and mRNA-driven misexpression of zebrafish ASC (Fig. III.1.5 and 1.6) support the notion that overexpression of ASC in zebrafish leads to speck formation without exposure to any exogenous inflammatory stimuli.

NLR oligomerization functions as a nucleation factor that then drives speck formation (Lu and Wu, 2014). In the case of speck formation as a consequence of overexpression, like the one we observe in zebrafish larvae, the requirement for a nucleating molecule is likely being bypassed. This is consistent with the observation that ASC behaves like a prion-like protein. Prions usually induce an energetically favored self-polymerization process in which the native protein is converted into the polymerized form ("prion switching") after a nucleation step (Ruland, 2014). However, since the frequency of prion switching depends on the concentration of the prion-like protein, the prion state can also be induced by overexpression (Cai et al., 2014). However, if only physiological amounts of the protein are present, the nucleating factor is required. During *in vitro* assembly of PYD_{ASC} filaments, physiological amounts of PYD_{ASC} did not polymerize unless NLRP3 (lacking the LRR) was added (Lu et al., 2014). Therefore, in our experimental set up of induced misexpression of ASC in zebrafish larvae, specks are likely being assembled as a consequence of overexpression.

2.2 ASC behavior in single cells

In the transgenic line *Tg(HSE:asc-mKate2)* (Fig. III.1.8), we observed that the total speck number reached a plateau in single larvae approximately 15hphs (Fig. III.1.8A and B). In this line, a single pulse in the form of a heat shock induces ASC expression. Therefore, by 15hphs, cells in which the pulse induced expression to a level sufficient to overcome the ASC concentration threshold required for speck formation, had already formed a speck.

In single cells we observed ASC is distributed throughout the cytoplasm, as has been reported in experiments *in vitro* (Bryan et al., 2009; Fernandes-Alnemri et al., 2007). Upon speck formation, all the available pool of the protein gets recruited to a single speck. This was true for epithelial cells, which endogenously express *asc* and muscle cells, which do not (Fig. III.1.1 and 1.2). The quantification of ASC-mKate2 in single epithelial cells showed no clear concentration threshold for activation (Fig. III.1.8D) and the amount of overexpressed ASC-mKate2 was not a good predictor for speck formation (Fig. III.1.8E). However, only the overexpressed ASC is detected in these experiments and the levels of endogenous ASC might vary between cells. Interestingly, we observed that cells in which ASC-mKate2 increased at higher rates formed a speck. Cells with a lowest rate of ASC-mKate2 increase did not form a speck, even though these cells eventually reached higher concentration levels of ASC-mKate than cells that did form a speck. Consistent with this observation, the rate of ASC-mKate2 increase was correlated with speck formation time point.

Although mechanisms to control cellular concentration of ASC exist, a sudden and rapid increase in concentration could give the cell very little time to adjust the endogenous levels of the protein, resulting in speck formation. If the increase in ASC is slower, perhaps degradation or post-translational modifications can keep the total protein concentration in check. The results we observed with single point mutations targeting predicted phosphorylation sites suggests that this regulatory mechanism, reported for mammalian ASC (Hara et al., 2013), could be conserved in zebrafish. Additional post-translational modifications could also play a role, especially in the light of

ASC being a ubiquitination target (Rodgers et al., 2014; Shi et al., 2012) or even the synthesis of other regulatory proteins, like the decoy CARD-only proteins or PYD-only proteins (known as COPs and POPs, respectively) (Dorfleutner et al., 2015).

Why do cells form a single speck? Data obtained by studying kinetics of speck formation in single epithelial cells (HeLa cells) support a model in which soluble cytoplasmic ASC molecules have a low affinity for each other, consistent with the weak interaction between PYD domains (Lechtenberg et al., 2014). This results in a very low probability of nucleation, but, after nucleation occurs, the affinity of aggregation increases significantly, leading to a fast recruitment of all soluble ASC in the cell. This process is only limited by diffusion speed and makes the formation of a second speck a highly unlikely event (Cheng et al., 2010). This is consistent with the behavior predicted for the cooperative formation of oligomeric complexes (Wu, 2013) in which a sharp transition in the response is observed as a function of ligand concentration.

3 Caspa recruitment and pyroptosis in epithelial cells

3.1 An alternate domain organization in zebrafish inflammasome

Masumoto et al. (2003) showed that if Caspa was coexpressed with zebrafish ASC in mammalian cells, it was recruited to ASC specks. Co-immunoprecipitation experiments showed that Caspa lacking its PYD domain was unable to interact with ASC (Masumoto et al., 2003). This indicates that Caspa is recruited to the speck via its PYD domain (PYD_{Caspa}) in mammalian cells. Our *in vivo* experiments showed that Caspa is recruited to the ASC speck live also via PYD_{Caspa} in zebrafish. Although expression of the PYD_{ASC} or PYD_{CARD} domain alone resulted in aberrant speck formation (Fig. III.1.17 and 1.18), the aggregates formed by overexpression of PYD_{ASC} recruited PYD_{Caspa} and Caspa and but not the caspase domain alone.

Current models of inflammasome assembly based on the oligomerization of PYD_{ASC} and $CARD_{ASC}$ domains into filaments (Lu and Wu,

2014) depict ASC filaments composed of an inner ring of homo-oligomerizing PYD_{ASC} domains with the $CARD_{ASC}$ flexibly linked in en external outer ring. The $CARD_{ASC}$ act as nucleating factors of caspase-1 when the protease docks onto them through CARD-CARD interactions and forms its own filaments. The structure of the caspase-1 CARD filaments assembled *in vitro* was recently solved using CryoEM (Lu et al., 2016). Caspase-1 CARD domains assemble in a helical manner to form a filament analogous to the one assembled by PYD_{ASC} domains. We observed no filament formation of PYD_{Caspa}-GFP (Fig. III.1.19B), which could reflect a difference between *in vitro* and *in vivo* experimental approaches or one between zebrafish and mammalian inflammasome assembly. Regardless, given that both PYD and CARD domains can form these high-order assemblies, we can hypothesize that inflammasome assembly in zebrafish has an inverted ASC filament structure with CARD domains located on the inside and Caspa assembling its own PYD filaments by docking on the outer PYD_{ASC} layer. Given that within the numerous zebrafish NLRs some have an N-terminal CARD (or PYD) domain there are many possible sensor molecules that could nucleate ASC assembly in this scenario (Laing et al., 2008; Stein et al., 2007). Confirming this hypothesis would require a more detailed structural analysis of the zebrafish inflammasome components.

3.2 Caspase-1 expression as a pyroptotic determinant

We observed a striking difference in the cellular response to speck formation depending on cell type. Epithelial cells underwent a rapid cell death after speck formation, displaying the archetypical morphological features of pyroptosis such as cell detachment, swelling and rounding (Jorgensen and Miao, 2015), whereas muscle cells seemed unaffected by speck formation at least for the following 20h. Treatment with the general caspase inhibitor Q-VD-OPh significantly reduced speck formation-induced cell death, confirming that the cell death is caspase-dependent (Fig. III.1.14).

The overexpression of Caspa was highly toxic for epidermal cells (Fig. III.1. 15A). Muscle cells also displayed an altered morphology upon Caspa

overexpression (Fig. III.1. 15D), although at a much later timepoint. It had been reported that Caspa or Caspb expression leads to cell death in mammalian cells (Masumoto et al., 2003), but within 20hphs only Caspa overexpression showed this response *in vivo*(Fig. III.1.15). A mouse model where caspase-1 was overexpressed in epidermal cells also caused high levels of epidermal cell death that led to dermatitis and ulcers (Yamanaka et al., 2000). *In situ* hybridization showed weak expression of *caspa* in epithelial cells (Fig. III.1.20). Altogether, this suggests that the expression of *caspa* must be kept tightly under control to prevent unintentional activation of the protease.

Fernandes-Alnemri et al. (2007) showed that HEK293 cells stably expressing physiological amounts of ASC–GFP were able to form a speck and remain viable. However, if pro-caspase-1 was coexpressed in this cell line, cells showed the morphological features of pyroptosis upon speck formation (Fernandes-Alnemri et al., 2007). We found no evidence for *caspa* or *asc* expression in muscle cells in naïve zebrafish larvae. Therefore, it is possible that muscle cells do not undergo pyroptosis after overexpression-induced speck formation because these cells lack the effector downstream of the initial inflammasome signaling. We took advantage of this fact to analyze ASC and Caspa domain interactions *in vivo*. However, it is possible that muscle cells are able to upregulate these genes in an inflammatory situation. In mice, the expression of NLRP3 inflammasome components is upregulated in primary mature muscle cells derived from a mice model of inflammatory muscle disease, whereas they were absent or strongly reduced in wild type mice. Furthermore, knocking down dysferlin from muscle cells in culture resulted in the release of mature IL-1β, although at levels 30x lower than those of a macrophage cell line after the same knockdown (Rawat et al., 2010). Therefore, although not expressed in a naïve situation, inflammasome components may be upregulated and activated under strong proinflammatory conditions in muscle cells.

Because Caspa was recruited to the ASC speck and neither Caspb nor Casp3a were, we generated a knockout of this gene using CRISPR/Cas9. Further experiments will address whether speck formation leads to

pyroptosis in epidermal cells in *caspa* mutant larvae. However, in the absence of Caspa, other caspases might be recruited to the speck, as has been reported for caspase-8 in mammals (Pierini et al., 2012; Sagulenko et al., 2013). Since the caspase-8 zebrafish orthologue, like caspase-8, has an N-terminal DED domain, this caspase could have a homologous role in zebrafish.

3.3 Speck assembly occurs in the cytoplasm and nucleus of epithelial cells

We found that, regardless of whether the speck is assembled in the cytoplasm or the nucleus of epidermal cells, it leads to cell death (Fig. III.1.12). This was also shown in HeLa cells, which do not undergo pyroptosis immediately upon speck formation (Cheng et al., 2010). In these cells, specks assemble by recruiting the entire compartment's (nucleus or cytoplasm) soluble pool of ASC within 15 min. Cheng et al. (2010) found that the second compartment's ASC pool also translocated into or out of the nucleus in order to assemble at the speck. The transport across to and from the nucleus occurred at a much slower rate than the diffusion observed within each compartment, indicating that the movement of ASC across the nuclear envelope is restricted. To what extent the fusion of a fluorescent protein to ASC for visualization purposes affects the transport is unclear (Cheng et al., 2010). Our data showed that zebrafish epidermal cells died before the second compartment's pool of ASC was depleted. We observed that the cell death seems to occur more rapidly if the speck is formed in the cytoplasm than in the nucleus (roughly three times faster, 15 min vs 45 min) suggesting that other components of the inflammasome also need to be translocated to the nucleus for cell death to take place. However, experiments with higher time resolution are required to confirm this observation.

3.4 Macrophage engulfment of specks

After epidermal cells undergo cell death upon ASC overexpression, ASC specks accumulate in the extracellular environment (Fig. III.1.13). Specks also accumulate in a caspase-1-dependent manner in the supernatant of

macrophage cell culture upon exposure to inflammasome-activating stimuli. The extracellular specks retain their ability to process extracellular caspase-1 and pro-IL-1β (Baroja-Mazo et al., 2014; Franklin et al., 2014). Franklin et al. (2014) also observed that adding specks of ASC-mCerulean assembled *in vitro* to a macrophage cell line expressing ASC-mCherry resulted in the engulfment of the specks (Franklin et al., 2014). In zebrafish, we observed that macrophages were able to engulf specks in phagosomes and degrade them. We also observed macrophages that had engulfed more than one speck. We did not detect macrophages undergoing pyroptotic cell death after having engulfed an extracellular speck. In the experimental setup by Franklin et al. (2014) the quantity of ASC-mCerulean detected in macrophage lysates peaks 6 hours after incubation and strongly diminished after 24h, indicating that some degradation of engulfed specks in the phagolysosomal compartment is taking place. However, 36 hours after incubation they observed cases in which soluble ASC-mCherry of the recipient cell was recruited to the engulfed ASC-mCerulean speck after the latter escaped from the phagolysosomal compartment into the cytosol. Whether this leads to the recipient cell's pyroptotic death was not investigated. Therefore, although macrophages can degrade engulfed specks, as we also observed, sometimes they are unable to do so. In the long term (namely 36 hours) the engulfed, undegraded speck can trigger lysosomal damage and be released into the cytosol, functioning as a nucleating factor for the recipient cell's soluble ASC (Franklin et al., 2014).

4 What causes speck formation *in vivo*?

4.1 Detection of endogenous speck formation using immunostainings

The antiASC antibody was able to recognize ASC also in its aggregated form (Fig. III.1.5) and antibody stainings have been used previously to recognize endogenous speck formation in macrophages (Sester et al., 2015). However, we were unable to detect endogenous specks by immunostaining larvae after exposure inflammatory stimuli (Fig. III.1.22). There are several

explanations for why this approach to visualize endogenous specks was not successful. It is possible that the treatments themselves did not stimulate inflammasome assembly or that fixation was not carried out at the right time point to visualize it. However, a technical issue could hinder detection by this method, since any cells in the epithelial surface that die upon speck formation would detach from the sample and be lost during fixation and washes included in the immunostaining protocol. Cells that remain in the sample would lose its cytoplasmic integrity and would no longer be discernable as single cells. Extracellular specks would unfortunately be indistinguishable from immunostaining artifacts.

4.2 The use of Crispr to generate a zebrafish knock-in

To find out whether zebrafish forms specks in a wild type situation we required a way to visualize this protein live without altering its endogenous concentration. We therefore chose to label the genomic *asc* copy itself. CRISPR/Cas9 genome editing has been used previously to insert exogenous DNA in zebrafish. In some cases integration relies on the exogenous fragment being integrated into the double stranded break by non-homologous end joining (homology independent repair) (Auer et al., 2014; Li et al., 2015) whereas others have taken advantage of homology directed repair (Hisano et al., 2015; Kimura et al., 2014). However, integration via homology independent repair can cause mutations at the junctions of the genomic DNA and the integrated fragment (Auer et al., 2014) and it has been reported to yield a smaller number of successful integration events than homology directed repair (Hisano et al., 2015). Therefore, we generated the *asc:asc-EGFP* line via homology directed repair with homology arms of the reported optimal length of 1kb (Irion et al., 2014), although homology regions as short as 40bp have been reported to successfully lead to integration (Hisano et al., 2015). The rate of injected embryos that showed GFP expression was significantly lower than those reported for GFP fusion to a CDS via homology directed repair (Hisano et al., 2015). When tagging the *krtt1c19e* locus, Hisano et al. (2015) reported 37% of injected embryos had some level of GFP

expression, although only less than 3% had broad GFP expression. In our hands less than 1% of injected embryos showed GFP signal, although the rate varied from 0 to 2% for every injection session. Because the only component that varied between injections was the Cas9 protein and the sgRNA aliquots, it is possible that in some aliquots the stability of the protein or the guide RNAs had been compromised. Regardless, when we screened the F0 founder fish by mating it with a wild type we observed 30% F1 positive embryos, which is in agreement with the values Hisano et al. (2015) reported for F0 founder fish (Hisano et al., 2015). When amplifying the *asc* locus in gDNA extracted from those F1 positive embryos we could detect one band corresponding to the wild type allele and one of larger size corresponding to the *asc-EGFP*. Sequence analysis of this fragment confirmed the integration of the exogenous DNA, thus confirming that the integration is heritable (Fig. III.1.24).

4.3 A zebrafish line to analyze speck formation *in vivo*

In spite of evidence that speck formation occurs in mouse and in humans under proinflammatory conditions (Broderick et al., 2015), the visualization of endogenous speck formation was limited to *in vitro* studies. Using the *asc:asc-EGFP* line we observed the endogenous pool of ASC recruited to form a speck (Fig. III.1.28). Furthermore, the speck-containing cells in the *asc:asc-EGFP* line displayed a the same morphology to cells in which speck formation occurred as a consequence of overexpression. This indicates that speck formation occurs *in vivo* in epidermal cells and leads to pyroptotic cell death. This finding represents a step forward in the understanding of inflammasome activation, but it also opens up many new questions and possibilities. For example, our study focused on the role of speck formation in epidermal cells, where *asc* is very prominently expressed. It will be interesting to investigate the role of *asc* in other cells that endogenously express *asc*, especially myeloid cells, where the phenomenon has been most prominently studied in mammals. Because these cells express levels of the protein that allow ASC-GFP to be easily imaged (Fig. III.1.27A

and B), the line could be used in zebrafish infection models where macrophage-pathogen interactions are important (Renshaw and Trede, 2012; Torraca et al., 2014). Pyroptosis in hematopoietic cells can lead to cytopenia and immunosuppression (Croker et al., 2014). Furthermore, inflammatory signaling was recently reported to be involved in hematopoiesis in both mice and zebrafish (Espín-Palazón et al., 2014; He et al., 2015). Given that we observed varying levels of ASC in cells within the caudal hematopoietic tissue (Fig. III.1.4D, 1.27C) an interesting application would be to use the *asc:asc-EGFP* line to study whether speck formation is involved in this process.

Another possible line of investigation would be the role of ASC in intestinal epithelial cells. Progatzky, et al. (2014) showed that the intestinal inflammation observed in response to a high cholesterol diet in zebrafish was dependent on inflammasome activation. Intestinal epithelial cells of adults fed with high cholesterol diet were stained positive for the activation of caspase-1-like proteases and knockdown of *asc* expression in intestinal epithelial cells diminished the recruitment of myeloid cells to the intestine in larvae (Progatzky et al., 2014). Whether high cholesterol diet leads to speck formation in intestinal epithelial cells was, however, not addressed by the study, and could be investigated live using our knock-in line.

5 IL-1 signaling in fish

5.1 Cleavage of IL-1 in medaka

Whether IL-1 is cleaved and the cleavage has an analogous function in teleost fish as in mammals is an open question (Ogryzko et al., 2014b). In this study we used medaka to approach this issue. We generated a transgenic *il1* reporter, *il1:EGFP-t2a-il1-HA* and tracked the transcriptional and post-translational activation of IL-1. We found that *il1* is expressed constitutively (Fig. III.2.3), but is also highly inducible in response to injury and infection in larvae (Fig. III.2.4). *Il1* was also expressed in the hematopoietic organs (head kidney and spleen) of adults (Fig. III.2.5). Furthermore, exposure of larvae to inflammatory stimuli reported to lead to the inflammasome-mediated

cleavage of IL-1α and IL-1β (Groß et al., 2012) also resulted in the cleavage of IL-1 in medaka. However, most of the IL-1 pool remained in its immature form, suggesting that cleavage only takes place in a small cell population in the larva. Cleavage of IL-1 occurred in the head kidney and spleen of adults in response to injection of bacterial debris (Fig. III.2.7). Mass spectrometry confirmed HA-specific antibodies pulled down IL-1 fragments of smaller size than the full-length protein (Fig. III.2.8). Overall our results indicate that medaka IL-1 is cleaved *in vivo* in response to inflammatory stimuli.

5.2 A fish IL-1 that is neither α nor β

IL-1α and IL-1β probably arose from the duplication of an ancestral gene (Sims and Smith, 2010). Although both genes were discovered at the same time (Dinarello, 2013), the role of IL-1α in inflammation has been less studied than that of IL-1β (Rider et al., 2013). Fish IL-1 homologues usually have the IL-1 family signature amino acid motif and slightly higher homology to IL-1β, and have therefore been considered and annotated as IL-1β orthologues (Ogryzko et al., 2014b). However, data from several fish species suggest that although fish IL-1 shares important characteristics with IL-1β, it is not an unambiguous genetic or functional orthologue.

A feature that distinguishes *il1β* from *il1α* is the high degree of inducibility of the gene under inflammatory conditions (Joosten et al., 2013). This characteristic is conserved in fish, whose *il1* expression is activated upon stimulation with bacteria or LPS (Secombes et al., 2011). We observed IL-1 upregulation in medaka larvae in response to sterile injury and LPS treatment, which had also been reported in zebrafish larvae (Novoa et al., 2009; Ogryzko et al., 2014a). In mammals, hematopoietic cells are the largest source of IL-1β. Medaka myeloid cells in adult blood expressed *il1* and carried out bacterial engulfment *in vivo* (Fig. III.2.5B). IL-1-expressing cells were also located in the fish hematopoietic organs, spleen and head kidney. We also observed that cells in the head kidney induced expression of *il1* in response to bacterial injection (Fig. III.2.5D). In zebrafish larvae, the *il1* increase in response to UVB irradiation is driven by myeloid cells (Banerjee and Leptin,

2014), as is the *il1* response after bacterial notochord infection, where it is expressed by macrophages and neutrophils *in vivo* (Nguyen-Chi et al., 2014).

In contrast, IL-1α is expressed constitutively in resting cells under homeostatic conditions (Rider et al., 2013). The medaka *il1* reporter line and a zebrafish *il1:GFP* line showed that the gene is expressed in a naïve situation (Nguyen-Chi et al., 2014). This constitutive level of expression is likely too low to be detected by *is*h in both species (Ogryzko et al., 2014a) (Fig. III.2.2). Furthermore, the expression pattern we observed, with *il1* expressed in gills, skin and intestine (Fig. III.2.3) is consistent with that of *il1α* in mammals, which express *il1α* in the entire gastrointestinal tract, kidney and skin keratinocytes (Rider et al., 2013).

An important aspect of IL-1β biology is the fact that its precursor is inactive and requires cleavage to bind to the IL-1 receptor, whereas IL-1α is able to bind to the IL-1 receptor in its immature and cleaved form (Afonina et al., 2015; Garlanda et al., 2013a; Joosten et al., 2013). Processing of IL-1β is carried out by caspase-1 after inflammasome activation, whereas calpain-like proteases cleave IL-1α in an inflammasome-dependent or independent manner (Groß et al., 2012). Although the caspase-1 site is not conserved in fish IL-1, when zebrafish IL-1 was co-expressed with Caspa or Caspb in HEK293 cells both enzymes cleaved IL-1 at distinct aspartic acid residues (Vojtech et al., 2012). Incubation of recombinant sea bass caspase-1 and IL-1 led to direct cleavage of the latter. These studies show that caspase-1 orthologues can cleave IL-1 in an artificial environment, but fail to show whether it happens *in vivo*. In a protein sequence analysis, we found that the IL-1α cleavage site is conserved in some species of teleost fish including zebrafish and medaka. We found that medaka IL-1 is cleaved upon inflammasome-activating stimuli like nigericin and bacterial infection (Fig. III.2.6), and in response to ionomycin treatment, which does not activate the inflammasome in macrophages, and instead leads to an intracellular Ca^{2+} increase that activates calpain proteases (Groß et al., 2012). Bacterial infection led to IL-1 cleavage in sea bream leukocytes in a caspase-1 independent manner, suggesting that other proteases may process IL-1 in fish *in vivo* (Angosto et al., 2012). Whether

calpains do cleave fish IL-1 *in vivo* requires further investigation.

Overall, IL-1 in teleost fish shares features of both IL-1α and of IL-1β. Considering it a direct orthologue of either one may bias interpretation of results.

5.3 IL-1 incorporation into inflammasome signaling

Although there is evidence that caspase-1 is activated in response to inflammatory stimuli in fish (Angosto et al., 2012; Banerjee and Leptin, 2014; Ogryzko et al., 2014a; Varela et al., 2014; Vincent et al., 2015), this activation might not directly lead to IL-1 cleavage. That activation of caspase-1 orthologues leading to pyroptotic cell death, however, does appear to be conserved. We can therefore imagine a scenario in which IL-1 in fish is cleaved *in vivo* as an indirect consequence of inflammasome activation, as is the case for IL-1α (Groß et al., 2012). This is consistent with our own results and that of others who see IL-1 cleavage in fish after exposure to inflammasome-activating stimuli. A possible evolutionary scenario is that incorporation of IL-1 into the inflammasome signaling cascade occurred after the divergence of fish and tetrapods (Angosto and Mulero, 2014), as part of the subfunctionalization of IL-1α and IL-1β, when only the latter acquired a site suitable for caspase-based cleavage (Denes et al., 2012; Ogryzko et al., 2014b).

5.4 The role of inflammasomes in the skin

Our own data and those of others (Chang et al., 2010) show that zebrafish ASC is expressed from early stages during embryo development. We show by *is*h that epidermis contributes to this early expression (Fig. III.1.1). As an immune organ, the skin provides protection from injury and infection. Keratinocytes function to relay environmental signals of immune cells, but also sense danger and execute a response which also serves to drive the infiltration of myeloid cells (Peeters et al., 2015). Mammalian keratinocytes express all inflammasome components *in vitro* and probably *in*

vivo (Feldmeyer et al., 2010). Furthermore, inflammasome components have been implicated in the inflammatory responses to UVB irradiation (Feldmeyer et al., 2007), contact hypersensitivity (Watanabe et al., 2007), HPV infection (Reinholz et al., 2013) and inflammatory disorders such as CAPS and atopic dermatitis (Dai et al., 2011; Feldmeyer et al., 2010). Crucial differences between mammalian and teleost skin epithelia are that the latter contains only living cells (Chang and Hwang, 2011). The skin in fish takes on an additional role as a barrier regulating salt and water homeostasis and in some species is used for nutrient acquisition and waste secretion (Glover et al., 2013). Therefore, control of skin microbial growth is crucial (Rakers et al., 2013), and the presence of an inflammation machinery is important from early development. This could explain why we observe that inflammasome components like ASC and IL-1 are present from early stages. However, there is also precedent for ASC in mice acting as a tumor suppressor gene in keratinocytes, and as a tumor promoter in myeloid cells (Drexler et al., 2012) implicating ASC in skin cancer. Given the accumulating evidence for the involvement of inflammasome signaling in cancer (Kolb et al., 2014), it is possible that similar links exists in inflammasome signaling in fish.

6 A reporter for NF-κB for imaging and quantitation

NF-κB is best known for its role as a master switch for the activation of proinflammatory genes, but it also regulates genes involved in growth, differentiation and cell death (Gilmore and Wolenski, 2012). This is achieved through binding sites for NF-κB dimers located upstream of coding sequences that act as regulatory sites (Natoli, 2006). Using a palindromic high affinity-binding site predicted by a recent analysis of NF-κB dimers' binding affinity, we generated a zebrafish NF-κB reporter line. Because the sequence is palindromic, we could place both the *EGFP* and *Renilla* luciferase genes downstream of the NF-κB regulatory sequences on opposing strands.

The zebrafish NF-κB reporter line allowed us to visualize both the endogenous expression patters and the inflammatory response after insult.

The endogenous activation pattern for the high affinity binding sites was largely consistent with those observed for the reporter line generated by Kanther et al, (2011). Namely, we also observed expression in the intestine, cloaca, and the lateral line, but observed stronger sporadic epithelial expression and less expression in pharyngeal arches (Kanther et al., 2011).

The expression in our line during the first 48hpf reflected previously reported roles for NF-κB. For example, activation during gastrulation (Liu et al., 2009) and the activation of cells in the notochord during somitogenesis most likely relate to NF-κB involvement in the formation of this structure (Correa et al., 2004). The severe malformation phenotypes we observed after *nfκbiαa* knockdown are consistent with those previously observed in zebrafish for NF-κB loss or gain of function experiments during early development (Correa et al., 2004; 2005).

A novel aspect of our reporter line compared to previously available zebrafish NF-κB reporters (Banerjee and Leptin, 2014; Kanther et al., 2011) is that it enables NF-κB activity quantification by bioluminescence measurement. The activity of the luciferase reflected the endogenous increase in NF-κB activity observed during development (Fig. III.3.2E), as well as the increase resulting from knockdown of the NF-κB inhibitor *nfκbiαa* (Fig. III.3.4A and E). Luciferase in each larva is measured individually in a well that contains the reagents required for luciferase activity without any permeabilization. Therefore, the larva is unharmed and can survive for several days, allowing for continuous tracking of reporter activity (Lahiri et al., 2014). This represents a significant improvement from a previously published method to measure NF-κB activity in zebrafish with a luciferase reporter in which lysis of the embryo was required for measurement (Alcaraz-Pérez et al., 2008).

Bioluminescence imaging of NF-kB expression in a luciferase transgenic mouse model has been used as a tool to screen for anti-NF-kB drug candidates (Robbins and Zhao, 2011). The zebrafish is a model ideally suited for whole-organism drug screening (Zon and Peterson, 2005) with fluorescence-based analysis of both reporter activity (Wang et al., 2015) and

bacterial count (Ordas et al., 2015; Veneman et al., 2013), and is used in high throughput screens to test for drug efficiency. We believe that our reporter could provide a cost-effective improvement for assays for drug discovery. Bioluminescence could be used to screen for whole-organism effects of drugs and tissue specific-effects could be visualized with the fluorescence reporter.

V. Closing remarks

The use of both zebrafish and medaka as developmental biology models has been significantly expanded to cover areas of immunology and cancer (Lin et al., 2016; Renshaw and Trede, 2012). Overall, given the increasing importance of visualization in the immunology field (Bousso and Moreau, 2012), there is great value in using models that enable visualization of defined immune processes in the context of the whole organism.

This work addressed the role of the inflammasome in teleost fish by generating reporters that enabled us to track signaling live. This allowed us to study ASC speck formation and to visualize the ensuing pyroptosis. Never before had this process been visualized in a living organism. Furthermore, the development of the *asc:asc-EGFP* knock-in line opens up new exciting research possibilities for the inflammasome research together with zebrafish immunity. Our work in medaka IL-1 led us to propose an alternate view on the role of this gene in fish and supports an evolutionary hypothesis for the incorporation of IL-1α and IL-1β into inflammasome signaling in mammals. Both projects point to the importance of inflammation in non-myeloid cells, where the inflammasome has been relatively scarcely studied.

Overall, through work on ASC, IL-1 and NF-κB we have significantly built on available knowledge in the functional role of the inflammasome in fish and its evolution. Because of the possibilities of discovery that the use of fish models offer, a more comprehensive characterization of innate immune signaling in fish will be useful in developing human disease models and understanding the evolution of our immune system.

VI. Materials and methods

1 Fish care, husbandry and genotyping

1.1 Zebrafish

Zebrafish (*Danio rerio*) were cared for as described previously (Westerfield, 2007). In short, fish were kept at 25°C on a 14-hour light-10-hour dark cycle. Mating crosses were set up late in the afternoon and eggs collected the following morning. In case of injection at one-cell stage, the pair was kept separate overnight and put together the following morning before injection. Eggs and larvae were kept in E3 medium (5 mM NaCl, 0.17 mM KCl, 0.33 mM $CaCl_2$, 0.33 mM $MgSO_4$) at 28°C. E3 medium was complemented with Methylene Blue at 0.0001% to prevent growth of mold only when embryos were not meant to be used for imaging purposes. In addition, the chemical 1-phenyl-2-thiourea (PTU, Sigma) was added to E3 medium at a concentration of 0.2 mM from 12 to 24hpf to inhibit melanization.

Throughout this study the Tupfel Long Fin (TLF) strain was used as a wild type with the Tübingen strain used for outcrossing. Additional transgenic lines generated prior to this study are described in Table VI.1.1.

Table VI.1.1. Published zebrafish transgenic lines used in this study.

Line	Reference
mpeg1:EGFP	(Ellett et al., 2011)
pU1:Gal4; UAS:tagRFP	(Sieger et al., 2012)
lysC:DsRed2	(Hall et al., 2007)
krt4:GFP	(Fischer et al., 2014)
krt19:Tomato-CAAX	(Fischer et al., 2014)
βactin:NLS-tagBFP	Lionel Newton, unpublished

1.2 Medaka

Medaka fish (*Oryzias latipes*) were kept in the same environmental conditions as those mentioned above for zebrafish. Eggs were collected from mouse cages containing both males and females daily. In the case of injections, males and females were kept in separate mouse cages overnight and put together the following day before injection. Eggs and larvae were kept in Embryo Rearing Media (ERM, 0.1% (w/v) NaCl, 0.003% (w/v) KCl, 0.004% (w/v) $CaCl_2$ x $2H_2O$, 0.016% (w/v) $MgSO_4$ x $7H_2O$). The Cab strain of wild type medaka were used throughout this study.

1.3 Genotyping

Larvae and adults were genotyped using the QuickExtract DNA Extraction Solution (Epicentre). A single larvae or a fin clip were placed in a PCR tube to which 100µl of the reagent were added. The mixture was vortexed for 15 s and incubated from 6 to 10 min at 65°C in a thermocycler. Sample was then vortexed again to fully disintegrate tissue and incubated for 2 min at 98°C. The genomic DNA (gDNA) in the supernatant was either used directly (5 µl per PCR) or stored at -20°C for its later use.

1.4 Injections

DNA, mRNA, morpholinos and proteins were routinely injected to embryos at the one-cell stage to alter gene expression. All reagents were injected in a solution containing 100 mM KCl unless otherwise indicated. More information on how expression vectors and mRNA and sgRNA were synthesized is included below. Morpholinos were used for gene knockdown and function by preventing splicing (splice morpholinos) or translation initiation (ATG morpholinos) of mRNA. Morpholinos were designed (when not previously described) and ordered through Gene Tools, LLC. All morpholinos used are listed in Table VI.1.2. Morpholinos were diluted in Nuclease-free H_2O to a concentration of 3 mM and kept at room temperature.

Table VI.1.2. Morpholinos used in this study.

Target	Sequence	Reference
asc (ENSDARG00000040076)	5′- GCTGCTCCTTGAAAGATTCCGCCAT-3'	This study
nfκbiαa (ENSDARG00000005481)	5′-TGCGGCTCTGTGTAAATCCATGTTC-3′	(He et al., 2015)

2 Inflammatory and Chemical treatments

2.1 Tail fin wounding

Assay was adapted from previously described methods (de Oliveira et al., 2013; Ogryzko et al., 2014a). Larvae were anesthetized with Tricaine, a Na+-channel inhibitor ethyl-m-aminobenzoate methanesulfonate (MESAB), by adding the compound to the media at a concentration of 40 μg/ml. Tricaine induces a temporary state of immobilization. While immobilized on a Petri dish, the tip of the caudal fin of each larvae was cut with a sterile surgical blade. Larvae were then placed in fresh medium and kept at 28°C until the time of sample collection.

2.2 UVB irradiation treatment

Larvae were exposed to UV radiation as previously described (Banerjee and Leptin, 2014). In short, larvae were placed on a Petri dish with as little media as possible and exposed to irradiation from broad-band UV lamps for periods corresponding to a maximum of 120 mJ/cm^2. After exposure media was added to the larvae and they were kept at 28°C until the time of sample collection.

2.3 Larval notochord injections

Bacterial notochord injections of zebrafish larvae were performed as described (Nguyen-Chi et al., 2014). In brief, larvae were anesthetized with

Tricaine by adding the compound to the media at a concentration of 40 µg/ml. Afterwards, fluorophore-conjugated *Escherichia coli* (*E. coli*, K-12 strain) were injected into the notochord. Larvae were immediately imaged.

2.4 Adult intraperitoneal injections

Adult medaka fish were infected using a previously published method (Aghaallaei et al., 2010). In short, medaka adults were anesthetized with Tricaine and injected with either fluorophore-conjugated *Escherichia coli* (*E. coli*, K-12 strain) or *Staphylococcus aureus* (wood strain, without protein A) debris via intraperitoneal injection. Three days after injection adults were sacrificed with a high dose of anesthetic and blood, head kidney and spleen were collected.

2.5 Chemicals

The chemicals used in this study are listed in Table VI.2.1. Chemicals were added directly to the medium.

Table VI.2.1. Chemicals used in this study.

Name	Purpose	Stock conc.	Working conc.	Source
Lipopolysaccharides from E. coli (LPS)	Signal 1 for inflammasome activation	1 mg/ml in H2O	50 µg/ml	Sigma-Aldrich
Ionomycin	Signal 2 for inflammasome activation	10 mM in DMSO	1- 50 µM	Sigma-Aldrich
Nigericin	Signal 2 for inflammasome activation	10 mM in DMSO	1- 50 µM	InvivoGen
Q-VD-OPh hydrate	Pan-caspase inhibitor	10 mM in DMSO	100 µM	Sigma-Aldrich
Mifepristone (RU-486)	Induce LexPR/LexOP expression	20 mM in EtOH	100 µM	Sigma-Aldrich

3 Cloning

3.1 Software

The software Geneious Version 6.1.7r was used for the design of all cloning strategies, analyses of sequencing data and sequence alignments. Primers were also occasionally designed using this software.

The kinase-specific prediction of phosphorylation sites in zebrafish ASC was carried out using the online software GPS 2.1.1 (Xue et al., 2011), with previously described parameters (Hara et al., 2013).

The software Prism Version 6.03 (GraphPad) was used for all statistican analyses and graphs.

3.2 Restriction digest cloning

Polymerase Chain Reaction for cloning purposes was performed using Phusion High-Fidelity DNA Polymerase (Thermo Fisher Scientific). PCR products were then run on a gel, extracted using MinElute Gel Extraction Kit (Qiagen) and digested with the appropriate FastDigest restriction enzymes (Thermo Fisher Scientific). Ligation with the digested vector treated with FastAP Alkaline Phosphatase (Thermo Fisher Scientific) was performed using T4 DNA Ligase (5 U/µl Thermo Fisher Scientific).

3.3 TOPO cloning

For TOPO cloning the PCR product was either gel extracted or directly used to set up a TOPO reaction. Because PCR products obtained using the Phusion polymerase are blunt (instead of having 3'A overhangs), the Zero Blunt TOPO PCR Cloning Kit (Invitrogen) was used.

3.4 Gateway cloning

Both BP and LR Gateway cloning reactions were performed according to manufacturer's instructions.

3.5 Golden GATEway cloning

Golden GATEway cloning was performed essentially as described (Kirchmaier et al., 2013). In short, 50 ng of entry vector (EV) plasmids numbered 1 to 6 and a vector backbone containing a different antibiotic resistance cassette as the rest, were digested with 0.5 µl of BsaI (Fast Digest, Thermo Fisher Scientific) and ligated with 0.5 µl of T4 DNA Ligase (30 U/µl, Thermo Fisher Scientific) in several rounds in one continuous reaction of 10 cycles consisting of 30 min at 37°C and 20 min at 16°C, followed by 5 min of 50°C and 5min of 80°C to inactivate both enzymes.

3.6 Fusion PCR

To join DNA fragments without restriction enzymes or DNA ligation fusion PCR was used. Most expression vectors used in this study containing a gene of interest fused to a fluorescent protein, among others, were cloned using this strategy. First, reverse and forward primers with overlapping 5' sequences were designed for the fragment to be cloned upstream and downstream, respectively. The corresponding primer pair for each fragment (namely a forward primer for the upstream fragment and a reverse primer for the downstream fragment) usually contained a restriction enzyme site. Fragments obtained with their corresponding primer pair by Phusion PCR were purified and then set up in a first round of amplification with PCR with low annealing temperature and few cycles (56°C, 13 cycles). No primers were added to this reaction as each fragment would serve as the primer for the other. In a second round of PCR, 3 µl of the previous product were used as template together with the forward and reverse primers that would amplify the joined fragment (fragment 1's forward primer and fragment 2's reverse primer). Standard PCR conditions were used for this second round of PCR. Because the strategy sometimes yielded unspecific products, the desired PCR product was always gel extracted.

3.7 Transformation

Several strains were used for transformation, depending on the size of the vector cloned and the complexity of cloning. For routine transformations the Subcloning Efficiency DH5α competent cells (Invitrogen) were used. For transformation of ligation, Gateway or Golden GATEway reactions a certain volume of the reactions was used directly for transformation by heat shock in either DH5α, TOP10 or Mach1 competent cells (Invitrogen). If blue/white colony screening was possible, the chromogenic substrate X-gal was added to the bacterial plates 1 h prior to bacterial plating after transformation.

3.8 Colony screening

Colonies grown in LB media with the appropriate antibiotic resistance and at 37°C overnight. To extract the plasmid, the QIAprep Spin Miniprep Kit (Qiagen) kit was used according to manufacturer's instructions. A restriction digest of the extracted plasmids was carried out to confirm correct ligation. The identity of the positive plasmids was further corroborated by sequencing (outsourced to GATC Biotech AG). If a large concentration of highly pure plasmid was required (i.e. for injection or *in vitro* transcription) a Midi was performed using the QIAfilter Plasmid Midi Kit (Qiagen).

3.9 Expression vectors

The following table contains all expression vectors generated in this study together with their purpose. Further information on the vectors used to generate transgenic lines can be found in the Section 4. A more detailed description of each expression vector's cloning strategy as well as primers designed for that purpose can be found in the Appendix, Section 3.

Table VI.3.1. Description of vectors used in this study.

Vector	Description
HSE:asc-mKate2, cmlc2:tagRFP	ASC (ENSDARP00000055920.5) fused to the fluorescent

	protein mKate2 (Evrogen) under the control of a heat shock promoter. Contains red heart marker.
HSE:mKate2, cmlc2:tagRFP	mKate2 under the control of a heat shock promoter. Contains red heart marker.
HSE:asc-mKate2-CAAX, cmlc2:tagRFP	ASC to mKate2 with membrane anchor control of a heat shock promoter. Contains red heart marker.
HSE:asc(4xmut)-mKate2, cmlc2:tagRFP	ASC-mKate2 with 4 missense mutations: T38A, Y152F, T160A and T170A, under the control of a heat shock promoter. Contains red heart marker.
HSE:asc(Y152F)-mKate2, cmlc2:tagRFP	ASC-mKate2 with Y152F mutation, contains red heart marker. Contains red heart marker.
HSE:asc-mKate2, cmlc2:tagRFP*	ASC-mKate2 containing 6 silent point mutations that prevent *asc* ATG morpholino knockdown under the control of a heat shock promoter. This morpholino-resistant version of *asc* is indicated by an asterisk (*asc**). Contains a red heart marker.
HSE:asc, cmlc2:tagRFP*	Untagged ASC* under the control of a heat shock promoter. Contains red heart marker.
HSE:asc-HA, cmlc2:tagRFP*	ASC* tagged with HA under the control of a heat shock promoter. Contains red heart marker.
HSE:PYD$_A$-mKate2, cmlc2:tagRFP	PYD domain of ASC (aa 1-90) fused mKate2 under the control of a heat shock promoter. Contains red heart marker.
HSE:CARD$_A$-mKate2, cmlc2:tagRFP	CARD domain of ASC (aa 112-203) fused mKate2 under the control of a heat shock promoter. Contains red heart marker.
HSE:tGFP, cmlc2:tagRFP	turboGFP (Evrogen) under the control of a heat shock promoter. Contains red heart marker.
HSE:caspa-EGFP, cmlc2:tagRFP	Caspa (ENSDARP00000034228.7) fused with GFP under the control of a heat shock promoter. Contains red heart marker.
HSE:caspb-EGFP, cmlc2:tagRFP	Caspb (ENSDARP00000068268.4) fused with GFP under the control of a heat shock promoter. Contains red heart marker.
HSE:casp3a-EGFP, cmlc2:tagRFP	Casp3a (ENSDARP00000006831.4) fused with GFP under the control of a heat shock promoter. Contains red heart marker.
HSE:PYD$_C$-EGFP, cmlc2:tagRFP	PYD domain of Caspa (aa 1-89) fused to GFP under the control of a heat shock promoter. Contains red heart marker.
HSE:casp$_C$-GFP, cmlc2:tagRFP	Caspase domain of Caspa (aa 134-383) fused to GFP under the control of a heat shock promoter. Contains red heart marker.
ubi:LexPR, LexOP:asc-mKate2, cry:ECFP	ASC-mKate2 is driven by LexPR/LexOP transactivation system. LexPR expression is controlled by ubiquitin

	promoter, contains cyan eye marker.
pCS2-*asc-mKate2*	Vector for *in vitro* transcription of ASC-mKate2 with SP6 promoter.
pCS2-*asc-tGFP*	Vector for *in vitro* transcription of ASC-tGFP with SP6 promoter.

4 Generation of transgenic or mutant lines

Throughout this study three different systems were used to generate transgenic fish. The medaka *il1:EGFP-t2a-il1-HA* and the zebrafish *nfκB:EGFP,luc* were generated using the meganuclease enzyme, the zebrafish *HSE:asc-mkate2* line using Tol2 transposon system, and the CRISPR-Cas9 system was used to generate the *caspa* mutant as well as the *asc:asc-EGFP* knock-in zebrafish lines. Each of these four cases will be described separately below.

4.1 Medaka *il1:EGFP-t2a-il1-HA* line

4.1.1 Vector design

This vector was constructed from the *il1:GFP* vector cloned by Baubak Bajoghli (unpublished). The *il1:GFP* vector contains the 7 kb region upstream of the medaka *interleukin 1 beta* gene (*il1b* , ENSORLG00000000217) (originally amplified from genomic DNA using primers Fwd: 5′-AGTCTCGAGGAGGAGGAGTGGAAGTTCC -3′; Rev: 5′-TATCCATGGTGCCGGCAAACAGAGACATTC -3′) upstream of the *EGFP* CDS. The *il1-HA* sequence was first amplified from a previously available vector (pGEMT-*il1b*) containing the CDS of *il1b* using a forward primer with 16 bp complementary to the *t2a* sequence (5′- GGAGAATCCCGGCCCTATGGAATCTGAGATGG -3′) and a reverse primer containing the *HA* sequence and a and *Spe*I site (5′GTCACTAGTTTAAGCGTAATCTGGAACATCGTATGGGTAACCGCCG CTCTGGCGGATGTGGAAGG-3′). To generate the *t2a-il1-HA* sequence two

oligos cointaining the *t2a* sequence
(Fwd: 5′- GAGGGCAGAGGAAGTCTTCTAACATGCGGTGACGTGGAG GAGAATCCCGGCCCT-3′;
Rev: 5′- AGGGCCGGGATTCTCCTCCACGTCACCGCATGTTAGAAGACTT CCTCTGCCCTC-3′) were annealed and then fused to the PCR product with fusion PCR using the afore mentioned reverse primer for *il1-HA* and a forward primer containing a *Bsp*1407I site
(5′- AGCTGTACAAGGAGGGCAGAGGAAGTCTTCTAAC -3′). This PCR product was digested and inserted, downstream and in frame with the *EGFP* using the *Bsp*1407I and *Spe*I restriction sites.

4.1.2 Injection and screening

An injection solution containing the plasmid (30-40 ng/µl), 0.5 units of *I-Sce*I meganuclease (New England Biolabs) and enzyme buffer was injected into blastomeres at the one-cell stage. Injected embryos were screened for GFP fluorescence at the larval stage and positive larvae were raised to adulthood (F0).

4.2 Zebrafish *nfκB:EGFP,luc* line

4.2.1 Vector design

The vector *nfκB:EGFP,luc* had been previously designed and cloned in the lab (Baubak Bajoghli). It contains 8 multimers of an artificial palindromic *nfκB* sequence flanked by a minimal CMV promoter on each side. The 5′ side contains an *EGFP* CDS downstream of the minimal promoter while the 3′ side contains a *Renilla* luciferase (*luc*) gene. The vector backbone also contains two *I-Sce*I cleavage sites for vector integration using meganuclease.

4.2.2 Injection and screening

An injection solution containing the plasmid (10-20 ng/µl), 0.5 units of *I-Sce*I meganuclease and enzyme buffer was at the one-cell stage. Injected

embryos were screened for fluorescence at the larval stage and positive larvae were raised to adulthood (F0).

4.3 Zebrafish *HSE:asc-mKate2* line

4.3.1 Vector design

The CDS from *asc* (ENSDARG00000040076) was initially amplified from zebrafish cDNA by Sanjita Banerjee
(Fwd: 5′- GCAGCCATGGCGGAATCTTTCAAGGAGC-3′, Rev: 5′-CGCCTCCACCCTCAGCATCCTCAAGGTCATCC -3′). The *asc* CDS was subcloned (Fwd: 5′- CTCGAATTCACCATGGCGGAATCTTTCAAGG -3′, Rev: 5′- ATCAGCTCGCTCACCATACCGCCTCCACCCTCAGC -3′) and fused to mKate2 (Evrogen)
(Fwd: 5′- GCTGAGGGTGGAGGCGGTATGGTGAGCGAGCTGAT-3′, Rev: 5′-ACGTCACTAGTTATCATCTGTGC-3′) via fusion PCR. The fused DNA fragment was inserted into pTH2 (cloned by Marleen Hanelt) a modified Gateway destination vector in which a heat shock element (Bajoghli et al., 2004) drives expression of a gene of interest. The vector backbone also contains Tol2 sites for transgenesis and a red heart (*cmlc2:tagRFP*) marker to facilitate screening for successful integration.

4.3.2 Injection and screening

Plasmid (10-20 ng/µl) and transposase mRNA (200 ng/µl) complemented with 100 mM of KCl were injected into fertilized eggs at the one-cell stage of the zebrafish TLF strain. Injected embryos were screened for red heart fluorescence at the larval stage and positive larvae were raised to adulthood (F0). No heat shock was given at this stage. The F0 generation was screened by outcrossing to Tubingen wild type strain. Larvae were screened for red heart fluorescence. Afterwards, positive larvae were given a heat shock to confirm insertion of the whole construct. A single founder whose progeny had a red heart and also expressed the ASC-mKate2 after heat shock induction was chosen and propagated.

4.4 Zebrafish *caspa* mutant

4.4.1 sgRNA design

Small guide RNAs (sgRNAs) targeting the first exon of zebrafish gene *caspa* (ENSDARG00000008165) were designed using the design tool at http://crispr.mit.edu, which finds and ranks all 23-bp sgRNA sequences ending in the NGG motif according target specificity and genome-wide off targets. In order for the sgRNA to be compatible with the two-oligo PCR method to produce sgRNA (see below) target sequences that did not start with a 5′-G were rejected. From the remaining candidates two sgRNAs were synthesized, Guide 1 *caspa*: 5′-GGACGCTTTAAGTAATATTGGGG-3′ and Guide 2 *caspa*: 5′-GCTGAAAGACGAGATAGATCTGG-3′ using the two-oligo PCR method (Section 6.2).

4.4.2 Injection

To test whether the sgRNAs were targeting the region of interest *in vivo*, sgRNAs were injected in varying concentrations (120-275 ng/µl) together with 1 µl of in-house (Protein Expression and Purification facility, EMBL Heidelberg) synthesized Cas9 (4 mg/ml) complemented with ca. 150 mM KCl into fertilized eggs at the one-cell stage of the zebrafish TLF strain. 24 hours after injection genomic DNA was extracted. Successful knockdown was verified by sequencing of an 800 bp PCR product from the targeted region of *caspa* (Fwd: 5′-TGGGTTAACTAGGCAAGTCAGGG -3′, Rev: 5′-AGGGTGTATCAGGACTTGGGCCC-3′). Using this strategy, Guide 1 was determined to be more efficient and was therefore injected a second time with larvae being raised to adulthood (F0).

4.4.3 Screening and breeding

At 6wpf 20 F0 fish were genotyped by fin clipping. 19/20 fish showed successful targeting of the region of interesting. These F0 fish were later incrossed and the F1 generation was raised to adulthood. The F1 fish were fin

clipped, and the targeted region was amplified and sequence. Among the genotyped F1 fish, three were found to have a *caspa* allele in which the 5′-AAATAATAA -3′ sequence inserted at the expected Cas9 cleavage site. This insertion resulted in the inclusion of two STOP codons (*caspa*^{K**} allele) in the first exon. To discover the second allele, an additional reverse primer was used (5′- CCACACATGGGAGGTGTGAA -3′) to amplify a larger region. The three genotyped F1 fish were found to have a band of 1 kb instead of the expected 1.8kb wild type band. Sequencing of this PCR product revealed that the second allele had a larger deletion of ca. 800 bp (*caspa*$^{\Delta 800}$). The deleted region included most of the first exon including the primer binding site used in the initial genotyping, thus explaining why this allele was not discovered in the first round of screening. The deletion also resulted in a nonsense mutation, thus confirming that these three F1 fish (2 males, one female) were *caspa* mutants and allowing them to be incrossed to obtain homozygous mutants with either the *caspa*^{K**} or the *caspa*$^{\Delta 800}$ deletion allele.

4.5 Zebrafish *asc:asc-EGFP* knock-in

4.5.1 Guide RNA design

Guide RNAs that targeted the last exon of *asc* were designed using the CRISPR/Cas9 target online predictor CCTop (http://crispr.cos.uni-heidelberg.de) (Stemmer et al., 2015). Two suitable hits, Guide 1 *asc*: 5′-ATTCCTGATGGATGACCTTG-3′ and Guide 2 *asc*: 5′-ATCTTCACTCAGCATCCTCA-3′ were synthetized using the oligo annealing method (described below) using the following primers listed in Table VI.4.1.

Table VI.4.1. Primers used for *asc* sgRNA synthesis.

Guide RNA	Primers used for amplification
Guide 1 *asc*	Fwd: 5'- TAGGTCCTGATGGATGACCTTG -3' Rev: 5'- AAACCAAGGTCATCCATCAGGA -3'
Guide 2 *asc*	Fwd: 5'- TAGGCTTCACTCAGCATCCTCA -3' Rev: 5'- AAACTGAGGATGCTGAGTGAAG -3'

4.5.2 Donor vector design

Donor vectors were cloned by Golden GATEway cloning. (Kirchmaier et al., 2013). All vectors except those whose cloning is explained below were kindly provided by the Wittbrodt lab. EV1 included the target site CRISPR 13 for plasmid linearization ('5- GGCGAGGGCGATGCCACCTACGG -3'), EV3 contained an *EGFP* CDS with a flexilinker for tagging of ASC, EV4 was empty and EV6 contained a STOP codon. Homology flanks specific for the 5' and 3' ends were cloned from gDNA into empty EV2 and EV5, respectively. Plasmids were designed according to integration sites and with different lengths of homology flanks and were PCR-amplified with forward primers containing a *Bam*HI cleavage site and reverse primers with a *Kpn*I site. The description of each can be found in Table VI.4.1.

Table VI.4.1. Primers used for amplification of *asc* homology arms from gDNA for each EV vector cloned.

Vector	Primers used for amplification
EV2-common_500bp	Fwd: '5-GCCGGATCCTAAACTTCATCGATGAGCACTGGA-3' Rev: '5-GCCGGTACCCTCAGCATCTTCCAAATCATCCATCAGG-3'
EV2-common_1kb	Fwd: '5-GCCGGATCCTAGCCAGAGCTTACTGTGCTG-3' Rev: '5-GCCGGTACCATCCTCAAGGTCATCCATCAGG-3'
EV5-common_1kb	Fwd: '5-GCCGGATCCTGAAGATTAAATCCTCTCAATCTGCA-3' Rev: '5-GCCGGTACCACAATAGTAATATATAGTGTTTGCTTTGCT-3'
EV5-common_2kb	Fwd: '5-GCCGGATCCTGAAGATTAAATCCTCTCAATCTGCA-3' Rev: '5-GCCGGTACCCATATTTGTACTGGCATATTTGAGCA-3'
EV5-asc2_1kb	Fwd: '5- GCCGGATCCCTGAGTGAAGATTAAATCCTCTC -3' Rev: '5- GCCGGTACCACAATAGTAATATATAGTGTTTGCTTTGCT-3'
EV5-asc2_2kb	Fwd: '5- GCCGGATCCCTGAGTGAAGATTAAATCCTCTC -3' Rev: '5- GCCGGTACCCATATTTGTACTGGCATATTTGAGCA -3'

4.5.3 Injection

First, we tested whether the sgRNAs guide 1 *asc* and guide 2 *asc* were targeting the region of interest *in vivo*, sgRNAs were injected in varying

concentrations (15-150 ng/µl) together with 1 µl of Cas9 (4 mg/ml) complemented with ca. 150 mM KCl into fertilized eggs at the one-cell stage of the zebrafish TLF strain. 24 hours after injection gDNA was extracted. Successful knockdown was verified by sequencing of a 1.3 kb PCR product from the targeted region of *asc*
(Fwd: 5'-CCTGTCTGACCATGTGAACATCTA-3',
Rev: 5'TTAGCATTTGTCCTTATCGCAAAC -3').

For homologous recombination, the DNA (20-50 ng/µl) was injected together with the sgRNA to target *asc* (15-150); the sgRNA for donor vector linearization, CRISPR 13 (150 ng/µl); and 1 µl of Cas9 (4 mg/ml) in a solution containing ca. 150 mM KCl.

4.5.4 Screening and breeding

Larvae were screened at 2dpf for correct recombination with the donor vector by looking for GFP expression in an expression pattern reflecting that of *asc*. Positive larvae were raised into adulthood. To look for founders, adults were outcrossed to TLF and the F1 was screened for GFP expression. F1 was genotyped using primers that bound upstream and downstream of sgRNA guide 2 *asc* target site (Fwd: 5'- AGAGTTATTAACAGGCCCAATCA -3', and Rev: 5'-ACCAATGACTTTGAGATGTG -3'). Because only GFP positive embryos carried the allele corresponding to a successful recombination of the donor vector, GFP embryos (F1) were raised to adulthood.

5 RNA extraction, cDNA synthesis and RT-PCR

5.1 Trizol RNA extraction and DNase treatment

Total RNA was extracted from larvae using TriFast (Peqlab) according to manufacturer's instructions. TriFast reagent was directly added to the larvae. Tissue was homogenized with an electrical homogenizer (Carl Roth GmbH) or by vortexing and was followed by a brief incubation at room temperature to dissociate nucleoprotein complexes. Afterwards, chloroform

was added to the sample and centrifuged to separate the sample into layers. The aqueous upper layer (containing RNA) was transferred to a new tube and isopropanol was added to precipitate the RNA. Samples were left overnight at -20°C to maximize extraction yield. The following day, samples were centrifuged at top speed at 4°C to pellet the RNA. The supernatant was removed and after two ethanol (75%) wash steps, samples were air dried. Each sample was dissolved in 10 to 30 µl of RNase-free water.

To prevent contamination form gDNA, samples were treated with RQ1 RNase-Free DNase (Promega) and then repurified using TriFast.

5.2 cDNA synthesis

To generate first strand cDNA from total extracted RNA was generated using the Superscript III ReverseTranscriptase enzyme (Invitrogen). Briefly, a reaction mix that included oligo(dT) primer, dNTPs and 1 µg of RNA was incubated at 65°C for 5 min and then cooled on ice. Afterwards, the reaction was complemented with enzyme buffer, DTT, RNase Inhibitor and reverse transcriptase. The RT reaction was carried out at 50°C, after which it was inactivated by heating up to 70°C for 5 min. The obtained cDNA was directly used for reverse transcription PCR.

6 RNA synthesis and clean up

6.1 mRNA synthesis

To produce RNA from DNA template, *in vitro* transcriptions (*iv*t) were carried out using the mMessage mMachine kit (Ambion), which yields capped RNA. First, the pCS2 + DNA vector containing the gene of interest to be used as template was linearized and gel extracted in sufficient amounts. The *iv*t reaction was set up according to manufacturer's instructions and contained, NTPs, CAP analog, Reaction buffer, linearized plasmid (template) and the SP6 RNA polymerase. After 2 hours of incubation, Turbo DNase was added to remove template DNA.

6.2 sgRNA synthesis

To synthesize the small guide RNAs (sgRNAs) targeting *caspa*, the two-oligo PCR method (Shah et al., 2015) was used. In the case of sgRNAs targeting *asc* sgRNA plasmids were cloned using oligo annealing (Stemmer et al., 2015).

6.2.1 Two-oligo PCR method

After sgRNA design a "Guide oligo" containing a 20 bp gene-specific sequence between a T7 RNA polymerase promoter and a 20 bp region homologous to the scaffold oligo (5'-AATTAATACGACTCACTATA[20bp target sequence]GTTTTAGAGCTAGAAATAGC-3') as well as a PAGE-purified Scaffold oligo:

(5'-GATCCGCACCGACTCGGTGCCACTTTTTCAAGTTGATAA CGGACTAGCCTTATTTTAACTTGCTATTTCTAGCTCTAAAAC-3')

containing the RNA loop structure required for recognition by Cas9 were synthesized. Both oligos are used to run a Phusion PCR reaction in which 10 µM of each oligo was used to synthesize the template DNA (ca. 120 bp) after both oligos anneal to one another. The thermocycler conditions used were 98°C for 30 s; 45 cycles of 98°C for 10 s, 60°C for 10 s, and 72°C for 15 s; and a final elongation time of 72°C for 5 min. The PCR product (5'-AATTAATACGACTCACTATA[20bp targetsequence]GTTTTAGAGCTAGAAATAGCAAGTTAAAATAAGGCTAG TCCGTTATCAACTTGAAAAAGTGGCACCGAGTCGGTGCGGATC-3) was cleaned up using QIAquick PCR Purification Kit (Qiagen).

6.2.2 Oligo annealing method

Oligo pairs (each 22 bp) corresponding to the same target site were annealed using 1 µl of 100 µM of each oligo with 18 µl H_2O and 20 µl annealing buffer (10 mM Tris, 30 mM NaCl) in a thermocycler. The following conditions were used: 95°C for 10 min, ramp down to 65°C and hold for 10 min, ramp down to 60°C and hold for 10 min, ramp down to 10°C.

Temperature was dropped a rate of 0.1°C/sec. Oligos were designed so that each contained a central complimentary region of 18 bp that was and a 5′ overhang of 4 bp complimentary to the sticky ends generated by *Bsa*I (Thermo Fisher Scientific) cleavage of the guide RNA expression vector DR274 (Addgene #42250). Ligation was carried out using 0.025 pmol of vector and 0.075 pmol of insert DNA.

To obtain the final DNA template, the DR274 plasmid containing the oligo insert was digested with *Dra*I (Thermo Fisher Scientific). The smaller fragment generated by this cleavage contained all elements required for its use as template for the *iv*t.

6.2.3 sgRNA *in vitro* transcription

Regardless of the origin of the template, all sgRNAs were transcribed using the T7 MEGAshortscript Kit (Ambion) according to manufacturer's instructions. In short a rection containing 300 ng of DNA template, NTPs, reaction buffer and T7 RNA polymerase was incubated for 4 hours at 37°C. Afterwards, DNase was added to degrade the template DNA.

6.3 RNA clean up

After *iv*t reaction, RNA was cleaned up using the RNA Clean & Concentrator-5 (Zymogen) according to manufacturer's inscructions. The concentration of both mRNA and sgRNAs was measured using a NanoDrop 8000 spectrophotometer (Thermo Fisher Scientific). If necessary, samples were diluted to desired concentration and afterwards aliquoted and stored at -80°C until their use.

6.4 *in situ* hybridization probe synthesis

The DNA template for *is*h probe synthesis was obtained either by linearizing a plasmid containing the sequence of interest or by amplifying the sequence to be used as probes with a forward primer containing the T3 promoter sequence (5′-AATTAACCCTCACTAAAGGGAAGA-3′) and a

reverse primer containing the T7 promoter sequence (5'-TAATACGACTCACTATAGGGAGA-3'). The advantage of the second method is that it allows for both the sense and antisense probes to be synthesized from the same PCR product, using the T3 and T7 RNA polymerase, respectively. Regardless of which method was used to obtain the DNA template or which RNA polymerase was being used, the *iv*t proceeded the same way, by use of the DIG RNA Labeling Kit (Roche). During the *iv*t digoxigenin-labeled UTP will be incorporated into an otherwise standard single stranded RNA. Probes were purified using SigmaSpin Post-Reaction Clean-Up Columns (Sigma–Aldrich) as previously described (Thisse and Thisse, 2008). Probes were stored at -80°C

7 ASC polyclonal antibody production

The antigen production and antibody purification were performed in-house by the Protein Expression and Purification Core Facility (EMBL, Heidelberg). The immunization procedure and all animal handling was carried out also in-house by the Laboratory Animal Resources.

7.1 ASC purification

ASC was purified using a SUMO3 and His tag. To fuse the CDS of ASC to both tags, the sequence was amplified from the previously constructed *HSE:asc-mKate* vector and cloned into the pETM-11 vector using a *Bam*HI and a *Hin*dIII site on the forward (5'-TCATCTGGATCCATGGCGGAATCTTTCAAGGAG-3') and reverse (5'-TCATCTAAGCTTTCACTCAGCATCCTCAAGGTC-3') primers. The vector was transformed into the *E. coli* BL21 (DE3) CodonPlus-RIL strain (Stratagene) and expressed in a large scale. After lysis and sonication most ASC-SUMO3 remained in the pellet, so it was resuspended in denaturing buffer conditions of 6 M Guanidine hydrochloride. ASC-SUMO3 was purified under these denaturing conditions in a Niquel- Nitrilotriacetic (Ni-NTA) columns. Eluted fractions containing ASC-SUMO3 were pooled and dialyzed

against 2 M Urea buffer. Digestion with Senp2 to cleave the SUMO3 tag was performed under these conditions. Because the protein precipitated after digest, it was resuspended once again in a denaturing buffer of 6 M Urea (final concentration 12.9 mg/ml), snap frozen in liquid nitrogen and stored at -80°C.

7.2 Immunization

Immunization was carried out in 2 female rabbits (New Zealand White, 2-2.5 kg). To prepare sample for injection, 300 µg of ASC were diluted 1:6 in H_2O and then 1:2 in TiterMax adjuvant. Prior to the primary immunization, a pre-immune bleed sample was taken. At day 14 after primary immunization a first boost was given, and a second boost two weeks later. 12 days afterwards a first bleed was taken and tested. The last 3 boosts were given at day 56, 84 and 112 after primary immunization, with second and third bleeds taken at day 66 and 94, respectively. The terminal bleed was performed under anesthesia at day 122.

7.3 Antibody purification

For antibody purification ASC protein was coupled to Cyanogen-Bromide-activated Sepharose. 10 ml of serum from the final bleed were used per ml of antigen-coupled resin. Suspension was transferred to a column for elution of antibody using low pH glycine buffer neutralized immediately after elution. Antibody-containing eluate fractions were pooled, complemented with 0.05% sodium azide and stored at 4°C.

8 Protein extraction, immunoprecipitation and Mass Spectrometry

8.1 Protein extraction

Protein extraction of both larvae and adult tissues was carried out in freshly prepared IP buffer (10 mM HEPES pH 7.5, 100 mM KCl, 2 mM $MgCl_2$,

0.1 mM $CaCl_2$, 5 mM EGTA pH 8.0, 1 mM NaF, 1 mM Na_3VO_4, 0.5% Triton, Protease inhibitor cocktail tablets [1 tablet/10 ml, Roche]). After collection, samples (one adult organ or up to 5 larvae) were submerged completely in 250 µl IP buffer and kept on ice. Samples were then sonicated to disintegrate tissue until no longer turbid. Tissue lysate was cleared by centrifugating at 4°C for 15 min at 14000 rpm and supernatant was transferred to a fresh tube on ice.

8.2 Immunoprecipitation

Immunoprecipitation was carried out using EZview Red Anti-HA Affinity Gel (Sigma Aldrich) according to manufacturer's instructions. Protein lysates were first precleared using EZview Red Protein A Affinity Gel (Sigma Aldrich) by incubating the lysate 1h at 4°C in IP buffer-equilibrated beads. Afterwards, samples were incubated with buffer-equilibrated Anti-HA beads overnight at 4°C, washed and eluted with HA peptide (Sigma Aldrich). To determine efficiency of immunoprecipitation, a small sample volume of the input and supernatant from wash before elution was collected for analysis. After collection 5xSDS Sample Buffer (10% SDS, 20% glycerol, 0.2M Tris-HCl pH 6.8, 0.05% Bromophenol Blue and 10% β-mercaptoethanol added right before use) was added to the samples, which were then denatured by boiling for 5 min at 95°C. Samples were afterwards stored at -20°C.

8.3 Immunoblotting

Prepared protein samples were separated by SDS-PAGE performed using the Mini-PROTEAN Vertical Electrophoresis Cell system (Bio-Rad) in 1x Lämmli running buffer (25 mM Tris, 192 mM glycine, 0.1% SDS). Proteins in the acrylamide gel were transferred to a polyvinylidene difluoride (PVDF) membrane (Immobilion-P) in a semi-dry transfer cell (Bio Rad). Gel, membrane (the latter after activation with methanol) and filter papers (Extra thick blot paper, Bio Rad) were submerged in transfer buffer (25 mM Tris, 192 mM glycine, 0.037% SDS, 20% methanol) and stacked, with the membrane

placed below the gel and both sandwiched between two filter papers. Proteins were transferred 13 V for 1 h. After transfer, the membrane was blocked with 10% dry milk powder (Reform Instant-Magermilchpulver, Frema) in PBST for 1 h to prevent non-specific background binding of the antibodies. Primary antibody was diluted in 5% dry milk powder in PBST at a given dilution and incubated overnight at 4°C with agitation. Afterwards, excess antibody was removed by washing with PBST 15 min three times. Secondary antibody was also prepared in 5% dry milk powder in PBST, but incubated only 1 h at room temperature with agitation. Excess secondary antibody was removed by washing with PBST 15 min three times. Detection was carried out using Luminata Crescendo Western HRP Substrate (Millipore) according to manufacturer's instructions. Chemiluminescent films (Amersham Hyperfilm ECL, GE Healthcare) were exposed to membranes and developed using an automated film developer.

8.4 Mass Spectrometry

All processing of samples and mass spectrometry was performed in house by the Proteomics facility at EMBL, Heidelberg. In brief, samples to be processes were run on an acrylamide gel and the gel was stained with Coomasie to visualize and cut bands of interest. Afterwards, an in-gel digest was performed with Trypsin. Peptides were then extracted from the gel and separated by HPLC (High Pressure Liquid Chromatography) in a NanoAcquity UPLC System (Waters). Peptides were afterwards identified and quantified by MS/MS in the hybrid linear ion trap-Orbitrap mass spectrometer LTQ Orbitrap Velos Pro (Thermo Fisher Scientific). Data was analyzed using Mascot (Matrix Science).

9 Flow Cytometry

Tissues from adult medaka (spleen, head kidney and blood) were collected essentially as described (Aghaallaei et al., 2010). Namely, after collection, all tissues were kept on ice. Blood was immediately diluted in 0.57

PBS/30 mM EDTA, and blood cells were pelleted (300 g for 5 min at 4°C) and resuspended in FACS buffer (5 mM EDTA, 10 U/ml Heparin in PBS). In the case of the head kidney and spleen, organs were submerged in FACS buffer directly after collection and, to obtain a single cell suspension, organs were disaggregated by using a cell strainer (40 μm Nylon, BD Falcon). Cell suspensions were sorted on a BD LSRFortessa Cell Analyzer (BD Biosciences).

10 Imaging

10.1 Mounting

For confocal microscopy, anesthetized larvae were mounted in 1.3% low-melting point agarose (Peqlab). The agarose was prepared beforehand in E3 medium, aliquoted in 1 ml and kept at 42°C during sample mounting. Anesthetized larvae were transferred to the agarose using a glass Pasteur pipette, pipetted back up from the agarose and then deposited in a glass bottom culture dish (P35G-1.5-10-C, MatTek). Immediately after, larvae were oriented using a needle or a micropipette tip. In the case of SPIM imaging, larvae were deposited in a Petri dish after being submerged in agarose and were subsequently sucked up a glass capillary using a plunger. The sample was then pushed out of the capillary (which became the sample holder) prior to imaging. The immersion media was supplemented with Tricaine so that larvae remain anesthetized during imaging.

10.2 Acridine Orange staining

Acridine Orange (AO) is a live dye that has previously been used to label dying cells in live zebrafish embryos (Peri and Nüsslein-Volhard, 2008). To stain larvae with AO, a 1:1500 dilution of a 10 mg/ml stock (Sigma Aldrich) was prepared in E3. Larvae were incubated for 45 min and then rinsed 3 times and kept 5 min in the last wash to get rid of excess dye. Larvae were anesthetized, mounted and imaged directly afterwards. Because AO is a light-sensitive dye, larvae were kept in the dark during staining.

10.3 Microscopes

Several microscopes were used during this study. Table lists all miscroscopes used.

Table VI.10.1. Microscopes used in this study.

Microscope	Objectives
Zeiss LSM 780 confocal microscope	5x NA 0.16 air 10x NA 0.45 air 20x NA 0.8 air 40x NA 1.1 water
Zeiss LSM 780 NLO 2-Photon confocal microscope	
Leica SP8 TCS confocal microscope	40x NA 1.1 water
Zeiss Lightsheet Z.1 microscope	20x water

Image acquisition and some occasional processing (such as tile merging) were carried out using the commercial software developed for each microscope by the manufacturer.

10.4 Image processing

Raw images were processed using ImageJ/Fiji (NIH) and Imaris x64 7.6.4 (Bitplane, AG). Deconvolution was carried out using Huygens Deconvolution (Scientific Volume Imaging).

10.5 Bioluminescence measurement

Luciferase activity of zebrafish larvae was measured as previously described (Lahiri et al., 2014) in collaboration with Nik Foulkes (KIT). In brief, individual larvae are placed in separate wells in 96-multiwell plates. Beetle luciferin reagent (Promega) is directly added to the medium of each well. The plate is then sealed. Afterwards, bioluminescence from whole larvae is assayed using a Packard Top-count NXT scintillation counter or an EnVision multilabel counter (Perkin Elmer).

11 *In situ* hybridization (*is*h)

11.1 Protocol

In situ hybridization was performed essentially as previously described (Thisse and Thisse, 2008). In short, larvae were fixed overnight in 4% paraformaldehyde (PFA) at 4°C. After washes with PBS and PBST (0.1% Tween 20 in PBS), samples were dehydrated in a graded series of methanol (MeOH) diluted in PBST (25% MeOH, 50% MeOH, 75% MeOH, 100% MeOH) at room temperature for 5 min and stored overnight in 100% MeOH at -20°C. Embryos were occasionally stored at this point for later processing. Larvae were rehydrated in the same graded series of MeOH. After several washes in PBST larvae older than 1dpf were permeabilized with a Proteinase-K (Roche) treatment according to age (15 min of 5 µg/ml for 2 dpf, 35 min of 10 µg/ml for 3 dpf, 35 min of 30 µg/ml for 4dpf). After treatment, samples were washed with PBST and postfixed with 4% PFA. Samples were washed with PBST to remove PFA before adding Hyb- mix and incubating 5 min at 67°C in a water bath. Hyb- mix was substituted with Hyb+ mix and kept at 67°C for 4 to 6 hours. Afterwards, 100 µl of Hyb+ containing approximately 100 ng of probe were added and samples were incubated overnight at 67°C for hybridization. Probe was removed the following day and samples were washed in formamide 50%/SSCT 2x twice for 30 min, in SSCT 2x for 15 min, and twice in SSCT 0.2x for 30 min. All washes were carried out at 67°C. Samples were then switched to room temperature and washed twice with Malate buffer before blocking with blocking buffer for 1 hour. Samples were then incubated overnight with a 1:4000 dilution of AntiDig-AP (Roche) in blocking buffer at 4°C. Following antibody incubation Malate buffer 2x was used to rinse samples and then to wash four times for periods of 25 min per wash. Sample was then equilibrated with staining buffer by washing 5 min three times. Staining buffer was then substituted with BM Purple AP substrate (Roche) and incubated in the dark until signal was visible. After staining, samples were washed with PBST, postfixed with 4% PFA, washed with PBST again. If

necessary, samples were cleared in 70% ethanol (EtOH) and 100% EtOH washes to diminish background. For long term storage samples were washed in 25% glycerol/PBS , transferred to 50% glycerol/PBS and kept at 4°C.

11.2 Plastic embedding and sectioning

In situ samples were sectioned using the Leica Historesin embedding kit (Leica Microsystems) according to manufacturer's instructions. Sample is first submerged in an intermediate infiltration solution (1:1.95% EtOH: Infiltration solution) and then transferred to infiltration solution. Embedding medium is prepared by mixing infiltration solution and a hardener powder. Only one specimen was immersed per well containing embedding medium in a Historesin Mold tray and left to harden. Sectioning was carried out manually using Leica RM2235 Manual Rotary Microtome (Leica Microsystems). Sections were placed on distilled water to remove wrinkles, mounted on glass slides (Super Frost, Thermo Fisher Scientific) and air dried.

11.3 Solutions

Table VI.11.1. Solutions and buffers used in this study.

Name	Components
PBST	0.1% Tween 20 in PBS.
20x SSC	NaCl 175.3 g, 88.2 g citric acid trisodium salt dissolved in 1 l H_2O pH adjusted to 7.0 with NaOH.
Hyb- mix	50% Formamide, 5x SSC, 0.1% Tween 20. Stored at -20°C.
Hyb+ mix	50 µg/ml Heparin, 5 mg/ml tRNA added to Hyb- mix. Stored at -20°C.
2x Malate buffer	200 mM Malate pH7.5, 300 mM NaCl, 0.1% Tween 20 added prior to use.
Blocking buffer	2% of Blocking Reagent (Roche), 50% 2x Malate Buffer with 0.1% Tween-20.
Staining buffer	100 mM Tris pH 9.5, 50 mM $MgCl_2$, 100 mM NaCl, 0.1% Tween 20 added just prior to use.

12 Immunostainings

Immunostainings were carried out using two different protocols, depending on the tissue being stained. They will be designated protocol 1 and 2. The second protocol allows for preservation of the epidermis and was therefore used to visualize the keratinocytes.

12.1 Protocol 1

For an immunostaining of internal tissues a previously published immunstaining protocol was followed (Varela et al., 2014). In short, larvae were fixed overnight in 4% PFA at 4°C. After several washes with PBS and PBST, samples were dehydrated in a graded series of MeOH diluted in PBST (25% MeOH, 50% MeOH, 75% MeOH, 100% MeOH) at room temperature while on a rocker for 5 min and stored overnight in 100% MeOH at -20°C. The following day embryos were rehydrated in a graded series of MeOH this time diluted in PBS-DTx (1% DMSO, 0.3% TritonX-100 in PBS). After several washes in PBS-DTx embryos were permeabilized with a PK treatment according to age (see in situ hybridization protocol for details on treatment). After PK digest samples were washed in PBS-DTx and blocked with blocking buffer (5%BSA in PBS-DTx) for 1 h at room temperature. Primary antibody was diluted in blocking buffer and samples were incubated overnight at 4°C. Samples were washed in PBS-DTx, incubated with secondary antibody 2 hours at room temperature, and washed again extensively with PBS-DTx.

12.2 Protocol 2

To visualize keratinocyte staining a much simpler and less abrasive protocol was used. The MeOH dehydration, PK treatment and postfixation were skipped entirely. Instead, fixed larvae were washed and then staining proceeded from blocking step, using PBST for all steps instead of PBS-DTx.

12.3 Antibodies

Table VI.12.1. Primary and secondary antibodies used in this study.

Antibody: Primary (p) or Secondary (s)	**Dilution and assay**	**Source**
antiASC (p, rabbit)	1:1000 (WB, IC)	Produced in house during this study
antiGFP (p, mouse)	1:1000 (IC) 1:10000 (WB)	Santa Cruz
antiLamin B2 (p, mouse)	1:200 (IC)	Thermo Fisher Scientific
anti-HA (p, rat)	1:200 (WB)	Roche
antiMouse-HRP (s)	1:5000 (WB)	Jackson ImmunoResearch
antiRabbit-HRP (s)	1:5000 (WB)	Jackson ImmunoResearch
antiRat-HRP (s)	1:5000 (WB)	Dianova
antiMouse-488 (s)	1:500 (IC)	Invitrogen
antiMouse-568 (s)	1:500 (IC)	Invitrogen
antiRabbit-488 (s)	1:500 (IC)	Invitrogen
antiRabbit-568 (s)	1:500 (IC)	Invitrogen
antiRabbit-647 (s)	1:300 (IC)	Invitrogen

VII. Appendix

1 Abbreviations

- aa: **a**mino **a**cid
- Ab: Antibody
- ASC: **A**poptosis-associated **s**peck-like protein containing a **C**ARD
- BSA: **b**ovine **s**erum **a**lbumin
- CAAX: CAAX prenylation sequence
- CARD: **c**aspase **a**ctivation and **r**ecruitment **d**omain
- Cas: **C**RISPR **a**ssociated **s**ystem
- cDNA: **c**omplimentary **DNA**
- CDS: **c**oding **D**NA **s**equence
- CHT: **C**audal **h**ematopoietic **t**issue
- CMV: **C**yto**m**egalo**v**irus
- CRISPR: **c**lustered **r**egularly-**i**nterspaced **s**hort **p**alindromic **r**epeats
- DAMPs: **D**anger-**a**ssociated **m**olecular **p**atterns
- DFD: **d**eath-**f**old **d**omain
- DTT: **D**i**t**hio**t**hreitol
- DMSO: **d**i**m**ethyl **s**ulf**o**xide
- dpf: **d**ays **p**ost **f**ertilization
- ECFP: **e**nhanced **c**yan **f**luorescent **p**rotein
- EGFP: **e**nhanced **g**reen **f**luorescent **p**rotein
- EM: **E**lectron **m**ycroscopy
- EtOH: Ethanol
- FACS: **f**luorescence-**a**ctivated **c**ell **s**orting
- Fwd: **f**or**w**ar**d** primer
- gDNA: **g**enomic **DNA**
- HA: **h**uman influenza hem**a**gglutinin
- hpf: **h**ours **p**ost **f**ertilization
- HPV: **H**uman **p**apilloma**v**irus
- HSE: **h**eat **s**hock **e**lement
- IEC: **I**ntestinal **e**pithelial **c**ells
- IP: **I**mmuno**p**recipitation
- *is*h: ***i**n **s**itu* **h**ybridization

- *ivt*: ***i****n vitro* **t**ranscription
- LPS: Bacterial **l**ipo**p**oly**s**accharides
- LRR: **l**eucine-**r**ich **r**epeats
- MeOH: Methanol
- min: **min**utes
- MS: **M**ass **S**pectrometry
- NBD: **n**ucleotide **b**inding **d**omain
- NF-κB: **N**uclear **f**actor **k**appa-light-chain-enhancer of activated **B** cells
- NHEJ: **N**on-**h**omologous **e**nd **j**oining
- NLR: **N**OD-**l**ike **r**eceptors
- NLS: **N**uclear **l**ocalization **s**ignal
- NOD: **n**ucleotide-binding and **o**ligomerization **d**omain
- PAGE: **p**oly**a**crylamide **g**el electrophoresis
- PAMPs: **P**athogen-**a**ssociated **m**olecular **p**atterns
- PBDTx: **p**hosphate-**b**uffered **s**aline plus 0.3%**D**MSO, 0.1%**T**riton-**x**
- PBS: **p**hosphate-**b**uffered **s**aline
- PBST: **p**hosphate-**b**uffered **s**aline plus 0.1% **T**ween- 20
- PFA: **p**ara**f**orm**a**ldehyde
- PHA: **p**hyto**h**aem**a**gglutinin
- PRR: **P**athogen **r**ecognition **r**eceptors
- PTM: **P**ost-**t**ranslational **m**odification
- PYD: **py**rin **d**omain
- Rev: **rev**erse primer
- RFP: **r**ed **f**luorescent **p**rotein
- ROS: **r**eactive **o**xygen **s**pecies
- RT-PCR: **r**everse-**t**ranscription **p**olymerase **c**hain **r**eaction
- SDS: **s**odium **d**odecyl **s**ulfate
- sgRNA: **s**mall **g**uide **R**NA
- SMOC: **s**upra**m**olecular **o**rganizing **c**enters
- T2A: viral 2A peptide
- TLR: **T**oll-**l**ike **r**eceptor
- WHD: **w**inged **h**elix **d**omain

2 RT-PCR Primers

Table VII.2.1. Reverse transcription primers used in this study.

Gene	Sequence (5′- -3′)
asc (zebrafish)	GATCAAGTGTATTGCAGTAGC
	CAATTCTTTCCAGTGCTCATCG
ef1a (zebrafish)	CTTCTCAGGCTGACTGTGC
	CCGCTAGCATTACCCTCC
interleukin-1 (medaka)	GAACCGCAGCACAGCTCACAGC
	ACATGTTCAGCTGGACTTTGC
nfκB (medaka)	AGCCACTGCCTCACTATGAGTC
	AGTAAAAAGTTCCGCCTCCTCC
ef1a (medaka)	AAGTTCGAGAAGGAAGCCGC
	GCTGGGTTGTAGCCGATCTT

3 Cloning strategies of expression vectors

Table VII.3.1. List of all expression vectors designed and cloned in this study, including cloning strategy and primers.

Vector	Description	Sequence (5′- -3′)	Cloning strategy
HSE:asc-mKate2, cmlc2:tagRFP	Fwd *asc*(*Eco*RI)	GCTTGAATTCACCATGGC GGAATC	Fusion PCR to fuse *asc* and mKate2 fragments. Restriction digest (*Eco*RI/*Eco*RV) to insert into final vector.
	Rev *asc-mKate2* fusion	ATCAGCTCGCTCACCATA CCGCCTCCACCCTCAGC	
	Fwd *asc-mKate2* fusion	GCTGAGGGTGGAGGCGG TATGGTGAGCGAGCTGAT	
	Rev *mKate2* (*Eco*RV)	CTAGTGATATCTCATCTG TGC	
HSE:mKate2, cmlc2:tagRFP	Fwd *mKate2* (*Eco*RI)	CTCGAATTCACTATGGTG AGCGAGCTGATTAAG	PCR and restriction digest (*Eco*RI/*Eco*RV) to insert into final vector.
	Rev *mKate2* (*Eco*RV)	ACGTCACTAGTTATCATC TGTGC	
HSE:asc-mKate2-CAAX,	Fwd *asc* (*Eco*RI)	GCTTGAATTCACCATGGC GGAATC	Fusion PCR to fuse *asc* and *mKate2-CAAX* fragments.
	Rev *asc-mkate2*	ATCAGCTCGCTCACCATA	

cmlc2:tagRFP	fusion	CCGCCTCCACCCTCAGC	Restriction digest (*Eco*RI/*Eco*RV) to insert into final vector.
	Fwd *asc-mKate2* fusion	GCTGAGGGTGGAGGCGG TATGGTGAGCGAGCTGAT	
	M13R (amplifies with *Eco*RV site)	CAGGAAACAGCTATGAC	
HSE:asc(4xmut)-mKate2, cmlc2:tagRFP	Fwd mut T38A	GGAGGCAGGAACCGCGC GTCGCAAAGTCTGCAATC GAAAAGCTG	Site-directed mutagenesis of *HSE:acs-mKate2, cmlc2:tagRFP* done in two rounds, first with primer pairs for T38A and T160A mutations. Second round of site-directed mutagenesis was carried out in that modified vector with primer pairs for Y152F and T170A mutations
	Rev mut T38A	CAGCTTTTCGATTGCAGA CTTTGCGACGCGCGGTTC CTGCCTCC	
	Fwd mut Y152F	CATCACAAATGAGGATTT CTGTACCATTCGTAATAA G	
	Rev mut Y152F	CTTATTACGAATGGTACA GAAATCCTCATTTGTGAT G	
	Fwd mut T160A	CCATTCGTAATAAGGAG GCTCCTCAAAAGAAGAT G	
	Rev mut T160A	CATCTTCTTTTGAGGAGC CTCCTTATTACGAATGG	
	Fwd mut T170A	GAGAGAGTTATTAGCAG GCCCAATCACATG	
	Rev mut T170A	CATGTGATTGGGCCTGCT AATAACTCTCTC	
HSE:asc(Y152F)-mKate2, cmlc2:tagRFP	Fwd mut Y152F	CATCACAAATGAGGATTT CTGTACCATTCGTAATAA G	Site-directed mutagenesis of *HSE:asc-mKate2, cmlc2:tagRFP* with primer pair for Y152F.
	Rev mut Y152F	CTTATTACGAATGGTACA GAAATCCTCATTTGTGAT G	
HSE:asc-mKate2, cmlc2:tagRFP*	Fwd mut G6A, A9G, T12A	GCTTGAATTCACCATGGC AGAGTCATTCAAGGAGC AGCTGCAG	To make *HSE:asc-mKate2, cmlc2:tagRFP asc* ATG morpholino-resistant a total of 6bp changes were made with two rounds of site-directed mutagenesis, first with primer pair G6A, A9G, T12A mutations.
	Rev mut G6A, A9G, T12A	CTGCAGCTGCTCCTTGAA TGACTCTGCCATGGTGAA TTCAAGC	
	Fwd mut G18A, G21A, G24A	CTCAAAAGCCTCCTGCAG TTGTTCTTTGAATGACTCT GCCATGGTG	

	Rev mut G18A, G21A, G24A	CACCATGGCAGAGTCATTCAAAGAACAACTGCAGGAGGCTTTTGAG	Second round of site-directed mutagenesis was carried out in that modified vector with primer pair for G18A, G21A, G24A.
HSE:zASC, cmlc2:tagRFP*	Fwd *asc** (*Nhe*I)	CACTATAGGGCTAGCTTGATTTA	PCR from *HSE:asc*-mKate2, cmlc2:tagRFP* and restriction digest (*Nhe*I).
	Rev *asc*	CTTCACTCAGCATCCTCAAGGTCATCC	
HSE:asc-HA, cmlc2:tagRFP*	Fwd *asc** (*Nhe*I)	CACTATAGGGCTAGCTTGATTTA	PCR from HSE:zASC*-mKate2, cmlc2:tagRFP and restriction digest (NheI).
	Rev HA tag	GATGTCGACTCAAGCGTAATCTGGAACATCGTATGGGTAACCGCCTCCACCCTCAGC	
HSE:PYD$_A$-mKate2, cmlc2:tagRFP	Fwd *zASC* (*Eco*RI)	GCTTGAATTCACCATGGCGGAATC	Fusion PCR to fuse *PYD$_A$* and *mKate2* fragments. Restriction digest (*Eco*RI/*Eco*RV) to insert into final vector.
	Rev *PYD$_A$* - *mKate2* fusion	ACCATACCGCCTCCACCTTGCCCTGTGTTCCTC	
	Fwd *PYD$_A$* - *mKate2* fusion	GAGGAACACAGGGCAAGGTGGAGGCGGTATGGT	
	Rev *mKate2* (*Eco*RV)	CTAGTGATATCTCATCTGTGC	
HSE:CARD$_A$-mKate2, cmlc2:tagRFP	Fwd *CARD$_A$* (*Bam*HI)	TTGAATTCAGAATGGTTGCTTTCTCCAAGG	PCR from *HSE:asc-mKate2, cmlc2:tagRFP* and restriction digest (*Bam*HI).
	Rev *mKate2* (*Eco*RV)	CTAGTGATATCTCATCTGTGC	
HSE:tGFP, cmlc2:tagRFP	Fwd *tGFP* (*Eco*RI)	GCTTGAATTCACCATGGAGAGCGACGAGAGCG	PCR from and restriction digest (*Eco*RI/*Eco*RV).
	Rev *tGFP* (*Eco*RV)	TCATCTGATATCTTATTCTTCACCGGCATCTGC	
HSE:caspa-EGFP, cmlc2:tagRFP	Fwd *caspa* (*Bam*HI)	TCAGGATCCAAGATGGCCAAATCTATCAAGGACC	PCR to amplify *caspa* from cDNA. Fusion PCR to fuse *caspa* and *EGFP* fragments. Restriction digest (*Bam*HI/*Eco*RV) to insert into final vector.
	Rev *caspa-EGFP* fusion	GCTCACCATGGTGGCGACCGGGAGTCCGGGGAACAGGTAGAAC	
	Fwd *caspa-EGFP* fusion	GTTCTACCTGTTCCCCGGACTCCCGGTCGCCACCATGGTGAGC	

	Rev *EGFP* (*Eco*RV)	CTAGATATCTTACTTGTACAGCTCGTCCATGC	
HSE:caspb-EGFP, cmlc2:tagRFP	Fwd *caspb* (*Bam*HI)	GTCGGATCCAGAATGGAGGATATTACCCAGC	PCR to amplify *caspb* from cDNA. Fusion PCR to fuse caspb and *EGFP* fragments. Restriction digest (*Bam*HI/*Eco*RV) to insert into final vector.
	Rev *caspb*	CAGTCCAGGAAACAGGTAGAACC	
	Rev *caspb-EGFP* fusion	CCTTGCTCACCATGGTGGCGACCGGCAGTCCAGGAAACAGG	
	Fwd *caspb-EGFP* fusion	CCTGTTTCCTGGACTGCCGGTCGCCACCATGGTGAGCAAGG	
	Rev *EGFP* (*Eco*RV)	CTAGATATCTTACTTGTACAGCTCGTCCATGC	
HSE:casp3a-EGFP, cmlc2:tagRFP	Fwd *casp3a* (*Bgl*II)	GTCAGATCTAAGATGAACGGAGACTGTGTGG	PCR to amplify *casp3a* from cDNA. Fusion PCR to fuse *casp3a* and *EGFP* fragments. Restriction digest (*Bgl*III/*Eco*RV) to insert into final vector.
	Rev *casp3a*	GGAGTGAAGTACATCTCTTTGG	
	Rev *casp3a-EGFP* fusion	GGAGTGAAGTACATCTCTTTGG	
	Fwd *casp3a-EGFP* fusion	GAGATGTACTTCACTCCTCCGGTCGCCACCATGGTGAGC	
	Rev *EGFP* (*Eco*RV)	CTAGATATCTTACTTGTACAGCTCGTCCATGC	
HSE:PYD$_C$-EGFP, cmlc2:tagRFP	Fwd *PYD$_C$* (*Bam*HI)	TTCGGATCCAAGATGGCCAAATC	Fusion PCR to fuse *PYD$_C$* and *EGFP* fragments. Restriction digest (*Bam*HI/*Eco*RV) to insert into final vector.
	Rev fusion *PYD$_C$ -GFP*	GCTCACCATGGTGGCGACCGGTTGCCCTGTGTTCTCCAAGAGC	
	Fwd fusion *PYD$_C$ -GFP*	GCTCTTGGAGAACACAGGGCAACCGGTCGCCACCATGGTGAGC	
	Rev *EGFP* (*Eco*RV)	CTAGATATCTTACTTGTACAGCTCGTCCATGC	
HSE:Casp$_C$-GFP, cmlc2:tagRFP	Fwd *Casp$_C$* with *Bam*HI	GTCGGATCCAGAATGACTTATGAAATAAAAGAC	PCR from *HSE:Caspa-EGFP*, *cmlc2:tagRFP* and restriction digest (*Bam*HI).
	Rev *EGFP* (*Eco*RV)	CTAGATATCTTACTTGTACAGCTCGTCCATGC	

ubi:LexPR, LexOP:asc-mKate2, cry:ECFP	Fwd *asc attB2R*	GGGGACAGCTTTCTTGTACAAAGTGGATATGGCGGAATCTTTCAAG	PCR to amplify *asc-mKate2* with *att* sites to insert into p3'E via BP reaction. LR reaction to produce final vector was done with *p*5'E:*ub*i and pME:*LexPR,LexOP* and pDEST *cry:ECFP*.
	Fwd *mKate2 attB3*	GGGGACAACTTTGTATAATAAAGTTGCTCATCTGTGCCCCAGTTTG	
pCS2- *asc-mKate2*	Fwd *asc* (*Eco*RI)	GCTTGAATTCACCATGGCGGAATC	PCR and restriction digest (*Eco*RI/*Eco*RV) to insert into final vector.
	Rev *mKate2* (*Eco*RV)	ACGTCACTAGTTATCATCTGTGC	
pCS2- *asc-tGFP*	Fwd *asc* (*Eco*RI)	GCTTGAATTCACCATGGCGGAATC	Fusion PCR to fuse *asc* and *tGFP* fragments. Restriction digest (*Eco*RI/*Eco*RV) to insert into final vector.
	Rev *asc-tGFP* fusion	CGCTCTCGTCGCTCTCCATACCGCCTCCACCCTCAGC	
	Fwd *asc-tGFP* fusion	GCTGAGGGTGGAGGCGGTATGGAGAGCGACGAGAGCG	
	Rev *tGFP* (*Eco*RV)	TCATCTGATATCTTATTCTTCACCGGCATCTGC	

4 Collaborations

- Thomas Thumberger, Centre for Organismal Studies (COS), Heidelberg, Germany
- Nik Foulkes, Karlsruhe Institute of Technology, Karlsruhe, Germany

5 Publications

- Bajoghli, B., **Kuri, P**., Inoue, D., Aghaallaei, N., Hanelt, M., Thumberger, T., Rauzi, M., Wittbrodt, J., and Leptin, M. (2015). Noninvasive In Toto Imaging of the Thymus Reveals Heterogeneous Migratory Behavior of Developing T Cells. The Journal of Immunology.

VIII. References

Aachoui, Y., Sagulenko, V., Miao, E.A., and Stacey, K.J. (2013). Inflammasome-mediated pyroptotic and apoptotic cell death, and defense against infection. Curr. Opin. Microbiol. *16*, 319–326.

Afonina, I.S., Müller, C., Martin, S.J., and Beyaert, R. (2015). Proteolytic Processing of Interleukin-1 Family Cytokines: Variations on a Common Theme. Immunity *42*, 991–1004.

Aghaallaei, N., Bajoghli, B., Schwarz, H., Schorpp, M., and Boehm, T. (2010). Characterization of mononuclear phagocytic cells in medaka fish transgenic for a cxcr3a:gfp reporter. Proc Natl Acad Sci USA *107*, 18079–18084.

Alcaraz-Pérez, F., Mulero, V., and Cayuela, M.L. (2008). Application of the dual-luciferase reporter assay to the analysis of promoter activity in Zebrafish embryos. BMC Biotechnol *8*, 81.

Angosto, D., and Mulero, V. (2014). The zebrafish as a model to study the inflammasome. Inflammasome.

Angosto, D., López-Castejón, G., López-Muñoz, A., Sepulcre, M.P., Arizcun, M., Meseguer, J., and Mulero, V. (2012). Evolution of inflammasome functions in vertebrates: Inflammasome and caspase-1 trigger fish macrophage cell death but are dispensable for the processing of IL-1β. Innate Immun.

Auer, T.O., and Del Bene, F. (2014). CRISPR/Cas9 and TALEN-mediated knock-in approaches in zebrafish. Methods *69*, 142–150.

Auer, T.O., Duroure, K., De Cian, A., Concordet, J.-P., and Del Bene, F. (2014). Highly efficient CRISPR/Cas9-mediated knock-in in zebrafish by homology-independent DNA repair. Genome Res. *24*, 142–153.

Badr, C.E., Niers, J.M., Tjon-Kon-Fat, L.-A., Noske, D.P., Wurdinger, T., and Tannous, B.A. (2009). Real-time monitoring of nuclear factor kappaB activity in cultured cells and in animal models. Mol Imaging *8*, 278–290.

Bajoghli, B., Aghaallaei, N., Heimbucher, T., and Czerny, T. (2004). An artificial promoter construct for heat-inducible misexpression during fish embryogenesis. Dev Biol *271*, 416–430.

Banerjee, S., and Leptin, M. (2014). Systemic response to ultraviolet radiation involves induction of leukocytic IL-1β and inflammation in zebrafish. The Journal of Immunology *193*, 1408–1415.

Barbé, F., Douglas, T., and Saleh, M. (2014). Advances in Nod-like receptors (NLR) biology. Cytokine Growth Factor Rev *25*, 681–697.

Baroja-Mazo, A., Martín-Sánchez, F., Gomez, A.I., Martínez, C.M., Amores-Iniesta, J., Compan, V., Barberà-Cremades, M., Yagüe, J., Ruiz-Ortiz, E., Antón, J., et al. (2014). The NLRP3 inflammasome is released as a particulate danger signal that amplifies the inflammatory response. Nat Immunol *15*, 738–748.

Bird, S., Zou, J., Wang, T., Munday, B., Cunningham, C., and Secombes, C.J. (2002). Evolution of interleukin-1beta. Cytokine Growth Factor Rev *13*, 483–502.

Boucher, D., Chen, K.W., and Schroder, K. (2014). Burn the house, save the day: pyroptosis in pathogen restriction. Inflammasome.

Bousso, P., and Moreau, H.D. (2012). Functional immunoimaging: the revolution continues. Nat Rev Immunol *12*, 858–864.

Broderick, L., and Hoffman, H.M. (2014). cASCading specks. Nat Immunol *15*, 698–700.

Broderick, L., De Nardo, D., Franklin, B.S., Hoffman, H.M., and Latz, E. (2015). The inflammasomes and autoinflammatory syndromes. Annu. Rev. Pathol. Mech. Dis. *10*, 395–424.

Broz, P., Moltke, von, J., Jones, J.W., Vance, R.E., and Monack, D.M. (2010a). Differential requirement for Caspase-1 autoproteolysis in pathogen-induced cell death and cytokine processing. Cell Host & Microbe *8*, 471–483.

Broz, P., Newton, K., Lamkanfi, M., Mariathasan, S., Dixit, V.M., and Monack, D.M. (2010b). Redundant roles for inflammasome receptors NLRP3 and NLRC4 in host defense against Salmonella. Journal of Experimental Medicine *207*, 1745–1755.

Bryan, N.B., Dorfleutner, A., Rojanasakul, Y., and Stehlik, C. (2009). Activation of Inflammasomes Requires Intracellular Redistribution of the Apoptotic Speck-Like Protein Containing a Caspase Recruitment Domain. The Journal of Immunology *182*, 3173–3182.

Bryant, C.E., and Monie, T.P. (2012). Mice, men and the relatives: cross-species studies underpin innate immunity. Open Biol *2*, 120015.

Cai, X., Chen, J., Xu, H., Liu, S., Jiang, Q.-X., Halfmann, R., and Chen, Z.J. (2014). Prion-like Polymerization Underlies Signal Transduction in Antiviral Immune Defense and Inflammasome Activation. Cell *156*, 1207–1222.

Carta, S., Lavieri, R., and Rubartelli, A. (2013). Different Members of the IL-1 Family Come Out in Different Ways: DAMPs vs. Cytokines? Front Immunol *4*, 123.

Chai, J., and Shi, Y. (2014). Apoptosome and inflammasome: conserved machineries for caspase activation. National Science Review *1*, 101–118.

Chang, M.X., Chen, W.Q., and Nie, P. (2010). Structure and expression pattern of teleost caspase recruitment domain (CARD) containing proteins that are potentially involved in NF-κB signalling. Dev Comp Immunol *34*, 1–13.

Chang, W.-J., and Hwang, P.-P. (2011). Development of zebrafish epidermis. Birth Defect Res C *93*, 205–214.

Chen, G.Y., and Nuñez, G. (2010). Sterile inflammation: sensing and reacting to damage. Nat Rev Immunol *10*, 826–837.

Chen, K.W., Groß, C.J., Sotomayor, F.V., Stacey, K.J., Tschopp, J., Sweet, M.J., and Schroder, K. (2014). The neutrophil NLRC4 inflammasome selectively promotes IL-1β maturation without pyroptosis during acute Salmonella challenge. CellReports *8*, 570–582.

Cheng, J., Waite, A.L., Tkaczyk, E.R., Ke, K., Richards, N., Hunt, A.J., and Gumucio, D.L. (2010). Kinetic properties of ASC protein aggregation in epithelial cells. J. Cell. Physiol. *222*, 738–747.

Chu, L.H., Gangopadhyay, A., Dorfleutner, A., and Stehlik, C. (2015). An updated view on the structure and function of PYRIN domains. Apoptosis *20*, 157–173.

Cookson, B.T., and Brennan, M.A. (2001). Pro-inflammatory programmed cell death. Trends in Microbiology *9*, 113–114.

Correa, R.G., Matsui, T., Tergaonkar, V., Rodriguez-Esteban, C., Izpisua-Belmonte, J.C., and Verma, I.M. (2005). Zebrafish IkappaB kinase 1 negatively regulates NF-kappaB activity. Curr Biol *15*, 1291–1295.

Correa, R.G., Tergaonkar, V., Ng, J.K., Dubova, I., Izpisua-Belmonte, J.C., and Verma, I.M. (2004). Characterization of NF-kappa B/I kappa B proteins in zebra fish and their involvement in notochord development. Mol Cell Biol *24*, 5257–5268.

Croker, B.A., O'Donnell, J.A., and Gerlic, M. (2014). Pyroptotic death storms and cytopenia. Curr Opin Immunol *26*, 128–137.

Dai, X., Sayama, K., Tohyama, M., Shirakata, Y., Hanakawa, Y., Tokumaru, S., Yang, L., Hirakawa, S., and Hashimoto, K. (2011). Mite allergen is a danger signal for the skin via activation of inflammasome in keratinocytes. J. Allergy Clin. Immunol. *127*, 806–14.e1–4.

de Alba, E. (2009). Structure and interdomain dynamics of apoptosis-associated speck-like protein containing a CARD (ASC). Journal of Biological Chemistry *284*, 32932–32941.

de Oliveira, S., Reyes-Aldasoro, C.C., Candel, S., Renshaw, S.A., Mulero, V., and Calado, A. (2013). Cxcl8 (IL-8) mediates neutrophil recruitment and behavior in the zebrafish inflammatory response. The Journal of Immunology

190, 4349–4359.

Denes, A., Lopez-Castejon, G., and Brough, D. (2012). Caspase-1: is IL-1 just the tip of the ICEberg? Cell Death Dis *3*, e338.

Dinarello, C.A. (2013). Overview of the interleukin-1 family of ligands and receptors. Semin Immunol *25*, 389–393.

Dorfleutner, A., Chu, L., and Stehlik, C. (2015). Inhibiting the inflammasome: one domain at a time. Immunol Rev *265*, 205–216.

Drexler, S.K., Bonsignore, L., Masin, M., Tardivel, A., Jackstadt, R., Hermeking, H., Schneider, P., Groß, O., Tschopp, J., and Yazdi, A.S. (2012). Tissue-specific opposing functions of the inflammasome adaptor ASC in the regulation of epithelial skin carcinogenesis. Proceedings of the National Academy of Sciences *109*, 18384–18389.

Ellett, F., Pase, L., Hayman, J.W., Andrianopoulos, A., and Lieschke, G.J. (2011). mpeg1 promoter transgenes direct macrophage-lineage expression in zebrafish. Blood *117*, e49–e56.

Elliott, E.I., and Sutterwala, F.S. (2015). Initiation and perpetuation of NLRP3 inflammasome activation and assembly. Immunol Rev *265*, 35–52.

Emelyanov, A., and Parinov, S. (2008). Mifepristone-inducible LexPR system to drive and control gene expression in transgenic zebrafish. Dev Biol *320*, 113–121.

Espín-Palazón, R., Stachura, D.L., Campbell, C.A., García-Moreno, D., Del Cid, N., Kim, A.D., Candel, S., Meseguer, J., Mulero, V., and Traver, D. (2014). Proinflammatory signaling regulates hematopoietic stem cell emergence. Cell *159*, 1070–1085.

Feldmeyer, L., Keller, M., Niklaus, G., Hohl, D., Werner, S., and Beer, H.-D. (2007). The Inflammasome Mediates UVB-Induced Activation and Secretion of Interleukin-1β by Keratinocytes. Current Biology *17*, 1140–1145.

Feldmeyer, L., Werner, S., French, L.E., and Beer, H.-D. (2010). Interleukin-1, inflammasomes and the skin. European Journal of Cell Biology *89*, 638–644.

Fernandes-Alnemri, T., Wu, J., Yu, J.-W., Datta, P., Miller, B., Jankowski, W., Rosenberg, S., Zhang, J., and Alnemri, E.S. (2007). The pyroptosome: a supramolecular assembly of ASC dimers mediating inflammatory cell death via caspase-1 activation. Cell Death Differ *14*, 1590–1604.

Fischer, B., Metzger, M., Richardson, R., Knyphausen, P., Ramezani, T., Franzen, R., Schmelzer, E., Bloch, W., Carney, T.J., and Hammerschmidt, M. (2014). p53 and TAp63 promote keratinocyte proliferation and differentiation in breeding tubercles of the zebrafish. PLoS Genet *10*, e1004048.

Franklin, B.S., Bossaller, L., De Nardo, D., Ratter, J.M., Stutz, A., Engels, G., Brenker, C., Nordhoff, M., Mirandola, S.R., Al-Amoudi, A., et al. (2014). The adaptor ASC has extracellular and "prionoid" activities that propagate inflammation. Nat Immunol *15*, 727–737.

Fukazawa, C., Santiago, C., Park, K.M., Deery, W.J., Gomez de la Torre Canny, S., Holterhoff, C.K., and Wagner, D.S. (2010). poky/chuk/ikk1 is required for differentiation of the zebrafish embryonic epidermis. Dev Biol *346*, 272–283.

Garlanda, C., Dinarello, C.A., and Mantovani, A. (2013a). The interleukin-1 family: back to the future. Immunity *39*, 1003–1018.

Garlanda, C., Riva, F., Bonavita, E., and Mantovani, A. (2013b). Negative regulatory receptors of the IL-1 family. Semin Immunol *25*, 408–415.

Gilmore, T.D., and Wolenski, F.S. (2012). NF-κB: where did it come from and why? Immunol Rev *246*, 14–35.

Glover, C.N., Bucking, C., and Wood, C.M. (2013). The skin of fish as a transport epithelium: a review. J. Comp. Physiol. B, Biochem. Syst. Environ. Physiol. *183*, 877–891.

Groß, O., Yazdi, A.S., Thomas, C.J., Masin, M., Heinz, L.X., Guarda, G., Quadroni, M., Drexler, S.K., and Tschopp, J. (2012). Inflammasome activators induce interleukin-1α secretion via distinct pathways with differential requirement for the protease function of caspase-1. Immunity *36*, 388–400.

Guo, H., Callaway, J.B., and Ting, J.P.Y. (2015). Inflammasomes: mechanism of action, role in disease, and therapeutics. Nat Med *21*, 677–687.

Hall, C., Flores, M.V., Storm, T., Crosier, K., and Crosier, P. (2007). The zebrafish lysozyme C promoter drives myeloid-specific expression in transgenic fish. BMC Dev Biol *7*, 42.

Hansen, J.D., Vojtech, L.N., and Laing, K.J. (2011). Sensing disease and danger: A survey of vertebrate PRRs and their origins. Dev Comp Immunol *35*, 886–897.

Hara, H., Tsuchiya, K., Kawamura, I., Fang, R., Hernandez-Cuellar, E., Shen, Y., Mizuguchi, J., Schweighoffer, E., Tybulewicz, V., and Mitsuyama, M. (2013). Phosphorylation of the adaptor ASC acts as a molecular switch that controls the formation of speck-like aggregates and inflammasome activity. Nat Immunol *14*, 1247–1255.

Hauenstein, A.V., Zhang, L., and Wu, H. (2015). The hierarchical structural architecture of inflammasomes, supramolecular inflammatory machines. Curr. Opin. Struct. Biol. *31*, 75–83.

He, Q., Zhang, C., Wang, L., Zhang, P., Ma, D., Lv, J., and Liu, F. (2015).

Inflammatory signaling regulates hematopoietic stem and progenitor cell emergence in vertebrates. Blood *125*, 1098–1106.

Hisano, Y., Sakuma, T., Nakade, S., Ohga, R., Ota, S., Okamoto, H., Yamamoto, T., and Kawahara, A. (2015). Precise in-frame integration of exogenous DNA mediated by CRISPR/Cas9 system in zebrafish. Sci Rep *5*, 8841.

Hoesel, B., and Schmid, J.A. (2013). The complexity of NF-κB signaling in inflammation and cancer. Mol. Cancer *12*, 86.

Hong, S., Zou, J., Collet, B., Bols, N.C., and Secombes, C.J. (2004). Analysis and characterisation of IL-1beta processing in rainbow trout, Oncorhynchus mykiss. Fish & Shellfish Immunology *16*, 453–459.

Hornung, V., Ablasser, A., Charrel-Dennis, M., Bauernfeind, F., Horvath, G., Caffrey, D.R., Latz, E., and Fitzgerald, K.A. (2009). AIM2 recognizes cytosolic dsDNA and forms a caspase-1-activating inflammasome with ASC. Nature *458*, 514–518.

Howe, K., Schiffer, P.H., Zielinski, J., Wiehe, T., Laird, G.K., Marioni, J.C., Soylemez, O., Kondrashov, F., and Leptin, M. (2016). Structure and evolutionary history of a large family of NLR proteins in the zebrafish. Open Biol *6*, 160009.

Huising, M.O., Stet, R.J.M., Savelkoul, H.F.J., and Verburg-van Kemenade, B.M.L. (2004). The molecular evolution of the interleukin-1 family of cytokines; IL-18 in teleost fish. Dev Comp Immunol *28*, 395–413.

Husain, M., Bird, S., van Zwieten, R., Secombes, C.J., and Wang, T. (2012). Cloning of the IL-1Î²3 gene and IL-1Î²4 pseudogene in salmonids uncovers a second type of IL-1Î² gene in teleost fish. Dev Comp Immunol *38*, 431–446.

Irion, U., Krauss, J., and Nüsslein-Volhard, C. (2014). Precise and efficient genome editing in zebrafish using the CRISPR/Cas9 system. Development *141*, 4827–4830.

Joosten, L.A.B., Netea, M.G., and Dinarello, C.A. (2013). Interleukin-1β in innate inflammation, autophagy and immunity. Semin Immunol *25*, 416–424.

Jorgensen, I., and Miao, E.A. (2015). Pyroptotic cell death defends against intracellular pathogens. Immunol Rev *265*, 130–142.

Kagan, J.C., Magupalli, V.G., and Wu, H. (2014). SMOCs: supramolecular organizing centres that control innate immunity. Nat Rev Immunol *14*, 821–826.

Kanther, M., Sun, X., Mühlbauer, M., Mackey, L.C., Flynn, E.J., Bagnat, M., Jobin, C., and Rawls, J.F. (2011). Microbial colonization induces dynamic temporal and spatial patterns of NF-κB activation in the zebrafish digestive

tract. Gastroenterology *141*, 197–207.

Kao, W.-P., Yang, C.-Y., Su, T.-W., Wang, Y.-T., Lo, Y.-C., and Lin, S.-C. (2014). The versatile roles of CARDs in regulating apoptosis, inflammation, and NF-κB signaling. Apoptosis *20*, 174–195.

Kayagaki, N., Stowe, I.B., Lee, B.L., O'Rourke, K., Anderson, K., Warming, S., Cuellar, T., Haley, B., Roose-Girma, M., Phung, Q.T., et al. (2015). Caspase-11 cleaves gasdermin D for non-canonical inflammasome signalling. Nature *526*, 666–671.

Kayagaki, N., Warming, S., Lamkanfi, M., Vande Walle, L., Louie, S., Dong, J., Newton, K., Qu, Y., Liu, J., Heldens, S., et al. (2011). Non-canonical inflammasome activation targets caspase-11. Nature *479*, 117–121.

Kim, B., Lee, Y., Kim, E., Kwak, A., Ryoo, S., Bae, S.H., Azam, T., Kim, S., and Dinarello, C.A. (2013). The Interleukin-1α Precursor is Biologically Active and is Likely a Key Alarmin in the IL-1 Family of Cytokines. Front Immunol *4*, 391.

Kim, J.H., Lee, S.-R., Li, L.-H., Park, H.-J., Park, J.-H., Lee, K.Y., Kim, M.-K., Shin, B.A., and Choi, S.-Y. (2011). High cleavage efficiency of a 2A peptide derived from porcine teschovirus-1 in human cell lines, zebrafish and mice. PLoS ONE *6*, e18556.

Kimura, Y., Hisano, Y., Kawahara, A., and Higashijima, S.-I. (2014). Efficient generation of knock-in transgenic zebrafish carrying reporter/driver genes by CRISPR/Cas9-mediated genome engineering. Sci Rep *4*, 6545.

Kirchmaier, S., Lust, K., and Wittbrodt, J. (2013). Golden GATEway cloning--a combinatorial approach to generate fusion and recombination constructs. PLoS ONE *8*, e76117.

Kolb, R., Liu, G.-H., Janowski, A.M., Sutterwala, F.S., and Zhang, W. (2014). Inflammasomes in cancer: a double-edged sword. Protein Cell *5*, 12–20.

Kono, H., Kimura, Y., and Latz, E. (2014). ScienceDirect Inflammasome activation in response to dead cells and their metabolites. Curr Opin Immunol *30*, 91–98.

Lahiri, K., Froehlich, N., Heyd, A., Foulkes, N.S., and Vallone, D. (2014). Developmental stage-specific regulation of the circadian clock by temperature in zebrafish. Biomed Res Int *2014*, 930308.

Laing, K.J., Purcell, M.K., Winton, J.R., and Hansen, J.D. (2008). A genomic view of the NOD-like receptor family in teleost fish: identification of a novel NLR subfamily in zebrafish. BMC Evol. Biol. *8*, 42.

Lamkanfi, M., and Dixit, V.M. (2014). Mechanisms and functions of inflammasomes. Cell *157*, 1013–1022.

LaRock, C.N., and Cookson, B.T. (2013). Burning down the house: cellular actions during pyroptosis. PLoS Pathog *9*, e1003793.

Latz, E., Xiao, T.S., and Stutz, A. (2013). Activation and regulation of the inflammasomes. Nat Rev Immunol *13*, 397–411.

Lawrence, T. (2009). The nuclear factor NF-kappaB pathway in inflammation. Cold Spring Harb Perspect Biol *1*, a001651.

Lechtenberg, B.C., Mace, P.D., and Riedl, S.J. (2014). Structural mechanisms in NLR inflammasome signaling. Curr. Opin. Struct. Biol. *29*, 17–25.

Li, J., Zhang, B.-B., Ren, Y.-G., Gu, S.-Y., Xiang, Y.-H., and Du, J.-L. (2015). Intron targeting-mediated and endogenous gene integrity-maintaining knockin in zebrafish using the CRISPR/Cas9 system. Cell Res. *25*, 634–637.

Li, S., Chen, X., Peng, W., Hao, G., Geng, X., Zhan, W., and Sun, J. (2016). Cloning and characterization of apoptosis-associated speck-like protein containing a CARD domain (ASC) gene from Japanese flounder Paralichthys olivaceus. Fish & Shellfish Immunology *54*, 294–301.

Lin, C.-Y., Chiang, C.-Y., and Tsai, H.-J. (2016). Zebrafish and Medaka: new model organisms for modern biomedical research. Journal of Biomedical Science 1–11.

Liu, X., Huang, S., Ma, J., Li, C., Zhang, Y., and Luo, L. (2009). NF-kappaB and Snail1a coordinate the cell cycle with gastrulation. The Journal of Cell Biology *184*, 805–815.

Lu, A., and Wu, H. (2014). Structural Mechanisms of Inflammasome Assembly. FEBS Journal.

Lu, A., Li, Y., Schmidt, F.I., Yin, Q., Chen, S., Fu, T.-M., Tong, A.B., Ploegh, H.L., Mao, Y., and Wu, H. (2016). Molecular basis of caspase-1 polymerization and its inhibition by a new capping mechanism. Nat Struct Mol Biol *23*, 416–425.

Lu, A., Magupalli, V.G., Ruan, J., Yin, Q., Atianand, M.K., Vos, M.R., Schröder, G.F., Fitzgerald, K.A., Wu, H., and Egelman, E.H. (2014). Unified Polymerization Mechanism for the Assembly of ASC-Dependent Inflammasomes. Cell *156*, 1193–1206.

Man, S.M., and Kanneganti, T.-D. (2015a). Regulation of inflammasome activation. Immunol Rev *265*, 6–21.

Man, S.M., and Kanneganti, T.-D. (2015b). Converging roles of caspases in inflammasome activation, cell death and innate immunity. Nat Rev Immunol *16*, 7–21.

Man, S.M., Hopkins, L.J., Nugent, E., Cox, S., Glück, I.M., Tourlomousis, P.,

Wright, J.A., Cicuta, P., Monie, T.P., and Bryant, C.E. (2014). Inflammasome activation causes dual recruitment of NLRC4 and NLRP3 to the same macromolecular complex. Proceedings of the National Academy of Sciences *111*, 7403–7408.

Mariathasan, S., Newton, K., Monack, D.M., Vucic, D., French, D.M., Lee, W.P., Roose-Girma, M., Erickson, S., and Dixit, V.M. (2004). Differential activation of the inflammasome by caspase-1 adaptors ASC and Ipaf. Nature *430*, 213–218.

Mariathasan, S., Weiss, D.S., Newton, K., McBride, J., O'Rourke, K., Roose-Girma, M., Lee, W.P., Weinrauch, Y., Monack, D.M., and Dixit, V.M. (2006). Cryopyrin activates the inflammasome in response to toxins and ATP. Nature *440*, 228–232.

Martinon, F., Burns, K., and Tschopp, J. (2002). The inflammasome: a molecular platform triggering activation of inflammatory caspases and processing of proIL-beta. Mol Cell *10*, 417–426.

Masters, S.L., Gerlic, M., Metcalf, D., Preston, S., Pellegrini, M., O'Donnell, J.A., McArthur, K., Baldwin, T.M., Chevrier, S., Nowell, C.J., et al. (2012). NLRP1 Inflammasome Activation Induces Pyroptosis of Hematopoietic Progenitor Cells. Immunity.

Masumoto, J., Taniguchi, S., and Sagara, J. (2001). Pyrin N-terminal homology domain- and caspase recruitment domain-dependent oligomerization of ASC. Biochem Bioph Res Co *280*, 652–655.

Masumoto, J., Taniguchi, S., Ayukawa, K., Sarvotham, H., Kishino, T., Niikawa, N., Hidaka, E., Katsuyama, T., Higuchi, T., and Sagara, J. (1999). ASC, a novel 22-kDa protein, aggregates during apoptosis of human promyelocytic leukemia HL-60 cells. J Biol Chem *274*, 33835–33838.

Masumoto, J., Zhou, W., Chen, F.F., Su, F., Kuwada, J.Y., Hidaka, E., Katsuyama, T., Sagara, J., Taniguchi, S., Ngo-Hazelett, P., et al. (2003). Caspy, a zebrafish caspase, activated by ASC oligomerization is required for pharyngeal arch development. J Biol Chem *278*, 4268–4276.

Mathew, J.A., Guo, Y.X., Goh, K.P., Chan, J., Verburg-van Kemenade, B.M.L., and Kwang, J. (2002). Characterisation of a monoclonal antibody to carp IL-1β and the development of a sensitive capture ELISA. Fish & Shellfish Immunology *13*, 85–95.

Matsuda, M., Tsukiyama, T., Bohgaki, M., Nonomura, K., and Hatakeyama, S. (2007). Establishment of a newly improved detection system for NF-kappaB activity. Immunol Lett *109*, 175–181.

McAuley, J.L., Tate, M.D., MacKenzie-Kludas, C.J., Pinar, A., Zeng, W., Stutz, A., Latz, E., Brown, L.E., and Mansell, A. (2013). Activation of the NLRP3

inflammasome by IAV virulence protein PB1-F2 contributes to severe pathophysiology and disease. PLoS Pathog *9*, e1003392.

Miao, E.A., Leaf, I.A., Treuting, P.M., Mao, D.P., Dors, M., Sarkar, A., Warren, S.E., Wewers, M.D., and Aderem, A. (2010). Caspase-1-induced pyroptosis is an innate immune effector mechanism against intracellular bacteria. Nat Immunol *11*, 1136–1142.

Miao, E.A., Rajan, J.V., and Aderem, A. (2011). Caspase-1-induced pyroptotic cell death. Immunol Rev *243*, 206–214.

Mogensen, T.H. (2009). Pathogen recognition and inflammatory signaling in innate immune defenses. Clin. Microbiol. Rev. *22*, 240–73–TableofContents.

Napetschnig, J., and Wu, H. (2013). Molecular basis of NF-κB signaling. Annu Rev Biophys *42*, 443–468.

Natoli, G. (2006). Tuning up inflammation: how DNA sequence and chromatin organization control the induction of inflammatory genes by NF-kappaB. FEBS Letters *580*, 2843–2849.

Newton, K., and Dixit, V.M. (2012). Signaling in innate immunity and inflammation. Cold Spring Harb Perspect Biol *4*, a006049.

Nguyen-Chi, M., Phan, Q.T., Gonzalez, C., Dubremetz, J.-F., Levraud, J.-P., and Lutfalla, G. (2014). Transient infection of the zebrafish notochord with E. coli induces chronic inflammation. Dis Model Mech *7*, 871–882.

Novoa, B., Bowman, T.V., Zon, L., and Figueras, A. (2009). LPS response and tolerance in the zebrafish (Danio rerio). Fish & Shellfish Immunology *26*, 326–331.

Ogryzko, N.V., Hoggett, E.E., Solaymani-Kohal, S., Tazzyman, S., Chico, T.J.A., Renshaw, S.A., and Wilson, H.L. (2014a). Zebrafish tissue injury causes upregulation of interleukin-1 and caspase-dependent amplification of the inflammatory response. Dis Model Mech *7*, 259–264.

Ogryzko, N.V., Renshaw, S.A., and Wilson, H.L. (2014b). The IL-1 family in fish: Swimming through the muddy waters of inflammasome evolution. Dev Comp Immunol 1–10.

Ordas, A., Raterink, R.-J., Cunningham, F., Jansen, H.J., Wiweger, M.I., Jong-Raadsen, S., Bos, S., Bates, R.H., Barros, D., Meijer, A.H., et al. (2015). Testing tuberculosis drug efficacy in a zebrafish high-throughput translational medicine screen. Antimicrob. Agents Chemother. *59*, 753–762.

Peeters, P.M., Wouters, E.F., and Reynaert, N.L. (2015). Immune Homeostasis in Epithelial Cells: Evidence and Role of Inflammasome Signaling Reviewed. Journal of Immunology Research *2015*, 1–15.

Peri, F., and Nüsslein-Volhard, C. (2008). Live imaging of neuronal degradation by microglia reveals a role for v0-ATPase a1 in phagosomal fusion in vivo. Cell *133*, 916–927.

Pierini, R., Juruj, C., Perret, M., Jones, C.L., Mangeot, P., Weiss, D.S., and Henry, T. (2012). AIM2/ASC triggers caspase-8-dependent apoptosis in Francisella-infected caspase-1-deficient macrophages. Cell Death Differ *19*, 1709–1721.

Pradhan, A., Khalaf, H., Ochsner, S.A., Sreenivasan, R., Koskinen, J., Karlsson, M., Karlsson, J., McKenna, N.J., Orbán, L., and Olsson, P.-E. (2012). Activation of NF-κB Protein Prevents the Transition from Juvenile Ovary to Testis and Promotes Ovarian Development in Zebrafish. J Biol Chem *287*, 37926–37938.

Progatzky, F., Sangha, N.J., Yoshida, N., McBrien, M., Cheung, J., Shia, A., Scott, J., Marchesi, J.R., Lamb, J.R., Bugeon, L., et al. (2014). Dietary cholesterol directly induces acute inflammasome-dependent intestinal inflammation. Nat Commun *5*, 5864.

Provost, E., Rhee, J., and Leach, S.D. (2007). Viral 2A peptides allow expression of multiple proteins from a single ORF in transgenic zebrafish embryos. Genesis *45*, 625–629.

Qu, Y., Misaghi, S., Newton, K., Maltzman, A., Izrael-Tomasevic, A., Arnott, D., and Dixit, V.M. (2016). NLRP3 recruitment by NLRC4 during Salmonella infection. Journal of Experimental Medicine jem.20132234.

Rakers, S., Niklasson, L., Steinhagen, D., Kruse, C., Schauber, J., Sundell, K., and Paus, R. (2013). Antimicrobial peptides (AMPs) from fish epidermis: perspectives for investigative dermatology. J Investig Dermatol *133*, 1140–1149.

Rast, J.P., Smith, L.C., Loza-Coll, M., Hibino, T., and Litman, G.W. (2006). Genomic insights into the immune system of the sea urchin. Science *314*, 952–956.

Rawat, R., Cohen, T.V., Ampong, B., Francia, D., Henriques-Pons, A., Hoffman, E.P., and Nagaraju, K. (2010). Inflammasome Up-Regulation and Activation in Dysferlin-Deficient Skeletal Muscle. The American Journal of Pathology *176*, 2891–2900.

Reinholz, M., Kawakami, Y., Salzer, S., Kreuter, A., Dombrowski, Y., Koglin, S., Kresse, S., Ruzicka, T., and Schauber, J. (2013). HPV16 activates the AIM2 inflammasome in keratinocytes. Arch Dermatol Res *305*, 723–732.

Reis, M.I.R., do Vale, A., Pereira, P.J.B., Azevedo, J.E., and Santos, dos, N.M.S. (2012). Caspase-1 and IL-1β Processing in a Teleost Fish. PLoS ONE *7*, e50450.

Renshaw, S.A., and Trede, N.S. (2012). A model 450 million years in the making: zebrafish and vertebrate immunity. Dis Model Mech *5*, 38–47.

Reynaud, E.G., Krzic, U., Greger, K., and Stelzer, E.H.K. (2008). Light sheet-based fluorescence microscopy: more dimensions, more photons, and less photodamage. Hfsp J *2*, 266–275.

Rider, P., Carmi, Y., Voronov, E., and Apte, R.N. (2013). Interleukin-1α. Semin Immunol *25*, 430–438.

Rinkenbaugh, A.L., and Baldwin, A.S. (2016). The NF-κB Pathway and Cancer Stem Cells. Cells *5*, 16.

Robbins, D., and Zhao, Y. (2011). Imaging NF-κB signaling in mice for screening anticancer drugs. Methods Mol Biol *716*, 169–177.

Rodgers, M.A., Bowman, J.W., Fujita, H., Orazio, N., Shi, M., Liang, Q., Amatya, R., Kelly, T.J., Iwai, K., Ting, J., et al. (2014). The linear ubiquitin assembly complex (LUBAC) is essential for NLRP3 inflammasome activation. Journal of Experimental Medicine *211*, 1333–1347.

Ruland, J. (2014). Inflammasome: putting the pieces together. Cell *156*, 1127–1129.

Sagulenko, V., Thygesen, S.J., Sester, D.P., Idris, A., Cridland, J.A., Vajjhala, P.R., Roberts, T.L., Schroder, K., Vince, J.E., Hill, J.M., et al. (2013). AIM2 and NLRP3 inflammasomes activate both apoptotic and pyroptotic death pathways via ASC. Cell Death Differ *20*, 1149–1160.

Sahillioglu, A.C., Sumbul, F., Ozoren, N., and Haliloglu, T. (2014). Structural and Dynamics Aspects of ASC Speck Assembly. Structure/Folding and Design *22*, 1722–1734.

Secombes, C.J., Wang, T., and Bird, S. (2011). The interleukins of fish. Dev Comp Immunol *35*, 1336–1345.

Sellin, M.E., Maslowski, K.M., Maloy, K.J., and Hardt, W.-D. (2015). Inflammasomes of the intestinal epithelium. Trends Immunol 1–9.

Sester, D.P., Thygesen, S.J., Sagulenko, V., Vajjhala, P.R., Cridland, J.A., Vitak, N., Chen, K.W., Osborne, G.W., Schroder, K., and Stacey, K.J. (2015). A novel flow cytometric method to assess inflammasome formation. The Journal of Immunology *194*, 455–462.

Shah, A.N., Davey, C.F., Whitebirch, A.C., Miller, A.C., and Moens, C.B. (2015). Rapid reverse genetic screening using CRISPR in zebrafish. Nat Meth.

Shi, C.-S., Shenderov, K., Huang, N.-N., Kabat, J., Abu-Asab, M., Fitzgerald, K.A., Sher, A., and Kehrl, J.H. (2012). Activation of autophagy by inflammatory signals limits IL-1β production by targeting ubiquitinated inflammasomes for destruction. Nat Immunol.

Shi, J., Zhao, Y., Wang, K., Shi, X., Wang, Y., Huang, H., Zhuang, Y., Cai, T.,

Wang, F., and Shao, F. (2015). Cleavage of GSDMD by inflammatory caspases determines pyroptotic cell death. Nature *526*, 660–665.

Sieger, D., Moritz, C., Ziegenhals, T., Prykhozhij, S., and Peri, F. (2012). Long-range Ca2+ waves transmit brain-damage signals to microglia. Dev Cell *22*, 1138–1148.

Siggers, T., Chang, A.B., Teixeira, A., Wong, D., Williams, K.J., Ahmed, B., Ragoussis, J., Udalova, I.A., Smale, S.T., and Bulyk, M.L. (2012). Principles of dimer-specific gene regulation revealed by a comprehensive characterization of NF-κB family DNA binding. Nat Immunol *13*, 95–102.

Sims, J.E., and Smith, D.E. (2010). The IL-1 family: regulators of immunity. Nat Rev Immunol *10*, 89–102.

Stein, C., Caccamo, M., Laird, G., and Leptin, M. (2007). Conservation and divergence of gene families encoding components of innate immune response systems in zebrafish. Genome Biol *8*, R251.

Stemmer, M., Thumberger, T., Del Sol Keyer, M., Wittbrodt, J., and Mateo, J.L. (2015). CCTop: An Intuitive, Flexible and Reliable CRISPR/Cas9 Target Prediction Tool. PLoS ONE *10*, e0124633.

Stephenson, H.N., Herzig, A., and Zychlinsky, A. (2015). ScienceDirect Beyond the grave: When is cell death critical for immunity to infection? 1–8.

Stutz, A., Horvath, G.L., Monks, B.G., and Latz, E. (2013). ASC speck formation as a readout for inflammasome activation. Methods Mol Biol *1040*, 91–101.

Sun, Y., Wang, J., Lao, H., Yin, Z., He, W., Weng, S., Yu, X., Chan, S., and He, J. (2008). Molecular cloning and expression analysis of the ASC gene from mandarin fish and its regulation of NF-κB activation. Dev Comp Immunol *32*, 391–399.

Takeuchi, O., and Akira, S. (2010). Pattern Recognition Receptors and Inflammation. Cell *140*, 805–820.

Tenthorey, J.L., Kofoed, E.M., Daugherty, M.D., Malik, H.S., and Vance, R.E. (2014). Molecular basis for specific recognition of bacterial ligands by NAIP/NLRC4 inflammasomes. Mol Cell *54*, 17–29.

Thisse, C., and Thisse, B. (2008). High-resolution in situ hybridization to whole-mount zebrafish embryos. Nat Protoc *3*, 59–69.

Thornberry, N.A., Bull, H.G., Calaycay, J.R., Chapman, K.T., Howard, A.D., Kostura, M.J., Miller, D.K., Molineaux, S.M., Weidner, J.R., Aunins, J., et al. (1992). A novel heterodimeric cysteine protease is required for interleukin-1|[beta]|processing in monocytes. , Published Online: 30 April 1992; | Doi:10.1038/356768a0 *356*, 768–774.

Ting, J.P.Y., Lovering, R.C., Alnemri, E.S., Bertin, J., Boss, J.M., Davis, B.K., Flavell, R.A., Girardin, S.E., Godzik, A., Harton, J.A., et al. (2008). The NLR gene family: a standard nomenclature. Immunity *28*, 285–287.

Torraca, V., Masud, S., Spaink, H.P., and Meijer, A.H. (2014). Macrophage-pathogen interactions in infectious diseases: new therapeutic insights from the zebrafish host model. Dis Model Mech *7*, 785–797.

Vajjhala, P.R., Lu, A., Brown, D.L., Pang, S.W., Sagulenko, V., Sester, D.P., Cridland, S.O., Hill, J.M., Schroder, K., Stow, J.L., et al. (2015). The Inflammasome Adaptor ASC Induces Procaspase-8 Death Effector Domain Filaments. J Biol Chem *290*, 29217–29230.

Van de Veerdonk, F.L., and Netea, M.G. (2013). New Insights in the Immunobiology of IL-1 Family Members. Front Immunol *4*, 167.

van der Vaart, M., Meijer, A.H., and Spaink, H.P. (2012). Pathogen Recognition and Activation of the Innate Immune Response in Zebrafish. Advances in Hematology *2012*, 1–19.

Vanaja, S.K., Rathinam, V.A.K., and Fitzgerald, K.A. (2015). Mechanisms of inflammasome activation: recent advances and novel insights. Trends Cell Biol *25*, 308–315.

Varela, M., Romero, A., Dios, S., van der Vaart, M., Figueras, A., Meijer, A.H., and Novoa, B. (2014). Cellular visualization of macrophage pyroptosis and interleukin-1β release in a viral hemorrhagic infection in zebrafish larvae. J Virol *88*, 12026–12040.

Veneman, W.J., Stockhammer, O.W., de Boer, L., Zaat, S.A.J., Meijer, A.H., and Spaink, H.P. (2013). A zebrafish high throughput screening system used for Staphylococcus epidermidis infection marker discovery. BMC Genomics *14*, 255.

Vincent, W.J.B., Freisinger, C.M., Lam, P.-Y., Huttenlocher, A., and Sauer, J.-D. (2015). Macrophages mediate flagellin induced inflammasome activation and host defense in zebrafish. Cellular Microbiology n/a–n/a.

Vojtech, L.N., Scharping, N., Woodson, J.C., and Hansen, J.D. (2012). Roles of Inflammatory Caspases during Processing of Zebrafish Interleukin-1β in Francisella noatunensis Infection. Infect Immun *80*, 2878–2885.

Wang, G., Rajpurohit, S.K., Delaspre, F., Walker, S.L., White, D.T., Ceasrine, A., Kuruvilla, R., Li, R.-J., Shim, J.S., Liu, J.O., et al. (2015). First quantitative high-throughput screen in zebrafish identifies novel pathways for increasing pancreatic β-cell mass. Elife *4*, e08261.

Watanabe, H., Gaide, O., Pétrilli, V., Martinon, F., Contassot, E., Roques, S., Kummer, J.A., Tschopp, J., and French, L.E. (2007). Activation of the IL-1β-Processing Inflammasome Is Involved in Contact Hypersensitivity. J Investig

Dermatol *127*, 1956–1963.

Watzke, J., Schirmer, K., and Scholz, S. (2007). Bacterial lipopolysaccharides induce genes involved in the innate immune response in embryos of the zebrafish (Danio rerio). Fish & Shellfish Immunology *23*, 901–905.

Westerfield, M. (2007). The Zebrafish Book.

Whitlock, K.E., and Westerfield, M. (2000). The olfactory placodes of the zebrafish form by convergence of cellular fields at the edge of the neural plate. Development *127*, 3645–3653.

Wu, H. (2013). Higher-order assemblies in a new paradigm of signal transduction. Cell *153*, 287–292.

Xue, Y., Liu, Z., Cao, J., Ma, Q., Gao, X., Wang, Q., Jin, C., Zhou, Y., Wen, L., and Ren, J. (2011). GPS 2.1: enhanced prediction of kinase-specific phosphorylation sites with an algorithm of motif length selection. Protein Eng. Des. Sel. *24*, 255–260.

Yamanaka, K., Tanaka, M., Tsutsui, H., Kupper, T.S., Asahi, K., Okamura, H., Nakanishi, K., Suzuki, M., Kayagaki, N., Black, R.A., et al. (2000). Skin-specific caspase-1-transgenic mice show cutaneous apoptosis and pre-endotoxin shock condition with a high serum level of IL-18. J Immunol *165*, 997–1003.

Yazdi, A.S., Drexler, S.K., and Tschopp, J. (2010). The Role of the Inflammasome in Nonmyeloid Cells. J. Clin. Immunol. *30*, 623–627.

Zhu, L.-Y., Nie, L., Zhu, G., Xiang, L.-X., and Shao, J.-Z. (2013). Advances in research of fish immune-relevant genes: A comparative overview of innate and adaptive immunity in teleosts. Dev Comp Immunol *39*, 39–62.

Zitvogel, L., Kepp, O., Galluzzi, L., and Kroemer, G. (2012). Inflammasomes in carcinogenesis and anticancer immune responses. Nat Immunol *13*, 343–351.

Zon, L.I., and Peterson, R.T. (2005). In vivo drug discovery in the zebrafish. Nat Rev Drug Discov *4*, 35–44.

Zychlinsky, A., Prevost, M.C., and Sansonetti, P.J. (1992). Shigella flexneri induces apoptosis in infected macrophages. Nature *358*, 167–169.

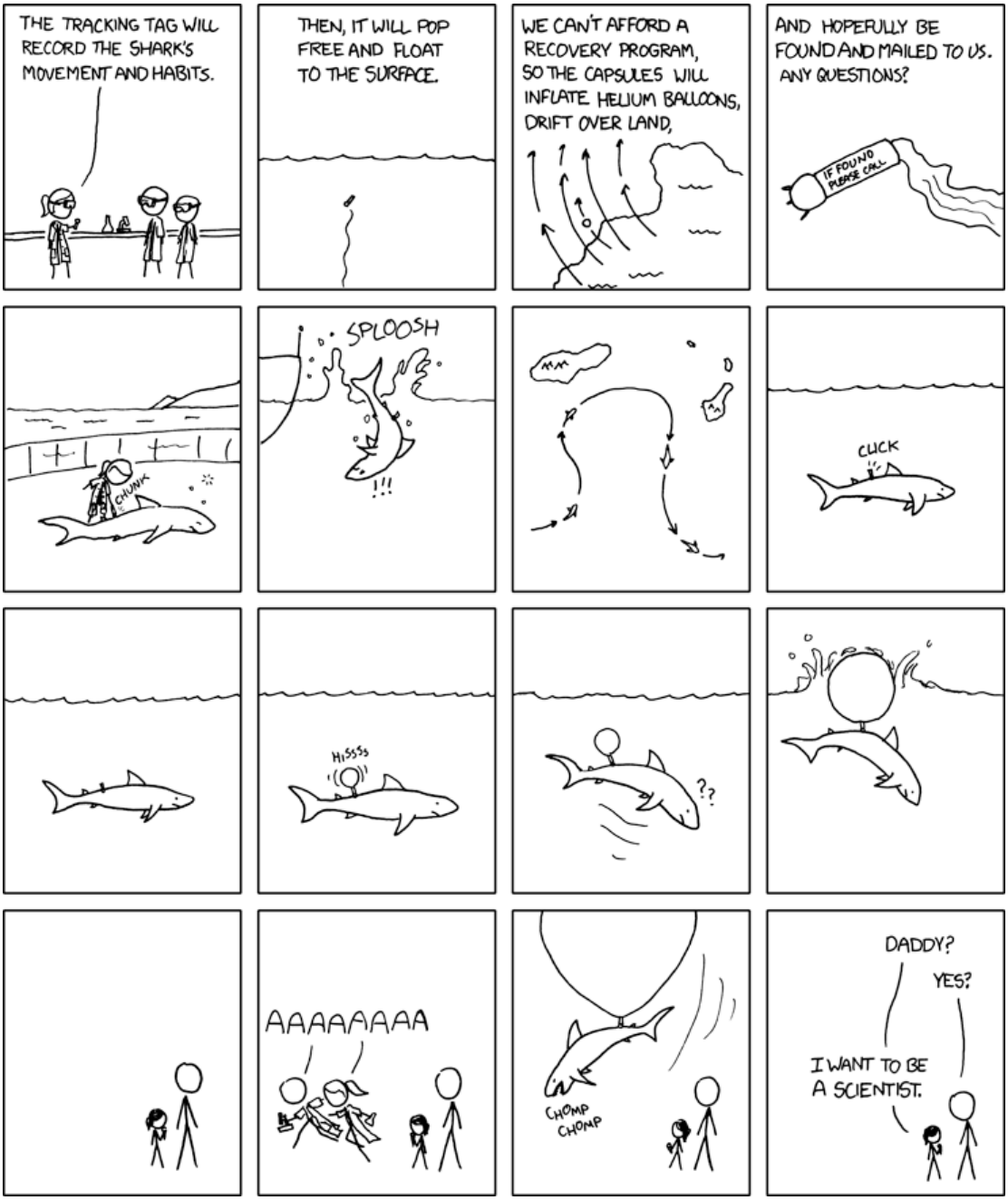

xkcd: Outreach

http://xkcd.com/585/